The Impacts of Glacial Runoff and pCO_2 on Centennial- to Millennial-Scale Climate Variability During the Last Glacial Cycle

by
© *Ryan Love*

A thesis submitted to the
School of Graduate Studies
in partial fulfilment of the
requirements for the degree of
Doctor of Philosophy

Department of *Physics and Physical Oceanography*
Memorial University of Newfoundland

December 2021

St. John's Newfoundland

Abstract

Freshwater is hypothesized to have a critical role in previous centennial- to millennial-scale climate variability (CMCV), e.g. Dansgaard Oeschger events, the Younger Dryas, and may play a central role in future climate change as ice sheet and glacier melt accelerates. Similarly, anthropogenic climate change demonstrates the need to understand the impact of carbon dioxide (pCO_2) on climate variability. The relationship between freshwater and rapid climate change in the paleoclimate records has been a subject of intense study, but past approaches have generally relied upon an approximation of freshwater entering the oceans via wide bands in the North Atlantic in 'hosing' experiments. This design element of hosing experiments, which supports the relationship between freshwater and climate cooling, artificially amplifies the climate response by introducing freshwater directly over sites of deep water formation. As well, previous studies have yet to characterize the role of either pCO_2 or freshwater on CMCV under appropriate boundary conditions.

This thesis explores the impact two likely controls of CMCV, freshwater and pCO_2 concentrations. I achieve this by first determining where coastally released freshwater is transported using an eddy permitting ocean model configured for the the Younger Dryas interval during the last deglaciation. It is found that by explicitly resolving features important for the transport of coastally released freshwater, such as mesoscale eddies, that hosing overestimates the amount of freshwater transported to sites of deepwater formation by $2 - 4\times$. Next, using these results I then derive a novel method of freshwater injection, the freshwater fingerprint, and examine the relative climate impact of different freshwater injection distributions. In comparing the fingerprint method against both conventional band hosing and regional injection methods I conclude that the fingerprint methodology allows for emulation of some features of the eddy permitting representation in a coarse resolution coupled climate model. Finally, I examine the impact that pCO_2 and freshwater has on a specific form of CMCV, Dansgaard-Oeschger events during Marine Isotope Stage 3 (MIS3), with boundary conditions consistent with the MIS3 interval. When examining characteristics of CMCV I find that both increasing freshwater and decreasing carbon dioxide levels lead to similar changes in interstadial & stadial durations.

Acknowledgements

I would like to thank my supervisor Dr. Lev Tarasov, who provided the initial concept and helped refine the project as it evolved. You have continued to push me to be a better scientist and communicator and I am much the better for it. As well, Dr. Heather Andres has been an exceptional mentor and guide over the final stretch of the thesis, you have been an extraordinary colleague to work with. My supervisory committee Dr. Brad de Young and Dr. Entcho Demirov provided useful advice and critique of both the thesis and research plans, you have helped keep things moving over the years. At the last stage the critique and commentary provided by Dr. James Munroe, Dr. Joe Wroblewski, and particularly Dr. Guido Vettoretti, was extremely valuable and your work is very much appreciated.

My thanks to those members of the Glacial Dynamics group, both past and present, who have volunteered time to read through the many drafts over the years. I am very grateful for both the camaraderie and support afforded by the ArcTrain, PALMOD, and ACDC programs as well as the colleagues and co-authors I have met through those endeavours. To the crew of PS115/2, both scientific and support, I thank you for the company and for providing perspective and memories I would otherwise never have. Finally, I'm thankful for my partner (now wife) Candice, you have supported and encouraged me from the first day of this work to the last.

— Ryan Love

Contents

List of Tables

List of Figures

List of Abbreviations

- AABW : Antarctic Bottom Water
- AMOC : Atlantic Meridional Overturning Circulation
- BA : Bølling-Allerød
- CBS : Closed Bering Strait
- CDO : Climate Data Operators
- CESM : Community Earth System Model
- CMCV : Centennial- to Millennial- Scale Variability
- CMIP5 : Climate Model Intercomparison Project phase 5
- DJF : Dec/Jan/Feb
- DO : Dansgaard-Oeschger
- dSv : deci-Sverdrup
- DWF : Deep Water Formation

- ECCO2 : Estimating the Circulation and Climate of the Ocean phase 2
- ECMWF : European Center EC for Medium Range Weather Forecasts ECMWF by developers at Hamburg HAM
- EMIC : Earth Model of Intermediate Complexity
- ESMs : Earth Systems Model
- ESPG : Eastern Subpolar Gyre
- FEN : Fennoscandia
- GHGs : Greenhouse Gasses
- GIN : Greenland-Iceland-Norwegian Seas
- GOM : Gulf of Mexico
- GRIP : Greenland Ice core Project
- GSL : Gulf of St. Lawrence
- GSM : Glacial Systems Model
- HE : Heinrich Event
- IRD : Ice Rafted Debris
- IPCC : International Panel on Climate Change
- JJA : June/July/August

- LGM : Last Glacial Maximum
- MAK : Mackenzie River
- MAM : March/April/May
- MIS : Marine Isotope Stage
- MITgcm : Massachusetts Institute of Technology general Circulation Model
- MPIOM : Max Plank Institute Ocean Model
- MWP1A : Meltwater Pulse 1A
- NADW : North Atlantic Deep Water Formation
- OBS : Open Bering Strait
- PMIP : Paleoclimate Model Intercomparison Project
- SIA : Sea Ice Area
- SON : September/October/November
- SSS : Sea Surface Salinity
- SST : Sea Surface Temperature
- THC : Thermohaline Circulation
- YD : Younger Dryas

Chapter 1

Introduction and Overview

1.1 Motivation and Overview

The Earth's climate is undergoing rapid anthropogenically driven changes towards an uncertain future. The potentially highest impact and also most uncertain aspects of such change arises from rapid climate change processes. It remains unclear how well current coupled climate models can capture such changes. A further challenge is that climate models are generally tuned to the current mean climate state. Such tuning is likely non-unique and it is therefore unclear to what extent model predictions are sensitive to the tuning. One option to address these uncertainties is to look to the past to try and understand the processes which led to rapid climate change at that time and to capture this behaviour with climate modelling tools. The paleoclimate record provides multiple instances of rapid, centennial- to millennial-scale climate change, with some similarities to anthropogenically derived climate change. As such, they offer the opportunity to test the question 'Can our tools capture the full range of climate variability under different mean states?'.

Centennial- to Millennial-Scale Climate Variability as seen in the available paleoclimate records is, at present, in the early stages of understanding from process and modelling viewpoints. Dansgaard-Oeschger (DO) events are the archetypal example of Centennial- to Millennial-scale climate variability (CMCV), first detected in deep ice cores from the Greenland ice sheet [Dansgaard et al., 1984], and are common during the Marine Isotope Stage 3 (MIS3) interval. During a DO event, Greenland surface temperatures can increase by up to $\approx 15^\circ$ C in a matter of decades [Kindler et al., 2014]. These events are not localized to Greenland and have global surface temperature and hydrological cycle signals [Corrick et al., 2020]. The warming over

Greenland is for many such events [Kindler et al., 2014] an order of magnitude greater then the regional difference between the pre-industrial interval and present day ($\approx 2^\circ$ C as of 2010 [Kobashi et al., 2011]). These instances of CMCV vary in duration [Rasmussen et al., 2014, $O(100-2500)$, when considering cold/warm intervals] over a wide range of atmospheric pCO_2 concentrations [Bereiter et al., 2015], ice sheet configurations [Batchelor et al., 2019], and orbital configurations [Laskar et al., 2011]. As such, these instances of CMCV provide an opportunity to compare our models to inferences of past climate and to assess their ability to represent large-scale climate change and variability.

These events take place in a background of an evolving glacial landscape, where glacial runoff enters the oceans in the form of freshwater and icebergs, the former of which has been connected with changes to overturning in the North Atlantic (see section 1.3.1). As well, the concentration of pCO_2 during the last glacial cycle varies on scales comparable to the differences between the pre-industrial interval and present day (pCO_2 variations during the MIS3 interval to the Holocene are a maximum range of ≈ 70 ppmv [Bereiter et al., 2015], preindustrial pCO_2 values were ≈ 280 ppmv and are presently ≈ 415 ppmv as per Keeling and Keeling [2017]). Both of these features, freshwater entering the oceans and pCO_2 concentrations, are changing rapidly at present due to anthropogenic influences and are also hypothesised to play a role in some forms of CMCV during the past. This thesis involves examining the role of freshwater and pCO_2[1] during two intervals of the last glacial cycle with notable CMCV: the Bølling-Allerød-Younger Dryas transition interval (≈ 12900 years ago,

[1]partial pressure of Carbon Dioxide, expressed in parts-per-million by volume (ppmv) hereafter

Rasmussen et al. [2006]), and the Marine Isotope Stage (MIS) 3 interval (57, 000 to 29, 000 years ago [Lisiecki and Raymo, 2005]).

In the following sections of this introduction I summarise the conceptual background and relevant recent literature, and develop the research questions of the thesis. I start with a discussion of pertinent forms of large-scale, glacial climate-system dynamics in Section 1.2, as well as a brief discussion of the records used to infer the existence of these processes or events. This discussion is continued by presenting information regarding the most recent millennial- to centennial-scale climate event, the Bølling-Allerød (BA)-Younger Dryas (YD) interval, which has been argued to be a Dansgaard-Oeschger event which occurred during the deglacial interval [Mangerud et al., 2010, Broecker et al., 2010], and Melt Water Pulse 1A (MWP1A), a large-scale glacial runoff event temporally proximal to the YD. Subsequently in Section 1.3, I discuss the challenges and progress made in studying glacial climates using numerical models, a discussion of some of the elements of my modelling tools is in Section A.1. I summarise the current Chapter in Section 1.4 and provide the broad research questions for this thesis.

1.2 Centennial to Millennial Scale Climate Variability During the Last Glacial Cycle

Here I provide context regarding Centennial- to Millennial Scale Climate Variability and the events this thesis examines. I start with a brief description of the types of proxy records which are used to understand CMCV along with their limitations.

While the thesis itself does not involve explicit study of these records, modelling is an effort to describe the behaviour of the climate system, not a climate model. As such, a familiarity with proxy records, their uses and limitations, is necessary to interpret and understand model behaviour. The dominant form of CMCV, Dansgaard-Oeschger events, are then discussed. Two significant climate events during the deglacial interval, the Younger-Dryas and Meltwater Pulse 1A, are examined to provide some context for Chapters 2 and 3.

1.2.1 Paleoclimate Records and Uncertainties

In order to determine if modelling results reflect the physical system, we have to compare them against measurements of the climate system, whether instrumental or via proxy records. In doing so, we need to account for both the uncertainties of the tools we use to measure system characteristics as well as the uncertainties arising from unresolved physical components or parametrized features of a climate model. For contemporary climate investigations (i.e. the preindustrial period to present), direct observations provide the most reliable source of information. However, for the intervals examined in this thesis, we are reliant on sparse and indirect measurements of climate features.

I provide a brief overview of ice and sediment cores and how they provide information on the climate system as well as associated uncertainties. A core is a record extracted from a medium which is deposited continually through time (though in some cases involving hiatuses) from which signals can be extracted (e.g. GHGs) or inferred (e.g. temperature via δ^{18}O). Translating core depths to absolute ages generally provides great uncertainty within a given record, as the deposition rate typically varies with time, and other features can modify the medium over time (e.g. compaction due to overburden in ice and sediment cores). However, the continual deposition means that the passage of time in a core is monotonic, unless the layering of a core is externally disturbed (e.g. bioturbation, distortions from ice flow).

Ice cores are a heavily relied-upon source of paleoclimate information, and deep ice-core drilling programs have been ongoing since the middle of the 20th century, when members of the United States Army successfully drilled a core through the full depth of the Greenland Ice Sheet [Langway, 2008]. One of the useful features of some ice core records is that they have an annual signal in some characteristics (e.g. soluble ions). For those ice cores (or subsections of ice cores where this analysis is possible, such as the upper or younger regions of the North Greenland Ice Core Project 2 (NGRIP2) core Rasmussen et al. [2006]), this feature allows for a direct mapping of ice core depth onto an absolute time axis. However, at greater depths and older times, advanced techniques to analyse an ice core on the millimetre or smaller scales is required to determine annual layers [e.g. Sneed et al., 2015].

Ice cores provide a relative wealth of data, two types of which I focus on here due to their relevance to the thesis. Firstly, measurements of isotopic ratios of the ice itself (e.g. $\delta^{18}O$ [2]) can be analysed to provide information with regards to local temperature [e.g. Kindler et al., 2014]. Secondly, atmospheric gasses are entrained

[2] $\delta^{18}O$ is the ratio of ^{18}O to ^{16}O in a sample relative to that same ratio for a standard. These are both stable isotopes of oxygen and this metric is used to infer changes in the past. The ratio in water which forms ice cores is primarily a function of temperature and the path of the precipitation between the evaporation in the tropics and the deposition at the site of interest. The concentration in benthic foraminifera is primarily a function of concentration in the ocean. For more details see Delaygue [2009]

during ice formation, and thereby provide a record of atmospheric greenhouse gas concentration over time [e.g. Bereiter et al., 2015, Loulergue et al., 2008, Schilt et al., 2010, respectivly]. Each of these types of data will be affected by the counting error discussed previously, but there are also several other sources of uncertainty. With respect to δ^{18}O, isotopic diffusion results in a slight time-averaging of the data, which make resolving sub-annual signals within the ice core difficult, if not impossible, depending upon the deposition rates and local climate [Cuffey and Steig, 1998]. With regards to atmospheric gasses, air is exchanged between the atmosphere and the snow-pack and firn layers until the firn to ice transition occurs and pore closure results. This interval of atmospheric exchange can be O(100 years) [Bales and Wolff, 1995], resulting in a temporal smearing of similar magnitude. Additionally, quantities such as entrained atmospheric gasses and δ^{18}O measurements are the result of discrete measurements which have a defined thickness over which the measurements are inherently averaged, taken along ice cores that are upwards of several kilometres in length. Furthermore, there are physical limits to the smallest sample size which can be processed to measure a specific quantity, thus resulting in an implicit time averaging. While technology has been developed to push sampling resolution down to sub-millimetre scale [Sneed et al., 2015] [where the previous sampling resolution was $\approx$ 1 cm Bigler et al., 2011] these appear to still be novel techniques and have yet to be implemented on the scale of an entire ice core record.

Marine sediment cores operate on similar principles to ice cores, in that the deposition of material(s) over time can be utilized to obtain information about the previous climate via indirect measurements. However, while ice cores record data on the scale of $100,000$ years, sediment cores operate on longer timescales (millions of years), as they are limited by when the ocean shelf is subducted on geological timescales (or limitations in coring technology) rather than internal ice sheet processes. A major advantage is that marine sediment cores can be obtained from a much wider geographic area than ice cores, which are limited to high latitudes and elevations above the ablation zone. Dating of marine sediment cores is less accurate than with ice cores as annual layers are usually not present. Marine core dating often relies on obtaining biological material throughout the core (for sections where carbon-14 dating can be employed) or via a comparison of signal changes which are expected to arise due to changes in the Earth's orbit [Lisiecki and Raymo, 2005, for cores beyond the range of direct dating methods]. For those cores which rely on dating biological material, an age model can be constructed by dating specific layers and making estimates of sedimentation rates, as well as by incorporating other techniques (e.g. referencing tephra [3] layers across other cores). The age model of a given core is one of the main uncertainties of these types of proxy records, as well as the variation in layer thickness due to rates of sedimentation. Again, the issue of discrete sampling arises as a source of uncertainty as in ice cores. Transitions between glacial and interglacial intervals can be determined via visual inspection of the sediment core itself as the composition of the sediment itself changes as a function of climate for some regions, see Fig. 1.1.

[3] Layers of volcanic ash deposited upon the surface. Tephra can generally be attributed to source regions/volcanoes via their composition, from which the scale of the event can be inferred.

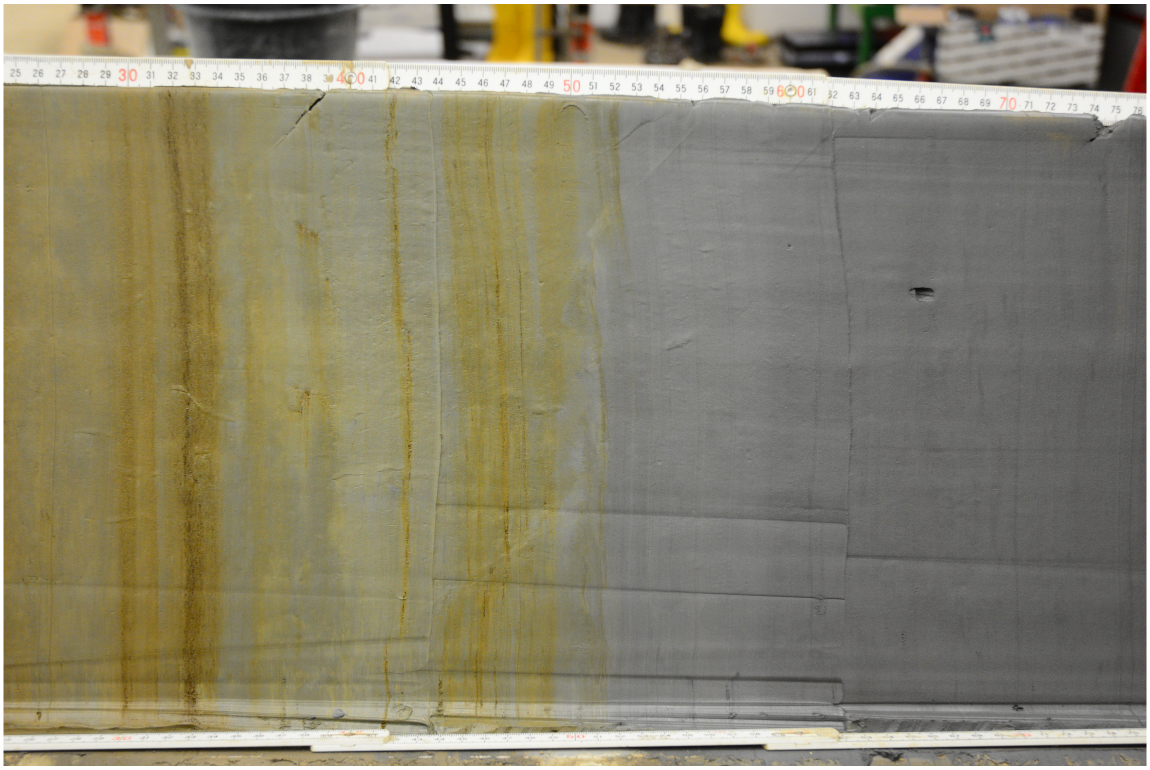

Figure 1.1: A section of the PS115/2_2_51-3 Kastenlot core taken at 80.964947N, 142.472960E. Time advances from right to left (top of the core to the left), with the transition from MIS6 to MIS5 roughly around the 51 cm mark as per the ruler at the top of the image [Stein, 2019]. While the differences between glacial and interglacial intervals is clear, the transition interval itself is not sharp, introducing uncertainty in ascribing the transitional interval to the depth of the core. For reference, of the various sediment cores taken at Lomonosov Ridge, this core has one of the highest resolutions with an average sedimentation rate of ≈ 5.8 cm/1000-years.

1.2.2 Dansgaard-Oeschger Events & Cycles

Dansgaard-Oeschger (DO) events are a form of Centennial- to Millennial scale Climate Variability (CMCV) which are documented in the paleoclimate record. Originally discovered via an examination of δ^{18}O signals in the Greenland ice core records [Dansgaard et al., 1969, 1982, 1984, 1993], they have since been found in paleoclimate proxy records from across the globe [e.g. Wang, 2001, Dokken et al., 2013]. Examples of DO events and cycles in the δ^{18}O records of Greenland ice cores and methane records of Antarctica are shown in Fig. 1.2. These intervals of rapid warming, followed by a gradual return towards stadial conditions terminating with a rapid decrease back to stadial conditions are called DO cycles while the rapid warming interval is the DO event [Gornitz, 2008]. Of interest is the lower rate of occurrence of this form of variability post Last Glacial Maximum (LGM) [4] as can be seen in Fig. 1.3. However, there are similarities between the Younger-Dryas(YD)/Bølling-Allerød(BA) intervals and DO events [Mangerud et al., 2010], which raises the question of whether the same processes of DO events played a role in the YD/BA intervals. This similarity is part of the reason for using the BA/YD transition as a backdrop in Chapter 2.

The DO signal can be seen globally in multiple paleoclimate proxy records, e.g. the speleothem records of Villars Cave in France [Genty et al., 2003] and Moomi Cave in the Indian Ocean [Burns, 2003], where the former records changes in temperature and the latter tracks changes in precipitation. By combining the multitude of available paleoclimate proxies it is possible to construct a global picture of trends

[4] hereafter in this document, LGM is considered to be at $\approx 21,000$ years ago

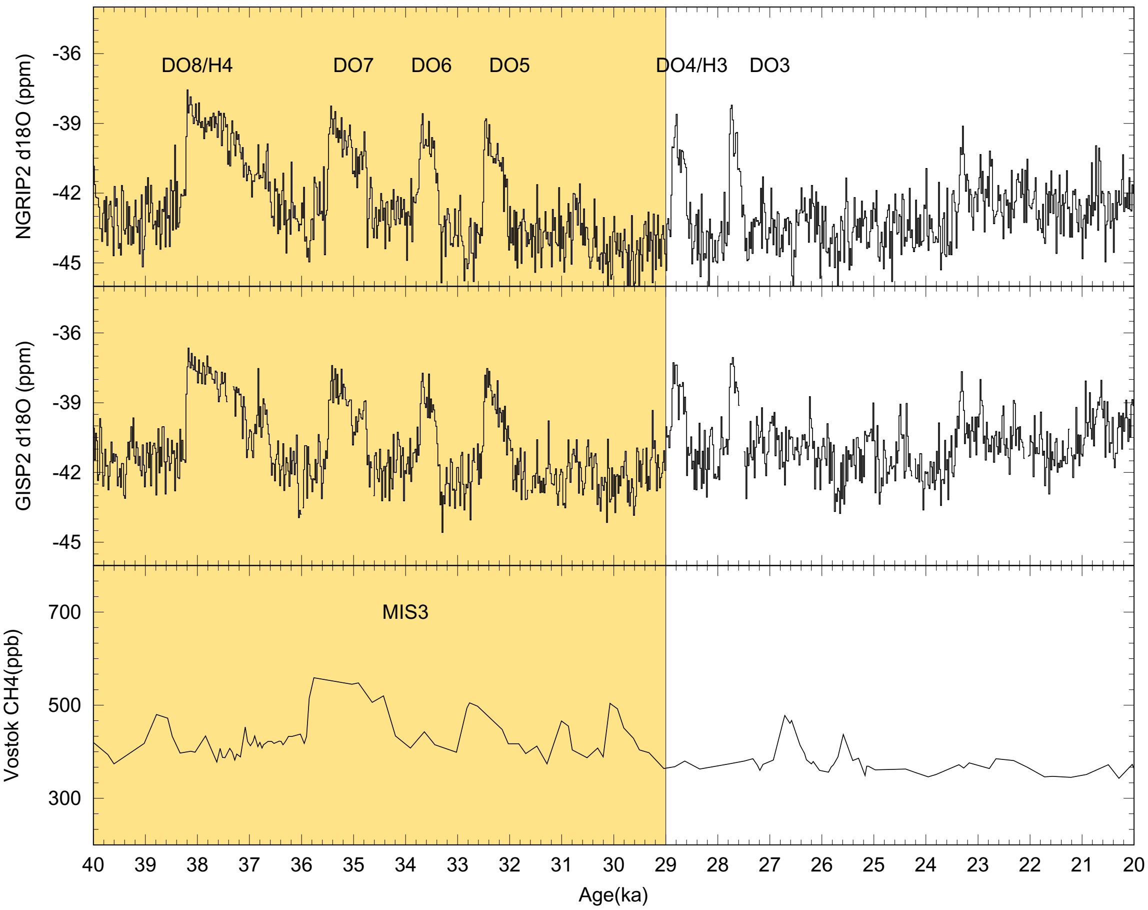

Figure 1.2: Various ice core records showing the signal from DOs in the paleoclimate record. Note the prevalence of the signal in the Greenland Cores (Greenland Ice Core Project, GRIP and NGRIP) relative to the Antarctic (Vostok). The Greenland data shows the relative concentration of δ^{18}O which can be broadly described as a proxy for Greenland temperature on timescales greater than a year. Conversely, the Antarctic cores plotted are showing the concentration of methane. It can be treated as a proxy for changes in the activity of tropical and high-latitude wetland, which is modulated by global temperature and precipitation changes. Thus, these cores reflect these changes. DO events can be clearly seen around $38,000$, $36,000$, $34,000$, and $32,500$ years ago along with several others as denoted. The NGRIP and GRIP core data utilises methods and techniques featured in Andersen et al. [2006], Svensson et al. [2006], Rasmussen et al. [2008] while the Vostok core data utilises those documented in Jouzel et al. [1987].

during the stadial and interstadial phases of a DO cycle. For example, proxies in the tropics and subtropics suggest that the East Asian Monsoon and the South American Monsoons are anti-phased during many of these glacial-interval, millennial-scale climate events [Wang et al., 2006, Voelker, 2002, Corrick et al., 2020]. Equator-ward shifts of the Southern Hemisphere westerly wind belt during the stadial interval are inferred from paleoclimate proxies[Lamy et al., 2000]. In Antarctica, a cooling trend during the interstadial interval and a warming trend during the stadial interval are observed (anti-phase relative to the Northern hemisphere) [Hinnov et al., 2002].

Several mechanisms have been proposed for the cause of DO cycles and the debate on the causes of DO cycles is still active. I summarise some of the more relevant proposed mechanisms here. One of the initial hypotheses was that DO cycles were driven by oscillations of salt in the North Atlantic mediated by glacial runoff [Broecker et al., 1990, Birchfield and Broecker, 1990]. During stadial intervals, salt build-up in the North Atlantic (driven by evaporation and reduced export of Atlantic water) eventually leads to the crossing of a critical density threshold. This crossing results in the re-invigoration of the Atlantic Thermohaline Circulation (THC) and the start of interstadial conditions. Upon the strengthening of the THC, northward heat transport is enhanced. The latter in turn enhances ice sheet melt, leading to increased freshwater discharge into the North Atlantic. Sea ice likely plays a vital role in these types of transitions, with switching between extensive stadial and reduced interstadial sea ice extents. This is discussed further in Section 1.3.4. Eventually, the enhanced freshwater discharge suppresses deep-water formation (DWF) and THC, leading to a resumption of stadial conditions and a repetition of the cycle.

This 'salt oscillator' mechanism is refined by the modelling work presented by Peltier and Vettoretti [2014], Vettoretti and Peltier [2016], who reproduce large parts of this mechanism using the Community Earth System Model (CESM) configured for last glacial maximum conditions. In the 'salt oscillator' mechanism, CMCV is the result of draw-down and build up of salinity in the Atlantic, moderated by glacial runoff as a result of the warming climate during interstadial intervals. The process of their simulated Centennial- to Millennial-scale Climate Variability (CMCV) largely follows that outlined in Broecker et al. [1990] but they do not require the addition of external freshwater and refine the region of oscillation to between the subpolar and subtropical gyres.

In contrast, a competing mechanism, the 'thermohaline oscillator' which is represented by oscillations of both heat and salinity is demonstrated by Brown and Galbraith [2016]. They achieve CMCV under similar glacial conditions, but find that heat transport to the sites of deep water formation is more important to the reinvigoration of Atlantic Meridional Overturning Circulation (AMOC). Proxy data from the Nordic Seas [Dokken et al., 2013] supports the gradual build-up of heat below a sea ice lid (as in Brown and Galbraith [2016]) as being responsible for the eventual resumption of DWF.

Freshwater plays a role in the thermohaline oscillator hypothesis, where it is responsible for establishing the halocline in the Nordic Seas, which suppresses DWF in the region and helps establish the stadial state. It is noted in both Dokken et al. [2013] and Brown and Galbraith [2016] that while not strictly required, freshwater can enhance these transitions. More details on both the thermohaline and salinity oscillator hypotheses are provided in Chapter 4.

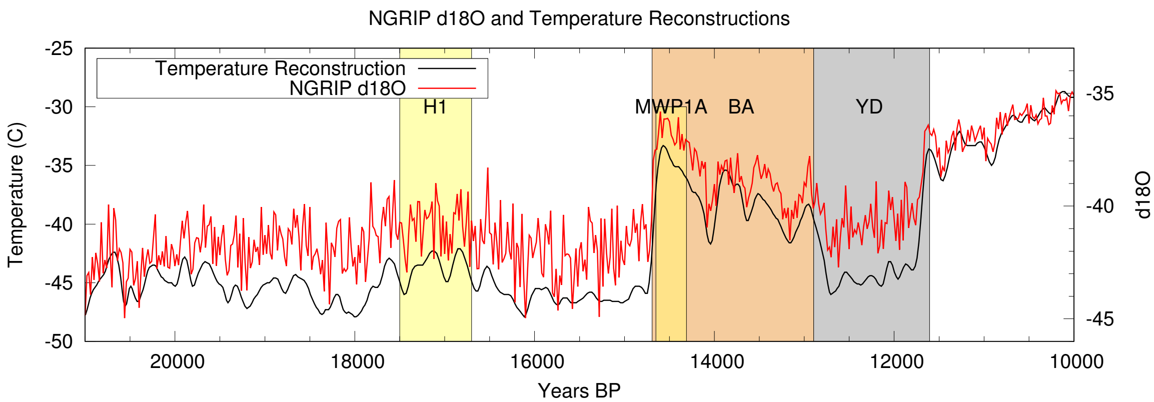

Figure 1.3: δ^{18}O timeseries from the NGRIP [Andersen et al., 2006, Svensson et al., 2006, Rasmussen et al., 2008] core from LGM into the Holocene with an accompanying temperature reconstruction [Kindler et al., 2014]. Highlighted are some of the millennial-scale, rapid, climate-change events: H1 being Heinrich Event 1, MWP1A being meltwater pulse 1A and YD being the Younger Dryas interval.

1.2.3 Meltwater Pulse 1A

Meltwater Pulse 1A (MWP1A) is a rapid increase in relative[5] sea level of $8.6-14.6$ m in < 500 years, which occurred from $14,650 - 14,310$ years ago [Deschamps et al., 2012, Liu et al., 2015] and is coincident with the onset of the Bølling-Allerød warm interval, this interval and the associated Relative Sea Level (RSL) rise is shown in Fig. 1.4. In section 1.2.2 the idea was introduced that freshwater added into the Nordic Seas can suppress DWF and initiate the stadial conditions of DO events. As such, it is unclear why despite a large rate of glacial runoff into the world's oceans, there was not a coincident sudden and extreme cooling event associated with

[5]Relative to present day

MWP1A. The sudden cooling event nearest in time to MWP1A is the Younger Dryas interval, which occurs more than 1000 years later. During the MWP1A interval, it is inferred that rate of glacial runoff entering the oceans exceeded 5 dSv[6] for an interval of several hundred years [Deschamps et al., 2012]. At present, the source(s) of this glacial runoff and the mechanism behind it remains uncertain. Recent studies favour contributions from the Northern Hemisphere [Tarasov et al., 2012, Gregoire et al., 2016, Brendryen et al., 2020]. Gregoire et al. [2016] finds that the North American ice sheets contribute between $3 - 4$ m and that the collapse of the saddle between the Laurentide and Cordilleran ice sheets increases this contribution to $5 - 6$ m. Comparatively, Tarasov et al. [2012] favour a greater contribution at 11.65 ± 1.6 m over a 500 year period.

Similarly, Brendryen et al. [2020] indicate a contribution from the Eurasian ice sheet during this interval that contributes 2 dSv directly to the Nordic Seas region. However, these results are at odds with the continued Bølling-Allerød warming. The flux rate provided by Brendryen et al. [2020] (and supported by Lin et al. [2021]), has been shown to be sufficient to suppress AMOC when introduced into the Nordic Seas in multiple studies under varying background climate conditions [Roche et al., 2009]. As such, it is apparent that there is a mis-match between inferred relative sea level changes due to glacial runoff (and thus associated freshwater fluxes) and the expected climate response. Barring a significant error in current inferences of MWP1A fluxes, this mismatch represents a major challenge to our understanding of how freshwater can affect the climate system. Aspects of this mis-match are explored

[6] $\mathrm{dSv} = 100{,}000\ \mathrm{m^3/s}$

in Chapter 2 of this thesis.

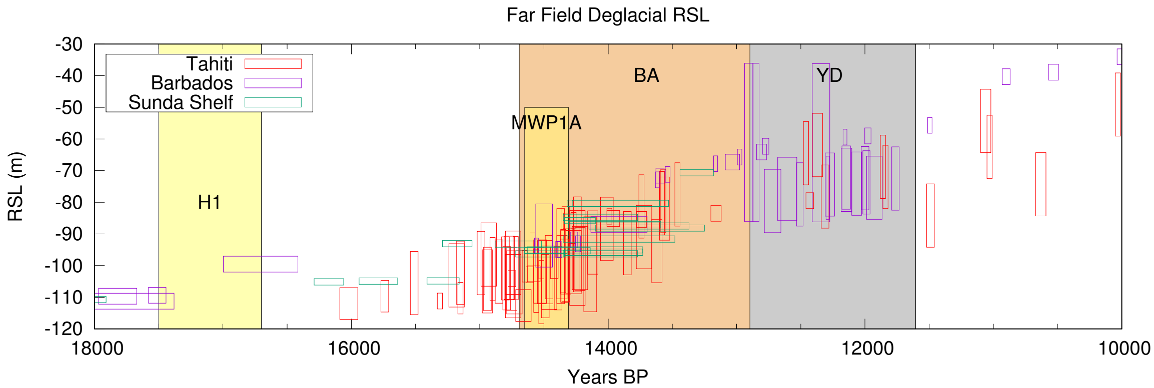

Figure 1.4: Relative sea level records from far-field data locations. Far-field RSL is considered to closely represent changes in eustatic sea level (i.e. how much sea level changes assuming a uniform distribution of water).

1.2.4 Younger Dryas

The YD was a climate reversal during the last deglaciation that approximately spanned $12,900$ to $11,600$ years ago [Bakke et al., 2009]. During this interval, proxy records indicate that the deglacial climate briefly and suddenly reverted to a near-glacial state, this reversion is shown in Fig. 1.3. This sudden reversal was exceptionally apparent in Northwestern and Central Europe, with decreases in regional temperatures of $20 - 30\ ^{\circ}$ C below present day [Isarin et al., 1998]. It was this large difference that helped to provide the name for this stadial interval, as it was spikes in *Dryas Octopetala* pollen which highlighted this interval in the paleoclimate record [Jessen, 1935, Mangerud et al., 1974].

While cold European temperatures were what helped define the YD, it has many other climatic features and has a climate signature that crosses the hemispheres. Using $^{231}\mathbf{Pa}/^{230}\mathbf{Th}$ ratios as a proxy for AMOC[7] strength, McManus et al. [2004] has provided evidence for a decrease in overturning during both the YD and Heinrich Event (HE) [8] 1. Proxy data analysis from Wang [2001] indicates a gradual decrease in the strength of the East Asian Monsoon during the YD, with a sharp return in strength at the end of the YD. The results of Wang [2001] compare well with those of the GISP2 record [Grootes and Stuiver, 1997, Stuiver et al., 1995, Meese et al., 1994, Steig et al., 1994, Grootes et al., 1993], which show a comparable δ^{18}O signal representative of a decrease in temperature over the same duration. Similarly, speleothem records examined in Wang et al. [2004] show a change in precipitation patterns in Brazil. They attribute these changes to massive and rapid changes in oceanic and atmospheric circulation patterns. In summary, paleo records indicate that this climate event, generally associated with freshwater release into the North Atlantic, has a multi-continent and cross-hemisphere scale signal.

1.3 Climate System Modelling in Glacial (115,000 to 7000 years ago) Contexts

Past Results and Key Issues

Here I provide a contextual summary of relevant research related to the subsequent chapters. The discussion begins by examining forcings to the climate system, namely

[7] The large-scale thermohaline and wind-driven overturning of heat and salt in the North Atlantic. The AMOC is responsible for large amounts of northward heat transport, and relatively strong AMOC states are associated with warm North American and European climate conditions while weak AMOC states are associated with glacial climate conditions for these same regions.

[8] Heinrich events are a feature of some of the coldest intervals between DO events and are defined by a large purging of icebergs from the North American ice sheets into the North Atlantic.

freshwater, ice sheets, and greenhouse gasses. Finally, the idea of the ‘Sea Ice Switch’ is introduced, primarily in the context of Dansgaard-Oeschger events.

The role of freshwater in climate change is a common thread throughout the thesis and frequently considered in subsequent chapters. In Section 1.3.1 I provide a brief overview of the range of experiments which have been conducted examining the role of freshwater and the climate system. Similarly, given previous work examining DO events generally does not utilize a consistent ice sheet configuration, effects of these differences are discussed next in Section 1.3.2. One of the primary means by which differences in ice sheets affect the global climate are through changes in atmospheric circulation, which subsequently result in changes to the oceanic circulation, so I expand upon this feature in particular. In Chapter 4, we explore a plausible range of pCO_2 values which occurred during the MIS3 interval, so some of the connections between changes in pCO_2 and the climate system are discussed here in Section 1.3.3.

These concepts and ideas are generally discussed in Chapters 2-4. However, the introduction in each chapter is necessarily limited by the format of a scientific publication. As such, this material is expanded upon here for the non-specialist, along with a review of the body of work in this subject.

1.3.1 Freshwater Forcing & Hosing Experiments

Rapid climate fluctuations during the last deglaciation like the initiation of the YD and HE1 have classically been attributed to changes in the strength of the AMOC [Manabe and Stouffer, 1999, Peltier et al., 2006]. The YD in particular has been hypothesized to be triggered by a sudden freshwater event that in combination with an associated re-routing of glacial runoff [Tarasov and Peltier, 2006, Teller, 2012] resulted in a sudden change in AMOC. The changes in AMOC strength are often attributed to the potential multi-stable nature of the AMOC [Rahmstorf, 2002]. This was first documented in Stommel [1961], through the use of an analytical box model, in which it was demonstrated that the AMOC has the potential for two stable flow regimes. Other abrupt climate events, such as stadial transitions during DO events, have been similarly thought to be initiated by freshwater perturbations.

Table 1.1 reveals that freshwater injections as a source of rapid climate change, among other paleoclimate phenomena, have been extensively investigated by numerical modelling. This range of experiments was initiated by studies such as Bryan [1986] and Manabe and Stouffer [1997], the latter of which can be considered the prototypical hosing experiment using a coupled ocean-atmosphere model. The structure of a typical 'hosing' experiment involves the injection of freshwater on the order of 1 to 100 dSv for a duration of 1 to 1000 years in a band across the North Atlantic between 50° N to 70° N. Some investigations will use a band slightly further south to better overlap with the Ruddiman Belt [9]. The Ruddiman Belt is chosen by some studies, as it is inferred that large quantities of icebergs melted in this region, and thus deposited ice-rafted-debris which has been found in sediment cores from the region[Ruddiman, 1977]. Few studies employ regional freshwater discharge distributions such as was done by Roche et al. [2009], instead opting for the simpler 'Hosing' distributions.

Common metrics for quantifying the results of hosing experiments are surface

[9] A region in the North Atlantic where enhanced levels of ice-rafted debris have been found, indicative of the path of icebergs during the last glacial cycle (these regions are shown in Fig. 1.5).

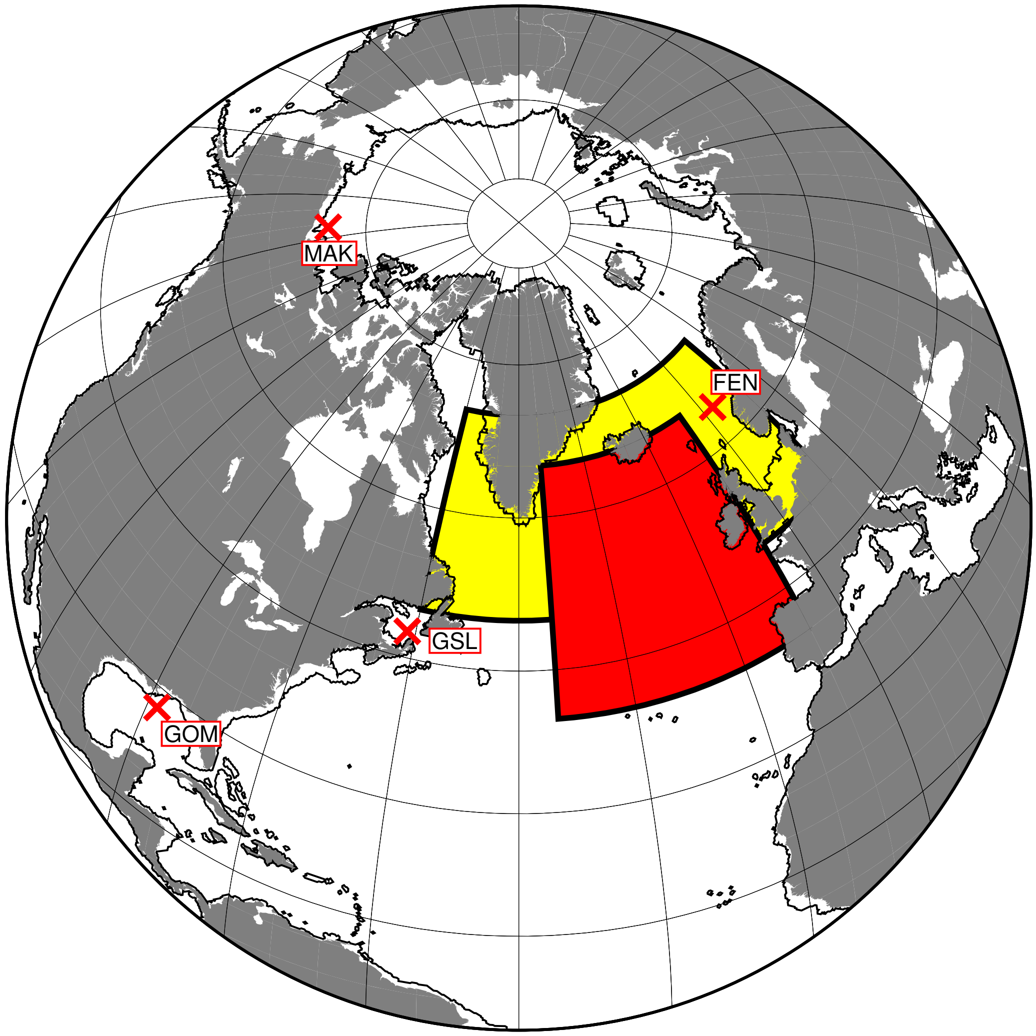

Figure 1.5: Labels and red 'X's indicate glacial runoff outlets or regions explored in this thesis and inferred to be important outlets during the last glacial cycle. MAK is the Mackenzie River, FEN is Fennoscandia, GSL is the Gulf of the St. Lawrence, and GOM is the Gulf of Mexico/Mississippi River. Highlighted regions indicate common freshwater injection bands as used in previous studies. Yellow is the common 50-70N band in the North Atlantic, while red is an approximate 'Ruddiman Belt' as per Ruddiman [1977]. It is worth noting that the extent shown is not necessarily consistent with what all studies use, as longitudinal extent (and in the case of the Ruddiman Belt, latitudinal extent in some cases) varies between studies. Present-day land-masses are shown in light grey, while an intermediate volume ($13,000$ years ago, but comparable to $38,000$ years ago as well) ice-sheet land-sea mask is contoured in black.

temperatures in the Northern Hemisphere along with the strength of the AMOC. However, few of these studies utilise the same metrics aside from overturning strength. Resultingly, comparing such features between studies proves difficult. Summarising the wide range of experimental results presented in Table 1.1, it is seen that every experiment presented here results in a net decrease in overturning strength until at least the end of the freshwater injection. This decrease in overturning is consistent despite the rather large variation in both forcing duration, magnitude, location and net volume into the world's oceans. The largest variation in the results pertain to whether the AMOC recovers and over what timescales it recovers, with some models not resuming normal circulation strength.

Other climate features which are strongly tied to overturning strength, such as sea-ice extent, display sensitivity to the forcing when such information is available. With regards to sea ice this is expected due to two physical connections tied to freshwater forcing: the reduction in Northward heat transport (and thus high-latitude cooling) associated with a reduction in overturning, and the freshening of the ocean surface in regions with sea ice. Both of these features contribute to enhanced sea ice growth. For the former, this is due to the direct cooling of the ocean surface. For the latter, this due to the raising of the freezing point of the ocean surface (the freezing point of freshwater is $\approx 2\ ^{\circ}$ C higher than that seawater when assuming an average salinity of ≈ 35 psu [Doherty and Kester, 1974]). However, sea ice itself plays a role in determining the location of DWF and in centennial- to millennial-scale climate variability, by acting as a barrier between the ocean and the atmosphere [Dokken et al., 2013]. The idea of sea ice exhibiting switching behaviour between two stable or quasi-stable states is explored in Section 1.3.4.

The interpretation of these studies is hampered by at least one of several common shortcomings in experimental designs: the use of simplified injection distributions (coupled with too-coarse resolution), over-large or unrealistic injection fluxes, inconsistent or inappropriate boundary conditions, and treating freshwater as a forcing and not an interactive component of the climate system. Firstly, the use of a 'hosing band' such as the 50-70N or Ruddiman belt regions are likely inaccurate descriptions of where freshwater is routed. Such an approach, with respect to the injection region, ensures that regions of DWF in numerical models are covered with a freshwater cap. This freshwater cap inhibits the formation of deep-water and overturning circulation in the North Atlantic.

Another component of this shortcoming is that the ocean model component of these simulations are too coarse resolution and unable to resolve features, such as boundary currents and mesoscale eddies, known to be important to the transport of freshwater from sites of glacial runoff. As such, the Hosing approach is considered an approximation to where glacial runoff would be eventually deposited. Previous studies [Condron and Winsor, 2012, Hill and Condron, 2014] show that this simplification of the transport of freshwater from regions of glacial runoff is inappropriate. The results of Condron and Winsor [2012] demonstrate that freshwater from the Gulf of St. Lawrence is transported well south of the typical Hosing region. For the Mackenzie River, the freshwater shows some overlap with the Hosing region, but again more freshwater is located further south than the 50-70N region, as highlighted in their salinity anomaly distribution figures. When considering these outlets as a source of freshwater which can initiate rapid climate change, as in the Mackenzie River which is hypothesized to be important in initiating the Younger Dryas [Tarasov and Peltier, 2005, Teller, 2012], this mismatch between where glacial runoff is hypothesized to be transported to (sites of DWF), and the actual proportion which arrives at these locations, and the resulting effect on climate change remains unexplored.

Secondly, some studies tend to use over-large fluxes of freshwater, ranging to upwards of 50 dSv, which is more than a factor of 20 greater than that inferred for the initiation of the Younger Dryas [Tarasov and Peltier, 2006] or for MWP1A [Deschamps et al., 2012][10]. Thirdly, some investigations use inconsistent topography or bathymetry when considering the role of glacial runoff during the deglacial interval, either using a fully glacial environment (i.e. LGM) or a pre-industrial climate. Finally, few studies explore the interactions between freshwater and the climate system (e.g. changing sea ice concentration due to surface freshening), instead focusing on it as a non-interactive component of the climate system and simply a means by which AMOC can be modified. I present a study which directly addresses these shortcomings in Chapter 2. In Chapter 3, I introduce and evaluate a new technique designed as a compromise for eddy parametrizing models.

[10] when considering the $10 - 15$ m increase in eustatic sea level over an interval of ≈ 300 years

Table 1.1: A brief summary of the multitude of freshwater forcing climate modelling experiments with respect to the strength of the AMOC (or THC, experiment depending). Note the rather large variation in both forcing duration, magnitude, location and net volume into the world ocean. Despite the large variations in experimental setup and choice of numerical model, every experiment presented here results in a net decrease in overturning strength until at least the end of the freshwater injection.

Authors	Model Description	Background climate	Forcing Description	Bulk Results	Sva	Eustatic (m)
Bryan [1986]	Primative equation ocean model with simplified geometry, no sea ice, prescribed surface conditions	Present Day	$-1°/_{\circ\circ}$ to $+2°/_{\circ\circ}$ salinity anomaly added to surface layer poleward of 45S/N	Negative salinity anomaly in SH reduces overturning, positive enhances overturning	N/A	N/A
Manabe and Stouffer [1997]	Coupled AOGCM; T15 Atmosphere and 3.7x4.0 ocean; no diurnal; thermodynamic sea ice	Present Day	0.1 Sv freshwater uniformly distributed over 50-70N of the North Atlantic for 500a	Reduction of AMOC to 4Sv from $\approx$ 18Sv	50	4.383
Manabe and Stouffer [1997]	Coupled AOGCM; T15 Atmosphere and 3.7x4.0 ocean; no diurnal; thermodynamic sea ice	Present Day	0.1 Sv uniformly distributed over 20.25-29.25N/52.5-90W over NA for 500a	Reduction of AMOC same as Northern injection but magnitude is $\approx$ 1/5	50	4.383
Manabe and Stouffer [2000]	Coupled AOGCM; T15 Atmosphere and 3.7x4.0 ocean; no diurnal; thermodynamic sea ice	Present Day	0.1 Sv freshwater uniformly distributed over 50-70N of the North Atlantic for 500a	Reduction of AMOC to 4Sv from $\approx$ 18Sv	50	4.383
Manabe and Stouffer [2000]	Coupled AOGCM; T15 Atmosphere and 3.7x4.0 ocean; no diurnal; thermodynamic sea ice	Presnt Day	0.1 Sv uniformly distributed over 20.25-29.25N/52.5-90W over NA for 500a	Reduction of AMOC same as Northern injection but magnitude is $\approx$ 1/5	50	4.383
Stouffer et al. [2006]	Model intercomparison study; see Stouffer et al. [2006]	Present Day	0.1 Sv freshwater uniformly distributed over 50-70N of the North Atlantic for 100a	Multimodel mean shows $\approx$c 30% reduction in THC strength	10	0.8766
Peltier et al. [2006]	NCAR CSM1.4; No information on model configuration provided	Present Day; Closed Bering Strait	0.3Sv for 100a over 50N to 70N latitude	Steadly declining decrease in AMOC strength to minima of $\approx$ 10Sv from $\approx$ 22Sv initial condition; gradual recovery over 200a after forcing ended	30	2.6298

Peltier et al. [2006]	NCAR CSM1.4; No information on model configuration provided	Present Day; Closed Bering Strait	0.3Sv for 100a over Arctic region occupied by the Beaufort Gyre	Same as NA configuration	30	2.6298
Stouffer et al. [2006]	Model intercomparison study; see Stouffer et al. [2006]		1 Sv freshwater uniformly distributed over 50-70N of the North Atlantic for 100a	THC rapdily decreases in strength and almost disappears in some ensemble members	100	8.766
Peltier et al. [2006]	NCAR CSM1.4; No information on model configuration provided	Present Day; Closed Bering Strait	1Sv for 100a over 50N to 70N latitude	Steadly declining decrease in AMOC strength to minima of $\approx$ 4Sv from $\approx$ 22Sv initial condition; gradual recovery over 200a after forcing ended	100	8.766
Peltier et al. [2006]	NCAR CSM1.4; No information on model configuration provided	Present Day; Closed Bering Strait	1Sv for 100a over Arctic region occupied by the Beaufort Gyre	Same as NA configuration	100	8.766
Vettoretti et al. [2009]	NCAR CSM1.4; T31 Atmosphere, 18 levels, $\approx 3.6°$ Ocean, thermodynamic sea ice	Preindustrial	0.1, 0.2, 0.3, 1.0 Sv for 100a, 50-70N region	AMOC decline not linear with strength of hosing, 0.1 & 0.2Sv forcings do not result in GISP2 SAT decrease	100	0.876, 1.752, 2.628, 8.766
Otto-Bliesner and Brady [2010]	CCSM3; T42 atmosphere; 1x1 degree ocean model, dynamic thermodynamic sea ice	LGM	0.1 Sv for 100a between 50-70N	Steady decline in AMOC strength over entire duration of forcing. Reduction of 29%	1	0.08766 [11]
Otto-Bliesner and Brady [2010]	CCSM3; T42 atmosphere; 1x1 degree ocean model, dynamic thermodynamic sea ice	LGM	0.1 Sv for 500a between 50-70N	Steady decline in AMOC strength over entire duration of forcing. Reduction of 40%	50	4.383 [11]

[11] Percent averaged over last 20 years of the freshwater hosing

Otto-Bliesner and Brady [2010]	CCSM3; T42 atmosphere; 1x1 degree ocean model, dynamic thermodynamic sea ice	LGM	0.25 Sv for 100a between 50-70N	Steady decline in AMOC strength over entire duration of forcing. Reduction of 50%	25	2.1915 [11]
Otto-Bliesner and Brady [2010]	CCSM3; T42 atmosphere; 1x1 degree ocean model, dynamic thermodynamic sea ice	LGM	0.28 Sv for 100a in the Gulf of Mexico	Steady decline in AMOC strength over entire duration of forcing. Reduction of 35%	28	2.45448 [11]
Otto-Bliesner and Brady [2010]	CCSM3; T42 atmosphere; 1x1 degree ocean model, dynamic thermodynamic sea ice	LGM	0.5 Sv for 100a between 50-70N	Steady decline in AMOC strength over entire duration of forcing. Reduction of 70%	50	4.383 [11]
Otto-Bliesner and Brady [2010]	CCSM3; T42 atmosphere; 1x1 degree ocean model, dynamic thermodynamic sea ice	LGM	0.5 Sv for 100a in the Gulf of Mexico	Steady decline in AMOC strength over entire duration of forcing. Reduction of 51%	50	4.383 [11]
Otto-Bliesner and Brady [2010]	CCSM3; T42 atmosphere; 1x1 degree ocean model, dynamic thermodynamic sea ice	LGM	1 Sv for 100a between 50-70N	Steady decline in AMOC strength over entire duration of forcing. Reduction of 81%	100	8.766
Condron and Winsor [2012]	MITGCM; 1/6x1/6 PE ocean, forced atmosphere (ERA40)	Present Day	5Sv at Mackenzie River outlet for 1a	Steady decline in AMOC strength over entire duration of simulation (25a); ending strength of $\approx$ 12.5Sv	5	0.4383
Condron and Winsor [2012]	MITGCM; 1/6x1/6 PE ocean, forced atmosphere (ERA40)	Present Day; Closed Canadian Archepeligo	5Sv at Mackenzie River outlet for 1a	Steady decline in AMOC strength over entire duration of simulation (25a); ending strength of $\approx$ 11.5Sv	5	0.4383
Condron and Winsor [2012]	MITGCM; 1/6x1/6 PE ocean, forced atmosphere (ERA40)	Present Day	5Sv at St. Lawrence outlet for 1a	Steady decline in AMOC strength over entire duration of simulation (25a); ending strength of $\approx$ 14Sv	5	0.4383

Bethke et al. [2012]	MIT IGSM2; 4x4 PE ocean, 4x4 zonally average statistical-dynamical atmosphere; thermodynamic sea ice	9kaBP	Freshwater flux over 20-50N varied in time from -0.250Sv to 0.250Sv	Hysteresis observed with rapid transistions at 0.125Sv and -0.050Sv. Minimum of ≈ 6Sv	N/A	N/A[12]
Bethke et al. [2012]	MIT IGSM2; 4x4 PE ocean, 4x4 zonally average statistical-dynamical atmosphere; thermodynamic sea ice	LGM	Freshwater flux over 20-50N varied in time from -0.250Sv to 0.250Sv	Hysteresis observed with rapid transistions at 0.260Sv and -0.050Sv. Minimum of ≈ 4Sv	N/A	N/A
Lohmann et al. [2016]	ECHAM5 T31 atmosphere, MPIOM 3x3 ocean, JSBACH surface model	LGM	0.2Sv for 150a in Southern Ocean; 52 - 62S, 40W - 62W	No significant change in AMOC strength	30	2.6298
Lohmann et al. [2016]	ECHAM5 T31 atmosphere, MPIOM 3x3 ocean, JSBACH surface model	LGM	0.2Sv for 150a over 40N-55N	Rapid reduction of AMOC to ∼5Sv from average of ≈ 18Sv; recovery after forcing ends	30	2.6298
Brown and Galbraith [2016]	CM2Mc coupled Ocean-Atmosphere, 3 degree ocean and amosphere components	PI, LGM, variable orbital	0.2Sv for 1000a over 40N-60N, 60-12W	Hosing results in AMOC reduction regardless of background configuration, resembles unforced oscillations but with faster changes	200	17

[12] Wide selection of results and boundary conditions presented; only key relevant studies are summarized here.

1.3.2 Ice Sheets

Another of the primary changes, and thus forcings, which may be important for CMCV during the MIS3 interval are changes to the continental-scale ice sheets. Relative to the volume of literature covering the response of numerical models to freshwater forcing, few studies have examined the isolated effects of varied ice sheets in a glacial climate.

The ice sheets that covered significant parts of the high Northern latitudes during the glacial era imposed a large change in surface topography and other surface characteristics relative to present day (present day vs. LGM topography as per the reconstruction from Tarasov et al. [2012] are shown in Fig. 1.6). Recent investigations have focused upon the orographic effects on atmospheric circulation and the consequences for glacial climate [Ullman et al., 2014, Zhang et al., 2014, Löfverström et al., 2014, Gong et al., 2015, Andres and Tarasov, 2019]. Changes in ice sheet orography can induce large-scale changes in the North Atlantic ocean circulation [Gong et al., 2015, Muglia and Schmittner, 2015], as the strength of ocean circulation is directly related to the wind stress at the ocean surface, as well as rapid changes in glacial climate [Zhang et al., 2014, Lohmann et al., 2016].

Results from the Paleoclimate Modeling Intercomparison Project (PMIP) have been inconclusive with respect to both the strength of the glacial AMOC and the AMOC strength difference between preindustrial and glacial intervals [Kageyama et al., 2021]. In PMIP3, it was consistently found that the glacial AMOC was both stronger and deeper [Muglia and Schmittner, 2015] by comparison to the preindustrial AMOC. The differences in this feature between PMIP2 and PMIP3 have been explored by Muglia and Schmittner [2015]. They utilised the output wind stress fields from PMIP 2 and 3 to force the uVic OGCM, so as to perform various sensitivity tests and isolate the orographic impact. They obtained results that led them to conclude that wind stress is a primary driver of AMOC strength. When their model was forced with the fields from the PMIP3 ensemble, they obtained an AMOC behaviour that was consistent with that of the OGCMs originally used: a net increase in AMOC strength along with an increase in depth. When they forced their model using the wind stress fields from the PMIP2 ensemble, the sign of the change in AMOC strength was variable between ensemble members, just as was found in the original PMIP2 ensemble. Gong et al. [2015] simulated several paleoclimate states using an AOGCM and obtained results which align with those of Muglia and Schmittner [2015].

The growth and decay of continental-scale ice sheets also have several other relevant impacts, such as changes to the albedo over land and changes in the relative sea level and ocean gateways. Ice and snow generally has a significantly higher albedo relative to deglaciated land [e.g. ranging from $\approx 40\%$ to $\approx 80\%$ reflection for dirty and pure snow and 20% for grass, Willeit and Ganopolski, 2018, Betts and Ball, 1997]. An increased albedo results in localized cooling, with feedbacks such as increased snowfall.

Changes in relative sea level and ice sheet volumes are strongly coupled. On the time scale of the last glacial cycle, water is either on land as snow, ice, and liquid water (lakes and inland seas), or in the oceans. The changes in relative sea level due to the presence of the North American and Fennoscandian ice sheets result in changes to ocean gateways. One such gateway inferred to be significant is the Bering Strait. Simulations of glacial oceans indicate that closing the Bering Strait can affect ocean circulation and intensify AMOC [Hu et al., 2007, 2012, 2015]. As previously discussed, changes in AMOC in turn alter heat transport from lower-latitudes to higher latitudes and as such may be significant for CMCV such as DO events.

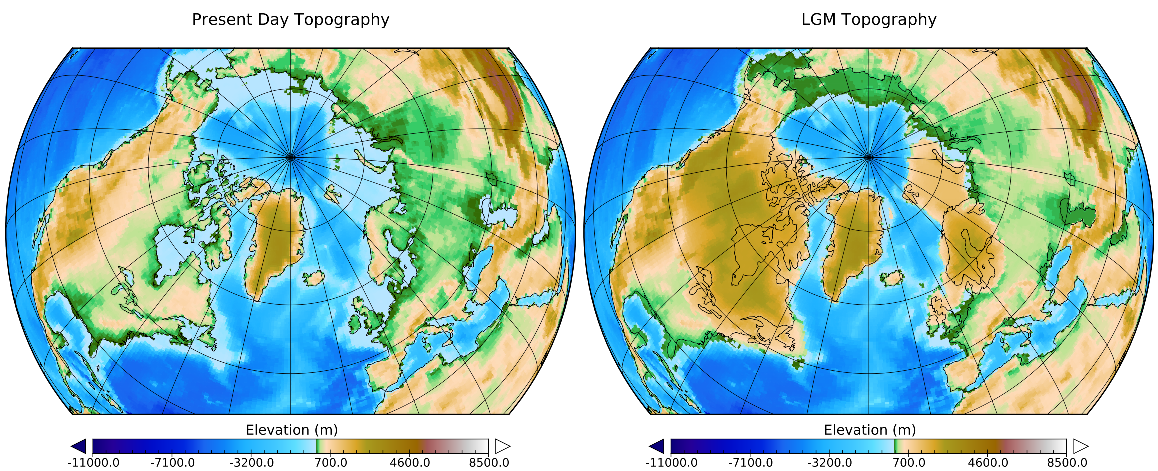

Figure 1.6: Northern hemisphere topography at the last glacial maximum and present day as given by the global calibration using the methodology presented in Tarasov et al. [2012]. Note that ice shelves are not shown in these plots. As well, the solid Earth response, geoidal deflection and relative sea level change is included.

1.3.3 Greenhouse Gases

Changes in well-mixed Greenhouse Gasses (GHGs) are generally discussed in the context of climate modelling experiments with regards to their changes in radiative forcing. Radiative forcing is the effective change in net energy flux through the Earth's atmosphere. In the context of my work, this change is due to changes in greenhouse gas concentrations. This forcing arises due to different greenhouse gasses interacting with radiation to absorb and re-emit different wavelengths of light. Incoming solar radiation is referred to as 'short wavelength' radiation, which does not largely interact with GHGs, while radiation emitted from the surface of the Earth is 'long wavelength' radiation and is mostly absorbed and retransmitted by GHGs.

In this thesis, the impact of pCO_2 concentration changes is examined primarily in the context of CMCV during MIS3. During this interval, it varies from as much as ≈ 225 ppmv to ≈ 185 ppmv [Bereiter et al., 2015]. This results in a ≈ 1 W/ m^2 [Etminan et al., 2016] difference between the lower and upper values, and represents just under a third of the increase between present-day and the pre-industrial concentrations due to anthropogenic pCO_2 emission.

Greenhouse gasses have varied over glacial intervals as a result of various processes in the climate system, see Fig. 1.7. The underlying mechanisms behind these changes are complex and beyond the scope of this thesis. Also, the tools used here do not incorporate these processes directly nor are transient changes in greenhouse gas concentrations evaluated. The radiative forcing changes are accounted for via configuration parameters in the utilized coupled climate model, whose radiation scheme incorporates this effect. In our simulations, we specify only CH_4, N_2O, and CO_2, and only use prescribed CO_2 concentration as a sensitivity parameter.

While pCO_2 alone does not directly influence the climate system, the effective increase in radiative forcing is amplified via the non-linear nature of the climate system. An example of such an amplification is via small changes in sea ice driven by minor warming as a result of pCO_2 changes. Increased pCO_2 concentrations lead to a reduction in sea ice extent via an increased effective radiative forcing (i.e. warming from the greenhouse effect). Under glacial conditions with subdued Atlantic meridional overturning, sea ice is generally extensive and covers sites of contemporary DWF in the Nordic Seas. A decrease in sea ice area and the associated retreat of the sea ice edge in the North Atlantic or Nordic Seas can result in greater heat release from the ocean and increased density at sites of DWF, and resultingly a re-invigoration or enhancement of overturning. This enhanced overturning leads to increased heat transport from lower latitudes to higher latitudes, resulting in a warming at higher latitudes, until a new equilibrium is reached. It is because of these types of feedbacks, and previous work (e.g. Brown and Galbraith [2016]) examining CMCV and pCO_2, that relationships between pCO_2 and the pacing of CMCV are anticipated. An understanding of these types of relationships are key to understanding future climate change, as it is projected that the Arctic ocean will likely be seasonally sea-ice free by ≈ 2050 under the pCO_2 intense RCP8.5 scenario [Collins et al., 2013].

Since these greenhouse gasses are considered well mixed, the effective change in radiative forcing is globally uniform. As well, unlike other potential mechanisms of affecting the energy balance of the Earth, such as varying orbital parameters[13], pCO_2 changes do not have a significant seasonal component. However, how this increase in radiative forcing due to pCO_2 interacts with the climate system is not uniform. Here again sea ice plays an important role in the climate system, as it has

[13] I note that changes in insolation which arise from changes in Earth's orbit are significant. However, an examination of this aspect is beyond the scope of this project. Additional details are provided in Section 1.4, Chapter 4, and expanded in 'Future Work'.

a much higher albedo relative to sea water, which results in an increased reflection of radiation [Wendler et al., 2004] and reduced localized warming from radiation. As such, under otherwise identical boundary conditions (i.e. orbital parameters, land-sea mask, land-ice configuration) a sea ice configuration which is extensive will reflect significantly more radiation than one which has less sea ice area. Thus sea ice changes can have an important role in the global climate system; this is discussed further in Section 1.3.4.

1.3.4 Sea Ice and the Switch Hypothesis

Sea-ice has the capacity to hold a central role in mechanisms of CMCV for numerous reasons. First and foremost, sea ice acts as an effective barrier to interactions between the ocean surface layer and the base of the atmosphere. As such, sea ice extent can exert major effects upon the climate system by moderating energy and momentum transfer between the ocean and the atmosphere. Due to these features, it has been proposed that CMCV, and longer timescale variability, can be explained in terms of a sea-ice switch [Gildor and Tziperman, 2003]. A conceptual model which arises from examination of a Nordic Sea sediment core invokes the growth and decay of sea ice as a key contributor to the storage and release of heat in the Nordic Seas during Dansgaard-Oeschger cycles [Dokken et al., 2013].

Two features of sea ice are strong indicators for the capacity for switch-like behaviour. First, in the presence of adjacent sea ice, the ocean surface is held close to the freezing point. Thus the SST is almost static in the presence of sea ice and can have much larger variability without. Resultingly, even minor changes in local tem-

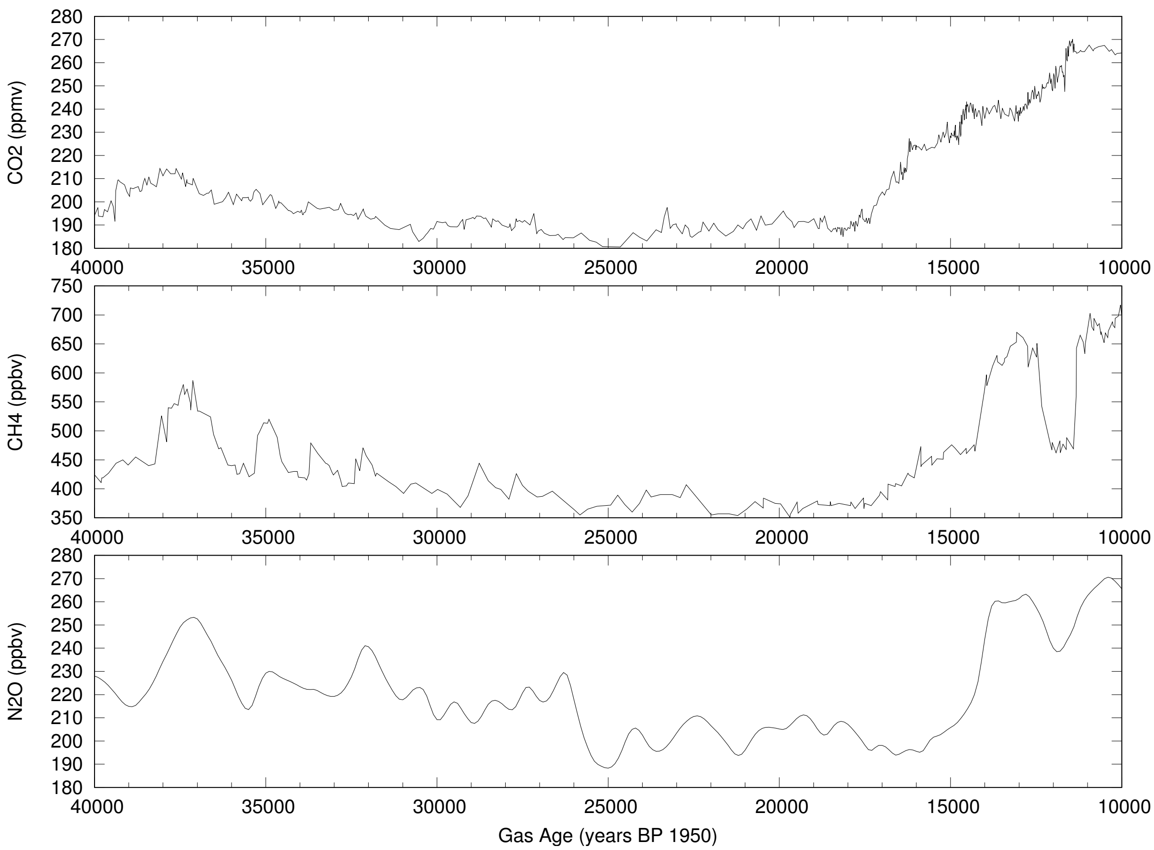

Figure 1.7: Greenhouse gas concentrations during the last glacial cycle. pCO_2, N2O, and CH4 are obtained from Bereiter et al. [2015], Schilt et al. [2010], Loulergue et al. [2008] respectively. These values are obtained from ice core records, where gasses are directly measured from air trapped within the ice itself.

peratures can lead to an expansion or retreat of sea ice. Second, the inherent change of sea ice from a solid (where it acts like a barrier) to liquid form, or the inverse, under appropriate conditions provides a mechanism for switch-like interactions between the atmosphere and ocean moderated by sea ice. Both of these features provide support for switch-like behaviour as sea ice extent rapidly expands and contracts in response to various components of the climate system [Gildor and Tziperman, 2003]. A key underpinning of the sea ice switch mechanisms for centennial- to millennial-scale climate variability is the presence of multiple sea ice configurations under the same land ice configuration [Ashkenazy et al., 2013, Gildor and Tziperman, 2003].

Studies examining DO-like CMCV [Klockmann et al., 2020, e.g.] provide the most conclusive support for this aspect of the sea-ice switch hypothesis. Generally, studies examining DO-like variability do not utilize transient ice sheets, and some achieve two different sea ice configurations [e.g. Klockmann et al., 2020]). The more extensive sea ice configuration corresponds with stadial/AMOC-weak conditions, while less extensive sea ice corresponds with the warmer interstadial/AMOC-strong intervals. However, of the various studies examining DO-like variability discussed in section 1.2.2, none explicitly invoke the sea-ice switch mechanism. This hypothesis, and the role of sea ice in general, is explored further in the context of CMCV in Chapter 4.

1.4 Thesis Overview and Research Questions

Current modelling efforts have, as of yet, been unable to replicate the full range of inferred CMCV over large spatial scales. As discussed, these events take place in a background of an evolving glacial landscape and changing radiative forcings. The potentially relevant key forcings which evolve on CMCV timescales are the following: the radiative forcing effects of changing orbital configurations and greenhouse gasses, orographic and land-surface changes arising from continental-scale ice sheets, and freshwater discharge into the ocean. However, an examination of all of these features is beyond the scope of a reasonable project, so the focus has been refined. To winnow these primary forcings, we can consider those which help to broaden the applicability of the work to both contemporary and paleo-climate contexts, and those that will simplify analysis.

While the future of the Greenland ice sheet under anthropogenic forcing is uncertain, changes in upper elevations (which affect ocean circulation via wind-stress) over the next century are inferred to be small, of the $O(10\text{ m})$ or $\approx 0.3\%$ of ice sheet thickness when considering the interior of the ice sheet [Vizcaino et al., 2015]. Similarly, orbitally derived variations in insolation are significant only on millennial time-scales, with changes resulting in only $\approx -0.003\text{ W/m}^2$ shift in global-mean, annually averaged insolation over the next century (or $\approx 0.175\text{ W/m}^2$ at 65° N, July monthly mean) [Laskar et al., 2004]. Comparatively, pCO_2 has increased by 150% since the pre-industrial interval [representing an increase of $\approx 2.2\text{W/m}^2$, Etminan et al., 2016] and ice melt (from all sources) may contribute to sea level rise as much as steric changes by the end of the 21st century [Love et al., 2016]. Of the primary forcings to be considered, both pCO_2 and freshwater are the most relevant for understanding future climate change.

When considering the domain of each of these forcings, they can be broadly categorized as primarily atmospheric and surface forcings (orbital, GHG, and ice sheets) or oceanic (freshwater via glacial runoff). Orbital changes result in spatially and temporally (when considering sub-annual time-scales) variable changes to insolation. While these sub-annual changes may be important to CMCV [Zhang, 2021], evaluating pCO_2, which is spatially uniform and in contemporary paleoclimate modelling does not vary on sub-annual time-scales, makes for a more straight-forward initial approach. Changes associated with ice sheets are multifaceted and would require disentangling the effects of orography, albedo, surface roughness, and other land-surface effects, all while in the context of a weakly constrained ice sheet distribution during MIS3 (as regards topography and areal extent). However, ice sheet volume is constrained via relative sea-level records and ocean sediment cores, and from these components we can infer glacial runoff and gateway changes. Being able to constrain ice sheet volume through time also allows for an examination of the impact of freshwater fluxes, as well as the impact of one gateway inferred to be important for glacial climates (the Bering Strait). In particular, we can use this information to examine recent CMCV with outstanding issues in understanding such as Meltwater Pulse 1A and the Younger-Dryas. Given the above, I chose pCO_2 and freshwater as the forcings to be tested during two intervals of the last glacial cycle with notable CMCV: the Bølling-Allerød-Younger Dryas transition interval, and the MIS3 interval.

Due to the restrictions of paleoclimate modelling on centennial to millennial timescales, features vital to the representation of freshwater transport in the ocean, eg. mesoscale eddies and boundary currents, are not explicitly resolved in the coupled climate model and are instead parametrized. As discussed in Section 1.3.1, it has been common practice to attempt to bypass these limitations by instead introducing freshwater directly to sites of deep water formation in the North Atlantic/Nordic Seas (also known as 'Hosing'), generally via the $50-70°$ N region. However, this simplification is likely inappropriate, as was demonstrated by Condron and Winsor [2012]. One key enigma in the context of the role of freshwater forcing is the expected climate response to freshwater entering the Atlantic and Arctic Oceans during MWP1A. Despite the large change in relative sea level during MWP1A, no sudden cooling took place but instead the next cooling interval, the YD, took place more than a millennium later. As such, a first step is ensuring that freshwater forcing and transports are appropriately represented in coupled climate model simulations.

To date, few studies examining CMCV during the MIS3 interval have employed consistent MIS3 boundary conditions. Previous studies examining CMCV during this interval generally utilize either full glacial maximum, pre-industrial, or blended, boundary conditions. Since CMCV during the last glacial cycle appears to be bounded by minimum and maximum ice sheet volumes there are likely mean-state dependences with respect to causal mechanisms of CMCV. How freshwater and pCO_2 interacts with and affects CMCV under boundary conditions consistent with MIS3 (i.e. GHGs, ice sheet volume, orbital configuration) remains unexplored.

With the above considerations, I have chosen the following specific questions:

- What proportion of freshwater is transported to sites of deep-water formation when it originates from one of several outlets of glacial runoff and small-scale processes of freshwater transport are resolved? How different is this from the 'Hosing' simplification and what are the implications for understanding events like the Younger Dryas and Meltwater Pulse 1A?

- How can I utilise model output from high-resolution freshwater injection experiments to compensate for the coarse ocean-model resolution required for paleo-timescale experiments? How do the modelled results affect the inferences made about centennial- to millennial-scale climate change due to freshwater forcing?

- What are the roles of freshwater and pCO_2 on changing stadial and interstadial durations of Dansgaard-Oeschger events during MIS3? What part of the range of variability seen in the paleoclimate record can be attributed to changes in these forcings?

In Chapter 2, in the context of MWP1A and the YD, I examine the relative freshening of key locations in the North Atlantic and adjacent ocean regions by utilizing an ocean model in a configuration which explicitly resolves these features while using glacial boundary conditions. In Chapter 3, I examine how much of a mis-match in freshwater distributions arises from the practice of freshwater Hosing, and the subsequent biases in inferring the role of freshwater in glacial climate introduced by use of this simplification. I also develop the novel 'freshwater fingerprint' method which captures some aspects of the eddy-permitting ocean model in eddy-parametrizing ocean models. This method will be of great benefit to climate modelling investigations where high-resolution modelling is not always appropriate or feasible, due to the great computational expense or long integration times required. In Chapter 4 I combine the techniques and understanding garnered in Chapters 2 and 3 to examine the sensitivity of DO events during MIS3 to glacial runoff and pCO_2, and to explore what range of variability in stadial/interstadial durations observed during MIS3 can be explained in response to these varying forcings. In Chapter 5 I provide an overall conclusion to the thesis and present future work that stems from this research.

This thesis is written in the 'Manuscript' format, rather than the 'Traditional' format. The main body of research is organized into 3 articles with the goal of eventual publication of each of these. Chapter 2 has already been published in the journal 'Climate of The Past', while Chapters 3 and 4 will be published on timelines beyond the submission of this thesis.

Bibliography

Katrine K Andersen, Anders Svensson, Sigfus J Johnsen, Sune O Rasmussen, Matthias Bigler, Regine Röthlisberger, Urs Ruth, Marie-Louise Siggaard-Andersen, Jørgen Peder Steffensen, Dorthe Dahl-Jensen, et al. The greenland ice core chronology 2005, 15–42ka. part 1: Constructing the time scale. *Quaternary Science Reviews*, 25(23):3246–3257, 2006.

Heather J. Andres and Lev Tarasov. Towards understanding potential atmospheric contributions to abrupt climate changes: characterizing changes to the north atlantic eddy-driven jet over the last deglaciation. *Climate of the Past*, 15(4):16211646, Aug 2019. ISSN 1814-9332. doi: 10.5194/cp-15-1621-2019. URL http://dx.doi.org/10.5194/cp-15-1621-2019.

Yosef Ashkenazy, Martin Losch, Hezi Gildor, Dror Mirzayof, and Eli Tziperman. Multiple sea-ice states and abrupt moc transitions in a general circulation ocean model. *Climate Dynamics*, 40 (7-8):1803–1817, 2013. ISSN 0930-7575. doi: 10.1007/s00382-012-1546-2. URL http://dx.doi.org/10.1007/s00382-012-1546-2.

Jostein Bakke, yvind Lie, Einar Heegaard, Trond Dokken, Gerald H. Haug, Hilary H. Birks, Peter Dulski, and Trygve Nilsen. Rapid oceanic and atmospheric changes during the younger dryas cold period. *Nature Geoscience*, 2(3):202205, Feb 2009. ISSN 1752-0908. doi: 10.1038/ngeo439. URL http://dx.doi.org/10.1038/ngeo439.

R. C. Bales and E. W. Wolff. Interpreting natural climate signals in ice cores. *Eos, Transactions American Geophysical Union*, 76(47):477477, 1995. ISSN 0096-3941. doi: 10.1029/95eo00293. URL http://dx.doi.org/10.1029/95EO00293.

Christine L. Batchelor, Martin Margold, Mario Krapp, Della K. Murton, April S. Dalton, Philip L. Gibbard, Chris R. Stokes, Julian B. Murton, and Andrea Manica. The configuration of northern hemisphere ice sheets through the quaternary. *Nature Communications*, 10(1), Aug 2019. ISSN 2041-1723. doi: 10.1038/s41467-019-11601-2. URL http://dx.doi.org/10.1038/s41467-019-11601-2.

Bernhard Bereiter, Sarah Eggleston, Jochen Schmitt, Christoph Nehrbass-Ahles, Thomas F. Stocker, Hubertus Fischer, Sepp Kipfstuhl, and Jerome Chappellaz. Revision of the epica dome c co2 record from 800 to 600 kyr before present. *Geophysical Research Letters*, 42(2):542–549, Jan 2015. ISSN 0094-8276. doi: 10.1002/2014gl061957. URL http://dx.doi.org/10.1002/2014GL061957.

Ingo Bethke, Camille Li, and Kerim H. Nisancioglu. Can we use ice sheet reconstructions to constrain meltwater for deglacial simulations? *Paleoceanography*, 27(2):n/an/a, Apr 2012. ISSN 0883-8305. doi: 10.1029/2011pa002258. URL http://dx.doi.org/10.1029/2011PA002258.

Alan K. Betts and John H. Ball. Albedo over the boreal forest. *Journal of Geophysical Research:*

Atmospheres, 102(D24):2890128909, Dec 1997. ISSN 0148-0227. doi: 10.1029/96jd03876. URL http://dx.doi.org/10.1029/96JD03876.

Matthias Bigler, Anders Svensson, Ernesto Kettner, Paul Vallelonga, Maibritt E. Nielsen, and Jrgen Peder Steffensen. Optimization of high-resolution continuous flow analysis for transient climate signals in ice cores. *Environmental Science & Technology*, 45(10):44834489, Apr 2011. ISSN 1520-5851. doi: 10.1021/es200118j. URL http://dx.doi.org/10.1021/es200118j.

G. Edward Birchfield and Wallace S. Broecker. A salt oscillator in the glacial atlantic? 2. a scale analysis model. *Paleoceanography*, 5(6):835843, Dec 1990. ISSN 0883-8305. doi: 10.1029/pa005i006p00835. URL http://dx.doi.org/10.1029/PA005i006p00835.

Jo Brendryen, Haflidi Haflidason, Yusuke Yokoyama, Kristian Agasoester Haaga, and Bjarte Hannisdal. Eurasian ice sheet collapse was a major source of meltwater pulse 1a 14,600 years ago. *Nature Geoscience*, 13(5):363–368, Apr 2020. ISSN 1752-0908. doi: 10.1038/s41561-020-0567-4. URL http://dx.doi.org/10.1038/s41561-020-0567-4.

Wallace S. Broecker, Gerard Bond, Millie Klas, Georges Bonani, and Willy Wolfli. A salt oscillator in the glacial atlantic? 1. the concept. *Paleoceanography*, 5(4):469477, Aug 1990. ISSN 0883-8305. doi: 10.1029/pa005i004p00469. URL http://dx.doi.org/10.1029/PA005i004p00469.

Wallace S. Broecker, George H. Denton, R. Lawrence Edwards, Hai Cheng, Richard B. Alley, and Aaron E. Putnam. Putting the younger dryas cold event into context. *Quaternary Science Reviews*, 29(9-10):10781081, May 2010. ISSN 0277-3791. doi: 10.1016/j.quascirev.2010.02.019. URL http://dx.doi.org/10.1016/j.quascirev.2010.02.019.

Nicolas Brown and Eric D. Galbraith. Hosed vs. unhosed: interruptions of the Atlantic Meridional Overturning Circulation in a global coupled model, with and without freshwater forcing. *Climate of the Past*, 12:1663–1679, 2016. doi: 10.5194/cp-12-1663-2016.

Frank Bryan. High-latitude salinity effects and interhemispheric thermohaline circulations. *Nature*, 323(6086):301304, Sep 1986. ISSN 1476-4687. doi: 10.1038/323301a0. URL http://dx.doi.org/10.1038/323301a0.

S. J. Burns. Indian ocean climate and an absolute chronology over dansgaard/oeschger events 9 to 13. *Science*, 301(5638):13651367, Sep 2003. ISSN 1095-9203. doi: 10.1126/science.1086227. URL http://dx.doi.org/10.1126/science.1086227.

Matthew Collins, Reto Knutti, Julie Arblaster, Jean-Louis Dufresne, Thierry Fichefet, Pierre Friedlingstein, Xuejie Gao, William J Gutowski, Tim Johns, Gerhard Krinner, et al. Long-term climate change: projections, commitments and irreversibility. In *Climate Change 2013-The Physical Science Basis: Contribution of Working Group I to the Fifth Assessment Report of the Intergovernmental Panel on Climate Change*, pages 1029–1136. Cambridge University Press, 2013.

A. Condron and P. Winsor. Meltwater routing and the younger dryas. *Proceedings of the National Academy of Sciences*, 109(49):1992819933, Nov 2012. ISSN 1091-6490. doi: 10.1073/pnas.1207381109. URL http://dx.doi.org/10.1073/pnas.1207381109.

Ellen C. Corrick, Russell N. Drysdale, John C. Hellstrom, Emilie Capron, Sune Olander Rasmussen, Xu Zhang, Dominik Fleitmann, Isabelle Couchoud, and Eric Wolff. Synchronous timing of abrupt climate changes during the last glacial period. *Science*, 369(6506):963969, Aug 2020. ISSN 1095-9203. doi: 10.1126/science.aay5538. URL http://dx.doi.org/10.1126/science.aay5538.

Kurt M. Cuffey and Eric J. Steig. Isotopic diffusion in polar firn: implications for interpretation of seasonal climate parameters in ice-core records, with emphasis on central greenland. *Journal of Glaciology*, 44(147):273284, 1998. ISSN 1727-5652. doi: 10.3189/s0022143000002616. URL http://dx.doi.org/10.3189/S0022143000002616.

W. Dansgaard, S.J. Johnsen, H.B. Clausen, D. Dahl-Jensen, N. Gundestrup, C.U. Hammer, and H. Oeschger. North atlantic climatic oscillations revealed by deep greenland ice cores. *Geophysical Monograph Series*, page 288298, 1984. ISSN 0065-8448. doi: 10.1029/gm029p0288. URL http://dx.doi.org/10.1029/GM029p0288.

W. Dansgaard, S. J. Johnsen, H. B. Clausen, D. Dahl-Jensen, N. S. Gundestrup, C. U. Hammer, C. S. Hvidberg, J. P. Steffensen, A. E. Sveinbjrnsdottir, J. Jouzel, and et al. Evidence for general instability of past climate from a 250-kyr ice-core record. *Nature*, 364(6434):218220, Jul 1993. ISSN 1476-4687. doi: 10.1038/364218a0. URL http://dx.doi.org/10.1038/364218a0.

Will Dansgaard, Sigfus J Johnsen, Jesper Møller, and Chester C Langway. One thousand centuries of climatic record from camp century on the greenland ice sheet. *Science*, 166(3903):377–380, 1969.

Willi Dansgaard, HB Clausen, N Gundestrup, CU Hammer, SF Johnsen, PM Kristinsdottir, and Niels Reeh. A new greenland deep ice core. *Science*, 218(4579):1273–1277, 1982.

Gilles Delaygue. *Oxygen Isotopes*, pages 666–673. Springer Netherlands, Dordrecht, 2009. ISBN 978-1-4020-4411-3. doi: 10.1007/978-1-4020-4411-3_163. URL https://doi.org/10.1007/978-1-4020-4411-3_163.

Pierre Deschamps, Nicolas Durand, Edouard Bard, Bruno Hamelin, Gilbert Camoin, Alexander L. Thomas, Gideon M. Henderson, Jun'ichi Okuno, and Yusuke Yokoyama. Ice-sheet collapse and sea-level rise at the boelling warming 14,600 years ago. *Nature*, 483(7391):559–564, Mar 2012. ISSN 1476-4687. doi: 10.1038/nature10902. URL http://dx.doi.org/10.1038/nature10902.

Brendan T Doherty and Dana R Kester. *Freezing point of seawater*. Sears Foundation for Marine Research, 1974.

Trond M. Dokken, Kerim H. Nisancioglu, Camille Li, David S. Battisti, and Catherine Kissel. Dansgaard-oeschger cycles: Interactions between ocean and sea ice intrinsic to the nordic seas. *Paleoceanography*, 28(3):491502, Sep 2013. ISSN 0883-8305. doi: 10.1002/palo.20042. URL http://dx.doi.org/10.1002/palo.20042.

M. Etminan, G. Myhre, E. J. Highwood, and K. P. Shine. Radiative forcing of carbon dioxide, methane, and nitrous oxide: A significant revision of the methane radiative forcing. *Geophysical Research Letters*, 43(24), Dec 2016. ISSN 1944-8007. doi: 10.1002/2016gl071930. URL http://dx.doi.org/10.1002/2016GL071930.

D. Genty, D. Blamart, R. Ouahdi, M. Gilmour, A. Baker, J. Jouzel, and Sandra Van-Exter. Precise dating of dansgaardoeschger climate oscillations in western europe from stalagmite data. *Nature*, 421(6925):833837, Feb 2003. ISSN 0028-0836. doi: 10.1038/nature01391. URL http://dx.doi.org/10.1038/nature01391.

Hezi Gildor and Eli Tziperman. Sea-ice switches and abrupt climate change. *Philosophical Transactions of the Royal Society of London A: Mathematical, Physical and Engineering Sciences*, 361 (1810):1935–1944, 2003. ISSN 1364-503X. doi: 10.1098/rsta.2003.1244.

Xun Gong, Xiangdong Zhang, Gerrit Lohmann, Wei Wei, Xu Zhang, and Madlene Pfeiffer. Higher laurentide and greenland ice sheets strengthen the north atlantic ocean circulation. *Climate*

Dynamics, 45(1-2):139150, Feb 2015. ISSN 1432-0894. doi: 10.1007/s00382-015-2502-8. URL http://dx.doi.org/10.1007/s00382-015-2502-8.

Vivien Gornitz. *Encyclopedia of paleoclimatology and ancient environments*. Springer Science & Business Media, 2008.

Lauren J. Gregoire, Bette Otto-Bliesner, Paul J. Valdes, and Ruza Ivanovic. Abrupt boelling warming and ice saddle collapse contributions to the meltwater pulse 1a rapid sea level rise. *Geophysical Research Letters*, 43(17):9130–9137, Sep 2016. ISSN 0094-8276. doi: 10.1002/2016gl070356. URL http://dx.doi.org/10.1002/2016GL070356.

PM Grootes and M Stuiver. Oxygen 18/16 variability in greenland snow and ice with 10- 3-to 105-year time resolution. *Journal of Geophysical Research: Oceans*, 102(C12):26455–26470, 1997.

PM Grootes, Minze Stuiver, JWC White, S Johnsen, and J Jouzel. Comparison of oxygen isotope records from the gisp2 and grip greenland ice cores. 1993.

Jenna C. Hill and Alan Condron. Subtropical iceberg scours and meltwater routing in the deglacial western north atlantic. *Nature Geoscience*, 7(11):806810, Oct 2014. ISSN 1752-0908. doi: 10.1038/ngeo2267. URL http://dx.doi.org/10.1038/ngeo2267.

Linda A Hinnov, Michael Schulz, and Pascal Yiou. Interhemispheric spacetime attributes of the dansgaardoeschger oscillations between 100 and 0ka. *Quaternary Science Reviews*, 21 (10):12131228, May 2002. ISSN 0277-3791. doi: 10.1016/s0277-3791(01)00140-8. URL http://dx.doi.org/10.1016/S0277-3791(01)00140-8.

A. Hu, G. A. Meehl, W. Han, A. Timmermann, B. Otto-Bliesner, Z. Liu, W. M. Washington, W. Large, A. Abe-Ouchi, M. Kimoto, and et al. Role of the bering strait on the hysteresis of the ocean conveyor belt circulation and glacial climate stability. *Proceedings of the National Academy of Sciences*, 109(17):64176422, Apr 2012. ISSN 1091-6490. doi: 10.1073/pnas.1116014109. URL http://dx.doi.org/10.1073/pnas.1116014109.

Aixue Hu, Gerald A. Meehl, and Weiqing Han. Role of the bering strait in the thermohaline circulation and abrupt climate change. *Geophysical Research Letters*, 34(5), Mar 2007. ISSN 0094-8276. doi: 10.1029/2006gl028906. URL http://dx.doi.org/10.1029/2006GL028906.

Aixue Hu, Gerald A. Meehl, Weiqing Han, Bette Otto-Bliestner, Ayako Abe-Ouchi, and Nan Rosenbloom. Effects of the bering strait closure on amoc and global climate under different background climates. *Progress in Oceanography*, 132:174196, Mar 2015. ISSN 0079-6611. doi: 10.1016/j.pocean.2014.02.004. URL http://dx.doi.org/10.1016/j.pocean.2014.02.004.

René FB Isarin, Hans Renssen, and Jef Vandenberghe. The impact of the north atlantic ocean on the younger dryas climate in northwestern and central europe. *Journal of Quaternary Science*, 13(5):447–453, 1998.

Knud Jessen. *Archaeological dating in the history of North Jutland's vegetation*. Munksgaard, 1935.

J Jouzel, C Genthon, C Lorius, JR Petit, and NI Barkov. Vostok ice core-a continuous isotope temperature record over the last climatic cycle (160,000 years). *Nature*, 329:403–408, 1987.

Masa Kageyama, Sandy P. Harrison, Marie-L. Kapsch, Marcus Lofverstrom, Juan M. Lora, Uwe Mikolajewicz, Sam Sherriff-Tadano, Tristan Vadsaria, Ayako Abe-Ouchi, Nathaelle Bouttes, and et al. The pmip4 last glacial maximum experiments: preliminary results and comparison with the pmip3 simulations. *Climate of the Past*, 17(3):10651089, May 2021. ISSN 1814-9332. doi: 10.5194/cp-17-1065-2021. URL http://dx.doi.org/10.5194/cp-17-1065-2021.

Ralph F Keeling and Charles D. Keeling. Atmospheric monthly in situ co2 data - mauna loa observatory, hawaii. in scripps co2 program data, 2017. URL https://library.ucsd.edu/dc/object/bb3859642r.

P. Kindler, M. Guillevic, M. Baumgartner, J. Schwander, A. Landais, and M. Leuenberger. Temperature reconstruction from 10 to 120 kyr b2k from the ngrip ice core. *Climate of the Past*, 10(2):887902, Apr 2014. ISSN 1814-9332. doi: 10.5194/cp-10-887-2014. URL http://dx.doi.org/10.5194/cp-10-887-2014.

M. Klockmann, U. Mikolajewicz, H. Kleppin, and J. Marotzke. Coupling of the subpolar gyre and the overturning circulation during abrupt glacial climate transitions. *Geophysical Research Letters*, 47(21), Nov 2020. ISSN 1944-8007. doi: 10.1029/2020gl090361. URL http://dx.doi.org/10.1029/2020GL090361.

Takuro Kobashi, Kenji Kawamura, Jeffrey P. Severinghaus, Jean-Marc Barnola, Toshiyuki Nakaegawa, Bo M. Vinther, Sigfs J. Johnsen, and Jason E. Box. High variability of greenland surface temperature over the past 4000 years estimated from trapped air in an ice core. *Geophysical Research Letters*, 38(21):n/an/a, Nov 2011. ISSN 0094-8276. doi: 10.1029/2011gl049444. URL http://dx.doi.org/10.1029/2011GL049444.

Lamy, Klump, Hebbeln, and Wefer. Late quaternary rapid climate change in northern chile. *Terra Nova*, 12(1):813, Feb 2000. ISSN 1365-3121. doi: 10.1046/j.1365-3121.2000.00265.x. URL http://dx.doi.org/10.1046/j.1365-3121.2000.00265.x.

Chester C. Langway. The history of early polar ice cores. *Cold Regions Science and Technology*, 52(2):101117, Apr 2008. ISSN 0165-232X. doi: 10.1016/j.coldregions.2008.01.001. URL http://dx.doi.org/10.1016/j.coldregions.2008.01.001.

J. Laskar, P. Robutel, F. Joutel, M. Gastineau, A. C. M. Correia, and B. Levrard. A long-term numerical solution for the insolation quantities of the earth. *Astronomy & Astrophysics*, 428(1): 261–285, Nov 2004. ISSN 1432-0746. doi: 10.1051/0004-6361:20041335. URL http://dx.doi.org/10.1051/0004-6361:20041335.

J. Laskar, A. Fienga, M. Gastineau, and H. Manche. La2010: a new orbital solution for the long-term motion of the earth. *Astronomy & Astrophysics*, 532:A89, Jul 2011. ISSN 1432-0746. doi: 10.1051/0004-6361/201116836. URL http://dx.doi.org/10.1051/0004-6361/201116836.

Yucheng Lin, Fiona D. Hibbert, Pippa L. Whitehouse, Sarah A. Woodroffe, Anthony Purcell, Ian Shennan, and Sarah L. Bradley. A reconciled solution of meltwater pulse 1a sources using sea-level fingerprinting. *Nature Communications*, 12(1), Apr 2021. ISSN 2041-1723. doi: 10.1038/s41467-021-21990-y. URL http://dx.doi.org/10.1038/s41467-021-21990-y.

Lorraine E. Lisiecki and Maureen E. Raymo. A pliocene-pleistocene stack of 57 globally distributed benthic δ18o records. *Paleoceanography*, 20(1):n/an/a, Jan 2005. ISSN 0883-8305. doi: 10.1029/2004pa001071. URL http://dx.doi.org/10.1029/2004PA001071.

Jean Liu, Glenn A. Milne, Robert E. Kopp, Peter U. Clark, and Ian Shennan. Sea-level constraints on the amplitude and source distribution of meltwater pulse 1a. *Nature Geoscience*, 9 (2):130134, Dec 2015. ISSN 1752-0908. doi: 10.1038/ngeo2616. URL http://dx.doi.org/10.1038/NGEO2616.

M. Löfverström, R. Caballero, J. Nilsson, and J. Kleman. Evolution of the large-scale atmospheric circulation in response to changing ice sheets over the last glacial cycle. *Climate of the Past*, 10

(4):14531471, Jul 2014. ISSN 1814-9332. doi: 10.5194/cp-10-1453-2014. URL http://dx.doi.org/10.5194/cp-10-1453-2014.

Gerrit Lohmann, Xu Zhang, and Gregor Knorr. Abrupt climate change experiments: the role of freshwater, ice sheets and deglacial warming for the atlantic meridional overturning circulation. *Polarforschung*, 85(2):161–170, 2016.

Laetitia Loulergue, Adrian Schilt, Renato Spahni, Valérie Masson-Delmotte, Thomas Blunier, Bénédicte Lemieux, Jean-Marc Barnola, Dominique Raynaud, Thomas F. Stocker, and Jérôme Chappellaz. Orbital and millennial-scale features of atmospheric ch4 over the past 800,000 years. *Nature*, 453(7193):383–386, May 2008. ISSN 1476-4687. doi: 10.1038/nature06950. URL http://dx.doi.org/10.1038/nature06950.

Ryan Love, Glenn A. Milne, Lev Tarasov, Simon E. Engelhart, Marc P. Hijma, Konstantin Latychev, Benjamin P. Horton, and Torbjrn E. Trnqvist. The contribution of glacial isostatic adjustment to projections of sealevel change along the atlantic and gulf coasts of north america. *Earths Future*, 4(10):440464, Oct 2016. ISSN 2328-4277. doi: 10.1002/2016ef000363. URL http://dx.doi.org/10.1002/2016EF000363.

Syukuro Manabe and Ronald Stouffer. The rle of thermohaline circulation in climate. *Tellus B*, 51(1), 1999. ISSN 1600-0889. URL http://www.tellusb.net/index.php/tellusb/article/view/16262.

Syukuro Manabe and Ronald J. Stouffer. Coupled ocean-atmosphere model response to freshwater input: Comparison to younger dryas event. *Paleoceanography*, 12(2):321336, Apr 1997. ISSN 0883-8305. doi: 10.1029/96pa03932. URL http://dx.doi.org/10.1029/96PA03932.

Syukuro Manabe and Ronald J Stouffer. Study of abrupt climate change by a coupled oceanatmosphere model. *Quaternary Science Reviews*, 19(15):285 – 299, 2000. ISSN 0277-3791. doi: http://dx.doi.org/10.1016/S0277-3791(99)00066-9. URL http://www.sciencedirect.com/science/article/pii/S0277379199000669.

JAN Mangerud, Svend T Andersen, BJÖRN E BERGLUND, and Joakim J Donner. Quaternary stratigraphy of norden, a proposal for terminology and classification. *Boreas*, 3(3):109–126, 1974.

Jan Mangerud, Steinar Gulliksen, and Eiliv Larsen. 14c-dated fluctuations of the western flank of the scandinavian ice sheet 45-25 kyr bp compared with boelling-younger dryas fluctuations and dansgaard-oeschger events in greenland. *Boreas*, 39(2):328–342, Apr 2010. ISSN 1502-3885. doi: 10.1111/j.1502-3885.2009.00127.x. URL http://dx.doi.org/10.1111/j.1502-3885.2009.00127.x.

J. F. McManus, R. Francois, J.-M. Gherardi, L. D. Keigwin, and S. Brown-Leger. Collapse and rapid resumption of atlantic meridional circulation linked to deglacial climate changes. *Nature*, 428(6985):834837, Apr 2004. ISSN 1476-4687. doi: 10.1038/nature02494. URL http://dx.doi.org/10.1038/nature02494.

DA Meese, RB Alley, T Gow, PM Grootes, P Mayewski, M Ram, K Taylor, E Waddington, and G Zielinski. Preliminary depth-age scale of the gisp2 ice core. *Special CRREL Report*, 94(1), 1994.

Juan Muglia and Andreas Schmittner. Glacial atlantic overturning increased by wind stress in climate models. *Geophysical Research Letters*, 42(22):98629868, Nov 2015. ISSN 0094-8276. doi: 10.1002/2015gl064583. URL http://dx.doi.org/10.1002/2015GL064583.

Bette L. Otto-Bliesner and Esther C. Brady. The sensitivity of the climate response to the magnitude and location of freshwater forcing: last glacial maximum experiments. *Quaternary Science Reviews*, 29(1-2):5673, Jan 2010. ISSN 0277-3791. doi: 10.1016/j.quascirev.2009.07.004. URL http://dx.doi.org/10.1016/j.quascirev.2009.07.004.

W. R. Peltier and G. Vettoretti. Dansgaard-Oeschger oscillations predicted in a comprehensive model of glacial climate: A "kicked" salt oscillator in the Atlantic. *Geophysical Research Letters*, 41:7306–7313, 2014. doi: 10.1002/2014GL061413.

W. R. Peltier, G. Vettoretti, and M. Stastna. Atlantic meridional overturning and climate response to arctic ocean freshening. *Geophysical Research Letters*, 33(6):n/a–n/a, 2006. ISSN 1944-8007. doi: 10.1029/2005GL025251. URL http://dx.doi.org/10.1029/2005GL025251. L06713.

Stefan Rahmstorf. Ocean circulation and climate during the past 120,000 years. *Nature*, 419(6903): 207214, Sep 2002. ISSN 0028-0836. doi: 10.1038/nature01090. URL http://dx.doi.org/10.1038/nature01090.

S. O. Rasmussen, K. K. Andersen, A. M. Svensson, J. P. Steffensen, B. M. Vinther, H. B. Clausen, M.-L. Siggaard-Andersen, S. J. Johnsen, L. B. Larsen, D. Dahl-Jensen, and et al. A new greenland ice core chronology for the last glacial termination. *Journal of Geophysical Research*, 111(D6), 2006. ISSN 0148-0227. doi: 10.1029/2005jd006079. URL http://dx.doi.org/10.1029/2005JD006079.

Sune O. Rasmussen, Matthias Bigler, Simon P. Blockley, Thomas Blunier, Susanne L. Buchardt, Henrik B. Clausen, Ivana Cvijanovic, Dorthe Dahl-Jensen, Sigfus J. Johnsen, Hubertus Fischer, and et al. A stratigraphic framework for abrupt climatic changes during the last glacial period based on three synchronized greenland ice-core records: refining and extending the intimate event stratigraphy. *Quaternary Science Reviews*, 106:14–28, Dec 2014. ISSN 0277-3791. doi: 10.1016/j.quascirev.2014.09.007. URL http://dx.doi.org/10.1016/j.quascirev.2014.09.007.

Sune Olander Rasmussen, Inger Kathrine Seierstad, Katrine Krogh Andersen, Matthias Bigler, Dorthe Dahl-Jensen, and Sigfus Johann Johnsen. Synchronization of the NGRIP, GRIP, and GISP2 ice cores across MIS 2 and palaeoclimatic implications. *Quaternary Science Reviews*, 27 (1):18–28, 2008.

Didier M. Roche, Ane P. Wiersma, and Hans Renssen. A systematic study of the impact of freshwater pulses with respect to different geographical locations. *Climate Dynamics*, 34(7-8): 9971013, May 2009. ISSN 1432-0894. doi: 10.1007/s00382-009-0578-8. URL http://dx.doi.org/10.1007/s00382-009-0578-8.

William F. Ruddiman. Late quaternary deposition of ice-rafted sand in the subpolar north atlantic (lat 40 to 65n). *Geological Society of America Bulletin*, 88(12):1813, 1977. ISSN 0016-7606. doi: 10.1130/0016-7606(1977)88⟨1813:lqdois⟩2.0.co;2. URL http://dx.doi.org/10.1130/0016-7606(1977)88<1813:LQDOIS>2.0.CO;2.

Adrian Schilt, Matthias Baumgartner, Jakob Schwander, Daphn Buiron, Emilie Capron, Jrme Chappellaz, Laetitia Loulergue, Simon Schpbach, Renato Spahni, Hubertus Fischer, and et al. Atmospheric nitrous oxide during the last 140,000years. *Earth and Planetary Science Letters*, 300(1-2):3343, Nov 2010. ISSN 0012-821X. doi: 10.1016/j.epsl.2010.09.027. URL http://dx.doi.org/10.1016/j.epsl.2010.09.027.

Sharon B. Sneed, Paul A. Mayewski, W.G. Sayre, Michael J. Handley, Andrei V. Kurbatov, Kendrick C. Taylor, Pascal Bohleber, Dietmar Wagenbach, Tobias Erhardt, and Nicole E. Spaulding. New la-icp-ms cryocell and calibration technique for sub-millimeter analysis of ice cores. *Journal of Glaciology*, 61(226):233242, 2015. ISSN 1727-5652. doi: 10.3189/2015jog14j139. URL http://dx.doi.org/10.3189/2015JoG14J139.

Eric J Steig, Pieter M Grootes, and Minze Stuiver. Seasonal precipitation timing and ice core records. *Science (Washington, DC);(United States)*, 266(5192), 1994.

Rüdiger Stein. The expedition ps115/2 of the research vessel polarstern to the arctic ocean in 2018. Technical report, 2019.

Henry Stommel. Thermohaline convection with two stable regimes of flow. *Tellus*, 13(2):224–230, 1961.

R. J. Stouffer, J. Yin, J. M. Gregory, K. W. Dixon, M. J. Spelman, W. Hurlin, A. J. Weaver, M. Eby, G. M. Flato, H. Hasumi, and et al. Investigating the causes of the response of the thermohaline circulation to past and future climate changes. *Journal of Climate*, 19(8):13651387, Apr 2006. ISSN 1520-0442. doi: 10.1175/jcli3689.1. URL http://dx.doi.org/10.1175/JCLI3689.1.

Minze Stuiver, Pieter M Grootes, and Thomas F Braziunas. The gisp2 δ 18 o climate record of the past 16,500 years and the role of the sun, ocean, and volcanoes. *Quaternary Research*, 44(3): 341–354, 1995.

Anders Svensson, Katrine K Andersen, Matthias Bigler, Henrik B Clausen, Dorthe Dahl-Jensen, Siwan M Davies, Sigfus J Johnsen, Raimund Muscheler, Sune O Rasmussen, Regine Röthlisberger, et al. The greenland ice core chronology 2005, 15–42ka. part 2: comparison to other records. *Quaternary Science Reviews*, 25(23):3258–3267, 2006.

Lev Tarasov and W.R. Peltier. Arctic freshwater forcing of the younger dryas cold reversal. *Nature*, 435(7042):662665, Jun 2005. ISSN 1476-4687. doi: 10.1038/nature03617. URL http://dx.doi.org/10.1038/nature03617.

Lev Tarasov and W.R. Peltier. A calibrated deglacial drainage chronology for the north american continent: evidence of an arctic trigger for the younger dryas. *Quaternary Science Reviews*, 25(7-8):659688, Apr 2006. ISSN 0277-3791. doi: 10.1016/j.quascirev.2005.12.006. URL http://dx.doi.org/10.1016/j.quascirev.2005.12.006.

Lev Tarasov, Arthur S. Dyke, Radford M. Neal, and W.R. Peltier. A data-calibrated distribution of deglacial chronologies for the north american ice complex from glaciological modeling. *Earth and Planetary Science Letters*, 315316:30 – 40, 2012. ISSN 0012-821X. doi: http://dx.doi.org/10.1016/j.epsl.2011.09.010. URL http://www.sciencedirect.com/science/article/pii/S0012821X11005243. Sea Level and Ice Sheet Evolution: A {PALSEA} Special Edition.

J. T. Teller. Importance of freshwater injections into the arctic ocean in triggering the younger dryas cooling. *Proceedings of the National Academy of Sciences*, 109(49):1988019881, Nov 2012. ISSN 1091-6490. doi: 10.1073/pnas.1218344109. URL http://dx.doi.org/10.1073/pnas.1218344109.

D. J. Ullman, A. N. LeGrande, A. E. Carlson, F. S. Anslow, and J. M. Licciardi. Assessing the impact of laurentide ice sheet topography on glacial climate. *Climate of the Past*, 10(2):487507, Mar 2014. ISSN 1814-9332. doi: 10.5194/cp-10-487-2014. URL http://dx.doi.org/10.5194/cp-10-487-2014.

Guido Vettoretti and W. Richard Peltier. Thermohaline instability and the formation of glacial

North Atlantic super polynyas at the onset of Dansgaard-Oeschger warming events. *Geophysical Research Letters*, 43:5336–5344, 2016. doi: 10.1002/2016GL068891.

Guido Vettoretti, Marc d Orgeville, William R. Peltier, and Marek Stastna. Polar climate instability and climate teleconnections from the arctic to the midlatitudes and tropics. *Journal of Climate*, 22(13):35133539, Jul 2009. ISSN 0894-8755. doi: 10.1175/2009jcli2481.1. URL http://dx.doi.org/10.1175/2009JCLI2481.1.

Miren Vizcaino, Uwe Mikolajewicz, Florian Ziemen, Christian B. Rodehacke, Ralf Greve, and Michiel R. Broeke. Coupled simulations of greenland ice sheet and climate change up to a.d. 2300. *Geophysical Research Letters*, 42(10):39273935, May 2015. ISSN 1944-8007. doi: 10.1002/2014gl061142. URL http://dx.doi.org/10.1002/2014GL061142.

Antje H.L. Voelker. Global distribution of centennial-scale records for marine isotope stage (mis) 3: a database. *Quaternary Science Reviews*, 21(10):11851212, May 2002. ISSN 0277-3791. doi: 10.1016/s0277-3791(01)00139-1. URL http://dx.doi.org/10.1016/S0277-3791(01)00139-1.

Xianfeng Wang, Augusto S. Auler, R. Lawrence Edwards, Hai Cheng, Patricia S. Cristalli, Peter L. Smart, David A. Richards, and Chuan-Chou Shen. Wet periods in northeastern brazil over the past 210 kyr linked to distant climate anomalies. *Nature*, 432(7018):740–743, Dec 2004. ISSN 1476-4687. doi: 10.1038/nature03067. URL http://dx.doi.org/10.1038/nature03067.

Xianfeng Wang, Augusto S. Auler, R. Lawrence Edwards, Hai Cheng, Emi Ito, and Maniko Solheid. Interhemispheric anti-phasing of rainfall during the last glacial period. *Quaternary Science Reviews*, 25(23-24):33913403, Dec 2006. ISSN 0277-3791. doi: 10.1016/j.quascirev.2006.02.009. URL http://dx.doi.org/10.1016/j.quascirev.2006.02.009.

Y. J. Wang. A high-resolution absolute-dated late pleistocene monsoon record from hulu cave, china. *Science*, 294(5550):23452348, Dec 2001. ISSN 1095-9203. doi: 10.1126/science.1064618. URL http://dx.doi.org/10.1126/science.1064618.

G. Wendler, B. Moore, B. Hartmann, M. Stuefer, and R. Flint. Effects of multiple reflection and albedo on the net radiation in the pack ice zones of antarctica. *Journal of Geophysical Research: Atmospheres*, 109(D6):n/an/a, Mar 2004. ISSN 0148-0227. doi: 10.1029/2003jd003927. URL http://dx.doi.org/10.1029/2003JD003927.

Matteo Willeit and Andrey Ganopolski. The importance of snow albedo for ice sheet evolution over the last glacial cycle. *Climate of the Past*, 14(5):697707, May 2018. ISSN 1814-9332. doi: 10.5194/cp-14-697-2018. URL http://dx.doi.org/10.5194/cp-14-697-2018.

X. Zhang. "Confidential Manuscript - Personal Communication", July 2021.

Xiao Zhang, Matthias Prange, Ute Merkel, and Michael Schulz. Instability of the atlantic overturning circulation during marine isotope stage 3. *Geophysical Research Letters*, 41(12):42854293, Jun 2014. ISSN 0094-8276. doi: 10.1002/2014gl060321. URL http://dx.doi.org/10.1002/2014GL060321.

Co-authorship Statement

Overall Thesis Project & Thesis Introduction

The overall research project was broadly described by the thesis supervisor, Dr. Lev Tarasov and further refined by R. Love. The thesis introduction was written by R. Love with editorial contributions from those contemporary members of the Glacial Dynamics group of Dr. Tarasov. As well, the thesis author's supervisory committee (Dr. Brad de Young and Dr. Entcho Demirov) provided advice and editorial contributions.

Freshwater Routing In Eddy-permitting Simulations Of The Last Deglacial:Impact Of Realistic Freshwater Discharge

R. Love prepared the experimental design, analysed the results, and wrote the manuscript with contributions from all authors. Alan Condron assisted with technical advise and details regarding the MITGCM configuration used. The initial manuscript was greatly enhanced through two reviewers (Dr. Pasha Karami and Anonymous) and one community based review during the publishing process with Climate of the Past.

Freshwater Fingerprints in Place of Freshwater Hosing

R. Love prepared the experimental design, analysed the results, and wrote the manuscript with contributions from all authors. X. Zhang assisted with data, utilities, and advise regarding the COSMOS Earth Systems Model. L. Tarasov assisted with additional refinements of the GLAC reconstruction used for this set of experiments

The Role of Glacial Runoff in Modulating Dansgaard-Oeschger-like Oscillations

R. Love prepared the experimental design, analysed the results, and wrote the manuscript with contributions from all authors. L. Tarasov assisted with additional refinements of the GLAC reconstruction used for this set of experiments H. J. Andres assisted via the contribution of an automated Dangaard-Oeschger event detection utility.

Editoral contributions to the thesis by coauthors and colleguges did not extend to providing substantive writing for any component. Editoral contributions amounted to assisting in clarifying language to enhance readability and suggestions for contextual content.

Chapter 2

Freshwater Routing In Eddy-permitting Simulations Of The Last Deglacial : Impact Of Realistic Freshwater Discharge

Freshwater Routing In Eddy-permitting Simulations Of The Last Deglacial:Impact Of Realistic Freshwater Discharge

Ryan Love[1], Heather J. Andres[1], Alan Condron[2], and Lev Tarasov[1]

[1]Department of Physics and Physical Oceanography, Memorial University of Newfoundland, St. John's, Newfoundland, Canada
[2]Geology & Geophysics, Woods Hole Oceanographic Institution, Woods Hole, Massachusetts, USA

2.1 Abstract

Freshwater, in the form of glacial runoff, is hypothesized to play a critical role in centennial to millennial scale climate variability such as the Younger Dryas and Dansgaard-Oeschger Events, but this relationship is not straightforward. Large-scale glacial runoff events, such as Meltwater Pulse 1A, are not always temporally proximal to subsequent large-scale cooling. As well, the typical design of hosing experiments that support this relationship tends to artificially amplify the climate response. This study explores the impact that limitations in the representation of runoff in conventional hosing simulations has on our understanding of this relationship by examining where coastally released freshwater is transported when it reaches the ocean. We focus particularly on the impact of: 1) the injection of freshwater directly over sites of deep-water formation (DWF) rather than at runoff locations (i.e. Hosing), 2) excessive freshwater injection volumes (often by a factor of 5), and 3) the use of present-day (rather than paleo) ocean gateways.

We track the routing of glaciologically-constrained freshwater volumes from four different inferred injection locations in a suite of eddy-permitting glacial ocean simulations using MITGCM under both open and closed Bering Strait conditions. Restricting freshwater forcing values to realistic ranges results in less spreading of freshwater across the North Atlantic and indicates that the freshwater anomalies over DWF sites depend strongly on the geographical location of meltwater input. In particular, freshwater released into the Gulf of Mexico generates a very weak freshwater signal over DWF regions as a result of entrainment by the turbulent Gulf Stream. In contrast, freshwater released into the Arctic with an open Bering Strait or from the Eurasian Ice sheet is found to generate the largest salinity anomalies over DWF regions in the North Atlantic and GIN Seas respectively. Experiments show that when the Bering Strait is open, the Mackenzie River source exhibits more than twice as much freshening of the North Atlantic deep-water formation regions as when the Bering Strait is closed. Our results illustrate that applying a freshwater 'hosing' directly into the North Atlantic with even "realistic" freshwater amounts still over-estimates the amount of terrestrial runoff reaching DWF regions. Given the simulated salinity anomaly distributions and the lack of reconstructed impact on deepwater formation during the Bølling-Allerød, our results

support that the majority of the North American contribution to MWP1A was not routed through the Mackenzie River.

2.2 Introduction

The most recent deglacial and glacial intervals are punctuated by large-scale centennial to millennial scale climate variability, including the Bølling-Allerød, Younger Dryas, and Dansgaard-Oeschger events. Changes in freshwater discharge into the ocean and subsequent transport are thought to play a significant role in this variability through their resultant impact on deepwater formation (DWF) in the North Atlantic [Broecker et al., 1989, Manabe and Stouffer, 1997, Teller et al., 2002]. However, recent earth system modelling [Peltier and Vettoretti, 2014, Zhang et al., 2014, Kleppin et al., 2015, Brown and Galbraith, 2016, Vettoretti and Peltier, 2016, Zhang et al., 2017, Klockmann et al., 2018] has also demonstrated that changing freshwater inputs into the oceans is not required to get such transitions.

Furthermore, there are clear intervals during the last deglaciation when strongly enhanced net freshwater injection into the oceans resulted in no temporally proximal cooling (see Fig. 2.1). In the case of Meltwater Pulse (MWP) 1-A, current best estimates of its timing indicate that, within dating uncertainties, the freshwater injection aligns with the Bølling-Allerød [Deschamps et al., 2012] warm interval. This is consistent with the physical reasoning that a warm interval coinciding with continental-scale ice sheets should result in enhanced glacial runoff. The onset of the subsequent cold Younger Dryas interval occurs more than a millennium later, which is longer than would be consistent with a direct physical linkage. Understanding the factors that control the impact of freshwater on climate is an important step toward understanding these past climate changes and predicting those in the future.

Climate models have generally supported the ability of freshwater to generate abrupt climate transitions in hosing experiments, where large volumes of freshwater ($1 - 10$dSv[1]) are imposed

[1] We use the more appropriately scaled unit of dSv, 1/10th of a Sverdrup, to better reflect the magnitude of realistic freshwater fluxes.

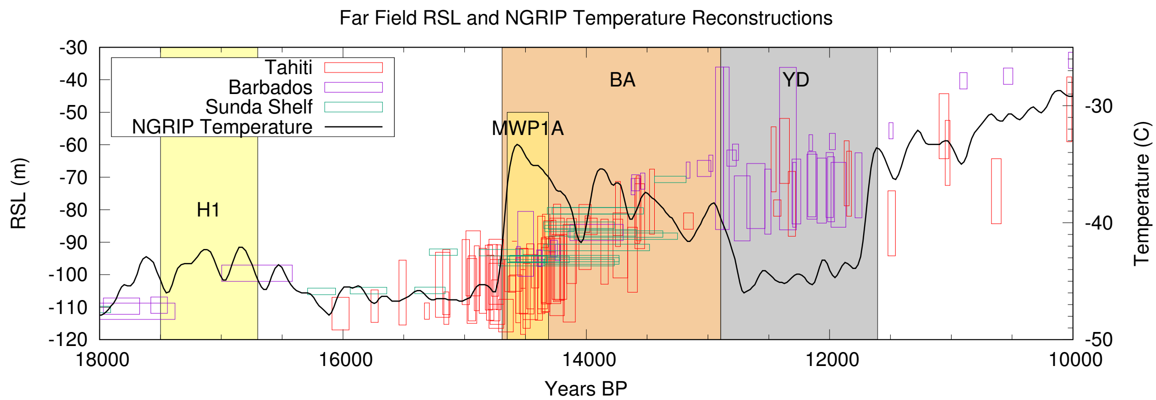

Figure 2.1: Far-field relative sea level records (i.e. sea level relative to present day, where the far-field sea level signal is roughly comparable to eustatic sea level) from Barbados [Fairbanks, 1989], Sunda Shelf [Hanebuth, 2000], and Tahiti [Deschamps et al., 2012] plotted along with a recent NGRIP temperature reconstruction for the deglacial [Kindler et al., 2014].

over sites of DWF [Kageyama et al., 2013]. Such hosings are meant to reproduce the effect of changing freshwater input into the oceans from regional ice sheet melt and iceberg discharge as well as rerouting of surface runoff [Tarasov and Peltier, 2005]. However, the climate model support for this connection between freshwater injection and climate transitions is problematic given at least three common experimental design problems that likely amplify climate system response compared to that which would ensue from more realistic freshwater injection experiments.

The first issue is the geographic distribution of freshwater injection. Given the transport mechanisms of coastally released freshwater, e.g. boundary currents and mesoscale eddies [Condron and Winsor, 2012, Hill and Condron, 2014, Nurser and Bacon, 2014], are well below the resolution of commonly used models, many studies opt to bypass the transport by injecting freshwater directly onto sites of DWF [e.g. Manabe and Stouffer, 1997, Peltier et al., 2006, Otto-Bliesner and Brady, 2010]. Often-times the freshwater is introduced directly over 50-70N or the Ruddiman/Ice-Rafted-Debris (IRD) belt, a region of ocean approximately between 40N and 50N in the North Atlantic, situated between Newfoundland, Canada and Portugal. These most common injection locations usually inhibit DWF through a persistent freshwater cap that results in near-immediate decreases in AMOC [Stouffer et al., 2006]. This attempt to compensate for coarse model resolution via hosing is problematic, since it assumes that all of the freshwater reaches the near-surface DWF zone intact. It is unclear if a more realistic representation of runoff routing would yield a similar freshwater signal at the zones of DWF. The only eddy-permitting and boundary-current resolving modelling of freshwater forcing from actual continental outlets to date under glacial boundary conditions suggests this is not the case [Condron and Winsor, 2012, Lohmann et al., 2020]. However both of these studies have design limitations which limit the interpretability of their results. The unstructured mesh of FESOM in Lohmann et al. [2020] has refined (but not quite eddy-permitting) grid resolution largely only over the Arctic ocean and at coastal boundaries but is unable to resolve the impact of mesoscale eddies on freshwater transport over the central North Atlantic. In order to offset the short one-year interval of injection, Condron and Winsor [2012] relied on fluxes of freshwater (50dSv) that were more than a factor of 20 larger than estimates derived from glaciological modelling over the Younger Dryas [Tarasov and Peltier, 2005, 2006].

The second significant issue we identify in modelling studies is the use of unrealistic volumes of freshwater in injection experiments. The amount of freshwater which is injected tends to be excessive, often of the order of 10dSv [e.g. Peltier et al., 2006]. If one considers the total discharge due to net ice mass loss during MWP1A, then a 10 to 15m rise of sea level over one third of a millennium [Deschamps et al., 2012] translates to a global excess (above background precipitation minus evaporation) discharge of 3 to 5dSv. This is the total contribution from outlets of all ice sheets. For North America, peak centennial-mean values of $1-1.5$dSv for any single discharge sector have been inferred from data-constrained glaciological modelling [Tarasov and Peltier, 2006]. For Eurasia, Brendryen et al. [2020] estimates a rate of discharge of 2dSv into the Norwegian Sea and Arctic Ocean from re-assessing Norwegian Sea sediment cores. It is understood that varying scales of freshwater injection can elicit wide ranges in climate behaviour [Roche et al., 2009, Kageyama et al., 2013]. A previous investigation covering a range of freshwater injection fluxes shows that the change in North Atlantic Deep Water (NADW) formation becomes less sensitive to the injection location as fluxes grow larger [Roche et al., 2009], due to an increasing amount of diffusive spread. Furthermore, results from Peltier et al. [2006] and Stouffer et al. [2006] demonstrate that the rate of change in AMOC and Greenland surface air temperature is much stronger for a 10dSv injection compared to that of a 3dSv injection.

The third limitation involves the use of present-day rather than paleo-bathymetry, and especially its effect on ocean gateways. The Bering strait in particular provides the sole connection between the Pacific and the Arctic, and has been shown to have global impacts on ocean circulation in previous studies [e.g. Hu et al., 2007, 2012, 2015]. As such, we also conducted an additional experiment examining the impact of uncertainties in the state of the Bering Strait. While it is clear that the Bering Strait was closed at the time of MWP1A, there is some evidence that it may have been open during the onset of the Younger Dryas [England and Furze, 2008] although the majority of available evidence indicates closure during this time [e.g. Jakobsson et al., 2017]. Hu et al. [2007, 2012, 2015] demonstrate that the transport of freshwater can be strongly affected by the state of the Bering Strait under various background climates, with the effect that a closed Bering Strait leads to a stronger AMOC. Also, when the strait is closed, freshwater injected into the 50-70N band remains in the Arctic Ocean longer and results in a delayed recovery of the AMOC from freshwater forcing. We explore the ambiguity of the Bering Strait for the one key injection region that most likely be affected by its state, the Mackenzie River in the Canadian Arctic.

The goal of this study is to directly address all of these limitations (i.e. unrealistically large volumes of freshwater injection, injection directly onto sites of DWF, and misrepresentation of gateways) via a more realistic experimental design, and to elucidate how these limitations may bias inferences about the connection between glacial runoff and salinity anomalies at sites of deep-water formation. This study provides one of the first assessments to simultaneously address all of these issues, using freshwater injection amounts constrained by the output of a calibrated ensemble of glaciological models (Tarasov and Peltier [2006] and ongoing work) applied to a range of plausible source regions in a suite of simulations that are eddy-permitting over all regions of freshwater transport except the Arctic, where mesoscale eddies tend to have spatial scales of $O(10\text{km})$ or less [Nurser and Bacon, 2014]. We achieve this by assessing the amount of freshwater transported to sites of DWF from the main Northern Hemisphere outlets. Given the importance of specific freshwater injection locations, we separately examine freshwater transported from the major outlet regions for the Northern Hemisphere posited to be important for these types of climate transitions: the Mackenzie River (MAK), Fennoscandia (FEN), the Gulf of St. Lawrence (GSL), and the Gulf of Mexico (GOM).

2.3 Experimental Design

We start our discussion of the experimental design with a brief overview of the model configuration, followed by information regarding the simulations conducted, ending with a discussion of the limitations of our configuration. All of the simulations were performed using the Massachusetts Institute of Technology General Circulation Model [MITgcm, Marshall et al., 1997] coupled global sea-ice/ocean model in a Cubed-Sphere 6x510x510 (CS510) configuration, which provides $\approx$ 18km spatial resolution with 50 vertical levels. This grid geometry and resolution is eddy-resolving to eddy-permitting for all ocean regions equator-ward of 60°N [Chelton et al., 1998, Nurser and Bacon, 2014]. Our configuration is of comparable complexity and resolution to most members of the multi-model ensemble of present-day simulations presented in Hirschi et al. [2020]. This resolution means the model is able to capture small-scale phenomena like coastal boundary currents and mesoscale eddies that are among the primary mechanisms responsible for the transport of terrestrial meltwater discharged into coastal, near-shore, environments [Condron and Winsor, 2012, Hill and Condron, 2014]. Most of the coarser resolution models used in current and previous PMIP and CMIP working groups are unable to do this explicitly [Yang, 2003]. A sample map of daily-mean salinity is shown in Fig. 2.2 in order to illustrate the turbulent characteristics of this model configuration. Generally, using eddy-resolving ocean model configurations results in a better representation (primarily greater current velocities) of small-scale features and a better agreement between models and observations for present day [Hirschi et al., 2020]. As well, some large-scale features, particularly the subpolar gyre, tend to be stronger at eddy-permitting resolutions [Treguier et al., 2005]. An overall increase in the transport speed of tracers at higher resolutions is notable in Weijer et al. [2012]. They find that a passive tracer released from the Greenland ice sheet covers the entirety of the subtropical gyre region within 2 years for a configuration at eddying resolution, whereas the non-eddying configuration of the same ocean model takes up to 5 years to even reach the eastern seaboard of North America. These features show that conducting simulations at eddy-permitting resolutions results in an overall more vigorous transport of glacial runoff relative to coarser, non-eddy-permitting resolutions.

All simulations and relevant setups/forcings are listed in the supplemental table B.1. The freshwater injection experiments were branched from one of two Younger Dryas control simulations, which were themselves initialized from a Last Glacial Maximum (LGM) simulation. The LGM simulation was run for ≈ 20 years using MITGCM and the same boundary conditions as Hill and Condron [2014]. This initial LGM simulation featured LGM bathymetry, sea level 120m lower than present, a glaciated Barents-Kara Sea and Canadian Archipelago, and a closed Bering Strait. The surface forcing used in the LGM simulation included winds, precipitation, 2m atmospheric temperatures, short and longwave radiation, surface runoff, and humidity from the CCSM3 working group's contribution to PMIP2 [Braconnot et al., 2007]. We do not use surface restoration in our experiments. Evaporation is handled internally by the model in the EXF (EXternal Forcing package) based on prescribed precipitation, relative humidity, and surface runoff fields. We used the 3D ocean salinity and temperature fields from the LGM simulation to initialise a control run with Younger Dryas bathymetry (including closed Bering Strait, CBS) and LGM surface forcing, which was integrated forward for an additional 10 years. The open Bering Strait (OBS) Younger Dryas control run was then branched from the CBS run, and both OBS and CBS control runs were integrated forward for an additional 10 years before the freshwater forcing simulations (MAK, FEN, GSL, and GOM) were branched off.

Sea level was adjusted in all Younger Dryas runs to that provided by the sea-level solver component of the Glacial Systems Model of Tarasov et al. [2012] at approx. 13ka. This sea level adjustment is not eustatic as was implemented in Hill and Condron [2014], but included major features which affect the geoid [Mitrovica and Milne, 2003] excepting the rotational component [Milne and Mitrovica, 1998], which has the weakest effect. The largest ensuing ocean gateway change at Younger Dryas compared to LGM is the opening up of the Barents-Kara Seas. Opening both the Barents-Kara Seas and the Bering Strait increases the flow into and out of the glacial

Arctic Ocean.

The freshwater injection runs were run for ≈ 20 years beyond the branch point, during which time the freshwater injection was applied continuously to one of four sites. These sites are the MAK outlet as in Condron and Winsor [2012], the GOM, the GSL, and a region off the coast of Norway in FEN (see table B.1 for more details). Figure 2.2 provides a map showing each injection outlet and the regions over which the salinity averages are calculated. We note that there is overlap between the North Atlantic deep-water formation zone (whose bounds were determined from the mixing region in our model, see Fig. B.1) and the GIN Seas region [whose bounds were obtained from Seidov et al., 2016]. As well, the GIN Seas region is more extensive than if it were constrained to what some models exhibit for their regions of deep-water formation in the GIN Seas. For our experiments, 2dSv of freshwater were continually imposed to be an analogue for the outflow of solid and liquid mass from the Northern Hemisphere ice sheets. This is about one and a half to twice the deglacial ice sheet sourced regional discharge flux (both meltwater and iceberg) when considering the centennial-mean peak for any single discharge region (for North America) in the data-constrained glaciological modelling of Tarasov and Peltier [2006], while being consistent with recent estimations for Fennoscandia [Brendryen et al., 2020]. While this flux is larger than the centennial-mean peak of Tarasov and Peltier [2006] for North America, this injection rate is both typical of previous studies exploring freshwater forcing during the Younger Dryas [such as Kageyama et al., 2013, Gong et al., 2013] and comparable to the Tarasov and Peltier [2006] estimates for glacial runoff, rather than orders of magnitude greater as previously discussed. Treating the outflow as mostly liquid and neglecting any differences in transport between icebergs and freshwater is a reasonable assumption for MAK, GSL and GOM. MAK and GSL liquid discharge is larger than solid discharge for almost all of the post ≈ 18ka deglacial interval, especially during discharge peaks [at least for the nn9894 and nn9927 GLAC1-D variants of Tarasov et al., 2012]. Similarly, all discharge into GOM would have been liquid during this interval. This assumption is likely not applicable for the flow of mass into the Hudson Strait/Baffin Bay region, where the majority of the discharge was in the form of icebergs until 11ka [at least in the data-constrained glaciological modelling of Tarasov et al., 2012]. As such, an investigation exploring the flow of glacial runoff from the Hudson Strait/Baffin Bay region would have to account for the differences in transport of icebergs versus freshwater, so we opted not to test this outlet.

Finally, we draw the readers attention to three possibly significant experimental design limitations: the short duration of the integrations, issues with the surface forcing, and the uncoupled nature of the ocean simulations. These issues do not negate the value of our experiments for the question of freshwater routing during the deglacial interval for the following reasons. Including the spin-up time, the injection runs are at longest ≈ 30 years due to computational constraints. By using the same surface forcing in the Younger Dryas simulations as was used in the LGM simulation and initializing from the temperature and salinity fields of the high-resolution LGM simulations, we were able to reduce the necessary spin-up time and thereby make efficient use of computational resources. As a result, these simulations are of sufficient duration to resolve surface ocean dynamical components [Le Corre et al., 2020], particularly the surface transports of freshwater by the glacial ocean, which is our primary focus here. However, they are of insufficient duration to spin up the deeper regions of the ocean, which require millennia. Cold-starting the YD simulations or initializing from present-day would have required substantially longer spin-up before the surface conditions would have been considered “reasonable approximations to YD.

We expect that the main effects of full equilibration of the deep ocean on the surface transports, relative to our state, would be enhanced overturning in the North Atlantic (see section B.3) and a latitudinal shift of the Gulf Stream. Nevertheless, in order to minimize the impact of any residual spin-up issues on the conclusions of this study (see supplemental section B.2 for a brief discussion on this topic), the OBS and CBS control simulations were also run forward in time by an amount equal to the injection experiments, so all results are interpreted with respect to changes in the control simulations. Further discussion of the implications of the short duration of experiments for the AMOC in particular can be found in the supplemental materials section B.3.

The Younger Dryas surface forcing fields we use are monthly values derived from a coupled climate model configured for LGM using ICE-5G boundary conditions. This ice sheet configuration has been shown to generate more zonal atmospheric circulation patterns than more recent reconstructions of LGM ice sheets [Ullman et al., 2014], and LGM winds are expected to be stronger and more southward-shifted over the North Atlantic than winds during the Younger Dryas [Andres and Tarasov, 2019, Löfverström and Lora, 2017]. These biases are expected to enhance zonal transport in the North Atlantic, as seen in comparison to a sensitivity experiment described in Supplemental Section B.5. Thus, we would expect freshwater transported across the North Atlantic to be routed further south than under forcing which does not have this bias.

Lastly, the configuration used is uncoupled and is lacking ocean-atmosphere interactions and feedback processes. At oceanic mesoscales, uncoupled configurations generally exhibit weaker AMOC relative to coupled configurations [Hirschi et al., 2020], and spatially variable sea surface temperature gradients can result in a wind stress curl which itself can modify sea surface temperatures [Chelton and Xie, 2010]. However, the expected magnitude of this latter effect is small. For example, our injections can result in sea surface temperature differences of several K (see Fig. B.2), which may result in local changes in 10m wind speeds of $\approx \pm 1$m/s [Song et al., 2009].

2.4 Results and Discussion

2.4.1 Control simulation climate

Our two control simulations are very similar, as is expected given they only differ in the state of the Bering Strait. An examination of the salinity fields in Fig. 2.2 and the velocity fields in Fig. B.3 reveals that the Gulf Stream in both simulations is highly zonal. This feature is due to the surface wind forcing as discussed in the Experimental Design section and in Section B.5. The sea ice extent is consistent between simulation years, with maxima varying between $15.75 - 16\text{km}^2$ for the closed Bering Strait (CBS) simulation and $17 - 18\text{km}^2$ for the open Bering Strait (OBS) simulation. Sea ice extent is larger in the OBS simulation due to two features: the expanded ocean area surrounding the open Bering Strait, and enhanced sea ice export, see Fig. B.4. Of note is the large region of sea ice cover off the eastern coast of North America, extending as far south as 40N in the winter (see Fig. 2.2 and Figs. B.3 and B.4). The absence of corresponding sea ice cover over the eastern North Atlantic indicates that there is substantial surface heat transport to this region, despite the zonal Gulf Stream. Both the GIN and Labrador Seas are covered with sea ice during the winter. Due to the extensive sea ice in this model, the main DWF zone lies south of the sea ice edge, in the region between Greenland, Iceland, and the British Isles (see also Fig. B.1). Mixed-layer depths in the Labrador Sea region are much shallower than in the northern North Atlantic and indicate that not much DWF is occurring there.

2.4.2 Freshwater transport paths

We begin our examination of the injection experiments by tracing the pathways of freshwater transport from each injection location. We present in Fig. 2.3 salinity anomalies at the surface for each of the four injection locations. Figures B.6, B.7, B.8, and B.9 show the salinity anomalies at 50m, 100m, and 150m depth. These anomalies are calculated as the differences between averages over the last 5 years of the injection experiments and the corresponding 5 years of the relevant control simulation. From Figures 2.3a, b, and c, it can be seen that freshwater from MAK, FEN, and GSL tends to follow a single, continuous pathway around the Arctic, into the East and then West Greenland Currents, and following the Labrador Current to the northern margin of the Gulf Stream. There, the freshwater accumulates at the separation point of the Gulf Stream from the eastern coast of North America and is advected eastward. At the western coast of Europe, the freshwater is mixed into the northern North Atlantic via the collapse of eddies. The main difference between different outlets along this pathway is the magnitude of freshwater at a given location, which is dependent on how far along this pathway the freshwater has traversed. The longer the pathway to that location, the greater opportunity for freshwater dilution through diffusion and eddy shedding and the greater time to get there. We note that if there is significant freshwater build-up along this pathway, it acts as a barrier, slowing down the transport of freshwater. This is exemplified in the case of the GSL in Fig. 2.3, which has much less freshwater in the eastern North Atlantic than the OBS MAK but much more entrainment of freshwater in the Gulf Stream at the location of its separation from the eastern coast of North America on the western North Atlantic.

The vertical distribution of freshwater along this pathway can be discerned by examining the

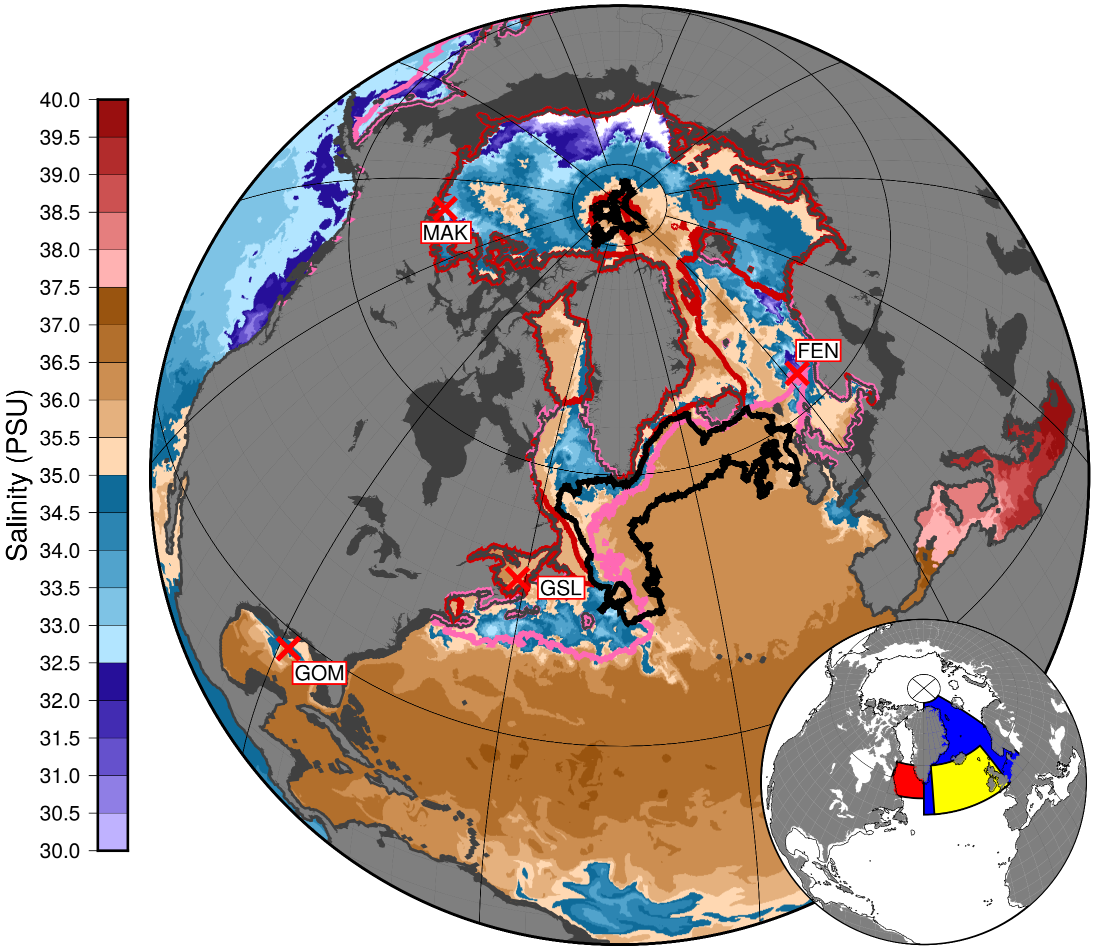

Figure 2.2: Sea surface salinity from a single day (i.e. daily mean data) at the end of the CBS Control run. Present day land-sea mask is shown in light grey while simulation land-sea mask is contoured in a darker grey. The dark red and pink contours denote the minimum and maximum sea ice extent respectively, of at least 15% sea ice coverage calculated over the last 5 years of the simulation. A 1000m mixed layer depth contour from the same time interval as the sea ice extent contours is shown in black. Comparison of the sea ice maximal extent to the mixed layer depth shown in Fig. B.1 (for the OBS case) while the black contour in the current plot indicates that deep convection is just off the outer limit of the sea ice maximum. The strong zonality of the Gulf stream is readily visible in the salinity field. The eddy resolving/permitting nature of the model configuration is evident in the plotted salinity colour bands. Inset panel shows each of the averaging regions highlighted with red for the Labrador Sea region, blue for the GIN Seas region, and yellow for the North Atlantic deep-water formation region.

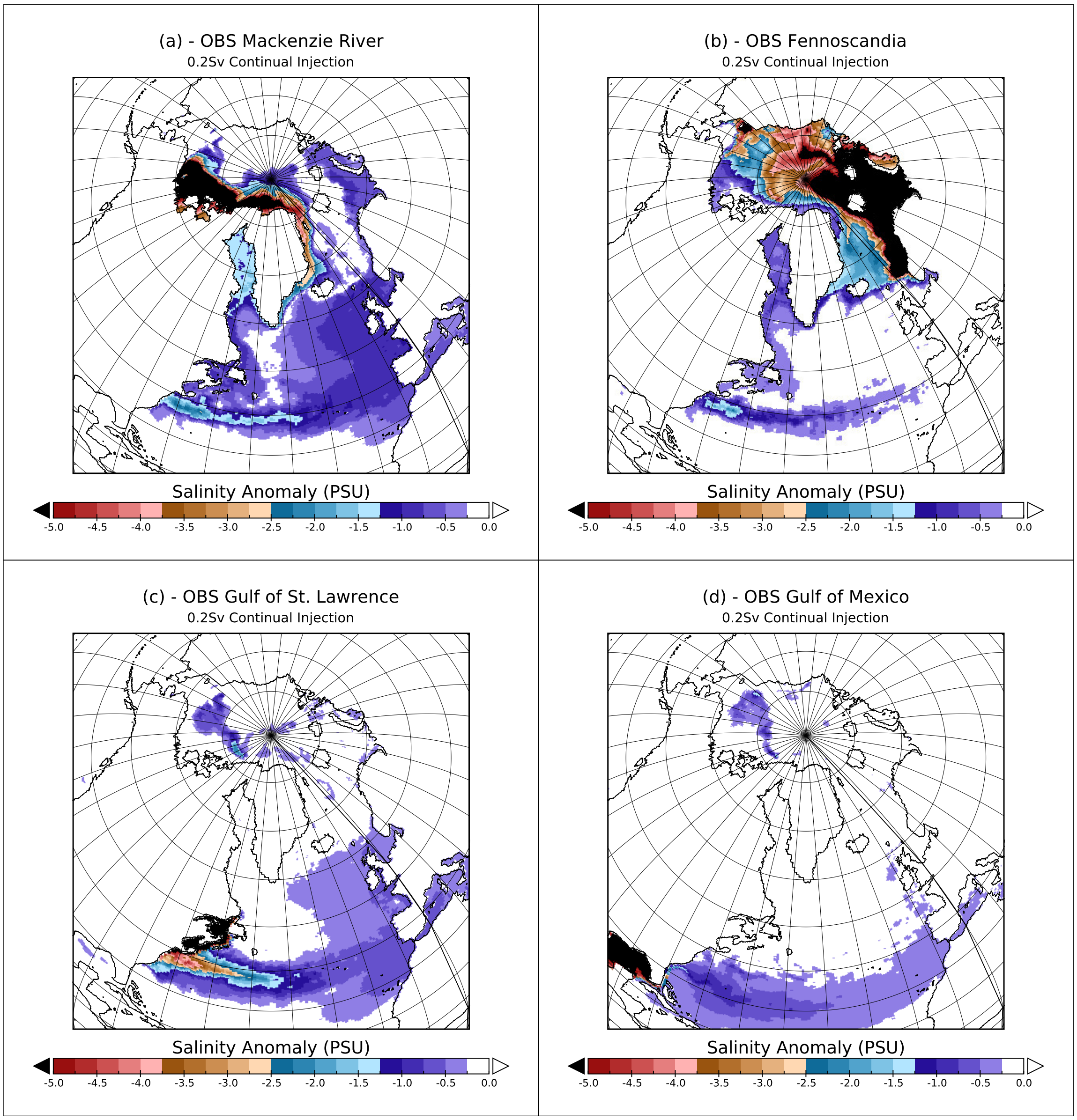

Figure 2.3: Time averaged sea surface salinity anomaly from the last 5 years of each of the OBS injection simulations, the CBS MAK experiment is available in the in Fig. B.5.

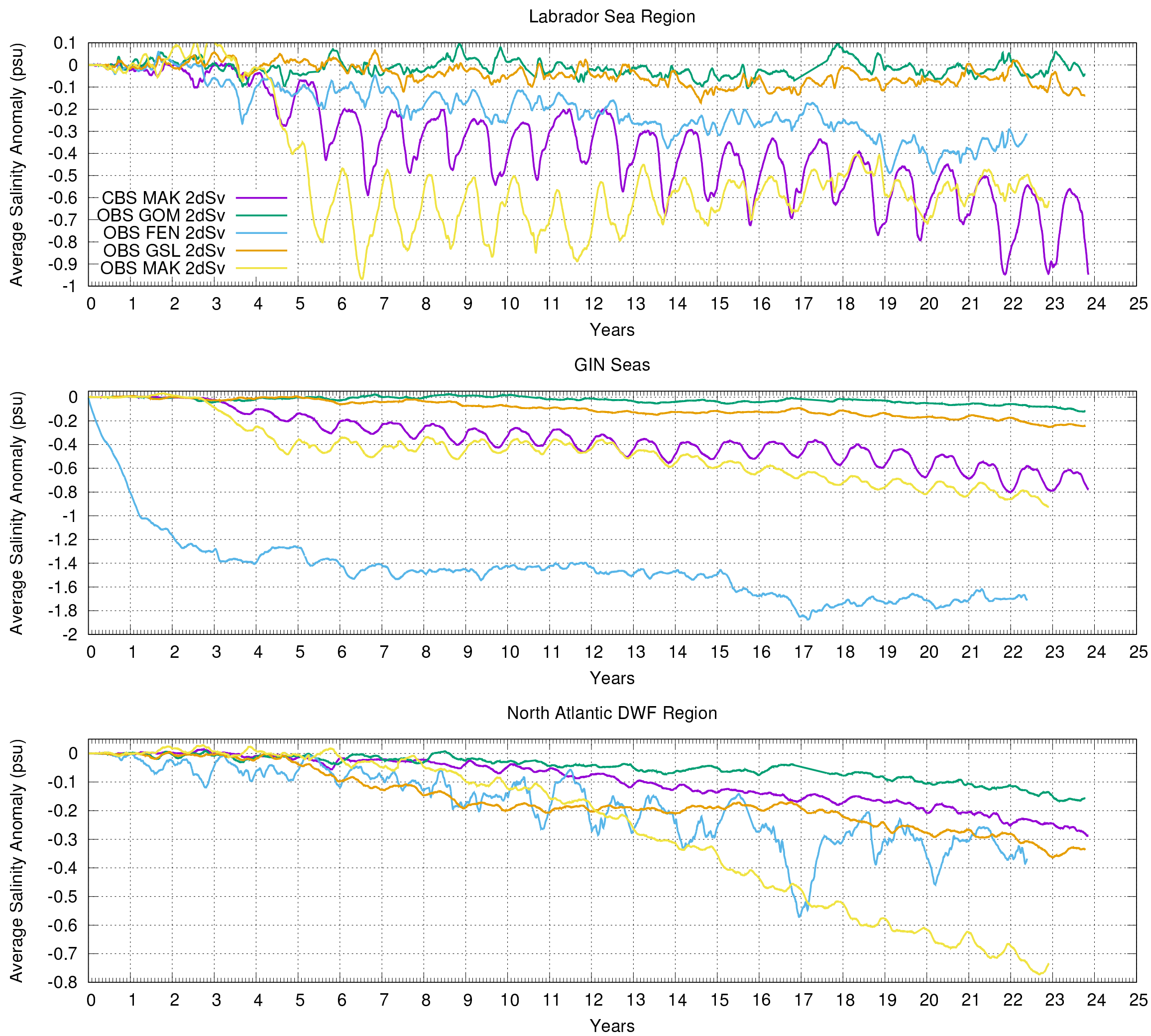

Figure 2.4: Sea surface salinity anomalies for each of our freshwater injection scenarios, calculated relative to their respective control runs. Each injection scenario uses 2dSv of freshwater continually injected at the location of their respective outlets. Each of the averaging regions is shown in the Fig. 2.2.

path traced by freshwater injected at the mouth of the MAK when the Bering Strait is closed as shown in Fig. B.5. Due likely in good part to the lack of wind stirring given perennial sea ice cover, the bulk of the salinity anomaly is located at the surface. As it fills the Canada basin, passes through Fram Strait along the continental shelf of Greenland, and joins the East Greenland Current, the freshwater remains primarily a surface signal. The concentration of freshwater in the surface current decreases dramatically, though, as it travels to the West Greenland Current and into the Labrador Sea and Baffin Bay. The large reduction in surface salinity anomaly along the east coast of Greenland coincides with the appearance of significant salinity anomalies at 100m depth and deeper. This is due to vertical mixing along the continental shelf of Greenland (with a local depth between 150-250m in this configuration) diluting the surface signature while introducing anomalies from the surface to 200m depth.

While the freshwater pathway when the Bering Strait is open in Fig. 2.3A and Fig. B.6 is broadly similar to that when it is closed, there are distinct features that provide insight into the mixing and transport processes occurring in a glacial ocean. Firstly, the Arctic surface salinity anomaly does not spread into the Canada Basin to the same degree, because it is constrained to lie between the Transpolar Current (not noticeably present in the CBS case) and the coast of the Canadian Archipelago. As a result, the surface freshwater concentrations carried along the East Greenland Current and West Greenland Current and into the Labrador Sea are much stronger than when the Bering Strait is closed. However, it is unclear that this contrast would persist if the simulation and injection were long enough to saturate accessible Arctic Ocean sectors. When comparing against OBS/CBS results from Karami et al. [2021] (with the closed Canadian Arctic Archipelago) it is apparent that this contrast is present even in unforced simulations. With an OBS there is less spreading into the subpolar gyre region and the Gulf Stream. When the Bering Strait is open there is a shift southward of the Gulf Stream and overall faster western boundary currents northwards and slower southwards of the Gulf Stream. Secondly, vertical mixing of the surface salinity anomaly appears to start earlier for the OBS case, in the shear zone of the Transpolar Current in the central Arctic. Thus, there is a stronger salinity anomaly at all depths to 150m off the northern coast of Greenland for the OBS case before becoming comparable to one-another along the eastern coast. The primary differences in this pathway from what is observed and simulated for the present is that freshwater sourced from the MAK tends to flow eastward along the coastal margin into the Canadian Archipelago [Fichot et al., 2013, Condron and Winsor, 2012], which is closed at the time of the Younger Dryas.

Freshwater from FEN tends to follow two different routes to DWF regions in Fig. 2.3B and Fig. B.7. One freshwater mass travels directly across the GIN Seas to eastern Greenland, following the surface currents shown in Fig. B.3. The second water mass is initially entrained in the Norwegian current, which carries the freshwater from the injection region northward to flood the Barents-Kara sea. The freshwater then circles around the Arctic basin before being transported southwards back into the GIN Seas and the North Atlantic via the East Greenland Current, following a similar pathway to the MAK. Similarly to the MAK experiments, the freshwater from FEN remains mostly in the top 50m of the water column until it reaches the continental margins of Greenland.

The freshwater from the GSL (Fig. 2.3C and Fig. B.8) gets entrained in the Gulf Stream and only spreads meridionally on the eastern side of the North Atlantic, where it also becomes mixed vertically as it passes over the shallow (200-300m depth) continental margins. As previously noted, the Gulf Stream in our simulations is more zonal than during present day. Given conditions during the Bølling-Allerød were closer to present day rather than full glacial, our configuration may not be an accurate representation of the Gulf Stream just prior to the Younger Dryas. A more modern Gulf Stream, where surface currents are more north-eastward, should result in greater freshwater transport to the North Atlantic DWF zone and GIN Seas, though again with substantial mixing.

Finally, freshwater released into the GOM initially fills that basin before leaking over the Florida shelf and into the Atlantic (see Fig. 2.3D and Fig. B.9). Inflow from the Yucatán Channel acts as a barrier to the freshwater that has filled the GOM, preventing it from expanding southward. The lower sea level around the Younger Dryas results in a more isolated GOM relative to present and helps to sequester the GOM from the Atlantic. As in the other scenarios, the freshwater remains in the uppermost layers as it passes over the Florida shelf. Afterwards, it mixes downward as it travels north and eventually becomes entrained in the Gulf Stream with freshwater present at least 200m deep. In neither the GSL nor the GOM injection is there evidence that the freshwater anomaly is able to cross the Gulf Stream as in Condron and Winsor [2012]. The zonality of the Gulf Stream in this configuration does not affect this conclusion substantially. When the GOM experiment is repeated using modern wind forcing from ERA40 [Uppala et al., 2005] in section B.5, the Gulf Stream is less zonal and closer to present-day observations. Yet, the majority of the freshwater remains primarily in a zonal band, while detectable pockets of freshwater now enter the subpolar North Atlantic. Finally, none of these simulations account for the effect of sediment in the glacial runoff which can lead to bottom-riding (hyperpycnal) flow in [Parsons et al., 2001]. Tarasov and Peltier [2005] suggested that outflow from the Mississippi (GOM) and the GSL at the magnitudes examined here would be heavily laden with sediment, rendering the outflow hyperpycnal with a resultant change in transport. By comparison, the MAK basin has limited surface sediments, and freshwater outflow would be much less affected by this process.

2.4.3 Injection site impact on DWF region salinity

Having traced the pathways of injected freshwater from each outlet, we now examine their respective contributions (Fig. 2.4) to three potential DWF regions: the Labrador Sea, the GIN Seas and the northern North Atlantic. Labrador Sea salinity is most strongly affected by freshwater injected into the MAK outlet. When the Bering strait is open, the peak freshening occurs within 7 years and appears to saturate after 10-15 years. In contrast, closing the Bering Strait reduces the freshening effect to half for the first decade of injection, after which its salinity anomaly gradually surpasses the OBS MAK. The FEN injection generates the next strongest anomaly in the Labrador Sea relative to the MAK outlets. None of the other tested outlets contribute noticeably to salinity anomalies in the Labrador Sea.

The GIN Seas region is most significantly affected by freshwater from the FEN injection, whose salinity anomaly is more than two times larger than that from the next largest contributor, the MAK. The reason for the importance of the FEN injection to GIN Seas salinity is largely due to its being within the averaging domain combined with the local ocean circulation directing FEN freshwater across the region.

Finally, the primary location of deep mixing in these simulations, the northern North Atlantic, is affected by injection into all of the outlets examined here. The strongest contribution is from the OBS MAK injection, which generates approximately twice the freshening of the next strongest outlets, the FEN and GSL. Notably, the salinity anomaly from the FEN injection location exhibits a much larger seasonal cycle compared to that of the other tested outlets. The GSLs freshening effect appears to increase in a step-wise fashion. None of the simulations appear to have reached equilibrium in the North Atlantic, with the exception of FEN. The prominent seasonal cycle of FEN, which exhibits the largest amount of variability on inter-annual timescales, reduces confidence in this conclusion. The CBS Mackenzie sourced simulation has a more delayed response compared to that of the corresponding OBS simulation, as expected with the enhanced boundary currents observed with an OBS, and it never reaches the rate of freshening achieved by the OBS over the duration of these simulations. Note that there is a detectable contribution to the salinity anomaly of the northern North Atlantic region from the GOM, although the salinity signal is not large enough in any single grid cell to be detectable in Fig. B.9. Of all our explored injection scenarios, the GOM scenario has the least impact with regards to salinity change in key DWF regions. The Mississippi River (primary meltwater drainage route to the GOM) therefore offers a possible escape valve for minimizing the impact of terrestrial meltwater injection on DWF, and therefore AMOC, at least on inter-annual to decadal timescales.

For comparison to conventional hosing studies, an order-of-magnitude calculation of the freshening effect of a 1-year 2dSv flux injected into each of the DWF regions (indicated in Fig. 2.2) is worth consideration. We assume that the freshwater displaces existing seawater from the regions, that the injection region is evenly inundated with freshwater, and the freshwater is evenly mixed over the top 50m of the water column. We do not account for the eventual flow of water in or out of the regions. For further details see Section B.6. Using the salinity field from the control run as our initial state, hosing directly onto the Labrador Sea region would result in a -4.2PSU change in salinity, which is more than 4x stronger a freshening effect than any of our equilibrated injection runs. Hosing the GIN Seas region results in a -0.65PSU salinity change, which is very similar to the top layer salinity shown in Fig. 2.4 after 1 year of injecting into the FEN injection location (located within the GIN Seas region). Finally, hosing in the North Atlantic DWF region results in a -1.26PSU salinity change. As in the Labrador Sea region, this represents an approximately 2-4x larger change than observed from any of the injection experiments presented herein.

Our results have significant differences compared to those of Condron and Winsor [2012] and Hill and Condron [2014], which both imposed a large 50dSv flux of freshwater for only the first year of the simulations. The much larger rate of freshwater injection in those studies generated much greater mixing at the boundaries of the coastal boundary currents and led to a greater spreading of the freshwater in the Arctic and Atlantic oceans. Also, the freshwater in Condron and Winsor [2012] and Hill and Condron [2014] is readily transported across the Gulf Stream, routing freshwater from either the GSL or the Hudson Strait to south of Cape Hatteras and into the GOM and vice versa. An examination of the freshwater distributions in Figs. B.5 and B.6 shows none of the overall flooding of the North Atlantic that is present in Condron and Winsor [2012]. The lower but continual flux in the simulations shown here also does not allow freshwater to penetrate the Gulf Stream as effectively by comparison to Condron and Winsor [2012]. Indeed, results from Condron and Hill [2021] indicate that our freshwater flux is not of sufficient magnitude to allow it to penetrate the Gulf Stream, which would require at least a 10 fold increase in flux. As such, the GSL injection delivers, relatively, significantly more freshwater to the GIN Seas and North Atlantic DWF region than the GSL run in Condron and Winsor [2012] despite both a much lower flux and overall volume of freshwater.

Additionally, we can compare our results to Roche et al. [2009] and Lohmann et al. [2020]. The former performed a wide suite of injection experiments using a much lower-resolution model with varying freshwater flux and injection location under LGM boundary conditions. The latter performed a set of 4 injection experiments using a model with enhanced grid resolution over large regions in the Arctic ocean and around the coasts while having the interior Atlantic grid resolution range upwards of 140km via their unstructured mesh approach. Since Roche et al. [2009] did not discuss the salinity signals at DWF sites directly, we interpret the freshening of the GIN Seas and northern North Atlantic DWF regions in this study to be analogous to changes in NADW export from their two sites of DWF. Our results are in broad agreement with both Roche et al. [2009]

and Lohmann et al. [2020] except with regards to freshwater injected into the GOM. Roche et al. [2009] found their GOM injection to generate comparable or greater effects on NADW export than injection from the GSL. The freshwater signal at DWF sites in Lohmann et al. [2020] from GOM was also stronger than in this study. We attribute both differences to the lower resolutions of the Florida Strait and Gulf Stream in those studies [approximately 18 times coarser in Roche et al. [2009] and $\approx 2-3$x coarser in Lohmann et al., 2020]. This lower resolution combined with the much longer duration of simulations in these studies would increase export rates and allow freshwater built up in the GOM time to flow out of the region and freshen the Atlantic. Finally, the higher resolution of the Gulf Stream in our set of simulations appears to make it a more effective barrier to freshwater transport than in either of these studies.

2.4.4 Implications for last deglacial interval

We now present the implications of our results to the routing of runoff during the deglacial interval. The glaciologically-modelled discharge time series from Tarasov and Peltier [2006] indicates there is a steady background discharge from NH ice sheets into the oceans from before Heinrich Event 1 to MWP1A, largely from the Gulf of Mexico. During this time interval, we would expect extensive sea ice over the GIN and Labrador Seas, and thus deep-water formation regions largely aligning with the NADW region in Fig. 2.2. As such, the runoff from Fennoscandia should have had a continual suppressing effect on deep-water formation during this time interval relative to present-day conditions. Examining the RSL data, we see there is almost no change in sea level during this time interval indicating that the freshwater flux is largely in balance with NH ice sheet changes (1dSv over 1000 years contributes $\approx$ 8.8m of eustatic sea level rise).

During the deglacial interval, the first major freshwater flux event is Heinrich Event 1 which is not well represented by our investigation that examines only liquid freshwater. However, we can make some inferences by combining our results with the iceberg modelling results of Hill and Condron [2014], Condron and Hill [2021]. Examining the iceberg distributions from these studies we can conclude that the resulting iceberg meltwater distribution would be most similar to our

Gulf of St. Lawrence outlet experiments, and as such would have one of the larger impacts upon deep-water formation in the North Atlantic. The first major liquid freshwater event we can discuss in the context of our results is MWP1A. It occurs early during the Bølling-Allerød interval, which is associated with rapidly increasing central Greenland temperatures, and increased freshwater discharge to the North Atlantic and brief century-scale minor reductions in AMOC [Obbink et al., 2010]. As MWP1A occurred during the near-interglacial climate state of the Bølling, DWF likely occurred in the GIN Seas. The reconstruction presented in Tarasov and Peltier [2006] largely attributes MWP1A runoff to the Mississippi River along with discharge into the Atlantic (from Newfoundland to Florida, with discharge via the Hudson River in contemporary New York State dominating). Paleoceanographic records from Orca Basin adjacent to the mouth of the Mississippi show the strongest deglacial freshening during this time interval [Broecker et al., 1989]. In contrast, some studies [such as Gregoire et al., 2016] appear to implicate freshwater routed through the Mackenzie River for MWP1A, whereby saddle collapse between the Cordilleran and Laurentide ice sheets is considered as the main mechanism for the rapid increase in outflow and sea level. As we have demonstrated, freshwater routed through the Mackenzie River is expected to have a stronger impact on freshening sites of deep-water formation relative to the Mississippi River, at least on decadal timescales. Similarly, the GSL [and very likely outlets south thereof, such as the Hudson River, Pendleton et al., 2021] also have relatively low impact on salinity over the GIN Seas. Therefore, a dominant North American freshwater discharge from the GSL and outlets south thereof, along with minimal freshwater discharge from the Mackenzie River and Fennoscandia may help to explain the lack of a strong climate system response to the enhanced freshwater input into the ocean during MWP1A.

However, this conclusion has to be understood in the context of the assumptions that went into these results, particularly the treatment of freshwater as an external forcing to the system and not part of a coupled ice-ocean-atmosphere system. It is worth noting that there is no evidence B-A warming occurred in response to a cessation of freshwater forcing [Tarasov and Peltier, 2006], as it was reproduced by in Liu et al. [2009], for example. If the B-A warming occurred as a manifestation of internally driven, Dansgaard-Oeschger-like variability, then it may be that the mechanisms that led to this warming could have also stabilized the AMOC against the freshwater resulting from the warming. It may be a similar mechanism also operated at the transition out of the Y-D and into the Holocene, when runoff is reconstructed to have derived from the GSL, which effectively reached North Atlantic deepwater formation sites in this study. Discerning whether this is indeed possible would require an analysis of the impact of freshwater on spontaneous Dansgaard-Oeschger-like variability, which we leave to future work.

Combining previous work highlighting the importance of glacial runoff from the MAK [Condron and Winsor, 2012, Keigwin et al., 2018], the impact of freshwater from FEN presented in Toucanne et al. [2009], and the results we present here, we conclude that the most plausible sources of glacial runoff to cause rapid cooling, while minimally impacting RSL, would be the Mackenzie River or Fennoscandia. The discharge data presented in Tarasov and Peltier [2006] supports this conclusion with respect to the Mackenzie River outlet. However, our results do not preclude non-linear effects from a short-lived freshwater discharge event from other outlets, such as a large flux/flooding event over a very short time interval [i.e. timescales below the resolution of studies such as Tarasov and Peltier, 2006] as discussed by Broecker [2006], Teller et al. [2002]. Nor does our work address a potential flush of freshwater from anywhere it has accumulated, such as in Baffin Bay for the MAK injections.

2.5 Conclusions

This study provides the first assessment of freshwater transport to deepwater formation regions under Younger Dryas conditions using realistic freshwater injection amounts applied to a range of plausible source regions in a suite of eddy-permitting simulations. We have addressed three main shortcomings in common practice for freshwater injection experiments that inflate the salinity anomalies at locations of DWF. The first shortcoming we address is the injection of freshwater directly over the locations of DWF rather than at its source location to mitigate unresolved O($<$ 50km) oceanic processes known to be important in the transport of glacial runoff. Using our model configuration, we find the transport of freshwater from the coast to sites of deepwater formation leads to a reduction in the effective freshwater forcing. We find in this study that one year of 2dSv injection at the mouth of the MAK (CBS) yields a freshening equivalent to direct regional hosing by amounts of $\approx$ 0.31dSv in the Labrador Sea, $\approx$ 0.33dSv in the northern North Atlantic, and $\approx$ 1.85dSv in the GIN Seas (using the same method and simplifications as in Section 2.4). Thus, while these practices may mitigate the inability of coarse resolution models to adequately resolve the small-scale features that are key to freshwater transport, like boundary currents and mesoscale eddies, applying 2dSv directly into these regions is an inaccurate representation of the transport processes involved. Since non-eddy-permitting models are currently and will likely continue to be used for paleoclimate studies, we are presently exploring better ways to mitigate this problem, the results of which are the subject of an upcoming study and outside the scope of this work.

The second shortcoming is the use of unrealistically large freshwater amounts. We find that limiting freshwater amounts to glaciologically-constrained values results in less diffusive spreading of the freshwater across the North Atlantic. In addition, the lower amounts are unable to traverse the Gulf Stream, isolating the salinity anomalies introduced north and south of the Gulf Stream.

The final shortcoming involves the use of present-day rather than paleo-bathymetry, and especially its effect on the Bering Strait. For the most proximal site to the Bering Strait, the Mackenzie River, we find that the opening of this gateway leads to a faster increase of freshwater export from the Arctic ocean and a larger downstream effect on the salinity of the northern North Atlantic.

We characterize which injection source region has the strongest freshening effect at three different potential deepwater formation (DWF) regions, the Labrador Sea, GIN Seas and northern North Atlantic. For DWF in the northern North Atlantic [most commonly occurring when the climate is in a glacial state with extensive sea ice Braconnot et al., 2011], freshwater introduced into the MAK outlet with an OBS imposes the largest freshening effect. Yet, we detect significant freshening from all injection outlets. For intermediate and DWF in the Labrador Sea, freshwater from the MAK generates the greatest freshening, with FEN having the next largest impact. Opening the Bering Strait approximately doubles the rate of freshening over the first 10 years of MAK injection. For GIN Seas DWF, freshwater from FEN is the strongest contributor to salinity anomalies. The implications of these results to our overarching question of how significant RSL changes, such as occurred during MWP1A, could occur without a consequent effect on DWF rates and climate is that the majority of freshwater from North American Ice Sheets needs to enter the ocean south of the Gulf Stream (along the coast of North America) to minimally impact sites of DWF. As well, the reduction in meridional transport of freshwater across the Gulf Stream observed in our results is a feature which ought to be equally applicable, and considered when not explicitly resolved, for both paleo-climate and future-climate investigations.

Finally, our results raise two questions which we leave to future work. Could a build-up and subsequent flushing (via changing oceanic gateways or changes in perennial sea ice) of freshwater in a partially isolated region, such as Baffin Bay, lead to a delayed onset of cooling after a change in routing or increase in glacial runoff? Additionally, can a transition from a stadial to an interstadial climate provide some means of stabilizing AMOC to the effects of freshwater and thus allow for both increased glacial runoff and increased warming such as seen at the onset of the Bølling-Allerød?

2.6 Acknowledgements

The authors would like to thank the anonymous reviewer and Pasha Karami for their assistance in improving this manuscript during the review process. The authors would also like to thank those at the GNU and Fedora projects,Kernel.org and in particular those responsible for GNU Parallel [Tange, 2011] whose software greatly sped up and streamlined the analysis in this work. This research was enabled in part by support provided by SciNet (www.scinethpc.ca) and Compute Canada (www.computecanada.ca) through both Resources for Research Groups allocations and the Rapid Access Service. This is a contribution to the ArcTrain program, which was supported by the Natural Sciences and Engineering Research Council of Canada. HA was funded by the German Federal Ministry of Education and Research (BMBF) as a Research for Sustainability initiative (FONA) through the project PalMod.

Bibliography

Heather J. Andres and Lev Tarasov. Towards understanding potential atmospheric contributions to abrupt climate changes: characterizing changes to the north atlantic eddy-driven jet over the last deglaciation. *Climate of the Past*, 15(4):16211646, Aug 2019. ISSN 1814-9332. doi: 10.5194/cp-15-1621-2019. URL http://dx.doi.org/10.5194/cp-15-1621-2019.

P. Braconnot, B. Otto-Bliesner, S. Harrison, S. Joussaume, J.-Y. Peterchmitt, A. Abe-Ouchi, M. Crucifix, E. Driesschaert, Th. Fichefet, C. D. Hewitt, and et al. Results of pmip2 coupled simulations of the mid-holocene and last glacial maximum part 1: experiments and large-scale features. *Climate of the Past*, 3(2):261–277, Jun 2007. ISSN 1814-9332. doi: 10.5194/cp-3-261-2007. URL http://dx.doi.org/10.5194/cp-3-261-2007.

P. Braconnot, S.P. Harrison, B. Otto-Bliesner, Ayako Abe-Ouchi, J. Jungclaus, and J.-Y Peterschmitt. The paleoclimate modeling intercomparison project contribution to cmip5. *CLIVAR Exchanges*, 56:15–19, 01 2011.

Jo Brendryen, Haflidi Haflidason, Yusuke Yokoyama, Kristian Agasster Haaga, and Bjarte Hannisdal. Eurasian ice sheet collapse was a major source of meltwater pulse 1a 14,600 years ago. *Nature Geoscience*, 13(5):363368, Apr 2020. ISSN 1752-0908. doi: 10.1038/s41561-020-0567-4. URL http://dx.doi.org/10.1038/s41561-020-0567-4.

W. S. Broecker. Geology: Was the younger dryas triggered by a flood? *Science*, 312(5777):11461148, May 2006. ISSN 1095-9203. doi: 10.1126/science.1123253. URL http://dx.doi.org/10.1126/science.1123253.

Wallace S. Broecker, James P. Kennett, Benjamin P. Flower, James T. Teller, Sue Trumbore, Georges Bonani, and Willy Wolfli. Routing of meltwater from the laurentide ice sheet during the younger dryas cold episode. *Nature*, 341(6240):318321, Sep 1989. ISSN 1476-4687. doi: 10.1038/341318a0. URL http://dx.doi.org/10.1038/341318a0.

Nicolas Brown and Eric D. Galbraith. Hosed vs. unhosed: interruptions of the Atlantic Meridional Overturning Circulation in a global coupled model, with and without freshwater forcing. *Climate of the Past*, 12:1663–1679, 2016. doi: 10.5194/cp-12-1663-2016.

Dudley Chelton and Shang-Ping Xie. Coupled ocean-atmosphere interaction at oceanic mesoscales. *Oceanography*, 23(4):5269, Dec 2010. ISSN 1042-8275. doi: 10.5670/oceanog.2010.05. URL http://dx.doi.org/10.5670/oceanog.2010.05.

Dudley B. Chelton, Roland A. deSzoeke, Michael G. Schlax, Karim El Naggar, and Nicolas Siwertz. Geographical variability of the first baroclinic rossby radius of deformation. *Journal of Physical Oceanography*, 28(3):433460, Mar 1998. ISSN 1520-0485. doi: 10.1175/1520-0485(1998)028⟨0433:

gvotfb⟩2.0.co;2. URL http://dx.doi.org/10.1175/1520-0485(1998)028<0433:GVOTFB>2.0.CO;2.

A. Condron and P. Winsor. Meltwater routing and the younger dryas. *Proceedings of the National Academy of Sciences*, 109(49):1992819933, Nov 2012. ISSN 1091-6490. doi: 10.1073/pnas.1207381109. URL http://dx.doi.org/10.1073/pnas.1207381109.

Alan Condron and Jenna C. Hill. Timing of iceberg scours and massive ice-rafting events in the subtropical north atlantic. *Nature Communications*, 12(1), Jun 2021. ISSN 2041-1723. doi: 10.1038/s41467-021-23924-0. URL http://dx.doi.org/10.1038/s41467-021-23924-0.

Pierre Deschamps, Nicolas Durand, Edouard Bard, Bruno Hamelin, Gilbert Camoin, Alexander L. Thomas, Gideon M. Henderson, Jun'ichi Okuno, and Yusuke Yokoyama. Ice-sheet collapse and sea-level rise at the bølling warming 14,600 years ago. *Nature*, 483(7391):559–564, Mar 2012. ISSN 1476-4687. doi: 10.1038/nature10902. URL http://dx.doi.org/10.1038/nature10902.

John H. England and Mark F.A. Furze. New evidence from the western canadian arctic archipelago for the resubmergence of bering strait. *Quaternary Research*, 70(1):6067, Jul 2008. ISSN 1096-0287. doi: 10.1016/j.yqres.2008.03.001. URL http://dx.doi.org/10.1016/j.yqres.2008.03.001.

Richard G. Fairbanks. A 17,000-year glacio-eustatic sea level record: influence of glacial melting rates on the younger dryas event and deep-ocean circulation. *Nature*, 342(6250):637642, Dec 1989. ISSN 1476-4687. doi: 10.1038/342637a0. URL http://dx.doi.org/10.1038/342637a0.

Cdric G. Fichot, Karl Kaiser, Stanford B. Hooker, Rainer M. W. Amon, Marcel Babin, Simon Blanger, Sally A. Walker, and Ronald Benner. Pan-arctic distributions of continental runoff in the arctic ocean. *Scientific Reports*, 3(1), Jan 2013. ISSN 2045-2322. doi: 10.1038/srep01053. URL http://dx.doi.org/10.1038/srep01053.

Xun Gong, Gregor Knorr, Gerrit Lohmann, and Xu Zhang. Dependence of abrupt atlantic meridional ocean circulation changes on climate background states. *Geophysical Research Letters*, 40(14):36983704, Jul 2013. ISSN 0094-8276. doi: 10.1002/grl.50701. URL http://dx.doi.org/10.1002/grl.50701.

Lauren J. Gregoire, Bette Otto-Bliesner, Paul J. Valdes, and Ruza Ivanovic. Abrupt blling warming and ice saddle collapse contributions to the meltwater pulse 1a rapid sea level rise. *Geophysical Research Letters*, 43(17):91309137, Sep 2016. ISSN 0094-8276. doi: 10.1002/2016gl070356. URL http://dx.doi.org/10.1002/2016GL070356.

T. Hanebuth. Rapid flooding of the sunda shelf: A late-glacial sea-level record. *Science*, 288 (5468):10331035, May 2000. ISSN 1095-9203. doi: 10.1126/science.288.5468.1033. URL http://dx.doi.org/10.1126/science.288.5468.1033.

Jenna C. Hill and Alan Condron. Subtropical iceberg scours and meltwater routing in the deglacial western north atlantic. *Nature Geoscience*, 7(11):806810, Oct 2014. ISSN 1752-0908. doi: 10.1038/ngeo2267. URL http://dx.doi.org/10.1038/ngeo2267.

Jol J.M. Hirschi, Bernard Barnier, Claus Bning, Arne Biastoch, Adam T. Blaker, Andrew Coward, Sergey Danilov, Sybren Drijfhout, Klaus Getzlaff, Stephen M. Griffies, and et al. The atlantic meridional overturning circulation in high-resolution models. *Journal of Geophysical Research: Oceans*, 125(4), Apr 2020. ISSN 2169-9291. doi: 10.1029/2019jc015522. URL http://dx.doi.org/10.1029/2019JC015522.

A. Hu, G. A. Meehl, W. Han, A. Timmermann, B. Otto-Bliesner, Z. Liu, W. M. Washington, W. Large, A. Abe-Ouchi, M. Kimoto, and et al. Role of the bering strait on the hysteresis of the ocean conveyor belt circulation and glacial climate stability. *Proceedings of the National Academy of Sciences*, 109(17):64176422, Apr 2012. ISSN 1091-6490. doi: 10.1073/pnas.1116014109. URL http://dx.doi.org/10.1073/pnas.1116014109.

Aixue Hu, Gerald A. Meehl, and Weiqing Han. Role of the bering strait in the thermohaline circulation and abrupt climate change. *Geophysical Research Letters*, 34(5), Mar 2007. ISSN 0094-8276. doi: 10.1029/2006gl028906. URL http://dx.doi.org/10.1029/2006GL028906.

Aixue Hu, Gerald A. Meehl, Weiqing Han, Bette Otto-Bliestner, Ayako Abe-Ouchi, and Nan Rosenbloom. Effects of the bering strait closure on amoc and global climate under different background climates. *Progress in Oceanography*, 132:174196, Mar 2015. ISSN 0079-6611. doi: 10.1016/j.pocean.2014.02.004. URL http://dx.doi.org/10.1016/j.pocean.2014.02.004.

Martin Jakobsson, Christof Pearce, Thomas M. Cronin, Jan Backman, Leif G. Anderson, Natalia Barrientos, Göran Björk, Helen Coxall, Agatha de Boer, Larry A. Mayer, and et al. Post-glacial flooding of the bering land bridge dated to 11 cal ka bp based on new geophysical and sediment records. *Climate of the Past*, 13(8):991–1005, Aug 2017. ISSN 1814-9332. doi: 10.5194/cp-13-991-2017. URL http://dx.doi.org/10.5194/cp-13-991-2017.

M. Kageyama, U. Merkel, B. Otto-Bliesner, M. Prange, A. Abe-Ouchi, G. Lohmann, R. Ohgaito, D. M. Roche, J. Singarayer, D. Swingedouw, and et al. Climatic impacts of fresh water hosing under last glacial maximum conditions: a multi-model study. *Climate of the Past*, 9(2):935953, Apr 2013. ISSN 1814-9332. doi: 10.5194/cp-9-935-2013. URL http://dx.doi.org/10.5194/cp-9-935-2013.

Mehdi Pasha Karami, Paul G. Myers, Anne de Vernal, L. Bruno Tremblay, and Xianmin Hu. The role of arctic gateways on sea ice and circulation in the arctic and north atlantic oceans: a sensitivity study with an ocean-sea-ice model. *Climate Dynamics*, May 2021. ISSN 1432-0894. doi: 10.1007/s00382-021-05798-6. URL http://dx.doi.org/10.1007/s00382-021-05798-6.

L. D. Keigwin, S. Klotsko, N. Zhao, B. Reilly, L. Giosan, and N. W. Driscoll. Deglacial floods in the Beaufort Sea preceded Younger Dryas cooling. *Nature Geoscience*, 11:599–604, 2018. doi: 10.1038/s41561-018-0169-6.

P. Kindler, M. Guillevic, M. Baumgartner, J. Schwander, A. Landais, and M. Leuenberger. Temperature reconstruction from 10 to 120 kyr b2k from the ngrip ice core. *Climate of the Past*, 10(2):887902, Apr 2014. ISSN 1814-9332. doi: 10.5194/cp-10-887-2014. URL http://dx.doi.org/10.5194/cp-10-887-2014.

Hannah Kleppin, Markus Jochum, Bette Otto-Bliesner, Christine A. Shields, and Stephen Yeager. Stochastic atmospheric forcing as a cause of Greenland climate transitions. *Journal of Climate*, 28:7741–7764, 2015. doi: 10.1175/JCLI-D-14-00728.1.

Marlene Klockmann, Uwe Mikolajewicz, and Jochem Marotzke. Two AMOC states in response to decreasing greenhouse gas concentrations in the coupled climate model MPI-ESM. *Journal of Climate*, 31:7969–7985, 2018. doi: 10.1175/JCLI-D-17-0859.1.

Mathieu Le Corre, Jonathan Gula, and Anne-Marie Trguier. Barotropic vorticity balance of the north atlantic subpolar gyre in an eddy-resolving model. *Ocean Science*, 16(2):451468, Apr 2020. ISSN 1812-0792. doi: 10.5194/os-16-451-2020. URL http://dx.doi.org/10.5194/os-16-451-2020.

Z. Liu, B. L. Otto-Bliesner, F. He, E. C. Brady, R. Tomas, P. U. Clark, A. E. Carlson, J. Lynch-Stieglitz, W. Curry, E. Brook, and et al. Transient simulation of last deglaciation with a new mechanism for bolling-allerod warming. *Science*, 325(5938):310314, Jul 2009. ISSN 1095-9203. doi: 10.1126/science.1171041. URL http://dx.doi.org/10.1126/science.1171041.

Marcus Löfverström and Juan M. Lora. Abrupt regime shifts in the north atlantic atmospheric circulation over the last deglaciation. *Geophysical Research Letters*, 44(15):80478055, Aug 2017. ISSN 0094-8276. doi: 10.1002/2017gl074274. URL http://dx.doi.org/10.1002/2017GL074274.

Gerrit Lohmann, Martin Butzin, Nina Eissner, Xiaoxu Shi, and Christian Stepanek. Abrupt climate and weather changes across time scales. *Paleoceanography and Paleoclimatology*, 35(9), Sep 2020. ISSN 2572-4525. doi: 10.1029/2019pa003782. URL http://dx.doi.org/10.1029/2019PA003782.

Syukuro Manabe and Ronald J. Stouffer. Coupled ocean-atmosphere model response to freshwater input: Comparison to younger dryas event. *Paleoceanography*, 12(2):321336, Apr 1997. ISSN 0883-8305. doi: 10.1029/96pa03932. URL http://dx.doi.org/10.1029/96PA03932.

John Marshall, Alistair Adcroft, Chris Hill, Lev Perelman, and Curt Heisey. A finite-volume, incompressible navier stokes model for studies of the ocean on parallel computers. *Journal of Geophysical Research: Oceans*, 102(C3):57535766, Mar 1997. ISSN 0148-0227. doi: 10.1029/96jc02775. URL http://dx.doi.org/10.1029/96JC02775.

Glenn A. Milne and Jerry X. Mitrovica. Postglacial sea-level change on a rotating earth. *Geophysical Journal International*, 133(1):119, Apr 1998. ISSN 1365-246X. doi: 10.1046/j.1365-246x.1998.1331455.x. URL http://dx.doi.org/10.1046/j.1365-246X.1998.1331455.x.

Jerry X. Mitrovica and Glenn A. Milne. On post-glacial sea level: I. general theory. *Geophysical Journal International*, 154(2):253267, Aug 2003. ISSN 1365-246X. doi: 10.1046/j.1365-246x.2003.01942.x. URL http://dx.doi.org/10.1046/j.1365-246X.2003.01942.x.

A. J. G. Nurser and S. Bacon. The rossby radius in the arctic ocean. *Ocean Science*, 10(6):967975, Nov 2014. ISSN 1812-0792. doi: 10.5194/os-10-967-2014. URL http://dx.doi.org/10.5194/os-10-967-2014.

Elizabeth A. Obbink, Anders E. Carlson, and Gary P. Klinkhammer. Eastern north american freshwater discharge during the bølling-allerød warm periods. *Geology*, 38(2):171174, Feb 2010. ISSN 0091-7613. doi: 10.1130/g30389.1. URL http://dx.doi.org/10.1130/G30389.1.

Bette L. Otto-Bliesner and Esther C. Brady. The sensitivity of the climate response to the magnitude and location of freshwater forcing: last glacial maximum experiments. *Quaternary Science Reviews*, 29(1-2):5673, Jan 2010. ISSN 0277-3791. doi: 10.1016/j.quascirev.2009.07.004. URL http://dx.doi.org/10.1016/j.quascirev.2009.07.004.

Jeffrey D. Parsons, John W. M. Bush, and James P. M. Syvitski. Hyperpycnal plume formation from riverine outflows with small sediment concentrations. *Sedimentology*, 48(2):465478, Apr 2001. ISSN 1365-3091. doi: 10.1046/j.1365-3091.2001.00384.x. URL http://dx.doi.org/10.1046/j.1365-3091.2001.00384.x.

W. R. Peltier and G. Vettoretti. Dansgaard-Oeschger oscillations predicted in a comprehensive model of glacial climate: A "kicked" salt oscillator in the Atlantic. *Geophysical Research Letters*, 41:7306–7313, 2014. doi: 10.1002/2014GL061413.

W. R. Peltier, G. Vettoretti, and M. Stastna. Atlantic meridional overturning and climate response to arctic ocean freshening. *Geophysical Research Letters*, 33(6):n/a–n/a, 2006. ISSN 1944-8007. doi: 10.1029/2005GL025251. URL http://dx.doi.org/10.1029/2005GL025251. L06713.

Simon Pendleton, Alan Condron, and Jeffrey Donnelly. The potential of hudson valley glacial floods to drive abrupt climate change. *Communications Earth & Environment*, 2(1), Aug 2021. ISSN 2662-4435. doi: 10.1038/s43247-021-00228-1. URL http://dx.doi.org/10.1038/s43247-021-00228-1.

Didier M. Roche, Ane P. Wiersma, and Hans Renssen. A systematic study of the impact of freshwater pulses with respect to different geographical locations. *Climate Dynamics*, 34(7-8):9971013, May 2009. ISSN 1432-0894. doi: 10.1007/s00382-009-0578-8. URL http://dx.doi.org/10.1007/s00382-009-0578-8.

Dan Seidov, Olga K. Baranova, Mathew Biddle, Timothy P. Boyer, Daphne R. Johnson, Alexey V. Mishonov, Christopher Paver, and Melissa Zweng. Greenland-Iceland-Norwegian Seas Regional Climatology (NCEI Accession 0112824). . 2016. doi: doi:10.7289/V5GT5K30.

Qingtao Song, Dudley B. Chelton, Steven K. Esbensen, Nicolai Thum, and Larry W. ONeill. Coupling between sea surface temperature and low-level winds in mesoscale numerical models. *Journal of Climate*, 22(1):146164, Jan 2009. ISSN 0894-8755. doi: 10.1175/2008jcli2488.1. URL http://dx.doi.org/10.1175/2008JCLI2488.1.

R. J. Stouffer, J. Yin, J. M. Gregory, K. W. Dixon, M. J. Spelman, W. Hurlin, A. J. Weaver, M. Eby, G. M. Flato, H. Hasumi, and et al. Investigating the causes of the response of the thermohaline circulation to past and future climate changes. *Journal of Climate*, 19(8):13651387, Apr 2006. ISSN 1520-0442. doi: 10.1175/jcli3689.1. URL http://dx.doi.org/10.1175/JCLI3689.1.

O. Tange. GNU Parallel - The Command-Line Power Tool. *;login: The USENIX Magazine*, 36(1):42–47, Feb 2011. URL http://www.gnu.org/s/parallel.

Lev Tarasov and W.R. Peltier. Arctic freshwater forcing of the younger dryas cold reversal. *Nature*, 435(7042):662665, Jun 2005. ISSN 1476-4687. doi: 10.1038/nature03617. URL http://dx.doi.org/10.1038/nature03617.

Lev Tarasov and W.R. Peltier. A calibrated deglacial drainage chronology for the north american continent: evidence of an arctic trigger for the younger dryas. *Quaternary Science Reviews*, 25(7-8):659688, Apr 2006. ISSN 0277-3791. doi: 10.1016/j.quascirev.2005.12.006. URL http://dx.doi.org/10.1016/j.quascirev.2005.12.006.

Lev Tarasov, Arthur S. Dyke, Radford M. Neal, and W.R. Peltier. A data-calibrated distribution of deglacial chronologies for the north american ice complex from glaciological modeling. *Earth and Planetary Science Letters*, 315316:30 – 40, 2012. ISSN 0012-821X. doi: http://dx.doi.org/10.1016/j.epsl.2011.09.010. URL http://www.sciencedirect.com/science/article/pii/S0012821X11005243. Sea Level and Ice Sheet Evolution: A {PALSEA} Special Edition.

James T Teller, David W Leverington, and Jason D Mann. Freshwater outbursts to the oceans from glacial lake agassiz and their role in climate change during the last deglaciation. *Quaternary Science Reviews*, 21(8-9):879–887, 2002.

S. Toucanne, S. Zaragosi, J.F. Bourillet, M. Cremer, F. Eynaud, B. Van Vliet-Lano, A. Penaud, C. Fontanier, J.L. Turon, and E. Cortijo. Timing of massive fleuve manche discharges over the last 350kyr: insights into the european ice-sheet oscillations and the european drainage network from mis 10 to 2. *Quaternary Science Reviews*, 28(13-14):12381256, Jun 2009. ISSN 0277-3791.

doi: 10.1016/j.quascirev.2009.01.006. URL http://dx.doi.org/10.1016/j.quascirev.2009.01.006.

A. M. Treguier, S. Theetten, E. P. Chassignet, T. Penduff, R. Smith, L. Talley, J. O. Beismann, and C. Bning. The north atlantic subpolar gyre in four high-resolution models. *Journal of Physical Oceanography*, 35(5):757774, May 2005. ISSN 0022-3670. doi: 10.1175/jpo2720.1. URL http://dx.doi.org/10.1175/JPO2720.1.

D. J. Ullman, A. N. LeGrande, A. E. Carlson, F. S. Anslow, and J. M. Licciardi. Assessing the impact of laurentide ice sheet topography on glacial climate. *Climate of the Past*, 10(2):487507, Mar 2014. ISSN 1814-9332. doi: 10.5194/cp-10-487-2014. URL http://dx.doi.org/10.5194/cp-10-487-2014.

S. M. Uppala, P. W. KÅllberg, A. J. Simmons, U. Andrae, V. Da Costa Bechtold, M. Fiorino, J. K. Gibson, J. Haseler, A. Hernandez, G. A. Kelly, and et al. The era-40 re-analysis. *Quarterly Journal of the Royal Meteorological Society*, 131(612):29613012, Oct 2005. ISSN 1477-870X. doi: 10.1256/qj.04.176. URL http://dx.doi.org/10.1256/qj.04.176.

Guido Vettoretti and W. Richard Peltier. Thermohaline instability and the formation of glacial North Atlantic super polynyas at the onset of Dansgaard-Oeschger warming events. *Geophysical Research Letters*, 43:5336–5344, 2016. doi: 10.1002/2016GL068891.

W. Weijer, M. E. Maltrud, M. W. Hecht, H. A. Dijkstra, and M. A. Kliphuis. Response of the atlantic ocean circulation to greenland ice sheet melting in a strongly-eddying ocean model. *Geophysical Research Letters*, 39(9):n/an/a, May 2012. ISSN 0094-8276. doi: 10.1029/2012gl051611. URL http://dx.doi.org/10.1029/2012GL051611.

Jiayan Yang. On the importance of resolving the western boundary layer in wind-driven ocean general circulation models. *Ocean Modelling*, 5(4):357379, Jan 2003. ISSN 1463-5003. doi: 10.1016/s1463-5003(02)00058-6. URL http://dx.doi.org/10.1016/S1463-5003(02)00058-6.

Xiao Zhang, Matthias Prange, Ute Merkel, and Michael Schulz. Instability of the atlantic overturning circulation during marine isotope stage 3. *Geophysical Research Letters*, 41(12):42854293, Jun 2014. ISSN 0094-8276. doi: 10.1002/2014gl060321. URL http://dx.doi.org/10.1002/2014GL060321.

Xu Zhang, Gregor Knorr, Gerrit Lohmann, and Stephen Barker. Abrupt North Atlantic circulation changes in response to gradual CO_2 forcing in a glacial climate state. *Nature Geoscience*, 10: 518–524, 2017. doi: 10.1038/NGEO2974.

Chapter 3

Exploring the Glacial Climate System Response to a Range of Freshwater Representations: Hosing, Regional, and Freshwater Fingerprints

Exploring the Glacial Climate System Response to a Range of Freshwater Representations: Hosing, Regional, and Freshwater Fingerprints

Ryan Love[1], Heather J. Andres[1], Xu Zhang[5,6], Alan Condron[2], Gerrit Lohmann[3,4], and Lev Tarasov[1]

[1]Department of Physics and Physical Oceanography, Memorial University of Newfoundland, St. John's, Newfoundland, Canada
[2]Geology & Geophysics, Woods Hole Oceanographic Institution, Woods Hole, Massachusetts, USA
[3]Group of Alpine Paleoecology and Human Adaptation (ALPHA), State Key Laboratory of Tibetan Plateau Earth System, Resources and Environment (TPESRE), Institute of Tibetan Plateau Research, Chinese Academy of Sciences, Beijing 100101, China
[4]Department of Environmental Physics & MARUM, University of Bremen, Bremen, Germany
[5]Group of Alpine Paleoecology and Human Adaptation (ALPHA), State Key Laboratory of Tibetan Plateau Earth System, Resources and Environment (TPESRE), Institute of Tibetan Plateau Research, Chinese Academy of Sciences, Beijing 100101, China
[6]Key Laboratory of Western Chinas Environmental Systems (Ministry of Education), College of Earth and Environmental Sciences, Lanzhou University, Lanzhou, 730000, China

3.1 Abstract

Freshwater, in the form of terrestrial runoff, is hypothesized to play a critical role in centennial to millennial scale climate variability like Dansgaard Oeschger events and the Younger Dryas, and it may play a central role in future climate change as ice sheet and glacier melt accelerates. Freshwater Hosing (i.e. injection across wide bands in the North Atlantic) is typically used as a means-to-an-end in eliciting a strong thermohaline circulation and climate response when investigating both past and future climate change, with little to no regard to other roles that freshwater plays in a complex coupled climate environment. We provide an alternative method for freshwater injection, our freshwater fingerprint, that is applicable for both glacial and river runoff which captures some of the small-scale behaviour that is not resolved in current paleoclimate models. We evaluate this method and compare against the Hosing methodology by addressing three primary questions. Firstly, where is freshwater routed at moderate resolution and is the use of a reduced effective Hosing justified? Secondly, does the freshwater fingerprint method capture eddy permitting behaviour? Thirdly, how do climate impacts vary between different forms of freshwater injection?

We find that freshwater released at the Mackenzie (MAK) and Fennoscandia (FEN) in a coarse resolution model results in similar distributions to their eddy permitting counterparts but generally do not travel as far downstream for the same time interval resulting in a relative time delay. Comparatively, freshwater released from the Mississippi River (GOM) and within the Gulf of St. Lawrence (GSL) demonstrates large-scale differences in their coarse resolution vs. eddy permitting distributions. Despite low sensitivity of AMOC to differences between our different injection methods, Hosing the North Atlantic results in stronger and earlier sea ice growth and surface cooling vs. more realistic methods (i.e. regional injection or fingerprint methods) , thereby over-representing the impact of freshwater in the climate system. For our coarse resolution FEN and MAK regional injections, we obtain AMOC changes comparable with that expected from the freshening observed in eddy permitting versions of the experiments. However, freshwater from the GOM gives rise to larger AMOC changes than freshwater from the GSL contrary to the eddy permitting experiments. When instead we use the freshwater fingerprint method, this relationship between GOM and GSL

sourced freshwater is reversed and the coarse resolution response aligns with the eddy permitting response. This reversal demonstrates that we are able to emulate some of the behaviour present at the eddy permitting scale in our coarse resolution configuration. Finally, given comparable AMOC responses between both the fingerprint and regional injection vs Hosing, we conclude that future investigations can mitigate the simplification of North Atlantic Hosing while still obtaining the desired results (i.e. large scale cooling and AMOC reduction) without exaggerating these same climate impacts.

3.2 Introduction

Ice caps, glaciers, and ice sheets are very likely to have an increased contribution to global-mean sea level under projected and current anthropogenic warming [Church et al., 2013, DeConto and Pollard, 2016], and most of this glacial melt enters the world's oceans in the form of freshwater. Polar amplification of anthropogenic climate change is likely to preferentially increase runoff at high latitudes [Collins et al., 2013], resulting in freshwater from Greenland continuing to be released near Northern Hemisphere sites of deepwater formation over the next decades and possibly centuries [Liu et al., 2017]. While preliminary evidence shows increasing runoff from Greenland will not be the dominant driver of Atlantic Meridional Overturning Circulation (AMOC) changes in the future [Ackermann et al., 2020], the AMOC is the weakest it has been in nearly two millennia., with the decrease in strength occurring mainly since midway through the 20th century [Caesar et al., 2021]. This decrease in AMOC is coincident with the ongoing decrease in terrestrial ice volume [Dyurgerov et al., 2005] as well as other major features of anthropogenic climate change, e.g. thermosteric sea level rise [Church et al., 2013], and may be associated with a complete loss of AMOC stability [Boers, 2021]. The paleoclimate archive indicates that freshwater entering the oceans can have a profound impact on global climate through the AMOC and associated northward heat transport by causing hemisphere-wide cooling on the order of decades to centuries, e.g. the Younger Dryas period [Teller et al., 2002] and the 8.2kaBP cooling event [Hoffman et al., 2012]. Since freshwater runoff has been an important contributor to climate variability in the past, predicting its potential contributions to climate variability in the future demands that we understand its role in the climate system.

Surface runoff, glacially sourced or otherwise, is understood to affect deep-water formation by producing a freshwater cap over regions of deep-water formation that stabilizes the water column. The ensuing reduction in vertical convection inhibits the generation of deep water, which results in a slowdown of AMOC and resultantly decreases northward surface heat transport. This reduction of heat transport results in abrupt (O(decades)) Northern Hemisphere-wide cooling which is inferred from various proxies, most notably the **GR**eenland **I**ce core **P**roject (GRIP) deep ice core record (see Kindler et al. [2014] for a recent temperature reconstruction). This mechanism may not be limited to glacial climates with continental-scale ice sheets over North America and Europe. Early model studies demonstrated this mechanism occurred in models configured under present day or pre-industrial configurations (e.g. Peltier et al. [2006]) and AMOC hysteresis under freshwater forcing is still a subject of study using contemporary climate models under present day climate Jackson and Wood [2018]. However, theoretical considerations indicate that freshwater can also have other effects on the climate system. For example, one would expect a fresher surface ocean to enhance sea ice growth (with associated climate system feedbacks), given one of the direct effects of freshening of the oceans surface is a rise in the freezing point of water[1]. Another important factor for future climate change is that changes in surface salinity and mixing can affect carbon dioxide uptake by the ocean [Rippeth et al., 2014]. Finally, freshwater is not a passive tracer, salinity directly affects both density and the relationship between density and temperature, thus affecting density driven circulation Stommel [1961].

The role of freshwater in simulated coupled climate systems has been explored by a large number of studies (some foundational examples are Stocker et al. [1992], Manabe and Stouffer [1997], Stouffer et al. [2006]), but they mostly focus on its effect on the AMOC. Furthermore, many studies use freshwater as a means-to-an-end to generate an AMOC response and achieve rapid climate change by releasing the freshwater directly into a band in the North Atlantic and bypassing

[1]there is an $\approx$ 2C increase in freezing point for completely fresh water (0psu vs. sea water (35psu), yielding a rate of change in freezing point per salinity change of ≈ -0.055C/psu, where freshening generates a negative salinity change [Doherty and Kester, 1974]

its transport from continental sources. These Hosing type studies[2] implicitly treat freshwater as a passive tracer until it reaches regions of deep-water formation, and they neglect other potential effects of the freshwater introduction (such as turbulent mixing with the ambient water as the meltwater initially enters coastal environments). As well, in some studies where Hosing is invoked, it is set up to replace either glacial runoff (e.g. Arctic-derived freshwater as in Peltier et al. [2006], or generalized ice-sheet runoff [He, 2011]) or freshwater sourced from iceberg armadas (i.e. the Ruddiman Belt as in TRACE21ka [He, 2011]). These assumptions likely amplify the expected response of continental runoff on deepwater formation and raise the question: do we understand the role of freshwater in the climate system fully enough to make robust predictions of climate change in the near future or distant past, even more so when relying on such simplified forms of forcing?

The primary justification for applying freshwater directly in the regions of deep-water formation is the inability of moderate-resolution ocean models, such as are commonly used in Earth System Models, to resolve the small-scale features (like boundary currents and mesoscale eddies) that are important to the transport and mixing of freshwater. Given the centennial to millennial timescales of many future or past climate experiments performed using these models, employing eddy-permitting ocean model configurations is not practical. However, previous work by Condron and Winsor [2012], Hill and Condron [2014], Love et al. [2021] demonstrates that the traditional Hosing band [Condron and Winsor, 2012] is not reflective of where freshwater is actually transported when released from runoff outlets such as the Mackenzie River. Love et al. [2021] shows as much as $50 - 75\%$ of freshwater might not reach a given site of deep-water formation within decades of commencing freshwater injection. The eddy permitting results raise the question of can Hosing be justified via the use a reduced flux to compensate for this difference downstream. Since an analysis has not yet been made regarding of the degree of mismatch associated with allowing an eddy-parametrizing model to route freshwater from continental outlets relative to where the freshwater is routed in an eddy-permitting or eddy-resolving model, it is unclear whether Hosing (at a reduced flux or otherwise) remains a valid option for some cases.

[2]herein this simplified form of freshwater forcing at any flux will be referred to as 'Hosing'

While the degree of mismatch between eddy-parameterized and eddy-permitting[3] freshwater routing has not yet been quantified explicitly, we can make some inferences from previous injection studies. One of the more comprehensive studies examining injection into different outlets is Roche et al. [2009], whose relatively low-resolution (3° horizontal in the ocean, 120x65x20, no enhanced resolution in the Arctic), eddy-parametrizing simulations are conducted using the LOVECLIM Earth system Model of Intermediate Complexity (EMIC) under LGM boundary conditions. Unfortunately, this study only presents their results in terms of their impact on the AMOC, so we interpret here the magnitude of AMOC changes as an indication of the amount of freshening at deep-water formation sites. Lohmann et al. [2020] provides a mix of eddy-parametrizing and eddy-permitting conditions through their use of an unstructured mesh approach. In that study, eddies are generally resolved along coastal boundaries, but in the oceans interior, including along the Gulf Stream, eddies are not explicitly resolved. Finally, Love et al. [2021] and Condron and Winsor [2012] both use a configuration of the MITgcm which is eddy permitting for all regions equatorward of 60°N. We note that no study discussed here is fully eddy permitting in the Arctic and so this limits our analysis. All of these studies show consistency in the routing of freshwater from the Mackenzie River and Fennoscandia. Differences arise when considering injection into either the Gulf of St. Lawrence or at the mouth of the Mississippi in the Gulf of Mexico. While the results of Roche et al. [2009] indicate that the Gulf of St. Lawrence injection is the least effective injection location at inhibiting NADW export (relative to the outlets studied here), both Love et al. [2021] and Lohmann et al. [2020] show that such injection results in a strong freshening in North Atlantic sites of deep-water formation. As regards to injection into the Gulf of Mexico, again both Love et al. [2021] and Lohmann et al. [2020] are in agreement with freshwater from the Mississippi resulting in the weakest reduction of AMOC. Conversely, injections into the Mississippi and Gulf of St. Lawrence generate AMOC responses of comparable magnitude in Roche et al. [2009], albeit of a weaker strength compared to other outlets examined. Yet, in all of these studies (except Love et al. [2021] and Condron and Winsor [2012], who did not simulate Hosing), direct Hosing into a

[3] Here we use eddy-permitting as having at least one grid cell per Rossby radius and eddy parameterizing for coarser horizontal resolutions as per Nurser and Bacon [2014].

band across the northern North Atlantic generates as strong of an, if not a stronger, effect on the AMOC than any outlet injection. In that manner, the results of Liu et al. [2017] appear incongruous. Their present-day simulations show that freshwater injected at the Northern end of the Greenland ice sheet, specifically their 79° N and Petermann glacier locations, is more effective than a Hosing band for the same freshwater flux. It is unclear if this inconsistency is a result of comparing an LGM experiment to a present day experiment, as the location of deep water formation is dependent upon the background climate, or a result of the differences in spatial resolution (Liu et al. [2017]'s ocean model is nominally 1° horizontal, and is at least twice as coarse a resolution as the configuration of Lohmann et al. [2020]). In summary, these inferences suggest that at least for injection locations near the Arctic, eddy-parametrizing freshwater routing is somewhat consistent with eddy-permitting routing, but this is not the case for injection locations further south. However, in none of these cases does it appear that direct Hosing is an appropriate replacement. It is one goal of this study to dig into the reasons behind these results by addressing this sort of mismatch explicitly through our use of varying scales of freshwater injection complexity.

Herein, we propose an option that allows ESM modellers to mitigate the low resolution of ocean models in a resource-efficient manner and generate more realistic freshwater distributions, the freshwater fingerprint method. This method can be applied to simulating the routing of future or past runoff from both ice sheets and glaciers as well as rivers in Earth System Models. Our novel methodology, a freshwater fingerprint, is a distribution mask generated from a model well capable of resolving the $O(< 50\text{km})$ features of surface ocean circulation. This mask is used to spatially weight freshwater injection fluxes in a coarser resolution model, rather than relying on either a Hosing band or regional injection. By placing the freshwater where an eddy-permitting model transports it, the freshwater fingerprint incorporates the effects of the freshwater on surface transports (i.e. not a passive tracer) at the same time as generating freshwater distributions that are more consistent with our best estimates from ocean-only eddy-permitting simulations.

Given the importance of understanding the role of freshwater in the climate system, freshwater runoff needs to be treated in as realistic a manner as possible within the limitations of the models being used. This issue is particularly crucial for capturing the coupling between ice sheets and climate via the oceans, which is a major source of uncertainty in future climate projections [DeConto and Pollard, 2016] and fundamental to our understanding of the past. This study aims to assess the impacts of three different methods of imposing freshwater in ocean models of moderate resolution (broad-band Hosing; regional, outlet-specific injections; and a freshwater fingerprint), one of which is a novel method: the freshwater fingerprint. This new and resource-efficient methodology allows coarse-resolution eddy-parametrizing ocean models to place freshwater where eddy-permitting models transport it. Our approach is to examine the climatic differences between these different representations of runoff in a contemporary Earth System Model, and highlight some of the direct climatological effects associated with the introduction of freshwater at various outlets around the Arctic and Atlantic Oceans.

These goals can be summarized by the following questions. Firstly, where is freshwater routed at moderate resolution and is the use of a reduced effective Hosing justified? Secondly, does the freshwater fingerprint method capture eddy permitting behaviour? Finally, how do climate impacts vary between different forms of freshwater injection?

3.3 Experimental Design & Methods

Two models of different complexity and spatial resolution were used to study the transport of freshwater in the ocean and the impact of this freshwater on climate. MITgcm was configured at an eddy-permitting resolution (see Love et al. [2021]; 1/6 deg) to study freshwater transport pathways and to generate spatial freshwater 'fingerprint' maps. COSMOS (a CMIP3-era, fully coupled atmosphere/ocean/sea-ice/land Earth System Model) was run at a much coarser (T31/3°) resolution to assess the different climate impacts of Hosing, regional freshwater release and freshwater 'fingerprinting' on the sensitivity of the climate system to glacial meltwater forcing.

We provide additional details about the various components of our methodology below, starting with describing the eddy-permitting simulations performed using the MITgcm in section 3.3.1. The subsequent processing to derive our fingerprints from the source salinity anomaly fields is expanded upon in section 3.3.2. In section 3.3.3 some of the major features of the fingerprints are explored, which are relevant for understanding the climatological differences that arise in subsequent sections. Section 3.3.4 describes the COSMOS model configuration used for all the freshwater forcing experiments. Finally, the experiments are listed in Table 3.1 and are described in more detail in Section 3.3.5.

3.3.1 Fingerprint Source Data

All of the fingerprint generation simulations were performed using the Massachusetts Institute of Technology General Circulation Model (MITgcm) as described in Love et al. [2021]. We summarise this configuration here for context. We run the coupled sea-ice/ocean model in a Cubed-Sphere 6x510x510 (CS510) configuration, which provides $\approx$ 18km spatial resolution globally with 50 vertical levels. This grid geometry is eddy permitting for most of the oceans [Chelton et al., 1998] with the exception of the Arctic [Nurser and Bacon, 2014]. It is well able to capture small-scale phenomena like coastal boundary currents more accurately than coarser resolution models such as those used in current and previous PMIP and CMIP working groups [Yang, 2003]. For our Younger Dryas background climate, we have adjusted sea level to that provided by the sea level solver component of the Glacial Systems Model of Tarasov et al. [2012] at approx 13kaBP, except as regards the state of the Bering Strait. For all injection experiments except that from the Mackenzie River outlet (the one most likely to be affected by this choice), the Bering Strait is open. For the MAK injection experiment, the Bering Strait is closed, consistent with sea level estimates from the Glacial Systems Model. The MITgcm was run in an uncoupled configuration with prescribed, monthly-mean surface forcings, cycled annually. Surface forcings are derived from a CCSM3 LGM simulation and have limitations with regards to overly zonal winds over the North Atlantic, which results in an overly zonal Gulf Stream. Love et al. [2021] showed that this feature results in freshwater introduced south of the Gulf Stream being transported more southward relative to a less zonal configuration (when considering the latitude at which freshwater impinges on eastern border of the Atlantic). It is also shown that when using less zonal winds (in the ERA40 simulations of Love et al. [2021]) that the freshwater was deposited slightly closer to sites of deep water formation as the Gulf Stream was

Run Short Name	Model	Freshwater Forcing	Background Climate
OBS-Ctrl-MIT	MITgcm	None	OBS Hybrid LGM/YD
CBS-Ctrl-MIT	MITgcm	None	CBS Hybrid LGM/YD
MAK-MIT	MITgcm	2dSv MAK Regional	CBS Hybrid LGM/YD
FEN-MIT	MITgcm	2dSv FEN Regional	OBS Hybrid LGM/YD
GSL-MIT	MITgcm	2dSv GSL Regional	OBS Hybrid LGM/YD
GOM-MIT	MITgcm	2dSv GOM Regional	OBS Hybrid LGM/YD
Control	COSMOS	None	38ka Orbital and GHG
Hosing-2d	COSMOS	50-70N 2dSv	38ka Orbital and GHG
Hosing-1d	COSMOS	50-70N 1dSv	38ka Orbital and GHG
Hosing-05d	COSMOS	50-70N 0.5dSv	38ka Orbital and GHG
MAK-R	COSMOS	2dSv MAK Regional	38ka Orbital and GHG
FEN-R	COSMOS	2dSv FEN Regional	38ka Orbital and GHG
GSL-R	COSMOS	2dSv GSL Regional	38ka Orbital and GHG
GOM-R	COSMOS	2dSv GOM Regional	38ka Orbital and GHG
MAK-FP	COSMOS	2dSv MAK Fingerprint	38ka Orbital and GHG
FEN-FP	COSMOS	2dSv FEN Fingerprint	38ka Orbital and GHG
GSL-FP	COSMOS	2dSv GSL Fingerprint	38ka Orbital and GHG
GOM-FP	COSMOS	2dSv GOM Fingerprint	38ka Orbital and GHG

Table 3.1: The background hybrid LGM/YD climate is as follows: 13kaBP Bathymetry, LGM Ocean Surface Forcing, and an open Bering Strait (with the exception of the MAK configuration which used a closed Bering Strait). The 38ka orbital and GHG values are as follows: 0.013676 eccentricity, 23.2675° obliquity, 25.94°longitude of perihelion, 185PPMV CO_2, 405PPBV CH_4, and 207.5PPBV N_2O. The MITgcm simulations were conducted using the cs510 grid which is roughly $\frac{1}{6}^{\circ}$/18km horizontal resolution with 50 vertical levels and are the same simulations as described in Love et al. [2021]. The COSMOS simulations use the GR30 ocean grid (120×101) which has a displaced pole in Greenland and is $\approx 3^{\circ}$ at the equator with finer resolution near the poles. Non-eustatic relative sea level changes are implemented with respect to the bathymetry in COSMOS, and the Bering Strait is closed in this configuration. The atmosphere, land, and vegetation components of COSMOS use a T31 grid which is $\approx 3.75^{\circ}$.

more north-easterly than with LGM winds. In this study, the impact of wind forcing is most relevant for the Gulf of Mexico and Gulf of St. Lawrence fingerprints. Glacial runoff from these outlets is mostly entrained by the Gulf Stream, but this entrainment more strongly affects the GOM as the Gulf Stream acts as a northern limit to freshwater transport, separating freshwater from the sites of deep water formation no matter the orientation. Our fingerprint resultantly deposits freshwater further south of sites of deep water formation relative to a fingerprint generated from a simulation where the Gulf Stream is more tilted like at present.

A freshwater injection scenario as well as a control simulation for each climate configuration are used. Of the simulations described in Love et al. [2021], we use the Mackenzie River (MAK), the Gulf of St. Lawrence (GSL), the Gulf of Mexico (GOM), and the Fennoscandian (FEN) injections, and their associated control simulations. Our freshwater fluxes are 2dSv continually for the duration of the simulation, to be an analogue for the outflow of solid and liquid mass from the ice sheets. Each simulation is $\approx 22 - 24$ years in duration, after a 10 year control simulation, due to computational constraints imposed by the high resolution nature of the model. Despite the short simulations, these experiments are of sufficient duration to resolve surface ocean transports of the freshwater signal [Le Corre et al., 2020]. We note that 2dSv of freshwater is an overestimate for FEN [Tarasov et al., 2014], but have elected to use this same value to allow for ease of comparison and overall consistency between the MITgcm and COSMOS runs.

3.3.2 Fingerprint Processing

Our fingerprints are generated as the difference in the salinity field of the injection experiment and the control simulation. However, to minimize the distorting effects of climate noise, differences of magnitude $< 3\sigma$ are set to zero. σ is the standard deviation of daily mean salinities with respect to the multi-year monthly mean in the control run. While the assumption of a Gaussian distribution for our σ is a simplification, an analysis of the distribution of salinity (not shown) reveals it is a reasonable approximation. To mitigate any trends due to our configuration, particularly the short duration of the simulations which results in a small drift near background runoff sites (largely in or adjacent to the Barents-Kara Seas), we de-trend the salinity fields prior to calculating the control run σ field. This de-trending is performed using a simple linear regression scheme. The difference between the injection experiment and its corresponding control is then averaged over 5 years of each model simulation. This time interval provides a compromise between eliminating background variability and obtaining a stable anomaly signal. We note that the interval over which the fingerprints are generated are partway through the simulations of Love et al. [2021]. This is an artefact of the timing of this investigation relative to Love et al. [2021]. We consider this to be an acceptable compromise for a first-order investigation quantifying the impact of the fingerprint methodology for the following reasons. The distributions are largely similar (the years over which the fingerprints were calculated versus the end of the simulations in Love et al. [2021]) with differences largely confined to the margins of the distributions. As well, the normalization of the anomaly field to generate the fingerprints reduces the weight of these low-anomaly regions. In calculating the salinity anomaly we consider only those values which are reflective of freshening. The few features which have saline anomalies are neither located near the injection region or large in magnitude indicating that they are unmitigated noise, as such these features are not considered in the fingerprint generation. At the next step in the procedure, the anomaly is vertically integrated over the whole water column to produce a 2D salinity distribution. Practically this integration has minimal effect on vertical salinity distributions in COSMOS, since the vast majority of the anomaly is within the mixed layer of MITgcm and ends up being mixed vertically in the corresponding layer in COSMOS. This distribution is area-weighted, then normalized to produce the fingerprint field. The fingerprints are provided at a global 1/6 degree resolution on a regular lat-lon grid; see Figs. C.1 and 3.1 for a comparison of the 1/6 degree grid relative to the GR30 grid used by MPIOM (the ocean component of COSMOS). The normalized fingerprint is conservatively remapped to the GR30 grid using the first-order, conservative regridding method provided by the Climate Data Operators (CDO) toolset [Schulzweida, 2019] and implemented as a weighted injection mask into COSMOS simulations. Plots of the fingerprints on the GR30 grid can be found in Figure 3.1.

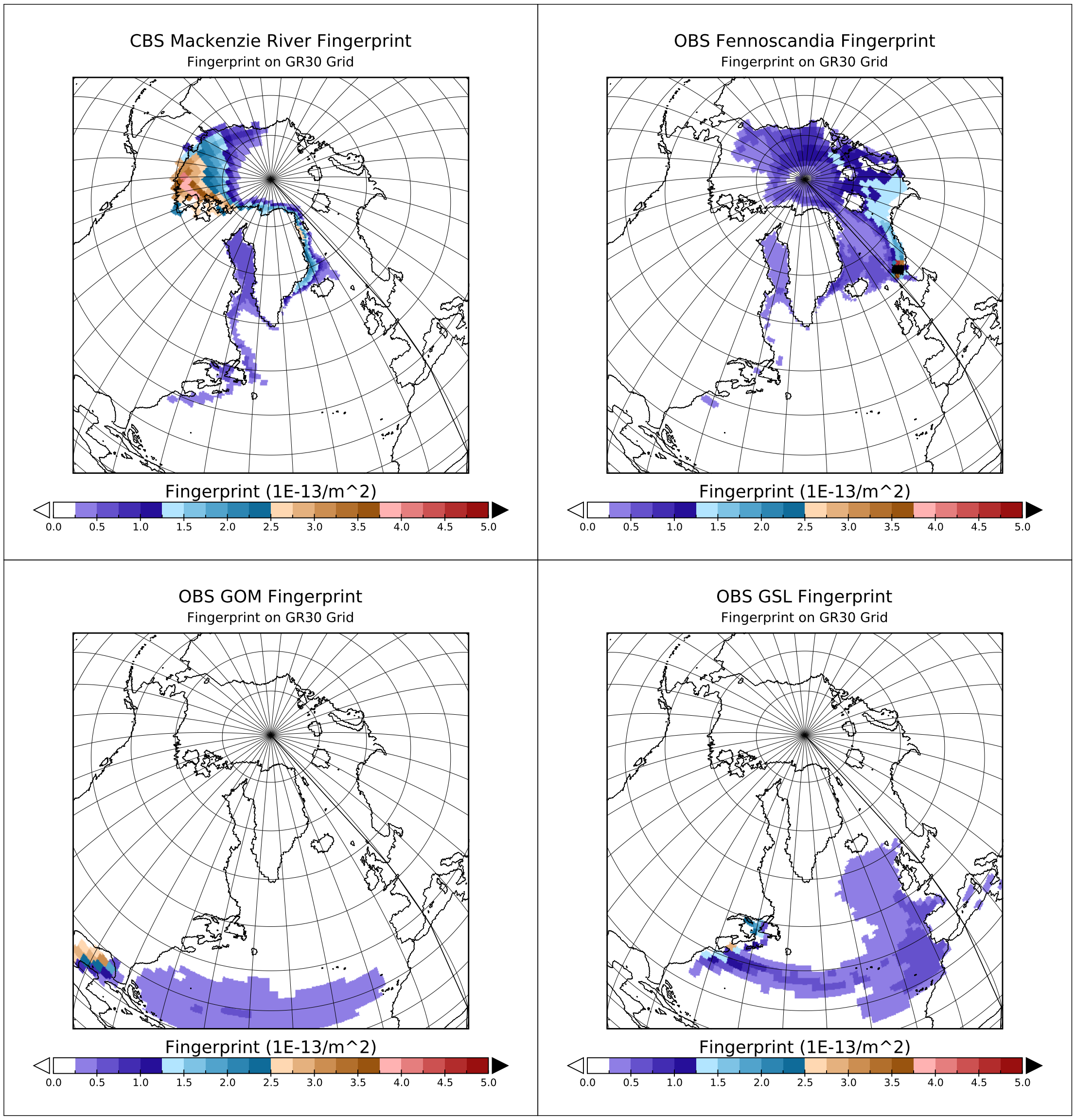

Figure 3.1: Each of the freshwater fingerprints used in this study. The fingerprints shown are remapped to the GR30 grid used by COSMOS. To obtain an injection rate in $\frac{m}{s}$ for a given fingerprint simply multiply the shown distribution by the desired volume flux in $\frac{m^3}{s}$. Fingerprints shown at $\frac{1}{6}^{\circ}$ resolution comparable to the native MITgcm resolution are shown in Fig. C.1.

3.3.3 Fingerprint Description

Here we highlight some of the major features of the three-dimensional salinity distributions which are used to generate our two dimensional fingerprints shown in Fig. 3.1 and C.1. For the MAK case, we find the bulk of the anomaly is located on the Canadian side of the Arctic Ocean, constrained to the East Greenland Current, and the Labrador Sea/Baffin Bay area with minimal amounts reaching the Gulf Stream. Freshwater has a tendency to accumulate in the Baffin Bay region from this outlet, and in Love et al. [2021] it is concluded that this provides the potential for a later surge of freshwater to propagate downstream should some mechanism flush the region (e.g. by opening the Canadian Arctic Archipelago). This fingerprint results in relatively little freshwater in the open ocean regions of the North Atlantic or GIN Seas. For the FEN case, the freshwater is carried northward into the Arctic ocean where it floods the Barents-Kara Sea. It is also carried westward across the GIN Seas, entrained in the East Greenland Current and eventually carried into the Labrador Sea. The entirety of the GIN Seas is thereby covered with freshwater when using this fingerprint, so it should strongly affect deep-water formation in this region. Freshwater from the GSL is carried southwards by the boundary current and transported eastward across the Atlantic via the Gulf Stream. At the coast of Europe, it splits into two, where the larger mass heads north along the coastline and the rest heads south. There also appears to be an accumulation of freshwater at the separation point of the Gulf Stream from the coast of North America from this outlet. Freshwater from the Mississippi/GOM primarily remains in the GOM. Any freshwater which escapes through the Florida strait is constrained to remain south of the Gulf Stream in the MITgcm simulations.

3.3.4 COSMOS Configuration

We use the COSMOS climate model for testing the three different injection methods. This model includes the MPIOM (the Max Planck Institute Ocean Model), the ECHAM5 (ECMWF Hamburg Version 5) atmosphere model, and the JSBACH land surface model. The atmospheric resolution is T31, with the land surface model sharing the same grid. The ocean grid is nominally 3 degrees (120x101x40), with a displaced pole over Greenland and the other at the geographic South Pole, and thus has enhanced resolution for the Arctic, Labrador Sea, and Greenland-Iceland-Norwegian (GIN) Seas. MPIOM is a primitive equation ocean model using the Boussinesq and hydrostatic approximations and uses a free-surface formulation [Jungclaus et al., 2006]. COSMOS readily allows for centennial to millennial scale climate simulations on the scale of days to weeks of wall-time using moderate computer resources (a single 40-core compute node per simulation in our case). Due to this efficiency, the moderate resolution of the comprehensive Atmosphere-Ocean-Sea Ice-Land configuration, and overall ease-of-modification, COSMOS has been used multiple times in paleoclimate modelling publications (eg. Gong et al. [2013], Zhang et al. [2013, 2014a,b]).

We have configured the model parameters for 38kaBP, which yields Dansgaard-Oeschger-like centennial to millennial scale internal climate variability in COSMOS. The 38ka land ice, topography, and sea level configuration is provided via the methods and work presented in Tarasov et al. [2012], with associated updates where new paleoclimate data has allowed for refinement of the GLAC reconstruction. Due to their availability, non-eustatic sea level adjustments have been included in the configuration specifications. These non-eustatic adjustments are obtained via the gravitationally self-consistent sea level and glacial isostatic adjustment sub-models incorporated into the GLAC reconstruction. This adjustments result in a thicker seawater column adjacent to ice sheets (i.e. near field regions) and a thinner seawater column for some regions distant from the ice sheet (i.e. far field regions). The Bering Strait and Canadian Arctic Archipelago are closed, and parts of the Arctic are glaciated further offshore than present land-sea boundaries. However, the Barents-Kara Sea remains open. These features result in a more isolated Arctic ocean by comparison to present day. Land surface types are as in COSMOS's pre-industrial datasets, but the plant functional types have been allowed to adjust to glacial conditions through the dynamic vegetation component of JSBACH.

We note that the boundary conditions specified by our land-ice/sea level reconstruction for 38kaBP are largely similar to the Younger Dryas configuration that was used to generate our fingerprints, in regards to the sea level, ice sheet volume, and land ice areal extent. See Fig. C.2 for the two paleo-land sea masks and Fig. C.3 for elevation and sea level differences between the time slices. Furthermore, both MIS3, which encompasses several DO events, and the Bølling-Allerød/Younger-

Dryas are periods with centennial-millennial scale variability between warm interstadial and cold stadial intervals. The main difference introduced by using MIS3 boundary conditions in COSMOS rather than YD boundary conditions is that the Bering Strait is closed, whereas it was open in all but the Mackenzie River injection experiments using the MITgcm. We consider the approximation of using OBS (Open Bering Strait) derived fingerprints in a CBS configuration to not be an impediment to this study for the following reasons. When we examine the salinity distributions for the Mackenzie River, the most proximal injection location to the Bering Strait, for both an open and a closed Bering Strait in Love et al. [2021] we find they are broadly similar except with regards to two features. The OBS Mackenzie River does not have freshwater directly adjacent to the Bering Strait due to the different local currents, and the Labrador Sea is fresher in the OBS configuration.

3.3.5 Freshwater Forcing Experiments

We use the configuration described in section 3.3.4 to test the relative impact of three methods of freshwater injections of varying complexity. These methods are, in order of increasing complexity, conventional Hosing (50-70N band), regional freshwater injection (i.e. injected at the outlets as represented by COSMOS), and our freshwater fingerprint (as described in section 3.3.2). Our injection scenarios are as listed in Table 3.1. Our Hosing experiment continuously and uniformly distributes 2dSv of freshwater over the 50-70N band in the North Atlantic. This type of forcing is typical for a scenario where the goal of Hosing is a strong reduction of thermohaline circulation in the North Atlantic (e.g. Manabe and Stouffer [1995], when testing climate sensitivity (e.g. Swingedouw et al. [2009]), or when loosely approximating the Ruddiman Belt ($40-65°$N as per Ruddiman [1977]). The regional injection involves directly injecting freshwater into the source regions for each of the outlets and allows us to compare the freshwater distribution generated by the COSMOS model to that generated by the MITgcm, as illustrated by the fingerprint. The regional injection locations are the same as in Love et al. [2021] but conservatively re-gridded (accounting for the differences in land-sea mask) to the GR30 grid. Finally, the freshwater fingerprint injection is implemented by taking our spatially variable, normalized freshwater fingerprint on the GR30 grid (as discussed in section 3.3.2) and scaling it by our 2dSv flux. All freshwater forcing is introduced into the combined liquid precipitation and surface runoff flux field directly within the ocean model. At 2 dSv, this is equivalent to an $\approx$ 1.5% increase in global precipitation. There is no direct modification of atmospheric components from the addition of this freshwater flux.

We compare all of our forcing experiments to a control simulation. This control simulation was branched from a previous 3000yr duration MIS3 simulation with slightly different atmospheric and orbital forcings. It has been integrated forward for roughly 1000yr under the current climate conditions prior to initializing the injection simulations. Our control and simulations all feature the following orbital and greenhouse gas forcings: 38ka orbital configuration (0.013676 eccentricity, 23.2675° obliquity, 25.94° longitude of perihelion), 185PPMV CO_2, 405PPBV CH_4, and 207.5PPMV N_2O. Our control simulation oscillates between a cold phase and a warm phase without the presence of any external forcing. To minimize the effect of these oscillations upon the results we begin the injections after the warm mode has hit a relatively steady state, several hundred years after a transition from a cold to a warm state and 400yr before a return to cold conditions. Furthermore, enhanced glacial runoff ought to be associated with warm background conditions, and as such we consider this the context of greater utility relative to injecting glacial runoff during a cold/stadial state. The exploration of the impact of freshwater injection under stadial boundary conditions, with an already reduced AMOC, is left to future work.

3.4 Results and Discussion

The results of this study are organized according to the research question they address. The main research questions are as follows.

- Where is freshwater routed at moderate resolution and is hosing justified?
- Does the fingerprint method capture eddy permitting behaviour?
- How do climate impacts vary between different forms of freshwater injection?

Our results and discussion will focus largely on the early decades after the initialization of freshwater injection. The reasons for this are twofold. Firstly, we wish to be able to draw comparisons between this work and the work of Love et al. [2021], who were limited to shorter durations due to using an eddy-permitting resolution model (our years 10-20 are most comparable to this previous investigation). Secondly, we find that all COSMOS simulations eventually reach a stadial-like state where the extensive interstadial to stadial climate signal dwarfs the more subtle freshwater injection signal. We leave the impact of freshwater injections on the characteristics of Dansgaard-Oeschger-like variability to future work.

3.4.1 Where is Freshwater Routed at Moderate Resolution, and Is Hosing Justified?

Comparisons between the COSMOS and MITgcm regional injection experiments indicate that the effectiveness of regional injection at moderate resolution depends on the location of injection. Injection sites nearer the displaced pole over Greenland (with consequently higher horizontal resolution) such as MAK-R and FEN-R (see Table 3.1) mostly reproduce the transport patterns in the eddy-permitting MITgcm simulations, but those nearer the Gulf Stream, such as GSL-R and GOM-R do not. These results are consistent with our inferences based on comparing Roche et al. [2009], Lohmann et al. [2020], Condron and Winsor [2012] and Love et al. [2021]. Overall, the primary differences we detect here between eddy-parametrized and eddy-permitting freshwater routing are a slower rate of freshwater transport, less accumulation of freshwater in marginal seas along the pathway of freshwater (e.g. Baffin Bay, mostly impacts MAK-R), and most significantly, greater freshwater transport across the Gulf Stream from both GSL-R and GOM-R. Each of these differences are discussed in more detail below.

Previous studies indicate that passive tracers tend to be transported more slowly at lower resolutions than at higher resolutions [Weijer et al., 2012], and we find evidence of a similar difference here in the rate of freshwater transport. Freshwater distributions averaged over years 10-20 of the regional injection experiments are shown in Fig. 3.2 where salinity anomalies are averaged vertically over the top 30m. MAK-R and FEN-R (Fig. 3.2E and J) both result in freshwater remaining mostly in the Arctic Ocean, with lesser amounts exiting via the East Greenland current than in the MITgcm simulations (as given by the fingerprint). Within the Arctic Ocean, the MAK-R freshwater spreads both east and west of the injection location, spreading as far west as the East Siberian Sea. While there is evidence of similar spreading in the fingerprint, a greater proportion heads eastward to the EGC in that experiment, rather than into the central Arctic. In contrast, the FEN-R freshwater mass fills the central Arctic comparatively much less, with a greater proportion circling around the GIN Seas instead. Thus, its not clear whether the slow progress of these freshwater masses along the coast of Greenland and into the Labrador Sea is entirely due to surface currents being slower or also whether circulation patterns in the Arctic differ in a way to trap the freshwater there. The freshwater in GSL-R most closely resembles its MITgcm counterpart when considering the progress of freshwater across the North Atlantic. However, given the differences in the Gulf Stream take-off point between the configurations this appears to be an artefact of the differences in the representation of the Gulf Stream between COSMOS and the MITgcm. Examining GOM-R relative to GOM-MIT we again see this delay, with much less freshwater on the eastern edge of the North Atlantic.

Examining the differences in freshwater accumulation in marginal seas, we find they are freshened less effectively at coarse resolutions. Baffin Bay experiences about half the freshening effect in the MAK-R simulation as in the MAK-MIT simulation over the same time interval. There is a similar difference between GOM-R or GSL-R and their MITgcm counterparts for the Mediterranean Sea. These differences are largely due to the slower rate of freshwater transport for those outlets, as discussed previously, coupled with the narrow entrances to the marginal seas (e.g. the Strait of Gibraltar is one ocean cell wide in MPIOM). For Baffin Bay and MAK-R, we see that it takes an additional decade (see Fig. C.4 before achieving comparable freshening to the MAK-MIT experiment, while GSL-R takes an additional $\approx$ 70years to freshen the Mediterranean Sea comparably to the levels seen in GSL-MIT. Thus, the net result is a fresher Mediterranean Sea and Baffin Bay after a given period of injection for comparable injection volumes at higher resolutions. For Baffin Bay, this has implications for rapid climate change, as this region can act as a reservoir of low-salinity water that could then rapidly spread into the North Atlantic should some climate

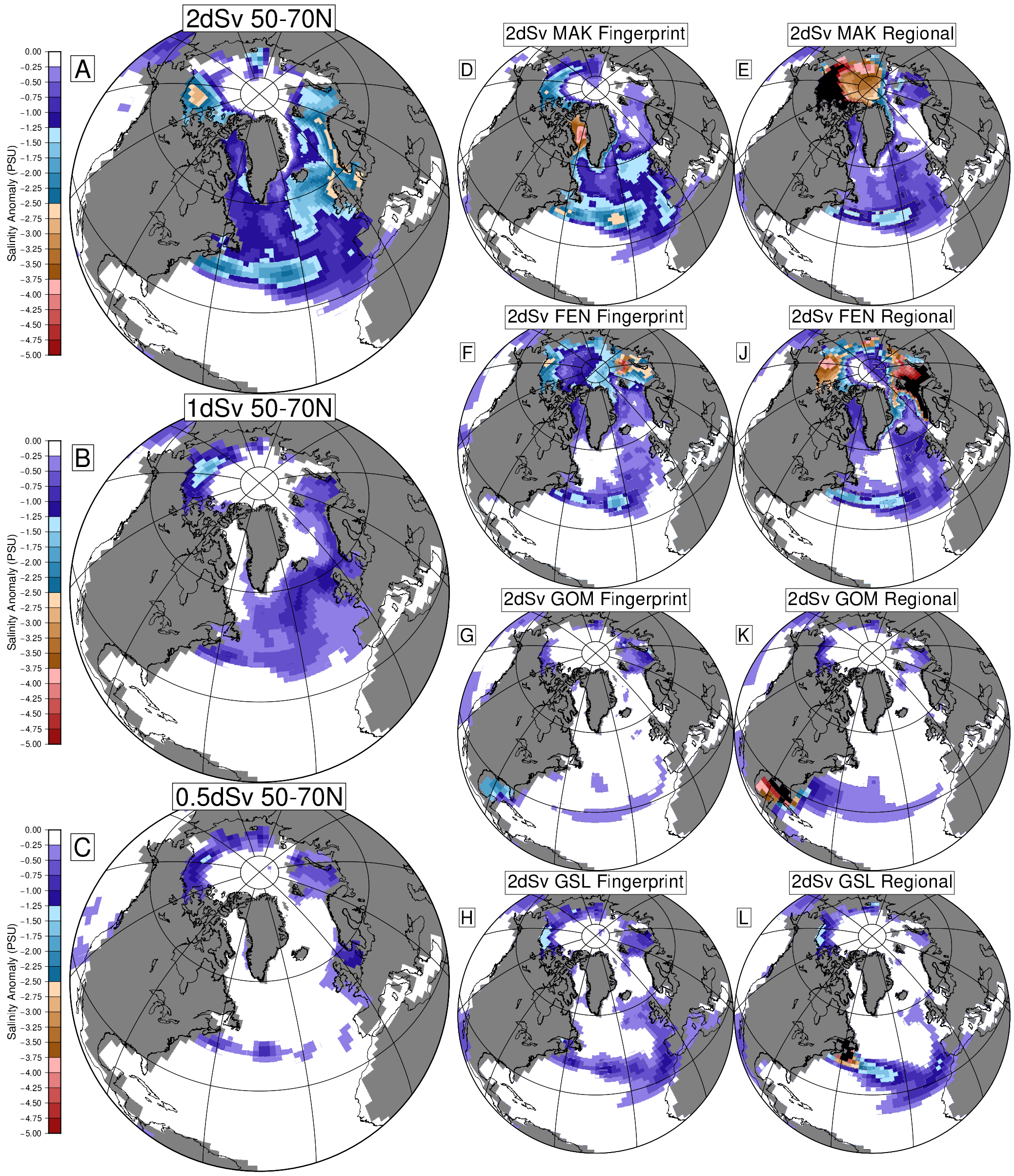

Figure 3.2: Salinity anomaly in the COSMOS simulations averaged over years $10-20$ of injection averaged over the top 30m of the water column. Subfigures a,b,c show the impact of a 50-70N injection, region highlighted in yellow in figure C.2, with varying fluxes uniformly distributed over the band. Subfigures d,f,g,h, show the salinity anomalies resulting from using the fingerprint distributions shown in figure 3.1 with a 2dSv flux. Similarly, subfigures e,j,k,l show the salinity anomalies resulting from the regional injection locations as shown in fig C.2.

feature result in a flushing action (e.g. deglaciation of the Canadian Arctic Archipelago or Nares Strait).

Similarly, we see more freshwater build up in GSL-MIT than GSL-R at the separation point of the Gulf Stream and North America. This may be a result of differences in the location of the separation point of the Gulf Stream from North America, which is further south in the MITgcm simulations than in COSMOS. In the GSL-MIT simulation, the freshwater flows southwards towards Cape Hatteras before flowing eastward across the Atlantic. Conversely, in the GSL-R simulation freshwater begins to cross the Atlantic via entrainment in the Gulf Stream as soon as it clears the Cabot Strait. Freshwater flows more readily across the Gulf Stream in GSL-R and GOM-R than in their MITgcm counterparts (at least along the eastern side of the North Atlantic, see Fig. 3.3). The bulk of the freshwater mass in GSL-R is directed south of the Gulf Stream into the sub-Tropical gyre when it reaches the coast of Europe. While this pathway is represented in the freshwater distributions of GSL-MIT, the bulk of the freshwater mass is redirected northward in that run instead. Freshwater in GOM-R more readily crosses the Gulf Stream than GOM-MIT along the East Coast of North America but otherwise follows a similar pathway as in the MITgcm. That is, they both follow the coastal boundary currents at the Cabot Strait. About midway across the Atlantic, the freshwater in the GOM-R experiment crosses the Gulf Stream and begins flowing northward. In comparison, freshwater in the GOM-MIT experiment only crosses the Gulf Stream at the western boundary of the Atlantic.

The excess northward transport across the Gulf Stream may be partly explained by the fact that the freshwater flows out of the GOM into the sub-Tropical North Atlantic more readily due to the lack of Caribbean Islands. At the equator, the grid resolution is too coarse to adequately resolve the Caribbean Islands without creating an artificial land-bridge to Central America or closing the Florida Strait. The effect of this ought to be greater exchange between the Gulf of Mexico and the Atlantic Ocean and thus more freshwater into the Atlantic. We note this feature is not unique to our configuration, at least both LOVECLIM (as in Bahadory et al. [2021], T. Bahadory, 2021

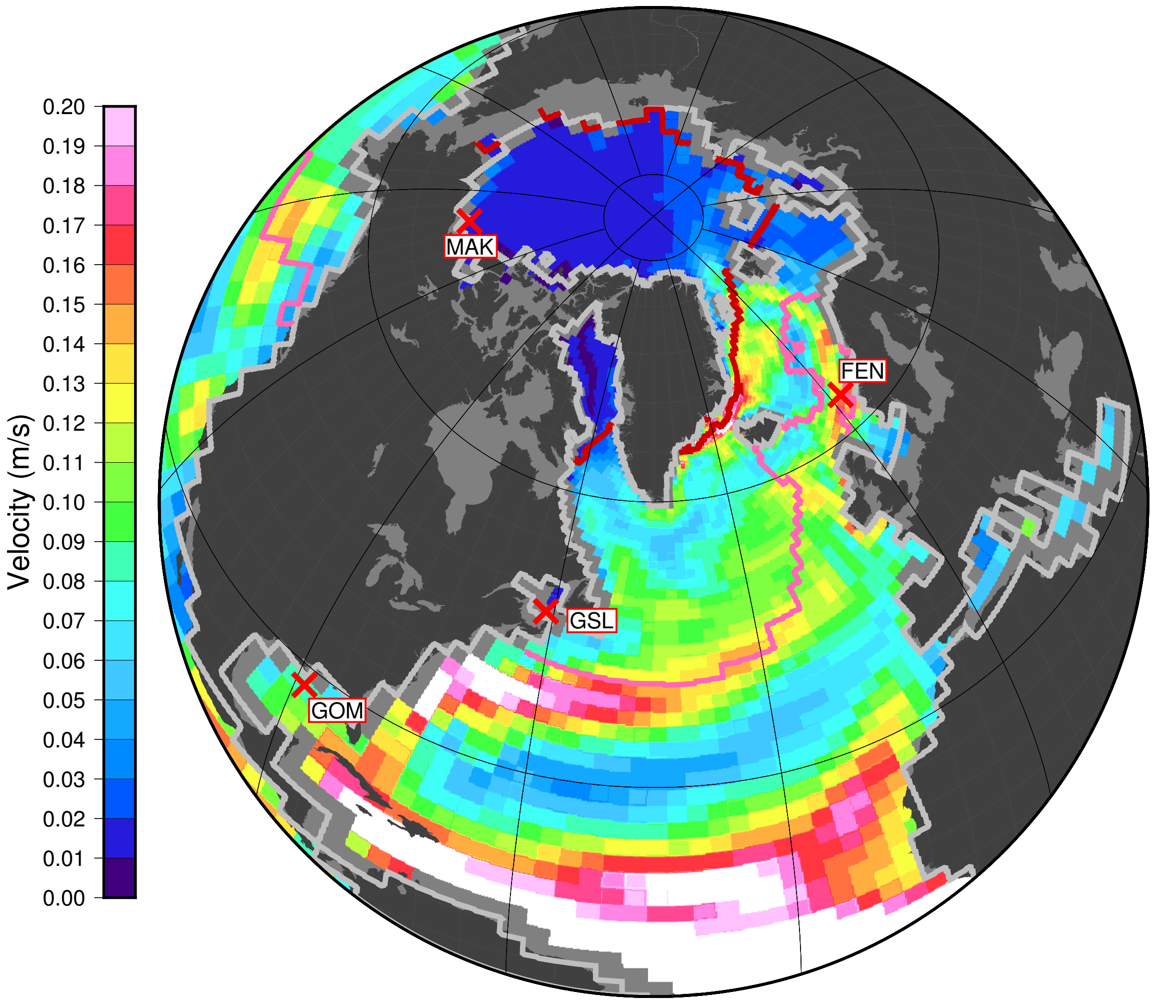

Figure 3.3: Average sea surface velocity for 100yr of the control run. Present day land-sea mask is shown in dark grey while simulation land-sea mask is contoured in a light grey. The dark red and pink contours denote the time minimum and maximum sea ice extent for the 100yr of the control run respectively, of at least 15% sea ice coverage. The Gulf Stream is less zonal and further North than the Gulf Stream in the MITgcm simulations presented in Love et al. [2021].

P. Comm[4]) and PLASIM (as in Andres and Tarasov [2019], H. Andres, 2021 P. Comm [5]) feature default model configurations with a similar representation. The net result of these differences is that our coarser-resolution configuration shows more rapid transport of freshwater to sites of deep-water formation from locations south of the Gulf Stream by comparison to the eddy-permitting configuration. However, one mitigating factor which is not considered in this study is the effect of bottom-riding (hyperpycnal) flow, a significant feature for outflow from the GOM (Broecker et al. [1989], Parsons et al. [2001], Tarasov and Peltier [2005], Aharon [2006]). This phenomenon should result in an even more significantly reduced surface freshening signal, with a resulting climate impact from diminished NADW formation and AMOC.

To get a more direct comparison between the regional injections at eddy-parametrizing and eddy-permitting resolutions, we process the COSMOS regional injection salinity distributions using the same methodology as was used to generate the MITgcm fingerprints, creating COSMOS fingerprints. When we compare these COSMOS-derived fingerprint fields to the MITgcm fingerprints in Figs. 3.1 and C.5 respectively, we find large-scale differences in the distributions that are not as readily visible when comparing the salinity distributions directly. Here again, the slower rate of freshwater transport is readily demonstrated, as all COSMOS regional injection experiments show much less freshwater downstream of the injection locations. The fingerprint marginal gradients in the eddy-permitting configuration are also generally sharper when compared to the coarse resolution configuration, readily demonstrating the strongly diffusive nature of the coarser resolution configuration. A significant proportion of MAK-R freshwater extends into the central Arctic (loosely following Lomonosov Ridge) relative to the MAK-MIT fingerprint, such that MAK-MIT has both a larger concentration of freshwater at the mouth of the Mackenzie and a greater transport of freshwater downstream into the North Atlantic than MAK-R for the same amount of injection. FEN-R shows minimal freshwater coverage over the interior of the GIN Seas or central Arctic relative to the FEN-MIT fingerprint, with much of the freshening occurring downstream in the Barents-Kara Seas and Beaufort Sea. Of note is a secondary salinity minimum at the mouth of the Mackenzie in

[4]Confirmed lack of Caribbean Islands in LOVECLIM
[5]Confirmed lack of Caribbean Islands in PLASIM

FEN-R that is not present in FEN-MIT. This feature is discussed in more detail in Supplemental Section C.2. GSL-R shows a markedly different distribution relative to the GSL-MIT fingerprint. The GSL-MIT fingerprint features southward advection along the North American coast toward Cape Hatteras, followed by a largely zonal band of freshening, which aligns with the Gulf Stream. Upon reaching the coast of Europe, the freshwater is mixed both northward and southward along the coast, with the majority of the freshwater heading north. Comparatively, the GSL-R fingerprint shows freshwater is transported directly south-east across the Gulf Stream and becomes entrained in the sub-Tropical gyre. GOM-R is the most similar to its respective fingerprint, but this is largely a result of freshwater entrapment within the Gulf of Mexico dominating the signal. Downstream from the injection location, fingerprint values, and thus salinity anomalies, are generally smaller than in the MITgcm fingerprint. Given these results, it appears the slower rate of tracer transport in the eddy parameterizing model counterbalances the lack of Caribbean Islands constricting flow out of the Gulf of Mexico.

Having explored the differences between the routing of freshwater at eddy-parametrizing and eddy-permitting ocean model resolutions, we now address the question of whether these differences are problematic enough to justify bypassing freshwater transport altogether and replacing it with Hosing. If we are to consider Hosing an acceptable simplification it needs to reproduce the major climatological effects of the eddy-permitting models, of which the AMOC is one of the most important. However, at present there are no readily accessible, fully-equilibrated, coupled climate model simulations which utilize an eddy-permitting ocean model to use as a reference to test this simplification. As such, the results of the regional injections with COSMOS, and work of Love et al. [2021] provide the best data against which we can compare the results of Hosing. Examining the differences in the AMOC response in our experiments, time series of which are shown in Fig. 3.4, we see that Hosing produces a larger and more rapid change than injection into any of the regions here for the same flux of freshwater. Thus, Hosing exaggerates the impact of freshwater on the AMOC, such that even the 1dSv hosing injection results in a greater peak reduction than MAK- or FEN-sourced freshwater at twice the injection rate. From these results we can conclude this exaggeration is problematically large when approximating freshwater sourced from either the Mackenzie

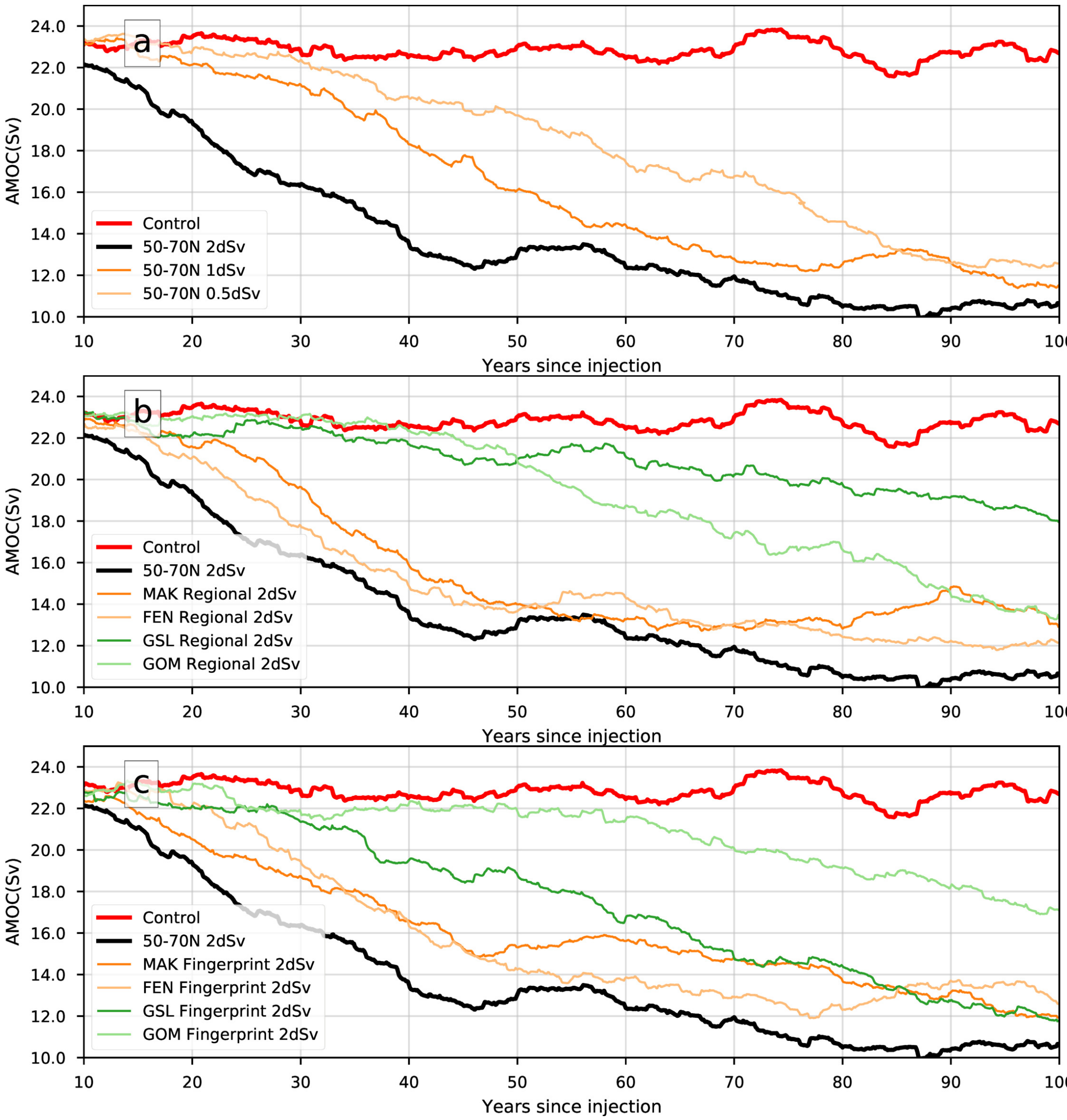

Figure 3.4: AMOC (maximum of the streamfunction in the North Atlantic below 400m) for each of the freshwater injection scenarios. In all panels the thick red line denotes the control simulation. A shows the Hosing scenarios for 3 different vales, B shows the different fingerprint scenarios all with 2dSv injection volumes, and C shows the regional injections where the freshwater flux (2dSv) is introduced at the locations shown in sfig. C.2. Data shown has been processed using 10yr window running mean.

River or Fennoscandia, which both generally reproduced eddy-permitting freshwater distributions.

Hosing also generally results in a stronger and faster cooling impact relative to regional injection, even when comparing 1dSv of Hosing to 2dSv of regional injection. Examining Figs. 3.5A,B,C we can readily see that for the same flux of freshwater, the simulated, maximum GRIP 2m temperature deviation is at least 1C colder than the MAK-R or FEN-R injections. Similarly, continental European 2m temperatures, Figs. 3.5D,E,F, demonstrate the same bias. As well, the cooling is spread over a much greater area, as seen in Fig. C.6, where equivalent fluxes applied via Hosing generate cooling covering much of North America, Europe, and North Asia, instead of the more regional cooling of the regional injection scenarios. Examining sea ice cover growth in Figs. 3.6, C.7, C.8, we see similar trends of a faster and stronger overall response relative to the regional injections.

It is not enough to use Hosing and account for differences in the results assuming that something as simple as a scale factor can account for the non-linear and spatial distribution differences between the Hosing simplification and routing in an coarse-resolution model. These results readily show that progressing from Hosing to regional injections yields an increase in realism (i.e. upstream salinity anomalies with associated impacts, less extreme climate responses) while still eliciting a strong AMOC response, and associated climate cooling, albeit not as swiftly or strongly as Hosing. Given the relative ease of implementing regional injection methods and the overarching similarities in AMOC responses, we conclude that for most situations, Hosing is not an acceptable simplification. However, there remains the significant problem that the excessive transport of freshwater across the Gulf Stream yields unrealistic freshwater amounts in deep-water formation regions from both GSL and GOM (and likely AMOC changes as a result). Given this representation problem and the overall transport pathway for the GSL, whose eddy permitting distribution overlaps with the Hosing band at least on the eastern half of the Atlantic, there may be some small merit to using a reduced flux (e.g. reduced by a factor of 4 as per the findings from Love et al. [2021]) with a hosing representation in limited circumstances. Besides which, Hosing may still be a valuable tool for comparing the climate sensitivity of models relative to one another. In summary, choosing to use the Hosing method of freshwater injection instead of regional injection will lead to an over-

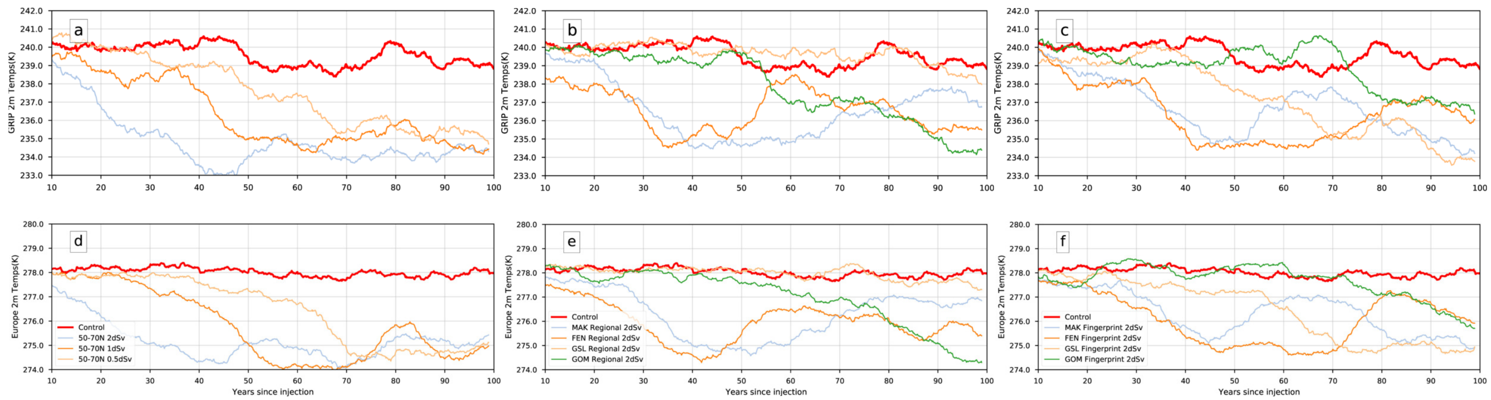

Figure 3.5: Surface temperatures at GRIP and continental Europe from each set of simulations. a and d show the Hosing scenarios,b and e show the regional injections as shown in sfig. C.2, while c and f show the fingerprint injection scenarios as in Fig. 3.1. Data shown has been processed using $10yr$ window running mean.

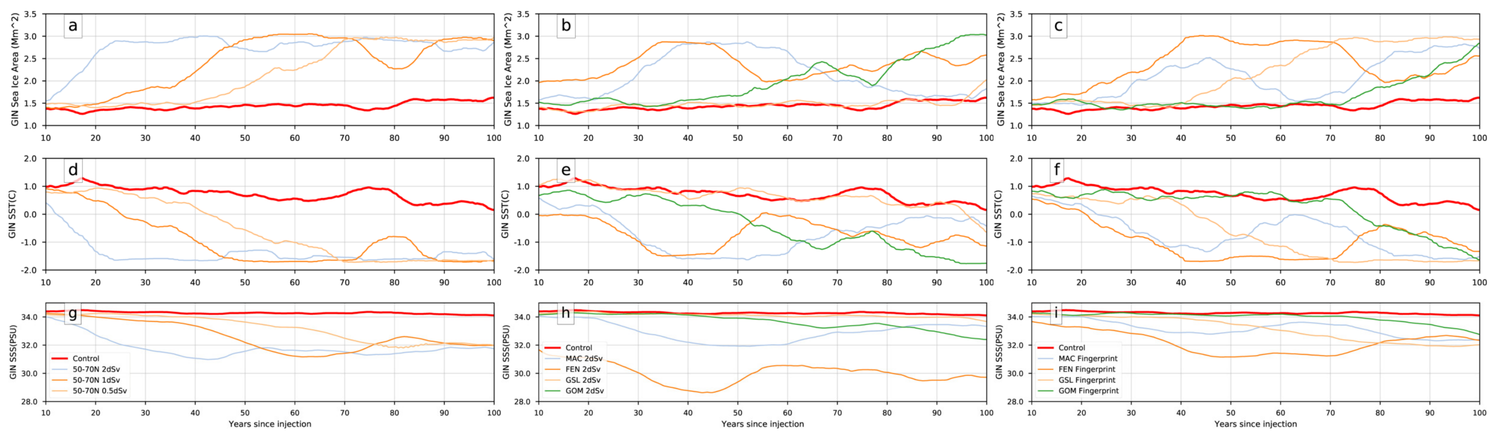

Figure 3.6: Ocean domain metrics for the upper layers of the Greenland-Iceland-Norwegian Seas. Each of the timeseries shown are boxcar running mean with a 10 year window.

estimation of surface cooling in Greenland and Europe, as well as an exaggerated growth of Northern Hemisphere sea ice. These biases ought to be accounted for when pursuing any investigations of climate stability or future climate projections.

3.4.2 Does the Fingerprint Method Capture Eddy-Permitting Behaviour?

Given our regional injection results and those of previous studies fail to adequately reproduce the salinity distributions from an eddy-permitting configuration for freshwater sourced from the Gulf of Mexico and the Gulf of the St. Lawrence, we require an alternative method that can better represent these distributions. As such, we present the freshwater fingerprint technique as described in section 3.3.2. The salinity distributions in the fingerprint forcing simulations shown in Fig. 3.2D,F,G,H, are largely similar to the fingerprint forcing distributions themselves. Consequently, we find that the fingerprint injection experiments can capture some of the features of the ocean-only eddy-permitting runs that were not reproduced in the regional injections. However, the fingerprint approach is not without shortcomings. The production of a fingerprints associated eddy-permitting simulation is an expensive and complicated pre-processing step. Mis-matches of climate features between the models can lead to some difficulties in use and interpretation. One such mismatch relevant here is the relative location of the Gulf Stream in the MITgcm versus COSMOS. Here we comment on how fingerprint injection affects each of the limitations identified in the regional injection experiments (the lagged transports, lack of freshwater accumulation in partially isolated basins, and transport across the Gulf Stream) and what new shortcomings may arise through the use of the freshwater fingerprint technique.

As highlighted in section 3.4.1, the lag in the rate of downstream transport of freshwater is one discrepancy between eddy-parametrizing and eddy-permitting freshwater routing. In contrast, due to the placing of freshwater in the fingerprint simulations where it has been transported after at least a decade of eddy-permitting simulation, the fingerprint injections would be expected to lead the eddy-permitting runs in the time to transport freshwater into deep-water formation zones.

However, when comparing Figure 4 of Love et al. [2021] to Figure 3.6i, it appears to still take longer to achieve the same salinity anomaly in the GIN Seas using the fingerprints, although for the MAK region at least, the lag is reduced relative to MAK-R. Whether this residual lag is again due to the slow transports in the eddy-parametrizing simulation or from some other process (e.g. a feedback due to the atmospheric coupling) is not clear. For at least the FEN-R injection this may be a disconnect in comparing a closed Bering Strait injection relative to the open Bering Strait configuration of the eddy permitting FEN-MIT experiment. As well, the maximum freshening of the GIN seas is reduced with the fingerprint method (see Fig. 3.6), likely due to the more diffuse nature of the fingerprint injection method. Aside from the transport to the GIN Seas, we find that the MAK-FP forcing leads to a much fresher North Atlantic and Labrador Sea when compared to the MAK-R forcing and much less accumulation in the central Arctic. Much like the MAK-MIT injection simulations, the bulk of the freshwater is transported from the Arctic to the North Atlantic via the East Greenland Current and the Labrador Sea. Similarly, the FEN-FP salinity distribution shows comparatively less freshening in the Beaufort Gyre region, which aligns with the FEN-MIT distribution, although its distribution otherwise resembles the FEN-R distribution in anomaly coverage. However, one of the main features of both the MITgcm and regional injection scenarios is not reproduced for MAK, which is the central core of freshwater built up around the site of the freshwater injection. Instead, the fingerprint by design emulates one of the main functions of this water mass (providing a reservoir for downstream freshwater flow), by virtue of sourcing the freshwater along the transport pathways from the total injection amount.

The second discrepancy between the COSMOS regional injections and the MITgcm transports discussed in section 3.4.1 was the lack of freshwater buildup in marginal seas. Using the Mackenzie River fingerprint results in the greatest observed freshening of the Labrador Sea of any of the simulations explored here, even exceeding the MITgcm results. Similarly, the GSL-FP simulation exhibits a freshening of the Mediterranean Sea comparable with the GSL-MIT simulation, but with no appreciable overshoot. The use of the GOM fingerprint does result in an earlier freshening of the Mediterranean Sea, but not as effectively as the GSL fingerprint. This discrepancy for freshening of marginal seas demonstrates the limitations of comparing model results for these regions to proxy evidence. Furthermore, the previously discussed flushing behaviour of a region like Baffin Bay would be very sensitive to the fingerprint. If exploring the concept of Baffin Bay as a reservoir of less saline water the use of the MAK fingerprint presented here would overemphasize the effects of the flushing.

Finally, one of the most important contrasts between the regional injections and their MITgcm counterparts is the rate of freshwater transport across the Gulf Stream. As discussed in section 3.4.1, GSL-Rs freshwater is largely entrained in the sub-Tropical gyre after crossing the North Atlantic, whereas GSL-MITs freshwater is largely directed northward to the DWF site. When using the fingerprint injection method for this outlet, the balance shifts and there is a greater amount of freshwater in the region of DWF. Examining the impact of this shift on AMOC in Fig. 3.4, it is readily apparent that this shift results in the GSL-FP having a more rapid effect on reducing AMOC. In comparison, using the GOM fingerprint results in a lesser rate of AMOC reduction by comparison to the regional injection. As discussed previously, GOM-Rs freshwater crosses the Gulf Stream midway across the North Atlantic. Through this pathway, the freshwater begins to flood the DWF region approximately 50yrs after the start of injection. Freshwater in the GOM-FP simulation does not follow this pathway and instead reaches the DWF region via the eastern edge of the Atlantic and not in as great a concentration as the regional injection. These differences result in a delay in AMOC reduction and a lesser rate of decrease relative to the regional injection. When comparing the relative rates of AMOC reduction between the regional and fingerprint injection methods for all outlets, we find that the relative impacts of the fingerprints injection methods more closely resemble the amounts of freshwater transported to sites of deep-water formation in the eddy-permitting MITgcm simulations in Love et al. [2021]. These results indicate that for at least the GSL and GOM outlets, our fingerprint injection has had the desired effect of letting us emulate at least one key climate impact, the AMOC.

The assessment of the effectiveness of the fingerprint method has also highlighted some issues associated with this method. Namely, by design, freshwater is instantaneously placed where it would have been transported over a decade or more of eddy-permitting simulation, and discrepancies in the background climate conditions (like the Gulf Stream) between the simulation generating the fingerprint and the one it is being applied to can have consequences. For example, freshwater from the GSL may be injected onto the southern margin of the Gulf Stream, rather than its northern flank with a northward shift in the Gulf Stream. As well, a fingerprint inherits any biases present in the eddy-permitting simulations (e.g. such as an overly zonal Gulf Stream as in Love et al. [2021]). Finally, the simulations that the fingerprints are derived from are an expensive pre-processing step whose utility may be outweighed by this expense depending upon the context of a given investigation. For example, if the fingerprints were to be used in a transient simulation it is unclear at present over what magnitude and temporal scales a given fingerprint remains valid. As such, it is unclear how many fingerprints would be required to replace a single outlet over an entire glacial cycle. However, we consider these initial results promising enough to warrant future further analyses of this question.

In summary, the freshwater fingerprint simulations adequately reproduce behaviour from the eddy permitting configuration for high latitude injections, more accurately represent the influence of GOM and GSL sourced freshwater on AMOC (relative to the freshening effects at eddy permitting resolutions), and are sensitive to climate mismatches between the coarse resolution simulations and the eddy permitting source simulations. Based on these results, we conclude that freshwater fingerprints provide an improved representation of freshwater routing in coarse resolution models, particularly for the GOM and GSL. Additionally, their use precludes the need of uncertain reduced flux Hosing estimates as discussed in Section 3.4.1. On this basis, we would argue that fingerprints ought to replace Hosing and regional injection for regions near the Gulf Stream. However, the situation is more complex for the MAK and FEN regions. For investigators using models in which the representation of coastal boundary currents is questionable due to resolution or parameterization issues (eg. EMICs such as LOVECLIM), we suggest the use of the fingerprints provided herein as a first-order means of capturing some of the major features of freshwater transport from these northern regions. For investigators using more complex GCMs (e.g. those comparable to COSMOS), which may represent high-latitude transports more accurately, deciding between using either regional injection or a freshwater fingerprint depends on the details of the goals of the analysis being performed.

3.4.3 How do Climate Impacts Vary Between Different Forms of Freshwater Injection?

Previously we established how freshwater routing changes between eddy permitting and eddy parameterizing model configurations and between different methods of freshwater injection, where we bridge the gap between these resolutions with the freshwater fingerprint technique. Here we discuss the associated climate impacts that arise from these differences, starting with the relative changes in the GIN Seas sea ice area (SIA), sea surface salinity (SSS) and sea surface temperature (SST). These features ought to change in parallel as they are tightly coupled. A fresher ocean or colder ocean surface results in sea ice growth, however sea ice growth results in brine rejection resulting in a more saline environment and also acts as a heat sink keeping the surface at the freezing point until melted.

Generally, changes in these characteristics of the GIN Seas reflect similar changes in the North Atlantic and the Arctic, so we only discuss these other regions in detail where differences arise. Time series of the data discussed are shown in figs 3.6, C.7, and C.9 for the GIN Seas, the North Atlantic, and the Arctic respectively. We find all GIN Sea metrics for the Hosing scenarios to increasingly trend away from the control scenario for ever increasing rates of injection, but not linearly. Hosing is highly effective at freshening the surface layers of the GIN Seas and North Atlantic for both the 2dSv and 1dSv cases, as is expected. The 0.5dSv case does not show a freshening effect within the first 10yr, taking $\approx$ 30yr of injection to have an overall negative salinity anomaly in the GIN Seas and North Atlantic, which correlates with the initial reduction in AMOC for that injection scenario. For 2dSv of injection, we also find GIN Seas sea ice grows at a rate of approximately 0.1Mm^2/yr, and both 1dSv and 0.5dSv grow at 0.05Mm^2/yr. [6]. Terrestrial temperature time series in Fig. 3.5 reproduce the sea ice behaviour. Hosing results in a faster and more sustained change in SIA, SSS, and SST relative to regional or fingerprint injections. This difference is more dramatic when examining 2m temperatures with 2dSv Hosing resulting in a peak cooling > 2C than any other injection method. We find similar relationships between the FEN-R and MAK-R in the North

[6]Rates calculated as a linear fit from zero sea ice change to peak sea ice coverage at $\approx$ 3Mm^2

Atlantic when comparing SIA, SSS, and SST changes (see Fig. C.7). This result is comparable to what was elucidated in Love et al. [2021] and further supports the idea that, for MPIOM, we are able to capture the relative relationships between the MAK and FEN outlets with similar accuracy as in the eddy-permitting configuration. Comparing these climate metrics and AMOC for GSL-R and GOM-R we find the same biases: freshwater from GOM results in an overall greater climate impact than GSL.

Comparing regional injections to their respective fingerprint counterparts, we find that injecting freshwater at the outlets results in earlier, but not faster, SIA/SST/SSS in the GIN Seas region for the MAK and FEN regions relative to the fingerprint methods. This relationship is also present when examining 2m temperature changes for Europe and at the GRIP ice core in Greenland (see Fig. 3.5. This temporal relationship is at odds with the lag difference discussed in section 3.4.2, where the fingerprints demonstrated less lag relative to the eddy permitting simulations. The amplitude of changes for MAK-R relative to MAK-FP is higher, whereby sea ice fully covers the GIN Seas at roughly the same rate as FEN-R. This feature is due in part to the enhanced surface runoff from Eastern Europe/North Asia, as discussed in section C.2. FEN-FP has similar results on GIN SIA and SSTs as FEN-R but these metrics remain at peak values for approximately twice as long a duration. Freshwater introduced in the GSL-R experiment does not result in any changes of note in the upper layers of the GIN Seas until close to the end of a century after the start of the injection, while the GSL-FP experiment begins freshening, cooling, and growing sea ice $\approx$ 40yrs after the start of injection. This difference corresponds with the relative balance of freshwater across the Gulf Stream from the GSL injection location as discussed in Section 3.4.2. GOM-R results in consistent growth of sea ice and freshening of the sea surface from $\approx$ 40yrs after the onset of injection despite being the furthest injection location from the GIN Seas. This is a result of the freshwater more effectively crossing the Gulf Stream as described in section 3.4.1. The GOM-FP compensates for this effect and is resultantly less effective than the GOM-R at freshening sites of DWF.

In summary, for traditional Hosing we obtain results that are readily expected based on first principles and previous studies (i.e. strong cooling in the NH, severe AMOC reductions, etc.)

For FEN-R and MAK-R we obtain relative sea ice area, SST, and SSS changes in the GIN Seas comparable with the freshening effects observed in Love et al. [2021]. However GOM-R shows a more effective change in the GIN Seas than GSL-R, contrary to these previous results. This ordering is reversed and results align with Love et al. [2021] when using the freshwater fingerprints, demonstrating that we are able to emulate some of the behaviour present at the eddy-permitting scale in our coarse resolution configuration using this methodology. The freshwater fingerprint runs show a delay in SIA, SSS, and SST in the GIN Seas and 2m temperatures over Greenland and Europe relative to their comparable regional injection simulations, due to the less concentrated injection regions

3.5 Conclusions

Freshwater transport, from both glacial and river runoff, may be poorly resolved in long simulations due to the necessarily coarse resolution required to conduct multi-centennial to multi-millennial scale experiments being at odds with the fine-scale transport mechanisms for coastally released freshwater. As such, freshwater Hosing (i.e. injection across wide bands in the North Atlantic) is often used as an approximation, assuming that glacial runoff will inevitably be transported to sites of deep water formation in the North Atlantic. However, this results in freshwater eliciting a disproportionately strong thermohaline circulation and climate response to realistic freshwater fluxes, and as such, inaccurately represents climate changes in response to freshwater injection. In order to better understand the role of glacial runoff in the climate system during the past and future and explore the biases introduced by the choice of freshwater injection method, we address the following questions: Where is freshwater routed at moderate resolution and when is hosing justified? Does the fingerprint method capture eddy permitting behaviour? How do climate impacts vary between different forms of freshwater injection?

To address these questions, we conduct several freshwater injection experiments using three different injection methods. Firstly, we uniformly spread freshwater over a band in the North Atlantic that covers common deep-water formation regions ($50 - 70°N$). Secondly, we inject freshwater at four major outlets in the Northern Hemisphere and allow the eddy-parameterizing model to transport the freshwater. Thirdly, we develop and test a freshwater fingerprint method that distributes the freshwater according to its pathway in an eddy-permitting model. To understand how well the coarse-resolution model represents freshwater transport, we compare the resulting salinity anomalies to those generated from the eddy-permitting model.

We find that regional freshwater injection in an eddy-parameterizing model can reproduce some, but not all, of the major features observed at the eddy permitting scale, with our investigation finding better agreement for the Mackenzie River (MAK) and Fennoscandia (FEN). Freshwater injected directly into these outlets in a coarse-resolution model such as was used here sufficiently represents freshwater transport relative to an eddy-permitting configuration, but does have two main shortcomings. Regional injections in our configuration resulted in slower freshwater transport relative to the eddy-permitting configuration, and marginal seas were not freshened as effectively at the coarser resolutions. The distributions of freshwater from the Gulf of St. Lawrence (GSL) and the Gulf of Mexico (GOM) are those most different from their eddy-permitting counterparts, due to discrepancies in the ability of freshwater to cross the Gulf Stream at eddy-permitting and eddy-parametrizing scales. The more ready crossing of the Gulf Stream impacts the freshwater transport to sites of deep water formation from these locations, over-emphasising the effect of freshwater from the GOM while diminishing the impact of freshwater from the GSL.

Despite these shortcomings, our results readily demonstrate that regional injections yield an increase in realism relative to Hosing. Furthermore regional injections still eliciting a strong AMOC response, and the associated climate cooling, albeit not as swiftly or strongly as Hosing. Given the relative ease of implementing regional injection methods and the overarching similarities in AMOC responses, we conclude that for most situations, Hosing is not an acceptable simplification when considering freshwater sourced from MAK or FEN. However, there remains the significant problem that the excessive transport of freshwater across the Gulf Stream. This excessive transport yields unrealistic freshwater amounts in deep-water formation regions and correspondingly unrealistic AMOC responses from both GSL and GOM, our fingerprint method is effective at reducing this effect.

In seeking to determine if our fingerprint method captures eddy permitting behaviour, we again compare the resulting distributions to those from the eddy-permitting configuration and focus on the specific shortcomings of the regional injection method. We find that the use of the freshwater fingerprint alleviates some, but not all, of the slower transport and subsequent lag in the freshwater anomaly field. Freshening of marginal seas is also improved for the Labrador Sea when using the MAK fingerprint. However, this results in overshooting the freshening observed in the eddy-permitting simulation. Similarly, the GSL-FP simulation exhibits a freshening of the Mediterranean Sea comparable with the GSL-MIT simulation, but with no appreciable overshoot. The use of the GOM fingerprint does result in an earlier freshening of the Mediterranean Sea, but not as effectively as the GSL fingerprint. When comparing the relative rates of AMOC reduction between the regional and fingerprint injection methods for all outlets, we find that the relative impacts of the fingerprints injection methods more closely resemble the amounts of freshwater transported to sites of deep-water formation in the eddy-permitting MITgcm. Thus, we conclude that the fingerprint method offers an improvement to both regional injection and Hosing for the GSL and GOM outlets with freshwater transports to deep water formation sites more closely resembling those from ocean-only eddy permitting simulations. Whether these improvements outweigh the added costs associated with the fingerprint, most notably the expense of configuring and running an eddy permitting model to produce the fingerprints, requires further investigation to quantify.

Finally, we examine how climate impacts vary between our different forms of freshwater injection. We find the overall climate response to Hosing is both faster and greater in magnitude compared to that of regional or fingerprint freshwater injection. When comparing the response of the climate system via AMOC we find that GSL regional injection results in less of a response than the GOM injection, in disagreement with results from the eddy permitting simulations for these outlets. Those same responses are inverted when using fingerprint simulations resulting in a more accurate response. Through either regional forcing or use of freshwater fingerprints, we find that there is no longer a need to rely on band Hosing to elicit AMOC responses. Choosing to use Hosing will lead to over-representation of surface cooling in Greenland and Europe, as well as an exaggerated growth of northern hemisphere sea ice. As such, these biases need to be addressed when pursuing any investigations of climate stability or future climate projections, if choosing to represent freshwater injection as a simple band over sites of deep water formation. The effects of using these freshwater fingerprints in place of Hosing and river runoff on longer duration simulations and Dansgaard-Oeschger-like variability are left to future explorations. We have demonstrated that the climate system is sensitive to the representation of freshwater injection and find that careful understanding of the biases involved from the choice of injection method is required to make robust climate predictions.

3.6 Acknowledgements

The authors would also like to thank those at the GNU and Fedora projects,Kernel.org and in particular those responsible for GNU Parallel [Tange, 2011] whose software greatly sped up and streamlined the analysis in this work. This is a contribution to the ArcTrain program, which was supported by the Natural Sciences and Engineering Research Council of Canada This work is also a contribution to the PALMOD project This research was enabled in part by support provided by SciNet (www.scinethpc.ca) and Compute Canada (www.computecanada.ca) through both Resources for Research Groups allocations and the Rapid Access Service.

Bibliography

L. Ackermann, C. Danek, P. Gierz, and G. Lohmann. Amoc recovery in a multicentennial scenario using a coupled atmosphere-ocean-ice sheet model. *Geophysical Research Letters*, 47(16), Aug 2020. ISSN 1944-8007. doi: 10.1029/2019gl086810. URL http://dx.doi.org/10.1029/2019GL086810.

Paul Aharon. Entrainment of meltwaters in hyperpycnal flows during deglaciation superfloods in the gulf of mexico. *Earth and Planetary Science Letters*, 241(1-2):260270, Jan 2006. ISSN 0012-821X. doi: 10.1016/j.epsl.2005.10.034. URL http://dx.doi.org/10.1016/j.epsl.2005.10.034.

Heather J. Andres and Lev Tarasov. Towards understanding potential atmospheric contributions to abrupt climate changes: characterizing changes to the north atlantic eddy-driven jet over the last deglaciation. *Climate of the Past*, 15(4):16211646, Aug 2019. ISSN 1814-9332. doi: 10.5194/cp-15-1621-2019. URL http://dx.doi.org/10.5194/cp-15-1621-2019.

Taimaz Bahadory, Lev Tarasov, and Heather Andres. Last glacial inception trajectories for the northern hemisphere from coupled ice and climate modelling. *Climate of the Past*, 17(1):397418, Feb 2021. ISSN 1814-9332. doi: 10.5194/cp-17-397-2021. URL http://dx.doi.org/10.5194/cp-17-397-2021.

Niklas Boers. Observation-based early-warning signals for a collapse of the atlantic meridional overturning circulation. *Nature Climate Change*, 11(8):680688, Aug 2021. ISSN 1758-6798. doi: 10.1038/s41558-021-01097-4. URL http://dx.doi.org/10.1038/s41558-021-01097-4.

Wallace S. Broecker, James P. Kennett, Benjamin P. Flower, James T. Teller, Sue Trumbore, Georges Bonani, and Willy Wolfli. Routing of meltwater from the laurentide ice sheet during the younger dryas cold episode. *Nature*, 341(6240):318321, Sep 1989. ISSN 1476-4687. doi: 10.1038/341318a0. URL http://dx.doi.org/10.1038/341318a0.

L. Caesar, G. D. McCarthy, D. J. R. Thornalley, N. Cahill, and S. Rahmstorf. Current atlantic meridional overturning circulation weakest in last millennium. *Nature Geoscience*, Feb 2021. ISSN 1752-0908. doi: 10.1038/s41561-021-00699-z. URL http://dx.doi.org/10.1038/s41561-021-00699-z.

Dudley B. Chelton, Roland A. deSzoeke, Michael G. Schlax, Karim El Naggar, and Nicolas Siwertz. Geographical variability of the first baroclinic rossby radius of deformation. *Journal of Physical Oceanography*, 28(3):433460, Mar 1998. ISSN 1520-0485. doi: 10.1175/1520-0485(1998)028⟨0433:gvotfb⟩2.0.co;2. URL http://dx.doi.org/10.1175/1520-0485(1998)028<0433:GVOTFB>2.0.CO;2.

John A Church, Peter U Clark, Anny Cazenave, Jonathan M Gregory, Svetlana Jevrejeva, Anders Levermann, Mark A Merrifield, Glenn A Milne, R Steven Nerem, Patrick D Nunn, et al. Sea level change. In *Climate Change 2013-The Physical Science Basis: Contribution of Working Group I to the Fifth Assessment Report of the Intergovernmental Panel on Climate Change*, pages 1136–1216. Cambridge University Press, 2013.

Matthew Collins, Reto Knutti, Julie Arblaster, Jean-Louis Dufresne, Thierry Fichefet, Pierre Friedlingstein, Xuejie Gao, William J Gutowski, Tim Johns, Gerhard Krinner, et al. Long-term climate change: projections, commitments and irreversibility. In *Climate Change 2013-The Physical Science Basis: Contribution of Working Group I to the Fifth Assessment Report of the Intergovernmental Panel on Climate Change*, pages 1029–1136. Cambridge University Press, 2013.

A. Condron and P. Winsor. Meltwater routing and the younger dryas. *Proceedings of the National Academy of Sciences*, 109(49):1992819933, Nov 2012. ISSN 1091-6490. doi: 10.1073/pnas.1207381109. URL http://dx.doi.org/10.1073/pnas.1207381109.

Robert M. DeConto and David Pollard. Contribution of antarctica to past and future sea-level rise. *Nature*, 531(7596):591597, Mar 2016. ISSN 1476-4687. doi: 10.1038/nature17145. URL http://dx.doi.org/10.1038/nature17145.

Brendan T Doherty and Dana R Kester. *Freezing point of seawater*. Sears Foundation for Marine Research, 1974.

Mark B Dyurgerov, Mark F Meier, et al. *Glaciers and the changing Earth system: a 2004 snapshot*, volume 58. 2005.

Xun Gong, Gregor Knorr, Gerrit Lohmann, and Xu Zhang. Dependence of abrupt atlantic meridional ocean circulation changes on climate background states. *Geophysical Research Letters*, 40(14):36983704, Jul 2013. ISSN 0094-8276. doi: 10.1002/grl.50701. URL http://dx.doi.org/10.1002/grl.50701.

Feng He. *Simulating transient climate evolution of the last deglaciation with CCSM 3*, volume 72. 2011.

Jenna C. Hill and Alan Condron. Subtropical iceberg scours and meltwater routing in the deglacial western north atlantic. *Nature Geoscience*, 7(11):806810, Oct 2014. ISSN 1752-0908. doi: 10.1038/ngeo2267. URL http://dx.doi.org/10.1038/ngeo2267.

Jeremy S. Hoffman, Anders E. Carlson, Kelsey Winsor, Gary P. Klinkhammer, Allegra N. LeGrande, John T. Andrews, and Jeffrey C. Strasser. Linking the 8.2 ka event and its freshwater forcing in the labrador sea. *Geophysical Research Letters*, 39(18), Sep 2012. ISSN 0094-8276. doi: 10.1029/2012gl053047. URL http://dx.doi.org/10.1029/2012GL053047.

L. C. Jackson and R. A. Wood. Hysteresis and resilience of the amoc in an eddy-permitting gcm. *Geophysical Research Letters*, 45(16):85478556, Aug 2018. ISSN 1944-8007. doi: 10.1029/2018gl078104. URL http://dx.doi.org/10.1029/2018GL078104.

J. H. Jungclaus, N. Keenlyside, M. Botzet, H. Haak, J.-J. Luo, M. Latif, J. Marotzke, U. Mikolajewicz, and E. Roeckner. Ocean circulation and tropical variability in the coupled model echam5/mpi-om. *Journal of Climate*, 19(16):39523972, Aug 2006. ISSN 1520-0442. doi: 10.1175/jcli3827.1. URL http://dx.doi.org/10.1175/JCLI3827.1.

P. Kindler, M. Guillevic, M. Baumgartner, J. Schwander, A. Landais, and M. Leuenberger. Temperature reconstruction from 10 to 120 kyr b2k from the ngrip ice core. *Climate of the Past*, 10(2):887902, Apr 2014. ISSN 1814-9332. doi: 10.5194/cp-10-887-2014. URL http://dx.doi.org/10.5194/cp-10-887-2014.

Mathieu Le Corre, Jonathan Gula, and Anne-Marie Trguier. Barotropic vorticity balance of the north atlantic subpolar gyre in an eddy-resolving model. *Ocean Science*, 16(2):451468, Apr 2020. ISSN 1812-0792. doi: 10.5194/os-16-451-2020. URL http://dx.doi.org/10.5194/os-16-451-2020.

Yonggang Liu, Robert Hallberg, Olga Sergienko, Bonnie L. Samuels, Matthew Harrison, and Michael Oppenheimer. Climate response to the meltwater runoff from greenland ice sheet: evolving sensitivity to discharging locations. *Climate Dynamics*, 51(5-6):17331751, Nov 2017. ISSN 1432-0894. doi: 10.1007/s00382-017-3980-7. URL http://dx.doi.org/10.1007/s00382-017-3980-7.

Gerrit Lohmann, Martin Butzin, Nina Eissner, Xiaoxu Shi, and Christian Stepanek. Abrupt climate and weather changes across time scales. *Paleoceanography and Paleoclimatology*, 35(9), Sep 2020. ISSN 2572-4525. doi: 10.1029/2019pa003782. URL http://dx.doi.org/10.1029/2019PA003782.

R. Love, H. Andres, A. Condron, and L. Tarasov. Eddy permitting simulations of freshwater injection from major northern hemisphere outlets during the last deglacial. *Climate of the Past Discussions*, 2021:1–16, 2021. doi: 10.5194/cp-2021-15. URL https://cp.copernicus.org/preprints/cp-2021-15/.

Syukuro Manabe and Ronald J. Stouffer. Simulation of abrupt climate change induced by freshwater input to the north atlantic ocean. *Nature*, 378(6553):165167, Nov 1995. ISSN 1476-4687. doi: 10.1038/378165a0. URL http://dx.doi.org/10.1038/378165a0.

Syukuro Manabe and Ronald J. Stouffer. Coupled ocean-atmosphere model response to freshwater input: Comparison to younger dryas event. *Paleoceanography*, 12(2):321336, Apr 1997. ISSN 0883-8305. doi: 10.1029/96pa03932. URL http://dx.doi.org/10.1029/96PA03932.

A. J. G. Nurser and S. Bacon. The rossby radius in the arctic ocean. *Ocean Science*, 10(6):967975, Nov 2014. ISSN 1812-0792. doi: 10.5194/os-10-967-2014. URL http://dx.doi.org/10.5194/os-10-967-2014.

Jeffrey D. Parsons, John W. M. Bush, and James P. M. Syvitski. Hyperpycnal plume formation from riverine outflows with small sediment concentrations. *Sedimentology*, 48(2):465478, Apr 2001. ISSN 1365-3091. doi: 10.1046/j.1365-3091.2001.00384.x. URL http://dx.doi.org/10.1046/j.1365-3091.2001.00384.x.

W. R. Peltier, G. Vettoretti, and M. Stastna. Atlantic meridional overturning and climate response to arctic ocean freshening. *Geophysical Research Letters*, 33(6):n/a–n/a, 2006. ISSN 1944-8007. doi: 10.1029/2005GL025251. URL http://dx.doi.org/10.1029/2005GL025251. L06713.

T. P. Rippeth, B. J. Lincoln, H. A. Kennedy, M. R. Palmer, J. Sharples, and C. A. J. Williams. Impact of vertical mixing on sea surfacepco2in temperate seasonally stratified shelf seas. *Journal of Geophysical Research: Oceans*, 119(6):38683882, Jun 2014. ISSN 2169-9275. doi: 10.1002/2014jc010089. URL http://dx.doi.org/10.1002/2014JC010089.

Didier M. Roche, Ane P. Wiersma, and Hans Renssen. A systematic study of the impact of freshwater pulses with respect to different geographical locations. *Climate Dynamics*, 34(7-8):9971013, May 2009. ISSN 1432-0894. doi: 10.1007/s00382-009-0578-8. URL http://dx.doi.org/10.1007/s00382-009-0578-8.

William F. Ruddiman. Late quaternary deposition of ice-rafted sand in the subpolar north atlantic (lat 40 to 65n). *Geological Society of America Bulletin*, 88(12):1813, 1977. ISSN

0016-7606. doi: 10.1130/0016-7606(1977)88⟨1813:lqdois⟩2.0.co;2. URL http://dx.doi.org/10.1130/0016-7606(1977)88<1813:LQDOIS>2.0.CO;2.

Uwe Schulzweida. Cdo user guide, October 2019. URL https://doi.org/10.5281/zenodo.3539275.

Thomas F. Stocker, Lawrence A. Mysak, and Daniel G. Wright. A zonally averaged, coupled ocean-atmosphere model for paleoclimate studies. *Journal of Climate*, 5(8):773797, Aug 1992. ISSN 1520-0442. doi: 10.1175/1520-0442(1992)005⟨0773:azacoa⟩2.0.co;2. URL http://dx.doi.org/10.1175/1520-0442(1992)005<0773:AZACOA>2.0.CO;2.

Henry Stommel. Thermohaline convection with two stable regimes of flow. *Tellus*, 13(2):224–230, 1961.

R. J. Stouffer, J. Yin, J. M. Gregory, K. W. Dixon, M. J. Spelman, W. Hurlin, A. J. Weaver, M. Eby, G. M. Flato, H. Hasumi, and et al. Investigating the causes of the response of the thermohaline circulation to past and future climate changes. *Journal of Climate*, 19(8):13651387, Apr 2006. ISSN 1520-0442. doi: 10.1175/jcli3689.1. URL http://dx.doi.org/10.1175/JCLI3689.1.

Didier Swingedouw, Juliette Mignot, Pascale Braconnot, Eloi Mosquet, Masa Kageyama, and Ramdane Alkama. Impact of freshwater release in the north atlantic under different climate conditions in an oagcm. *Journal of Climate*, 22(23):63776403, Dec 2009. ISSN 0894-8755. doi: 10.1175/2009jcli3028.1. URL http://dx.doi.org/10.1175/2009JCLI3028.1.

O. Tange. GNU Parallel - The Command-Line Power Tool. *;login: The USENIX Magazine*, 36(1): 42–47, Feb 2011. URL http://www.gnu.org/s/parallel.

L Tarasov, A Hughes, R Gyllencreutz, OS Lohne, J Mangerud, and JI Svendsen. The global glac-1c deglaciation chronology, melwater pulse 1-a, and a question of missing ice. In *IGS Symposium: Contribution of Glaciers and Ice Sheets to Sea-Level Change, Chamonix, France*, pages 26–30, 2014.

Lev Tarasov and W.R. Peltier. Arctic freshwater forcing of the younger dryas cold reversal. *Nature*, 435(7042):662665, Jun 2005. ISSN 1476-4687. doi: 10.1038/nature03617. URL http://dx.doi.org/10.1038/nature03617.

Lev Tarasov, Arthur S. Dyke, Radford M. Neal, and W.R. Peltier. A data-calibrated distribution of deglacial chronologies for the north american ice complex from glaciological modeling. *Earth and Planetary Science Letters*, 315316:30 – 40, 2012. ISSN 0012-821X. doi: http://dx.doi.org/10.1016/j.epsl.2011.09.010. URL http://www.sciencedirect.com/science/article/pii/S0012821X11005243. Sea Level and Ice Sheet Evolution: A {PALSEA} Special Edition.

James T Teller, David W Leverington, and Jason D Mann. Freshwater outbursts to the oceans from glacial lake agassiz and their role in climate change during the last deglaciation. *Quaternary Science Reviews*, 21(8-9):879–887, 2002.

W. Weijer, M. E. Maltrud, M. W. Hecht, H. A. Dijkstra, and M. A. Kliphuis. Response of the atlantic ocean circulation to greenland ice sheet melting in a strongly-eddying ocean model. *Geophysical Research Letters*, 39(9):n/an/a, May 2012. ISSN 0094-8276. doi: 10.1029/2012gl051611. URL http://dx.doi.org/10.1029/2012GL051611.

Jiayan Yang. On the importance of resolving the western boundary layer in wind-driven ocean general circulation models. *Ocean Modelling*, 5(4):357379, Jan 2003. ISSN 1463-5003. doi: 10.1016/s1463-5003(02)00058-6. URL http://dx.doi.org/10.1016/S1463-5003(02)00058-6.

X. Zhang, G. Lohmann, G. Knorr, and X. Xu. Different ocean states and transient characteristics in last glacial maximum simulations and implications for deglaciation. *Climate of the Past*, 9(5): 23192333, Oct 2013. ISSN 1814-9332. doi: 10.5194/cp-9-2319-2013. URL http://dx.doi.org/10.5194/cp-9-2319-2013.

Xiao Zhang, Matthias Prange, Ute Merkel, and Michael Schulz. Instability of the atlantic overturning circulation during marine isotope stage 3. *Geophysical Research Letters*, 41(12):42854293, Jun 2014a. ISSN 0094-8276. doi: 10.1002/2014gl060321. URL http://dx.doi.org/10.1002/2014GL060321.

Xu Zhang, Gerrit Lohmann, Gregor Knorr, and Conor Purcell. Abrupt glacial climate shifts controlled by ice sheet changes. *Nature*, 512(7514):290294, Aug 2014b. ISSN 1476-4687. doi: 10.1038/nature13592. URL http://dx.doi.org/10.1038/nature13592.

Chapter 4

The Role of CO2 and Glacial Runoff in Modulating Dansgaard-Oeschger Oscillations in an Earth Systems Model

The Role of CO2 and Glacial Runoff in Modulating Dansgaard-Oeschger Oscillations in an Earth Systems Model

Ryan Love[1], Heather J. Andres[1], and Lev Tarasov[1]

[1]Department of Physics and Physical Oceanography, Memorial University of Newfoundland, St. John's, Newfoundland, Canada

4.1 Abstract

The last glacial cycle is punctuated by multiple instances of large-scale climate change occurring at centennial to millennial timescales. A prototypical example of this form of Centennial- to Millennial-scale Climate Variability (CMCV) are Dansgaard-Oeschger events, which are characterized by global-scale thermal and hydrological changes. During the last glacial cycle, Dansgaard-Oeschger events occur most commonly during the 57ka − 29ka interval. Previous studies have modelled various aspects of this phenomenon but at present the role of pCO_2, which varied by ≈ 40 ppmv over the MIS3 interval, and glacial runoff, remain poorly explored but are understood to be significant. As such, we seek to elucidate the roles of freshwater and atmospheric pCO_2 on this form of variability through the use of a coarse-resolution, fully coupled Earth System Model in a set of configurations appropriate for MIS3 that demonstrates CMCV. This set of configurations brackets the range of pCO_2 values during the MIS3 interval, features multiple freshwater injection approaches of varying complexity and injection rates, and uses orbital parameters and ice sheet distributions appropriate for 38 ka.

We find that interstadial durations are sensitive to increases in pCO_2, such that increasing pCO_2 increases the duration of interstadial (warm/interglacial) intervals. This feature is consistent with the Thermohaline Oscillator hypothesis of Dansgaard-Oeschger events, which proposes the pacing of stadial to interstadial durations is set by the rate of heat export to sites of deep water formation. We find these relationships are due to an enhanced temperature gradient between the subsurface Atlantic waters and Nordic Seas waters as pCO_2 increases. Comparatively, our results do not indicate that the average stadial (cold/glacial) duration is dependent on the background pCO_2, although the maximum stadial duration is reduced by 75% when comparing 175 ppmv to 207 ppmv. The wide range of stadial durations and sparseness of events from which to obtain a distribution weaken the strength of any conclusions regarding the relationship between average stadial durations and pCO_2.

We find freshwater can modulate CMCV in one of three ways depending upon both the injection region and rate. As with pCO_2 decreases, we find freshwater decreases interstadial durations when

directly using glacial runoff in accordance with ice sheet volume changes at 38 ka as per the GLAC1E reconstruction. At fluxes greater than 0.5 dSv, continual freshwater forcing in either the $50-70°$ N band or from the Mackenzie River is enough to suppress the AMOC and drive the model into a perennial stadial mode. For both of these injection regions, fluxes $<$ 0.5 dSv yield regularly periodic CMCV, whose period depends upon the injection region rather than the rate. Injections into the $50-70°$ N band result in the fastest oscillations.

4.2 Introduction

The last glacial cycle is punctuated by multiple instances of large-scale climate change occurring at centennial to millennial timescales. A canonical example of such variability is Dansgaard-Oeschger (DO) events, notable during Marine Isotope Stage 3 (MIS3) ($\approx$ 57 kaBP $-$ 29 kaBP), which are identified as centennial- to millennial- scale excursions in δ^{18}O values from Greenland ice core records. During a DO event, Greenland surface temperatures increase by $\approx 6.5-15°$ C[1] on the time-scale of decades [Kindler et al., 2014]. This magnitude of warming is comparable to the difference in Greenland surface temperatures between the last glacial maximum (LGM, $\approx -45°$ C) [Kindler et al., 2014] and preindustrial period ($\approx -32°$ C)[Kobashi et al., 2011]. While DO events were initially identified in Greenland ice core records, as in Dansgaard et al. [1984], and indicate temperature changes there, they are also recorded in other paleoclimate records. These records indicate changes in surface temperatures over Europe [Genty et al., 2003], oceanographic features (e.g. temperature, salinity, sea ice cover) in the Nordic Seas [Dokken et al., 2013], and hydrologic cycle changes for the South American and South Asian monsoon regions [Corrick et al., 2020]. Corrick et al. [2020], Adolphi et al. [2018] find that most interstadials identified in Greenland ice cores can be identified in multiple speleothem records that include the South American Monsoon region, the South Asian Region, and Southern Europe. In addition, a climate proxy record from a marine sediment core in the Greenland-Iceland-Norwegian (GIN) Seas reflect these climate events and indicates that changes associated with DO events affect the structure of the entire water column

[1]Range provided for MIS3

[Dokken et al., 2013]. These features are used to decipher the mechanisms underlying DO cycles.

Despite the intense interest in DO events, a complete mechanistic understanding of this type of variability remains elusive. Historically, explanations have focussed on one of two main mechanisms: the 'salinity oscillator' as described by Broecker et al. [1990], Birchfield and Broecker [1990] and the modelling work of Ganopolski and Rahmstorf [2001], Peltier and Vettoretti [2014], Klockmann et al. [2020], and the 'thermohaline oscillator' described by Shaffer [2004], Dokken et al. [2013], and Brown and Galbraith [2016]. These two mechanisms are not necessarily mutually exclusive, but they emphasize different regions and processes in the evolution of DO events. They are outlined below, beginning with the salinity oscillator.

The salt oscillator mechanism posits that transitions between two states of Atlantic Meridional Overturning Circulation (AMOC), and resultantly Northern Hemisphere climate, are modulated by periods of salt build-up and salt drain-down in the Atlantic. The abrupt transitions between them triggered by the passing of critical density thresholds. The AMOC is understood to switch between 'on' and 'off' quasi-stable states, where 'on' is comparable to present day. The 'off' state is described as a mode with reduced heat release from the northern North Atlantic and reduced export of North Atlantic deep water (NADW) to the Southern Ocean, similar to its configuration at LGM [Broecker et al., 1990, Birchfield and Broecker, 1990]. In a contemporary context, these modes are better described as Greenland interstadial and stadial modes of operation, as per Rahmstorf [2002], where the term 'off mode' is reserved for an even lower AMOC state associated with Heinrich events. While the salt oscillator mechanism depends critically on the accumulation and advection of relatively saline and fresh seawater masses, the understanding of the cause and location of the accumulation of salinity have changed with time. In Broecker et al. [1990], Birchfield and Broecker [1990], salt accumulates in the North Atlantic via the atmospheric transport of evaporated freshwater westward into the Pacific Ocean catchment. It is counterbalanced during AMOC on states by a warming of northern high latitudes that increases glacial melt, which enters the North Atlantic as freshwater runoff. AMOC transitions to 'on' are initiated by the passing of a critical density threshold wherein the density of deep water formed in the North Atlantic is greater than that of the surrounding oceans, permitting the transport of North Atlantic deep water out of the Atlantic basin and thereby reinvigorating the AMOC. This balance between evaporation and freshwater input in the Nordic Seas was found to control Centennial- to Millennial-scale Climate Variability (CMCV) in the CLIMBER Earth Model of Intermediate complexity (EMIC) under glacial boundary conditions [Ganopolski and Rahmstorf, 2001]. Indeed, transitions were found to be self-reinforcing, such that regardless of the magnitude of the triggering, once the density threshold was exceeded, the AMOC made a full transition to the opposite state.

More recent interpretations of the salinity oscillator mechanism, as in Peltier and Vettoretti [2014], Vettoretti and Peltier [2016], Klockmann et al. [2020], do not invoke changing freshwater input into the ocean to counterbalance the saline signal from evaporation and thereby terminate the interstadial state. In the unforced CMCV of these studies with more complex Earth System Models (ESMs) [Peltier and Vettoretti, 2014, Vettoretti and Peltier, 2016, Klockmann et al., 2020], salinity oscillates between the North Atlantic subpolar and subtropical gyres, leading to a redistribution of relatively fresh and saline water masses within the North Atlantic. The subtropical gyre exhibits anomalously high salinity values during Greenland stadial states, at the same time as salinity in the north-eastern North Atlantic is anomalously low. Klockmann et al. [2020] demonstrates that this state arises in MPI-ESM due to the subpolar gyre extending into the north-eastern North Atlantic, where deepwater forms at that model configuration. This restricts the northward flux of saline water from the subtropical gyre region, leading to the accumulation of salinity there, and weakens the AMOC by filling the deepwater formation zone with relatively fresh, subpolar water. In Vettoretti and Peltier [2016], the transition to an interstadial state is triggered by the gradual salinification of the surface layer and thinning of sea ice in the northern North Atlantic that undermines local stratification, opens a polynya, and leads to vertical convection. This results in an enhanced northward flux of salinity from the subtropical gyre region and an accompanying increase in AMOC [Peltier and Vettoretti, 2014]. In Klockmann et al. [2020], a reduction in sea ice cover in the North Atlantic initiates a transition by transferring heat to the atmosphere that strengthens the Icelandic Low and directs additional warm air to the sea ice margin. The warm winds melt additional sea ice and strengthen the subpolar gyre in the north-eastern North Atlantic, which increases the northward transport of subtropical water to sites of deepwater formation and initiates convection there. No mechanism for the reduction in sea ice cover is discussed, but its occurring randomly is proposed. When the subpolar gyre eventually weakens and contracts, saltier subtropical-sourced water dominates the eastern North Atlantic, and the AMOC is strong. In these studies, the return to stadial conditions occurs as sea ice starts to regrow and northward salt fluxes decrease in response to a reduction in the relative salinity difference between the subtropics and subpolar regions. Recent work by Vettoretti and Peltier [2018] also invokes the role of sea ice export from the Arctic to sites of deep water formation as enhancing the stratification and thereby reducing deep water formation.

The thermohaline oscillator mechanism is similar to the salt oscillator in its dependence on density differences driving AMOC changes, but the heat transport to regions of deep water formation, heat build-up under sea ice in regions of deep water formation, and its effect on vertical mixing all play a much more important role. Fundamental to this mechanism is the accumulation of sub-surface heat in the northern North Atlantic during a Greenland stadial that eventually leads to a vertical temperature inversion that destabilizes the water column and induces deep convection [Olsen et al., 2005, Shaffer, 2004, Dokken et al., 2013, Brown and Galbraith, 2016]. A transition back to stadial conditions arises in a range of studies, from a box-model approach [Olsen et al., 2005], to a highly simplified EMIC [Shaffer, 2004], and a more complex ESM [Brown and Galbraith, 2016], when a strong halocline develops in the northern North Atlantic under Greenland interstadial conditions. In Brown and Galbraith [2016], this halocline develops in response to renewed sea ice growth, particularly when freshwater is added to the surface of the northern North Atlantic. In Shaffer [2004], the halocline develops in response to the reduction in poleward salinity transport associated with a weakening AMOC under cooling lower latitudes. Their observed cooling is a result of colder water infiltrating from below, as the deep Atlantic has been filled by Antarctic Bottom Water (AABW) at this point in the mechanism, and importing of colder water from southern latitudes. In both investigations, the halocline suppresses vertical convection in the northern North Atlantic, and the AMOC weakens and shoals. Under a weak AMOC, the deep Atlantic fills with cold Antarctic Bottom Water (AABW), while the interior of the North Atlantic above 2500 m warms in response to a downward diffusion of heat at low latitudes. Some of this accumulated heat is transported towards the northern North Atlantic via weak circulation and horizontal mixing, contributing once more to the accumulation of sub-surface heat. In contrast, after the onset of the AMOC strong mode, North Atlantic-sourced water fills the deep North Atlantic, and the interior above 2500 m cools due to convection.

The thermohaline oscillator mechanism is consistent with the progression of events inferred from a marine sediment core situated in the Nordic Seas and the conceptual model based on them described in Dokken et al. [2013]. An interpretation of the marine sediment core provided in Dokken et al. [2013] reveals that the Nordic Seas switched between two distinct modes numerous times during the MIS3 interval. During Greenland stadial intervals, the surface is relatively fresh (as a result of melting and calving of the adjacent Fennoscandian ice sheet during interstadial intervals) with a subsurface halocline supported by continual sea ice formation and brine rejection along the coastline [Jensen et al., 2018]. As in Shaffer [2004], Brown and Galbraith [2016], warmer Atlantic water circulates below the halocline and transports heat to the region, resulting in a build-up of subsurface heat and eventually leading to a convective instability and overturning. This overturning results in the melting of sea ice in the Nordic Seas and the release of subsurface heat to the atmosphere. Interstadial conditions in the region are comparable to the present: the Nordic Seas are free of sea ice, have a weakly stratified water column, and readily release heat from the ocean to the atmosphere. Dokken et al. [2013] does not provide a mechanism by which interstadial intervals transition to stadial intervals but notes that there is a constant decrease in salinity towards the termination of interstadials. This decrease in salinity is in agreement with the termination of interstadials in the results of Vettoretti and Peltier [2018], Brown and Galbraith [2016], and Shaffer [2004].

The investigations summarised above all generally examine their mechanisms of CMCV from the perspective of high-latitude climate changes, however the role of low-latitude climate changes on CMCV has also been examined. For example, the role of the inter-tropical convergence zone (ITCZ) on thermohaline circulation (THC) centennial scale variability has been discussed in Vellinga and Wu [2004] where it is found that oscillations in the THC are coupled to changes in the ITCZ. Enhanced northward ocean heat transport associated with a strong THC results in an enhanced and more northerly ITCZ. This associated increase in precipitation in the tropical North Atlantic eventually leads to a freshwater anomaly which propagates to the subpolar North Atlantic with a lagged (on the order of several decades) THC response. While the results of Vellinga and Wu [2004] indicate a much faster response than is associated with DO events, the overall pattern of low-latitude changes leading to oscillations in the THC has been demonstrated on longer timescales in Zhang [2021].

In summary, the salt oscillator may be generalized as the oscillation of salt between the subtropical and subpolar regions, where transitions may be triggered by changes in sea ice, density contrasts, or via freshwater influx. The thermohaline oscillator instead focuses on the resumption of AMOC via thermally destabilizing the water column in the region of DWF and entering the weak mode of AMOC via the regrowth of a strong halocline in the northern North Atlantic, possibly in response to sea ice changes and/or temperature gradients. As mentioned earlier, these two proposed mechanisms to describe DO events are not mutually exclusive, and their common dependence on changes in sea ice extent and the opening of polynyas during stadial-interstadial transitions suggests that they may both be contributing simultaneously to different aspects of DO variability.

The idea of a 'sea ice switch' mechanism modulating large-scale glacial transitions is posited by Gildor and Tziperman [2003] and is proposed to be one means of explaining both $100,000$ year variability and CMCV. They argue that sea ice feedbacks provide a ready means of producing rapid climate transitions, so long as two different quasi-stable sea ice configurations exist under the same boundary conditions. This is due to the ability of sea ice to moderate fluxes of heat and moisture between the ocean and atmosphere and to respond on short (annual to decadal) time scales. The former feature is core to both hypotheses with anomalies of heat or salinity being built up under a sea ice lid.

The boundary conditions applied to models in previous work have been shown to affect both sea ice states and CMCV. Previous work with the ESM used in this study, COSMOS, and a largely comparable one, MPI-ESM, demonstrates that these models exhibit aspects of both mechanisms as they respond to changes in ice sheet height [Zhang et al., 2014a, Klockmann et al., 2018], greenhouse gases [Zhang et al., 2017, Klockmann et al., 2018], and orbital forcing [Zhang, 2021]. We summarize here their and others conclusions regarding the relationships of these climate forcings and DO event characteristics. We first look at the relationships with ice sheet volume.

Increased global ice volume is associated with shorter interstadials in statistical modelling performed of DO events from the NGRIP ice core record [Lohmann and Ditlevsen, 2018]. As well, there appears to be a threshold above which no events occur given that DO events and other CMCV like the Younger Dryas only occur at intermediate ice volumes (according to ice sheet reconstructions such as Tarasov et al. [2012] and the relative sea level record of the last glacial cycle [Lambeck, 2001]). This limiting threshold for CMCV with respect to ice volume during the last glacial cycle is supported by box-modelling results [Sima et al., 2004]. Similarly, there is no CMCV during the 100 ka to 90 ka interval, so there may be a minimum ice volume threshold as well (see Fig. 4.1). However, this threshold behaviour is not necessarily reproduced in modelling studies. Published examples of simulated CMCV discussed above are in some cases produced with either present day ice sheets (such as Klockmann et al. [2020]) or last glacial maximum ice sheets (such as Peltier and Vettoretti [2014], Vettoretti and Peltier [2016]). In COSMOS, hysteresis exists for the AMOC in response to ice sheet height changes only over a range of approximately 18m ESL (where the North American ice complex area is fixed to an LGM configuration) [Zhang et al., 2014a]. Also, when in this sensitive range, a change in the height of the Northern Hemisphere ice sheets corresponding to as little as a 2m ESL change (40% to 45% LGM height) can be enough to induce a transition via changes in atmosphere-ocean-sea ice feedbacks that modify the heat distribution and sea ice concentration in the North Atlantic.

Orbital configurations with higher summer insolation in the Northern Hemisphere are associated with shorter stadial durations in Lohmann and Ditlevsen [2018] and overall higher frequency variability in Brown and Galbraith [2016]. Zhang [2021] find that these configurations generate competing influences on deepwater formation, whose interplay results in CMCV transitions in COSMOS. On one hand, increased summer insolation reduces sea ice extent, which leads to greater heat loss from the subpolar North Atlantic and increased North Atlantic deepwater formation. On the other hand, it also reduces the export of moisture from the tropical Atlantic via modulating trade-wind strength, resulting in greater freshening when this water reaches sites of DWF.

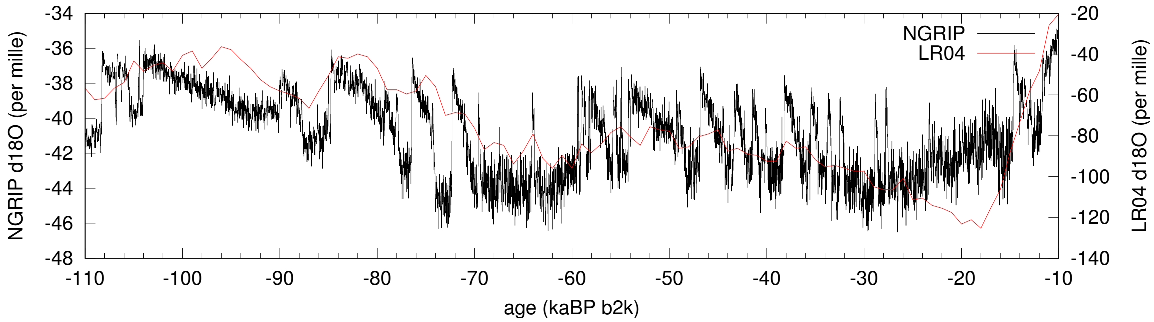

Figure 4.1: δ^{18}O for the NGRIP Greenland ice core [Seierstad et al., 2014] representing local Greenland temperatures and the LR04 stack [Lisiecki and Raymo, 2005] representing ice sheet volume.

Across multiple studies, there appears to be a narrow range of pCO_2 concentrations which support CMCV and allow it to occur spontaneously. Klockmann et al. [2018] identifies the window of pCO_2 values over which AMOC variability is enhanced and CMCV is observed between $195 - 217$ ppmv pCO_2 and only with a pre-industrial ice sheet configuration. Comparatively, Brown and Galbraith [2016] found only 180 ppmv supported CMCV and again only with pre-industrial ice sheets. However, they tested very large steps between prescribed pCO_2 values (120, 147, 180, 220, and 270 ppmv), so there is a large degree of uncertainty in the actual range. Besides being a control on the potential for CMCV, previous work also indicates that the durations of the strong and weak modes are sensitive to pCO_2 concentrations. Zhang [2021] and Klockmann et al. [2018] find that the durations of AMOC strong modes increase with greater values of pCO_2.

While neither of the presented DO mechanisms rely on Hosing [2], these climate events occur in a background of an evolving glacial landscape, one aspect of which is glacial runoff. It is well established that freshwater introduced into the North Atlantic can induce rapid and geographically wide-spread climate change by suppressing the AMOC [Kageyama et al., 2013]. For this reason, freshwater has been used to set the pacing of CMCV in transient climate simulations [He, 2011]. Brown and Galbraith [2016] investigates the impact of Hosing with their configuration and note several significant differences in CMCV features as a result. When incorporating freshwater Hosing,

[2]freshwater applied in wide bands across the North Atlantic either over or adjacent to sites of deep water formation

they find their cold intervals become longer due to surface freshening and enhanced stratification. By comparison, their un-forced simulations demonstrate the same AMOC inhibition associated with cold intervals but with lesser magnitudes. Finally, the transition between stadial and interstadial modes is gradual in their un-hosed simulations and abrupt in their Hosed simulations.

Previous investigations, while providing important insight into potential mechanisms and sensitivity to boundary conditions, have some limitations which need to be considered. Of the more recent studies which examine unforced CMCV in the context of DO events, Peltier and Vettoretti [2014], Vettoretti and Peltier [2016], Klockmann et al. [2020] do not use boundary conditions consistent with intervals which exhibit this form of CMCV (e.g. MIS3). Peltier and Vettoretti [2014], Vettoretti and Peltier [2016] use LGM boundary conditions for both ice sheets and orbital configurations, while Klockmann et al. [2020] use present-day ice sheets with LGM orbital parameters. An examination of the paleoclimate archive (see Fig. 4.2 and discussion in Lohmann and Ditlevsen [2018]) shows CMCV are sensitive to both these parameters and occur only under intermediate ice sheet volumes. This disconnect between modelled CMCV and observations suggests that this form of variability is dependent on the model mean state. Shaffer [2004] and Ganopolski and Rahmstorf [2001] both rely on simplified and coarse resolution EMICs in their investigations, the former of which resolves only basin-scale features, making an examination of regional dependencies difficult if not impossible. As well, the latter employs both negative (freshwater) and positive (evaporation) salinity anomalies varying sinusoidally about an average of 0. While increased freshwater fluxes during a period of glacial evolution can be readily assumed, evaporation of a comparable amount over a comparatively small domain is difficult to justify.

While no study as of yet has bracketed the range of stadial/interstadial durations observed in the paleoclimate records while under self-consistent glacial conditions using a fully coupled ice-ocean-atmosphere Earth Systems model, it is clear that progress towards this goal has been made. As summarised above, recent studies demonstrate that there are a wide range of factors which can affect the characteristics of CMCV and, to a lesser extent, the mechanism itself. We choose to focus on two such factors, pCO_2 and glacial runoff/freshwater, for the following reasons. Freshwater input was chosen as a sensitivity parameter both because it is known to have the potential to affect

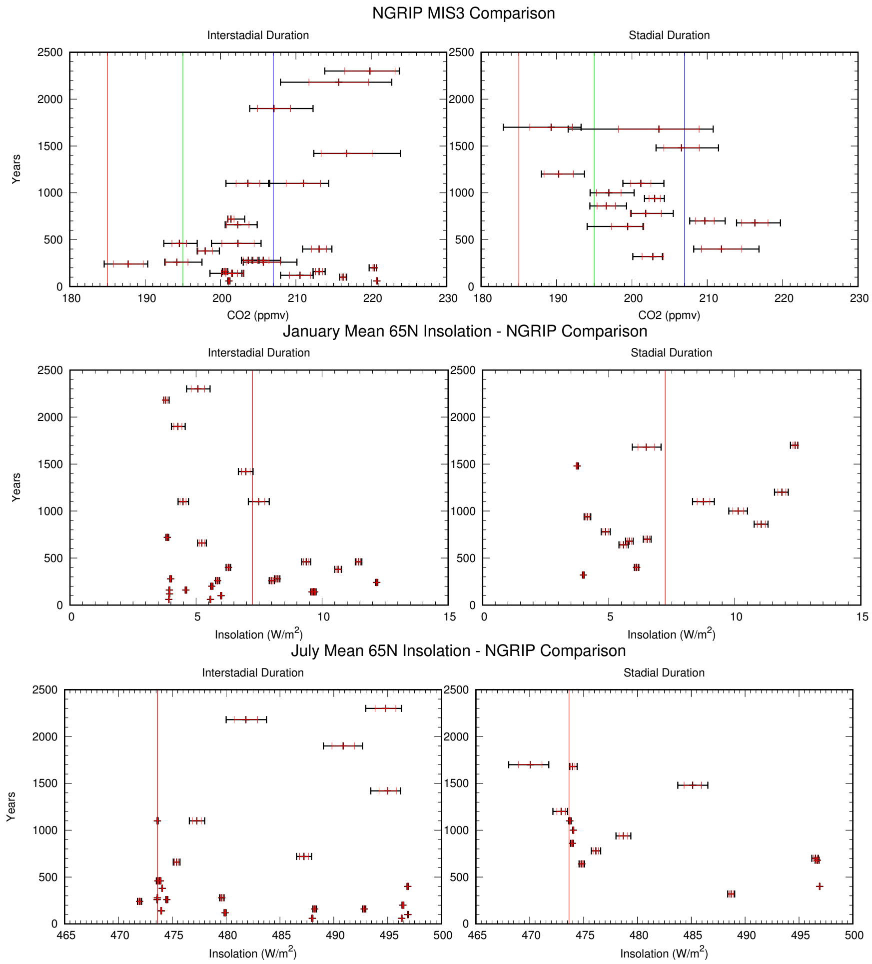

Figure 4.2: Stadial/Interstadial durations as a function of pCO_2, insolation at 65N for January and July during MIS3. Durations determined from the event years as per Rasmussen et al. [2014] with corresponding pCO_2 values from Bereiter et al. [2015]. Insolation values shown are monthly mean and determined from Laskar et al. [2004]. Black lines indicate max-min values during the intervals while thin red lines indicate 1σ. pCO_2 and insolation values were linearly interpolated annually to determine mean and standard deviation. Events from GS-5.1 to GI16.1a are shown. Vertical lines in the top panel indicate the background pCO_2 values we explore in this study, red is 185ppm, green is 195ppm, and blue is 207ppm. Similarly, the red line in the bottom two panels show the insolation for our orbital configuration. When considering interstadial durations greater than 500 years, pCO_2 is more strongly correlated than July insolation at 65° N, with R^2 values of $\approx$ 0.65 and $\approx$ 0.18 respectively.

aspects of the main mechanisms presented and because MIS3 is a period of glacial evolution where regional freshwater discharge is changing due to evolving ice sheets. One important source of uncertainty associated with freshwater is its location of injection and we anticipate some sensitivity to the location of the injection due to the differences in transport pathways. This is due to both the AMOC sensitivity to injection location and method as described in Love et al. [2021b] and the accumulation-discharge behaviour for Mackenzie River sourced freshwater from Condron and Winsor [2012]. Hence, in this study, we use multiple representations of freshwater injection with different spatial distributions: namely, broad-band Hosing, regional injection from probable sites of glacial runoff, a direct mapping of glacial runoff, as well as the novel freshwater fingerprint method as described in Love et al. [2021b]. Specifically, we seek to elucidate the roles of freshwater and pCO_2 on this form of variability through the use of a coarse-resolution, fully coupled Earth System Model in a set of configurations which features CMCV.

pCO_2 was chosen as a sensitivity parameter as previous studies (e.g. Brown and Galbraith [2016], Klockmann et al. [2018], Zhang [2021]) have demonstrated that simulated CMCV are sensitive to pCO_2. Furthermore pCO_2 varied significantly during MIS3 (see Fig. 4.2) [Bereiter et al., 2015] As well, under the thermohaline oscillator hypothesis, changing the background temperature via pCO_2 ought to affect the pacing of the oscillations directly via changing oceanic distributions of heat, its rate of transport, and via changing sea ice margins.

There are other boundary conditions that varied during the MIS3 interval which may be considered, such as orbital and orographic forcing (via changes to ice sheet geometry). Changes to orbital parameters can result in complex changes in the spatial and temporal distribution of insolation, such as the enhancement of boreal seasonality via changes in obliquity. While radiative changes due to pCO_2 variation are not spatially uniform Huang et al. [2016], the overall distribution should be similar for the range of pCO_2 which occurred during MIS3. We elect to leave orbital forcing to future work and instead focus on pCO_2 as our source of radiative forcing due to pCO_2's spatial and temporal simplicity by comparison to orbital forcing. This uniformity should simplify the examination of the impacts of radiative forcing changes on simulated CMCV. With regards to exploring the sensitivity of CMCV to changes in ice sheet geometry, one component of our configuration cannot be automated at present. As such, comprehensively exploring this component of the parameter space with our numerical model would be inefficient at this time, as such this is left to future work.

4.3 Experimental Design

4.3.1 Model Configuration

We use the COSMOS Earth System Model to explore the relationships between glacial runoff or background carbon dioxide levels and centennial- to millennial-scale climate variability (CMCV) This model has been used multiple times in paleoclimate modelling publications (eg. Zhang et al. [2014a,b], Love et al. [2021b]) and is utilized here due to its balance between complexity and computational efficiency as well as its ability to exhibit CMCV. COSMOS is a CMIP3-era, coarse-resolution, fully coupled Earth System Model composed of the MPIOM (the Max Planck Institute Ocean Model), the ECHAM5 (ECMWF Hamburg Version 5) atmosphere model, and the JSBACH land surface model. COSMOS readily allows for millennial timescale climate simulations on the scale of days to weeks of wall-time using moderate computer resources (a single 40-core compute node per simulation in our case). ECHAM5 is run at T31 spherical harmonic grid resolution with 20 vertical levels. MPIOM is a primitive-equation ocean model using the Boussinesq and hydrostatic approximations with a free-surface formulation [Jungclaus et al., 2006]. It is run in the GR30 grid configuration, which has a nominal horizontal resolution of 3 degrees (120x101x40) at the equator with 40 vertical levels. The GR30 grid also features a displaced pole in Greenland which yields enhanced horizontal resolution in the Arctic Ocean, GIN Seas, and Labrador Sea. MPIOM exchanges information with ECHAM via the OASIS coupling software at daily intervals. The enhanced northern horizontal resolution results in average and minimum horizontal resolutions of ≈ 160 km and ≈ 20 km, respectively, versus the ≈ 270 km global average.

The horizontal ocean grid resolution is much coarser than required to explicitly resolve mesoscale eddies [Nurser and Bacon, 2014] and is thus eddy parametrizing using the Gent-McWilliams eddy parametrization [Gent and Mcwilliams, 1990]. Vertical mixing is accomplished via a modified

Pacanowski-Philander (PP) scheme (Pacanowski and Philander [1981]), where an additional wind-induced stirring parameter is introduced Marsland et al. [2003] to account for under-representation of near surface mixing. Recent work [Gutjahr et al., 2021] examined the effects of this parameterization on simulated present-day climate, by comparison to other parameterizations such as the KPP parameterization used in Peltier and Vettoretti [2014], and found that this scheme performs well but induces several biases relative to other mixing schemes. The largest biases resulting from the PP scheme are a colder central North Atlantic, thicker Arctic sea ice, and a weaker AMOC, each of these we discuss here in turn. A colder central North Atlantic is not impactful to our results as surface temperatures in this region do not impact our CMCV. In this study, thicker Arctic sea ice should not impact our results, however it would need consideration for future work examining the impact of sea ice export to sites of deep water formation on CMCV, as in Vettoretti and Peltier [2018]. Finally, a weaker AMOC may affect the timing of our CMCV stadial/interstadial durations. However quantifying this impact is beyond the scope of this study.

We choose boundary conditions consistent with the 38 ka interval, as it is the approximate time of the most recent long period MIS3 Dansgaard-Oeschger cycle in Greenland ice core records and it thereby has somewhat better-constrained boundary conditions compared to earlier long period events in MIS3 events. However, it is worth noting that the ice sheet configuration is the least constrained boundary condition and also poses one of the larger differences with respect to comparable studies. We use the GLAC1E.NA3085 reconstruction for the 38 ka land ice, topography, and sea level configuration. The NA3085 North American component is a variant of the nn9927 chronology from an approximate Bayesian calibration of a glaciological model [Tarasov et al., 2012] against a large set of relative sea level, geological, and geodetic datasets. The imposed modifications on the glacial index for the climate forcing and a few ice sheet model ensemble parameters enabled consistency of NA3085 with new MIS3 ice extent constraints [Carlson et al., 2018]. These modifications also significantly reduced ice volume and area over the 55 to 31 ka interval compared to that of nn9927. The remaining global ice sheet chronologies are that of the default GLAC1D reconstruction [Tarasov and Peltier, 2003, Briggs et al., 2014, Tarasov et al., 2014]. Non-eustatic sea level adjustments (as per the sea-level model of Mitrovica and Milne [2003] but without the rotational component [Milne and Mitrovica, 1998]) have been included. Details of the method used to generate the paleo-bathymetry and topography inputs for COSMOS are available in supplemental Section D.2. The Bering Strait and Canadian Arctic Archipelago are closed, and parts of the Arctic are glaciated further offshore than present land-sea boundaries. However, the Barents-Kara Sea remains open. These features result in a more isolated Arctic ocean by comparison to the present. Incoming solar radiation changes due to changes in the Earth's orbit are handled internally by COSMOS [Berger, 1978] with values set to 38kaBP. For greenhouse gases, we use values guided by the reconstructions of Bereiter et al. [2015], Loulergue et al. [2008], Schilt et al. [2010] for pCO_2, CH4, and N2O respectively. We use 405 PPBV CH4, and 207.5PPBV N2O for all simulations and pCO_2 ranging from 165-207 PPMV (see table 4.1 for a full listing). Drainage data for the river transport model is calculated offline prior to the simulation using tools from the Max Planck Institute (Pers. Comm., Tobias Stacke). Land surface data required by the JSBACH model is set to preindustrial conditions but modified to be consistent with the land ice reconstruction with regards to land ice extent. This largely consists of replacing pre-industrial grid-cell values with those appropriate for land ice coverage in glaciated areas according to existing values in the model input datasets. Vegetation types are as in COSMOS's pre-industrial datasets, but the plant functional types have been allowed to adjust to glacial conditions through the dynamic vegetation component of JSBACH.

4.3.2 Experiments and Forcings

Our experiments consist of a series of simulations with fixed boundary conditions whose members differ both in carbon dioxide concentrations as well as freshwater forcings. See Table 4.1 for a full list of experiments. pCO_2 values range between $165 - 207$ ppmv. These values capture the range of pCO_2 recorded during the MIS3 interval around 38 ka as per the reconstruction of Bereiter et al. [2015], both before and after the DO event occurring then, with additional lower-end members to capture the sensitivity of our model to this forcing. Additional low-end members were chosen as initial results indicated that lower-pCO_2 values provided greater stadial durations more representative of the paleoclimate record. Similarly, to explore the sensitivity of CMCV in COSMOS to freshwater forcing, we use four different injection distributions that represent glacial runoff at varying levels of complexity. These 4 injection distributions can be briefly summarised as: Hosing, regional, glacial-routing, and fingerprint freshwater distributions. The reasoning behind our choice to explore multiple different forms of freshwater injection, rather than use only the prototypical $50-70°$ N band in the North Atlantic (i.e. Hosing), is multi-fold. Firstly, it has been shown in multiple investigations that injecting into the $50-70°$ N band in the North Atlantic is not representative of where freshwater is advected from multiple probable outlets of glacial runoff [Condron and Winsor, 2012, Love et al., 2021a,b]. The use of this Hosing band is also understood to result in more rapid and stronger AMOC reduction and climate changes [Love et al., 2021b]. While using regional outlet injection is a more realistic representation of glacial runoff, this method has biases for specific regions of glacial runoff which can be addressed by the use of the freshwater fingerprint approach [Love et al., 2021b]. Finally, we use the glacial runoff distribution from GLAC1E over regional injection alone as this scenario is the most reflective of glacial runoff during this period. Each of the four employed freshwater injection distributions are discussed in detail below. For each of the injection simulations the freshwater is injected continually for the duration of the simulation.

The simplest injection distribution of our ensemble deposits freshwater uniformly over a band spanning $50-70°$ N across the North Atlantic, a distribution that will be referred to as 50-70N or Hosing throughout this investigation. Hosing is used to initiate a significant decrease in AMOC and associated northward heat transport, and to compare climate changes between models (as in Kageyama et al. [2013]). It is similarly used to replace either glacial runoff (e.g. Arctic-derived freshwater as in Peltier et al. [2006], or generalized ice-sheet runoff [He, 2011]) or freshwater sourced from iceberg armadas (i.e. the Ruddiman Belt as in TRACE21ka [He, 2011]). We run Hosing experiments with 3 different flux magnitudes into the $50-70°$ N band (0.5 dSv, 1 dSv, and 2 dSv), whose value approximately bracket peak inferred rates of discharge [Tarasov and Peltier, 2006]. As discussed, this distribution choice introduces biases in the AMOC response, however we elect to include this form of freshwater injection to provide a comparison to other studies. All injection methods add freshwater to the ocean via the liquid freshwater flux field to the ocean.

The regional freshwater distribution adds increased complexity by releasing freshwater from several of the major drainage outlets for the North American Ice Complex or the Fennoscandian ice sheet. The North American Ice Complex outlets include the Mackenzie River (MAK), the Gulf of the St. Lawrence (GSL), and the Mississippi River into the Gulf of Mexico (GOM), while the Fennoscandian (FEN) ice sheet injection location is a region off the coast of Norway. Fluxes of 2 dSv are used for all of these outlets, with additional values of 0.25 dSv, 0.5 dSv, and 1 dSv for the Mackenzie River regional injection location.

In addition to the outlet-specific direct injections, we also injected freshwater along the coastal regions of North America and Eurasia, following the rates of volumetric ice change of the GLAC1E reconstruction at 38ka and its associated drainage routing map. This corresponds to a total flux of ≈ 0.43 dSv. We also conduct experiments where we double the injection volumes used for this method to test the sensitivity of the system to increased freshwater amounts.

The most complex injection distribution uses the freshwater fingerprint approach explored in Love et al. [2021b] for each of these outlets. The fingerprint method allows us to approximate features not explicitly resolved by our relatively coarse-resolution ocean model by distributing freshwater according to a weighted distribution map created from an eddy-permitting, ocean-only model [Love et al., 2021b]. All of the fingerprints used in this investigation are presented in Fig. 1 of Love et al. [2021b]. For the freshwater fingerprint injection, we use constant freshwater injections rates of 2 dSv. These values are in line with both typical freshwater injection rates as used in previous studies [Kageyama et al., 2013] and bracket estimates for fluxes associated with the triggering of stadial conditions. Peak centennial-mean values of $1 - 1.5$ dSv for any single discharge sector of the North American Ice Sheets have been inferred from data-constrained glaciological modelling for the initiation of the Younger Dryas interval [Tarasov and Peltier, 2006]. For a full listing of injection scenarios see table 4.1.

The COSMOS model oscillates between stadial and interstadial states in the absence of freshwater forcing under the described boundary conditions; these unforced oscillations are discussed in section 4.4.1. Our simulations originate from control simulations using similar MIS3 boundary conditions which have been integrated for > 4000 years. In keeping with the idea that enhanced glacial runoff is a result of warming, we conduct our injections at the peak of an interstadial period (the vertical blue line in Fig. D.1). This also allows us to evaluate the impact which a sudden increase in freshwater entering the oceans has upon CMCV and if the flux of freshwater can terminate an event already in progress. Each injection is run continually for the duration of the simulation, with durations of ≈ 1500 years.

We note that the impact of Heinrich Event scale fluxes of solid freshwater is not negligible and the role of this impact of this form of freshwater forcing upon CMCV remains poorly constrained at present. However, there remains outstanding issues with the timing of Heinrich events during stadial intervals Rasmussen et al. [2014] and it is reasonable to assume that the climate impact of a Heinrich event has some dependence on the timing of the event itself. Indeed, some recent work proposes that Heinrich events are a result of DO events and not a contributing factor Boers et al. [2018]. As such, an exploration of this form of freshwater forcing is beyond the scope of this study.

Finally, we point the reader to several shortcomings in our experimental design and model configuration worth noting. Our simulations are only O(2000) years in duration, which lets us obtain several cycles but remains limiting with respect to obtaining robust statistics. As well, there is at least one noted bias in the MPIOM component of COSMOS which may be significant here: the subpolar gyre is too extended to the east under present day boundary conditions [Jungclaus et al., 2006]. This region is noted as significant for the CMCV in Klockmann et al. [2020], where changes in the relative intensities of wind-driven and density-driven components of the sub-polar gyre are key to the mechanism of their simulated CMCV (see Section 4.4.1 for additional detail). Finally, we only examine the impact of glacial runoff introduced during interstadial periods. It is reasonable to assume, based on previous freshwater injection experiments [Kageyama et al., 2013], that the introduction of freshwater during a stadial interval should extend the stadial via AMOC suppression. Examination of such a response is left to future work.

Run Name	pCO_2	Freshwater Forcing Distribution	Freshwater Flux (dSv)
aso_1E38OXLC2	165	None	0
aso_1E38OMXLC	175	None	0
aso_1ELoCo2	185	None	0
aso_1EMiCo2	195	None	0
aso_1EHiCo2	207	None	0
aso_1E38OLCFWp5	185	GLAC1E	0.215
aso_1ELC2FW1	185	GLAC1E	0.43
aso_1E38OLCFW2	185	GLAC1E	0.86
aso_1EMC2FW1	195	GLAC1E	0.43
aso_1E38OMCFW2	195	GLAC1E	0.86
aso_1EHC2FW1	207	GLAC1E	0.43
aso_1E38OHCFW2	207	GLAC1E	0.86
aso_1ELC2DF8	185	$50 - 70°$ N	0.5
aso_1ELC2DF7	185	$50 - 70°$ N	1
aso_1ELC2DF5	185	$50 - 70°$ N	2
aso_1ELC2DF9	185	MAK Fingerprint	2
aso_1ELC2DFB	185	FEN Fingerprint	2
aso_1ELC2DFC	185	GOM Fingerprint	2
aso_1ELC2DFD	185	GSL Fingerprint	2
aso_1ELC2DFJ	185	MAK Regional	0.25
aso_1ELC2DFI	185	MAK Regional	0.5
aso_1ELC2DFH	185	MAK Regional	1
aso_1ELC2DF3	185	MAK Regional	2
aso_1ELC2DFE	185	FEN Regional	2
aso_1ELC2DFF	185	GOM Regional	2
aso_1ELC2DFG	185	GSL Regional	2

Table 4.1: Experiments performed with the COSMOS Earth Systems Model. All experiments use the same global ice reconstruction, orbital configuration, and concentrations for Methane and Nitrous oxide: these are GLAC1E, 38ka as determined by COSMOS internally [Berger, 1978], and 405 PPBV CH4, and 207.5PPBV N2O, respectively. The simulations aso_1ELC2D3,5,7,8,9,B,C,D,E,F,G,H,I were all initialized at the peak of the first interstadial in aso_1ELoCo2. Each of the aso_1ELC2D**X** simulations was integrated for ≈ 1400 years while all others were integrated for ≈ 2200 years. As such, aso_1ELoCo2 may be considered the 'Control' run for those freshwater injection simulations. All other simulations were branched from a previous MIS3 control simulation and share the same initialization data. For scale, 1dSv of glacial runoff for 1000 years is equivalent to ≈ 8.7m of eustatic sea level rise.

4.3.3 CMCV Detection

We use the maximum of the overturning stream function in the Atlantic as the primary metric for classifying our simulations as operating in a stadial or interstadial mode. The AMOC was chosen, since it exhibits a lower noise level than other variables which readily show these signals, such as sea ice area or Greenland surface air temperatures. We diagnose and characterise the CMCV in the COSMOS runs using an automated algorithm which determines the start and end of an event for a given set of parameters, applied to annually-averaged AMOC time series.

This algorithm detects potential onsets of an abrupt stadial-interstadial transition via the identification of outliers. For every data point in a given AMOC time series, the mean and standard deviation of the time series prior to that data point are calculated over a pre-determined interval. In this case, the predetermined interval was chosen to be 20 years. Then, the consistency of the AMOC value at that point was compared to these prior statistical characteristics. If the AMOC value exceeded two standard deviations and at least 3Sv above the prior mean, it was identified as a candidate event. The end of the event was then identified as the first instance after the abrupt increase that the AMOC again fell within two standard deviations of the mean prior to the abrupt transition. Candidate events were winnowed according to two criteria. First, the event had to last longer than 40 years. Second, the event could not lie within another event. This second criterion was chosen to prevent multiple events being detected during the same abrupt, but multi-year transition. Given a suitable choice of parameters, this automated event detection method was found to successfully identify events in the GRIP time series, as well as D-Olike events generated by two different climate models estimated via visual inspection. In the time series presented here, some events were not identified using the selected parameters, namely those of smaller magnitude and more gradual initial transitions. However, we choose to identify events via this automated method rather than visual inspection to ensure consistency in the definitions of events for our comparisons between runs.

4.4 Results and Discussion

Here we discuss the main features and mechanisms of the CMCV in our runs and characterise this variability in terms of the salt and thermohaline oscillator hypotheses presented in Section 4.2. We first compare the attributes of the CMCV simulated here to the data record and two recent studies examining CMCV using comparable numerical models under different boundary conditions. These comparisons allow us to situate our sensitivity experiments in both a historical context and relative to studies that examine the influence of ice sheet geometry and orbital configuration on CMCV. We then examine how consistent the mechanisms of the CMCV detected in the simulations presented here are with the salinity and thermohaline oscillator hypotheses. This provides a framework from which we can interpret the impact of the pCO_2 and freshwater changes.

4.4.1 Features of Unforced Centennial- to Millennial-Scale Climate Oscillations

We characterize CMCV in terms of four attributes of D-O and D-Olike cycles: the durations of the Greenland interstadial and stadial intervals, and the magnitudes of stadial to interstadial changes in Greenland temperatures and in the AMOC. Using these attributes, we compare our results to the paleoclimate record and two contemporary investigations that use either the same coupled climate model as used here [Zhang, 2021] or a similar coupled climate model, the MPI-ESM [Klockmann et al., 2018, 2020] [3]. The CMCV in our ensemble exhibit stadial (AMOC-weak) periods ranging from $\approx 30 - 780$ years and interstadial (AMOC-strong) periods ranging from $\approx 40 - 600$ years (see Fig. 4.3). The durations of stadial/interstadial intervals in our ensemble overlap with the range spanned by the paleoclimate archive. However our oscillations have a lower maximum duration than the paleoclimate archive, as seen when comparing Figs. 4.2 and 4.3. During MIS3 ($29 - 57$ ka based on Lisiecki and Raymo [2005]), the paleoclimate record indicates Greenland stadials range

[3]Klockmann et al. [2020] uses MPI-ESM, whose main difference from COSMOS is an updated version of the atmospheric component [Jungclaus et al., 2013], ECHAM, and any parameter changes associated with tuning the model configuration.

from $320 - 1700$ years while interstadials range from $60 - 2300$ years [Rasmussen et al., 2014].

When compared to the temperature reconstruction for MIS3 [Kindler et al., 2014], our simulated events have peak to peak (on monthly time-steps with an annual running-mean boxcar window) surface temperature changes over Greenland of comparable magnitude as shown in Fig. 4.4. However the large annual to decadal scale variability in our modelling results is not resolved in reconstructions such as Kindler et al. [2014]. Greenland surface temperature changes in our simulations are weaker when comparing to time-averaged 2 m temperatures at the NGRIP location in COSMOS shown in Fig. 4.4 (to emulate the smoothing processes involved in ice core records [Bales and Wolff, 1995]). The temperature changes over Greenland during MIS3 are inferred to be $6.5 - 16.5°$ C [Kindler et al., 2014] where ours are $\approx 5°$ C for the 185ppm simulation.

Having examined the paleoclimate archive we now shift focus to comparable studies examining CMCV. Zhang [2021] uses glacial ice sheet boundary conditions that are comparatively larger [4] than the GLAC1E reconstruction used here, along with a range of orbital and GHG values (we focus on the constant forcing 34 ka orbital and 40 ka GHG conditions simulation here for comparison). Considering the statistical analysis results of Lohmann and Ditlevsen [2018], this more extensive ice sheet configuration, particularly with regards to the Fennoscandian ice sheet, ought to result in a relatively higher frequency of events (and thus shorter intervals) when compared to our 195ppm pCO_2 simulation. However, this is not what we observe. Instead, Zhang [2021] features oscillations where the stadial period varies in duration from $\approx 200-500$ years and interstadial durations from $\approx 700-1200$ years, with a peak-to-peak difference of $\approx 1000-1400$ years, which represent less frequent transitions than our comparable 195ppm pCO_2 simulation. This discrepancy may be explained by differences in land ice volume counterbalancing the differences in orbital configurations (the daily mean, top-of-atmosphere solar flux at 65N during the summer solstice at 38 ka being $\approx 5.5\text{W/ m}^2$ greater than at 34 ka per Laskar et al. [2011]). Comparing against Klockmann et al. [2020], who uses present-day ice sheet boundary conditions with LGM orbital values and 206ppmv pCO_2, we ought to expect a lower rate of occurrence (and consequently, longer durations) [Lohmann and Ditlevsen,

[4]Their ice sheet distribution is generated by extrapolating MIS3 ice sheets from the sum of PMIP3 LGM ice sheets and an anomaly from the ICE5G chronology

2018] as both their ice sheet volume and insolation (a difference of $\approx 34\text{W}/\text{ m}^2$ using the same metric as above) are lower. Indeed their configuration produces stadial periods that last $\approx 1000-1300$ years with interstadial periods of $\approx 500-700$ years, and a peak-to-peak periodicity of $\approx 1500-2000$ years, compared to $80-210$ years stadial and $460-580$ years interstadial durations for our comparable configuration. This variation in CMCV characteristics between models demonstrates sensitivity to both the ice sheet configuration and orbital configuration.

Next, we compare our results to the mechanisms described in 4.2. We start with the salt oscillator mechanism and the mechanism presented in Klockmann et al. [2020]. We find general agreement, such as the extension of the more saline subtropical gyre waters extending towards the eastern North Atlantic in Fig. 4.5 and the exchange of salt between the subpolar and subtropical gyres shown in Fig. D.2. However there are some disparities which likely arise due to the differences in the configuration, namely continental ice sheets and the orbital configuration. As discussed previously, our ice sheet configuration for the Northern hemisphere at 38 ka (shown in Fig. D.3) is more extensive than the present day configuration of Klockmann et al. [2020], despite it being a relatively small configuration by comparison to other viable ensemble members. This leads to large differences in atmospheric circulation over the North Atlantic ocean. The main atmospheric circulation difference is expected to be that a glacial configuration results in an intensification of zonal winds and a southern shift in the peak of winds [Andres and Tarasov, 2019], and a resulting difference in sea ice distributions [Zhang et al., 2014a]. These differences would have significant implications for Klockmann et al. [2020]s CMCV sub-polar gyre hypothesis, given they argue that Sverdrup transport (which would be enhanced with intensified wind stress) in the eastern subpolar gyre is a significant influence on AMOC.

As shown in Fig. 4.5, deep-water formation in the North Atlantic and GIN seas is suppressed during the weak AMOC phase in our experiments. However, the location of deep water formation in our configuration is further North relative to Klockmann et al. [2020]. The deepest mixing in our configuration occurs in the center of the Norwegian Sea rather than in the North Atlantic south of Iceland as in Klockmann et al. [2020]. This contrast in deep-water formation sites likely arises due to the differences in the orbital configuration between our experimental setups. A more glacial/colder orbital configuration should lead to more extensive sea ice. However, this feature would also be affected by the lack of continental scale ice sheets. A result of a more southerly sea ice margin is that deep water formation should be pushed south into the North Atlantic rather than the Nordic seas. To evaluate this we can examine the results of Love et al. [2021a], who use LGM surface boundary conditions but comparable bathymetry. Comparing sea ice margins and mixed layer depth fields between the simulations presented here and in Love et al. [2021a] this southern shift of the sea ice margin and deep water formation zone is precisely the behaviour seen. The differences in orbital configurations between the simulations shown here and those of Klockmann et al. [2020], result in overall greater insolation during NH winter and less during NH summer, resulting in warmer NH winters and colder NH summer in our configuration [Laskar et al., 2011]. For both strong and weak AMOC configurations, our winter (Dec/Jan/Feb, DJF) sea ice margins (red lines in Fig. 4.5) are further north over the eastern North Atlantic than those of Klockmann et al. [2020]. We attribute this to less extensive sea ice growth during the warmer winters in our configuration.

When comparing the oscillation of salinity between the subpolar and subtropical gyre regions, we find the anticipated relationship that during the AMOC strong intervals subtropical salinity decreases while subpolar salinity increases. However, this oscillation is not as clear a signal as in other salinity oscillator studies due to variability in the signal (e.g Peltier and Vettoretti [2014], Klockmann et al. [2020]) and the decrease is only at the onset of the AMOC strong intervals as seen in Fig. D.2. This weaker relationship is also found when comparing the density differences across the subpolar gyre as in Klockmann et al. [2020]. Comparing the density differences using our further north deep-water formation site, we find better agreement but the density contrast is not as clear as in previous studies. As such, we conclude that we can describe some of the behaviours of our CMCV via the salinity oscillator hypothesis but the relationships and progression are not as good a fit as in previous studies.

Here we compare against the Nordic Sea sediment core data and the conceptual model based on it put forth by Dokken et al. [2013] and the thermohaline oscillator model described earlier. We find several points of agreement. The overall progression of DO transitions as described by the conceptual model of Dokken et al. [2013] also well describe our transitions when considering Nordic seas sea ice cover, subsurface temperatures and salinity, and Greenland surface temperatures as shown in Fig. 4.4. As well, their results show that the Nordic seas were ≈ 2 C warmer during Greenland stadials by comparison to interstadials. Subsurface temperatures in this study increase by between 3C and 4C at the location of the sediment core as shown in Fig. 4.4d with a gradual build up of subsurface heat increasing downward is seen in Fig. D.5. Furthermore, Dokken et al. [2013] predicts a shift in the storm track between stadials and interstadial conditions, during interstadial conditions the stormtrack extends into the Nordic seas and delivers heat to the region inhibiting the growth of sea ice. Examining 200hPa eddy kinetic energy as in Li and Battisti [2008] to evaluate storm tracks in our simulations, we find agreement with the predictions of Dokken et al. [2013] with a slight shifting of the storm track when diagnosing this via eddy kinetic energy in Fig. D.6.

There are some disparities between our results and those of Dokken et al. [2013]. Dokken's work proposes an overshoot in Greenland surface temperatures at the onset of an interstadial which we do not observe. The overshoot does not seem to be consistent between studies. When comparing AMOC in Peltier and Vettoretti [2014] and Zhang [2021] both show an overshoot at the onset of an interstadial, [5]. while Klockmann et al. [2020] and our results do not when examining Greenland surface temperatures or AMOC. The overshoot may be a result of greater subsurface heat build-up in the Nordic seas present in the simulations of Peltier and Vettoretti [2014] and Zhang [2021] (relative to this study and Klockmann et al. [2020]) which results in a stronger initial impulse of heat release adjacent to the Greenland ice sheet. Finally, comparing against the thermohaline mechanism described in Section 4.2, our configuration reproduces the progression of changes in Greenland surface air temperatures, GIN Seas sea ice extent and sub-surface temperature in the Nordic seas much more effectively than it does the salinity oscillator mechanism.

As discussed above, a feature that is common to both the thermohaline and salinity oscillator hypotheses is the opening of sea ice at the transitional period from a stadial to an interstadial. In Vettoretti and Peltier [2016] this takes the form of a 'super polyna' driven by subsurface heat.

[5]Note that Peltier and Vettoretti [2014] and Zhang [2021] do not provide surface temperatures for Greenland and as such we examine AMOC for presence of an overshoot. This study and Klockmann et al. [2020] both provide this metric.

While in Dokken et al. [2013] and Klockmann et al. [2020] a polyna is not invoked, in the former sea ice reduction is also the result of subsurface heat build-up while the latter could not attribute a mechanism to the sea ice reduction. Similarly, sea ice is extensive during stadial intervals and retracted during interstadials. This switching of sea ice between two states has been raised as a potential component of CMCV by Gildor and Tziperman [2003] where it is argued that sea ice can act as a switch for the climate system between two quasi-stable states provided some criteria are met. One of these criteria is that multiple sea ice configurations exist under the same land ice configuration. It is unclear if Peltier and Vettoretti [2014] achieve this, as their NH sea ice area begins growing at the onset of their interstadial intervals [Vettoretti and Peltier, 2018]. This indicates their interstadial intervals are less stable than their stadial intervals, where sea ice remains at a maximum for several hundred years before transitioning. Comparatively, our results demonstrate two stable sea ice states consistently across all our simulations which exhibit CMCV, some examples of which are shown in Fig. D.7. Similarly, Klockmann et al. [2020] presents two stable sea ice states in their simulation. Phase analysis to explore the pacing of our simulated events has not proven fruitful due to the signal-to-noise ratio in our climate simulations, so determining if sea ice changes are responsible for initiating the transitions or are simply responding to them would require further sensitivity tests. However, work presented in Vettoretti and Peltier [2018] demonstrates that sea ice export from the Arctic Ocean provides enough freshwater to initiate a transition from interstadial to stadial conditions. At present we cannot directly compare our results to those of Vettoretti and Peltier [2018] as MPIOM's sea ice component does not have an (at least documented) output option for sea ice melt flux, as such we leave this comparison to future work. Future work examining this feature will have to account for the ice thickness bias associated with the PP mixing scheme as discussed in Section 4.3. An examination of sea ice cover, the AMOC, and heat flux through the oceans surface at the site of deep water formation in the Nordic Seas indicates that sea ice changes generally lead changes in AMOC when transitioning from stadial intervals to interstadials. However, this lead is several years in magnitude and not always consistent for stadial intervals that have brief excursions of reduced sea ice cover in this region. At the least, it is clear that sea ice changes can amplify the transitions in our simulations via the sudden release of stored subsurface heat.

In summary, we find our CMCV exhibit features of both the salinity oscillator and thermohaline oscillator mechanisms of Dansgaard-Oeschger variability. Our results indicate that CMCV in our ensemble are more dependant upon the transport of heat (as in the thermohaline oscillator) rather than exclusively salt (as in the salinity oscillator). However, our configuration does not reproduce all aspects of the salinity oscillator hypothesis as effectively as those of the thermohaline oscillator hypothesis. We note that our ensemble does not represent the full range of variability of the paleoclimate record during MIS3, being unable to reproduce the longer duration intervals. However, our ensemble does capture the shorter- to intermediate-duration events sufficiently to assess some of the impacts of freshwater and pCO_2 with regards to modulating features of our CMCV.

4.4.2 What are the impacts of glacial runoff?

We explore the sensitivity of our models CMCV to not only the freshwater itself, but also the location over which it is applied when exploring the impact of freshwater. Given we identify two different mechanisms and sets of processes involved in DO events that characterize our CMCV, predicting the impact of a given flux of freshwater is non-trivial. However, previous work demonstrates that we ought to expect several trends with regards to freshwater injection. Stadial durations should increase with the addition of freshwater, the magnitude of overturning between stadial and interstadial ought to be greater for simulations with freshwater injection, and there should be different rates of stadial-interstadial transition for simulations with and without freshwater injection [Brown and Galbraith, 2016]. However, differences may arise as Brown and Galbraith [2016] did not perform continuous freshwater injection as was done in these sets of experiments. We examine the impact of freshwater forcing on our CMCV from the perspective of stadial duration, interstadial duration, and AMOC increase during interstadials. In doing so, we find freshwater can modulate CMCV in one of three ways depending upon both the injection region and rate. It can either decrease interstadial durations, completely suppress AMOC, or alter the periodicity of CMCV. We first establish some general trends then examine each of these types of variability in turn.

As freshwater flux increases in Fig. 4.3, both the duration of interstadial periods and the variability in the duration decreases. The simulations which have no freshwater injection exhibit the longest interstadials and freshwater at the highest rates of injection evaluated here completely suppresses AMOC. The former observation is unsurprising given it is well established that freshwater can inhibit deep water formation and the AMOC [Kageyama et al., 2013], while the latter was anticipated primarily for the hosing injection method. However, it is notable that for all cases the introduction of freshwater terminated the interstadial state within ≈ 200 years. For values of freshwater that permit CMCV, we find that both the average and maximum values of interstadial AMOC anomaly (relative to stadial) exhibit a negative correlation with freshwater forcing. This relationship with regards to amplitude is in agreement with the results of Brown and Galbraith [2016], but it is weak when considering our range of AMOC values. With regards to the nature of the transitions between stadial and interstadial, we observe transitions comparably abrupt (i.e. transitions which take place over century and sub-century intervals as shown in Fig. 4.6) in the presence of freshwater forcing as observed in Brown and Galbraith [2016]. Barring the trivial case of sufficient freshwater flux to entirely suppress the AMOC, there is no clear relationship between freshwater flux and stadial duration.

For regional and fingerprint injection methods, injecting > 0.5 dSv suppresses the AMOC below our threshold of CMCV detection, although visual inspection of Fig. 4.6 indicates the presence of CMCV for some simulations. At 2 dSv, the AMOC remains in a stadial state over the entirety of the simulation, as seen in Fig. 4.6. Previous work by Roche et al. [2009] suggests that a cessation of the freshwater flux should lead to an AMOC recovery in all tested cases despite this not being explicitly tested. This type of behaviour has been used to set the pacing of large scale climate oscillations in previous transient experiments [He, 2011] and previous sensitivity studies [Brown and Galbraith, 2016]. As in Love et al. [2021b], the Hosing injection scenarios result in the strongest damping of AMOC for the same freshwater injection flux, with the 2 dSv Hosing resulting in an average AMOC 1Sv lower than the next strongest damping (GOM-R), and 2Sv lower than the average of all other 2 dSv injections, whose average AMOC is ≈ 7 Sv as is seen in Fig. 4.6. This trend is also present when examining other climate indicators, such as global sea ice area, and global-mean sea-surface temperatures. The response sensitivity to the injection location identified in Love et al. [2021b], such as the greater impact of freshening from the GOM vs. GSL, is replicated in the longer simulations here. Similarly, the use of the freshwater fingerprint method offsets the overly-strong freshening effect from GOM relative to GSL even on the longer timescales.

For regional and Hosing injections of < 1 dSv, we observe regular oscillations in the AMOC in Fig. 4.6, where the period depends more strongly on the injection location (of those tested here) than the injection rate. Hosing results in a faster oscillation by comparison to Mackenzie regional injection, with a period of ≈ 150 years for Hosing and ≈ 225 years for MAK-R. Examining the differences in the salinity fields between the 0.5 dSv Hosing and MAK injections during AMOC-strong intervals in Fig. D.8, we see that the Hosing results in greater freshening of the Nordic Seas and the associated deep-water formation site. Given the limited evidence, we conclude that the oscillation is related to the ability of a given injection scenario to freshen the sites of deep-water formation and trigger the weakened AMOC state, but more testing is required.

We can make some predictions regarding the different oscillatory behaviours for different outlets using the results of the impact of freshwater injection on AMOC presented in Love et al. [2021b]. Assuming the relative ordering of oscillation period follows that of AMOC reduction, we can predict that Fennoscandia would have a similar frequency to MAK (if not slightly faster), GOM would be next fastest, while GSL would be the slowest. The fingerprint injections should be comparable, but slightly slower for MAK and FEN by comparison to their regional counterparts. This threshold behaviour with respect to transitions due to freshwater forcing and the resulting periodic behaviour has been seen in other DO investigation studies [Ganopolski and Rahmstorf, 2001]. Ganopolski and Rahmstorf [2001] finds their CMCV, which they liken to DO events, are triggered by the addition of freshwater forcing exceeding a threshold and find the structure of an event is the same regardless of the forcing as long as the threshold is exceeded. Similarly, the 2xGLAC1E forcing, which is equivalent to ≈ 0.86 dSv, demonstrates a threshold behaviour, while the 1xGLAC1E does not provide enough freshening to drive the periodic behaviour (and so transitions do not have a regular pacing) but rather reduces interstadial durations.

In summary, we find in our simulations that freshwater can play multiple roles in our simulated climate and have varying effects depending upon both injection location and injection rate. Injections at fluxes greater than ≈ 0.86 dSv suppress CMCV for our configuration, with no sensitivity to the source region or injection method. Interstadial duration decreases with increasing freshwater fluxes below this value while stadial duration is not sensitive to this parameter. Both the average and maximum of AMOC changes from stadial to peak interstadial decrease as freshwater flux increases. Regional and hosing injections with injection rates ≤ 0.5 dSv drive CMCV into a regular periodic regime where the period depends on the location of forcing (see Fig. 4.6). Finally, the introduction of freshwater can terminate an interstadial interval within ≈ 200 years for our configuration.

4.4.3 What are the impacts of background pCO_2 concentrations?

Here we explore the impacts of pCO_2 on attributes of the simulated CMCV and compare those to how these features are related in the paleoclimate record. DO events are known to occur over a range of background pCO_2 values, see Fig. 4.3, where pCO_2 provides an effective radiative forcing modifier. Again we can appeal to previous work to make some predictions with regards the impacts of changing pCO_2 concentrations: there ought to be a narrow range of concentrations over which oscillations can be sustained [Klockmann et al., 2018] and interstadial durations should be correlated with pCO_2 [Zhang, 2021] and Figure 4.2.

We find some parallels to the freshwater forcing results when examining the impact of pCO_2 on our CMCV characteristics in Fig. 4.3. Interstadial durations show a clear relationship with changes in pCO_2; as pCO_2 concentration increases, so does the observed interstadial durations, especially when no freshwater forcing is applied. Mean stadial durations do not show a strong relationship with pCO_2, and due to the large uncertainties involved, we cannot conclude if there is any dependence or simply a weak one. However, the maximum stadial duration does show a clear decrease with increasing pCO_2, with our 175 ppmv configuration producing a stadial event almost 800 years in duration, while 207 ppmv stadial durations do not exceed 210 years. In contrast with freshwater, pCO_2 does not appear to affect the magnitude of AMOC changes between the stadial and peak interstadial in our ensemble. Comparing our findings to a similar set of sensitivity studies conducted by Zhang [2021], we see correspondence between our results in that when they increase (decrease) their background pCO_2 values, their interstadials increase (decrease) in duration. However, by comparison to Klockmann et al. [2018], we have demonstrated a relatively wider range of background pCO_2 concentrations under which CMCV spontaneously occur. Given the observed trends, extending the range of pCO_2 concentrations ± 10 ppmv may be enough to suppress CMCV into either a stable stadial or interstadial state.

Our findings are in agreement with the thermohaline oscillator hypothesis, whereby the pacing of stadial events should be set by how swiftly heat can be transported to the location of DWF. As such, a greater temperature gradient between the Atlantic and the GIN Seas as a result of increased pCO_2 should lead to shorter stadial intervals. The behaviour of shorter stadial durations is observed in Fig 4.3 when considering maximum stadial duration. We observe temperatures increasing with pCO_2 at both the surface and at 200 m depth (0.24° C/ ppmv pCO_2) in the Atlantic and North Atlantic during both stadial and interstadial periods. By comparison, the GIN Seas 200 m potential temperature during stadials does not change with increasing pCO_2. Examining Figs. D.9 and D.10, we can see the temperature and salinity gradient between the Atlantic Ocean and the GIN seas increases with pCO_2 during the stadial intervals. Despite the increased salinity in the Atlantic due to increased evaporation as a function of pCO_2 increase ($\approx 10\%$ increase in evaporation between 165ppm and 207ppm), the increase in subsurface temperatures in the North Atlantic results in a greater density change.

Our modelling results for nominal pCO_2 dependence are reflected in the paleoclimate record. Fig. 4.2 shows that interstadial durations in the paleoclimate record are somewhat correlated (0.65) with pCO_2 while stadial durations have negligible (-0.16) correlation. However, the latter nominal non-correlation obscures that the longest (shortest) duration stadials occur at the lowest (highest) levels of pCO_2. This is consistent with our model results (fig. 4.3). Furthermore, without our modelling results, the interpretation of the causative role of changing pCO_2 is confounded by its dependencies on climate [e.g. temperature changes enhancing drawdown of CO_2 in the Southern

Ocean, Bauska et al., 2021]. It is also evident from the paleo climate record that stadial and interstadial dependencies on radiative forcing are non-trivial. Interstadial dependence on July $65N$ insolation is negligible (0.18) while stadial duration has a weak correlation with July $65N$ insolation (-0.35) and negligible correlation (-0.16) with pCO_2.

As well, it is clear that the ice core records show a greater range of stadial/interstadial durations than our modelling results produce, and there are a comparable numbers of short-duration ($<$ 500 years) interstadials at relatively high pCO_2 values as there are long-duration interstadials. In particular, we are unable to reproduce the longer duration stadials or interstadials as seen in the paleoclimate record. However, we have shown that the introduction of freshwater can terminate an interstadial interval, and if the flux is sufficient, force a stadial state for at least the duration of the injection. While we have not demonstrated that our configuration will revert to an interstadial state after the cessation of freshwater injection, other studies have shown this (e.g. Brown and Galbraith [2016]).

In summary, our results, those of comparable studies, and the paleoclimate record all indicate a correspondence between increasing pCO_2 and increasing interstadial durations during MIS3, while we demonstrate that increases in pCO_2 concentration decrease the maximum stadial duration.

4.5 Conclusions

This study examines the relationships between background pCO_2 concentration, freshwater, and attributes of centennial- to millennial- scale climate variability (CMCV) like Dansgaard-Oeschger events. We do this using a comprehensive, coarse-resolution Earth System model configured for 38 ka during MIS3 with a range of pCO_2 concentrations and freshwater injection scenarios.

When exploring the role of freshwater on CMCV, we find that freshwater injections can result in one of three different behaviours depending both upon the flux amount and the location of the injection. Continual freshwater injection of 2 dSv results in a complete suppression of AMOC and a continual stadial state for all injection locations and methods investigated. Intermediate injections of $0.25 - 0.5$ dSv using regional injection locations and the $50 - 70°$ N band in the North Atlantic result in oscillations with a consistent period. In these simulations the period depends more strongly on the location of the injection than the injection amount, with the $50-70°$ N band having a higher frequency. Finally, when using the glacial runoff distribution from an ice sheet reconstruction, we find freshwater decreases interstadial durations but does not impact stadial durations.

We find that there is a clear relationship between pCO_2 and interstadial durations, where increasing pCO_2 leads to longer interstadial intervals in our Earth Systems model. This relationship is also present in the paleoclimate record when examining the pCO_2 variations over the MIS3 interval. Maximum stadial duration is more strongly related to background pCO_2 concentration, where increasing background pCO_2 results in an upper limit on the duration of stadial intervals, reducing it from a maximum of $\approx$ 800 years for 185 ppmv pCO_2 to $\approx$ 200 years at 207 ppmv pCO_2. This feature of our simulated events is also seen in the paleoclimate record, but there are limited stadial events in the paleoclimate record at higher pCO_2 values to draw conclusions from. The pacing of our simulated events appears to be coupled to the subsurface temperature gradient between the Atlantic and the GIN seas.

Our results are broadly compatible with the paleoclimate record and previous investigations. However we do not capture the full range of stadial/interstadial durations present in the climate records, being unable to reproduce the longer-duration/lower-frequency events during the MIS3 interval. Two other primary forcings were not examined in this investigation but are inferred to be significant for CMCV: the effects of varied ice sheet geometry and orbital configurations. As such, these results raise the question of how impactful differences in ice sheet geometry, and particularly its areal extent which remains untested at present, and orbital configurations are upon these CMCV characteristics given we could not reproduce the longer-duration/lower-frequency events during the MIS3 interval via freshwater or pCO_2 forcings.

4.6 Acknowledgements

The authors would also like to thank those at the GNU and Fedora projects,Kernel.org and in particular those responsible for GNU Parallel [Tange, 2011] whose software greatly sped up and streamlined the analysis in this work. This is a contribution to the ArcTrain program, which was supported by the Natural Sciences and Engineering Research Council of Canada This work is also a contribution to the PALMOD project This research was enabled in part by support provided by SciNet (www.scinethpc.ca) and Compute Canada (www.computecanada.ca) through both Resources for Research Groups allocations and the Rapid Access Service.

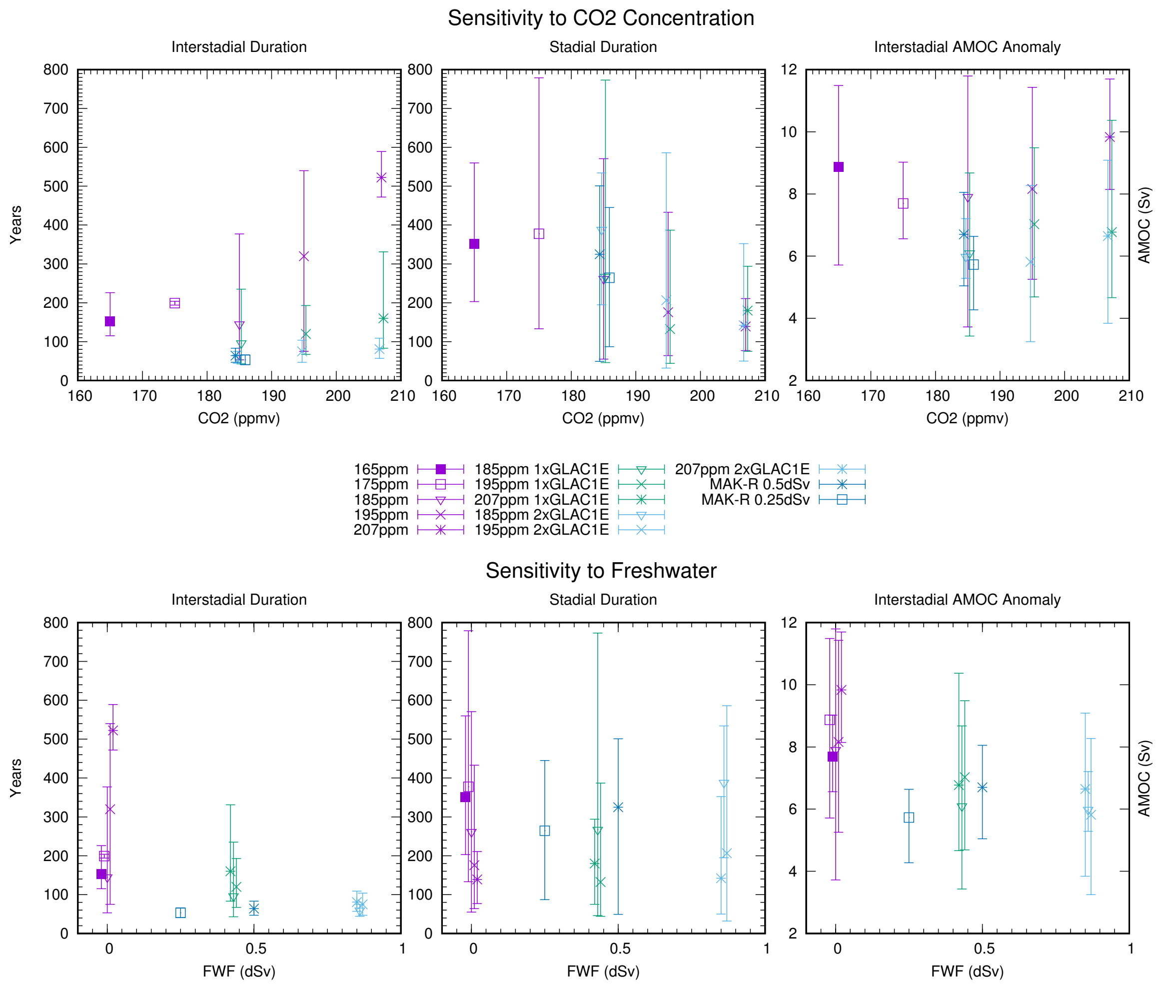

Figure 4.3: The relationship between freshwater flux, pCO_2, stadial and interstadial durations, and peak amplitude of the interstadial AMOC value. Vertical error bars are indicative of the maximum/minimum values for the interstadial/stadial durations or AMOC peak. Stadial/interstadial durations for configurations in which no CMCV were detected are not shown. As a result, the only regional injection simulations shown are MAK-R at 0.5 dSv and 0.25 dSv. Where values overlap due to using the same flux value (0, 0.43, 0.86 dSv) or same pCO_2 value (185,195,207 ppmv) they have been offset on the x-axis by a small amount to assist clarity. The full range of freshwater fluxes can be seen in Fig. D.4.

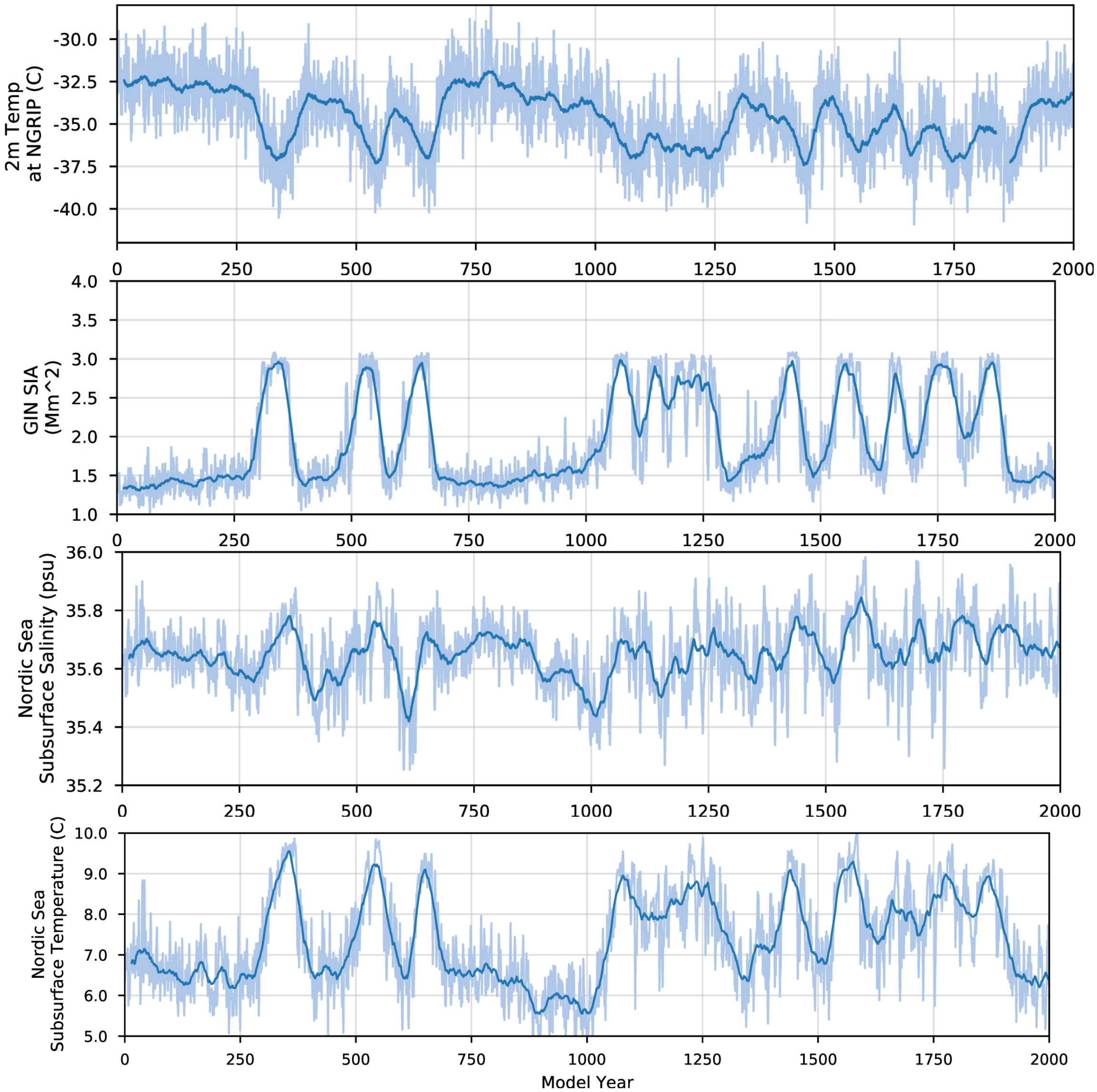

Figure 4.4: Data from the 185ppm pCO_2 run focusing on the oscillation around year 550 with equivalent fields to the conceptual model shown in Fig. 5 of Dokken et al. [2013]. A 30 year running mean has been applied to the data shown in the darker line, while a 12 month running mean has been applied to the lighter line, data points shown are at monthly intervals. Subsurface salinity and temperature is the average over 150m to 600m depth at the Nordic sea sediment core MD992284 location. Top panel is the model's 2m temperature at the location of the NGRIP core.

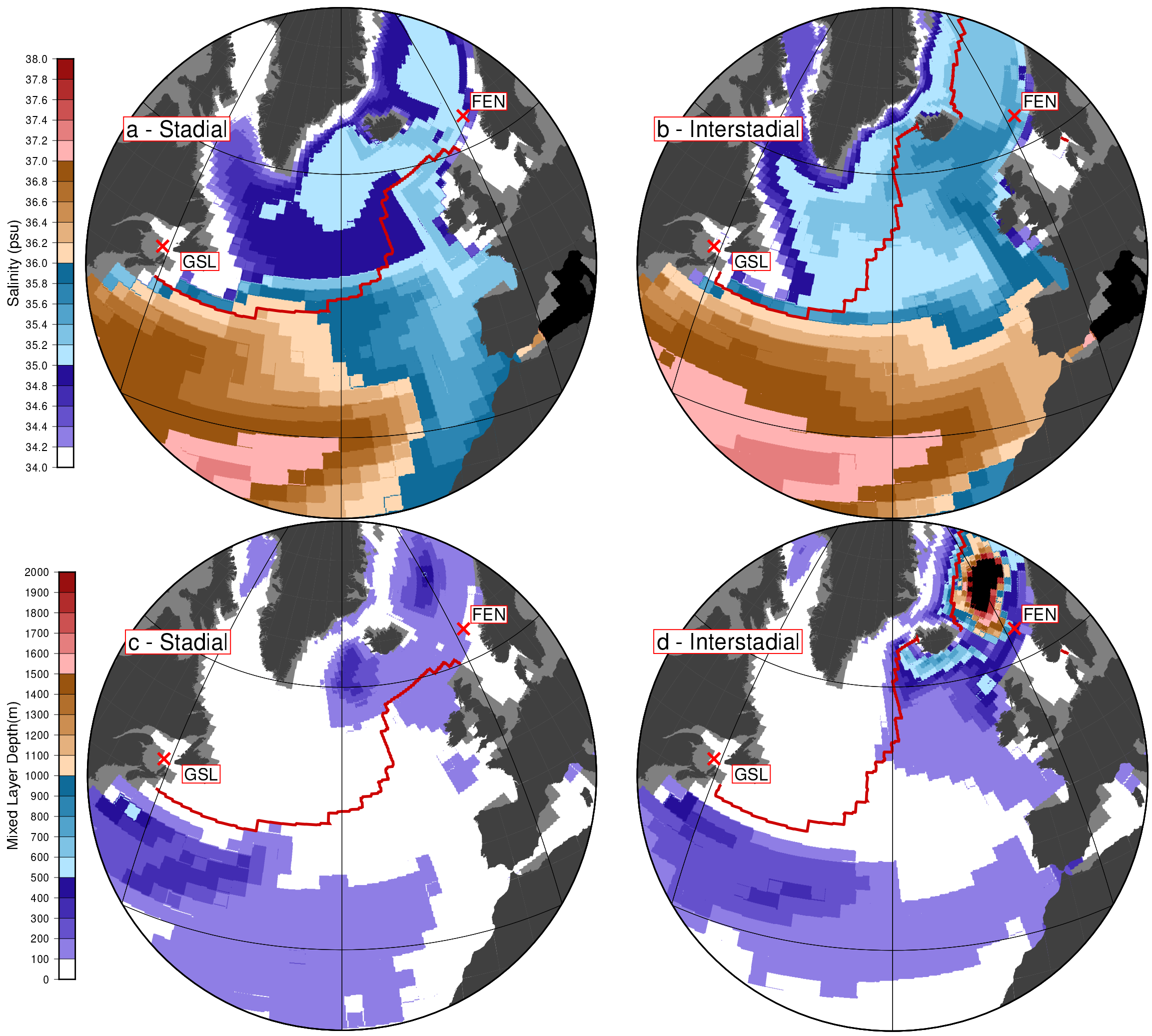

Figure 4.5: Salinity (top panels) and DJF mixed layer depth (bottom panels) for the weak AMOC interval (panels a and c) and the strong AMOC interval (panels b and d). Present day land-sea mask is shown in dark grey, the red line represents the 90% DFJ sea ice area boundary.

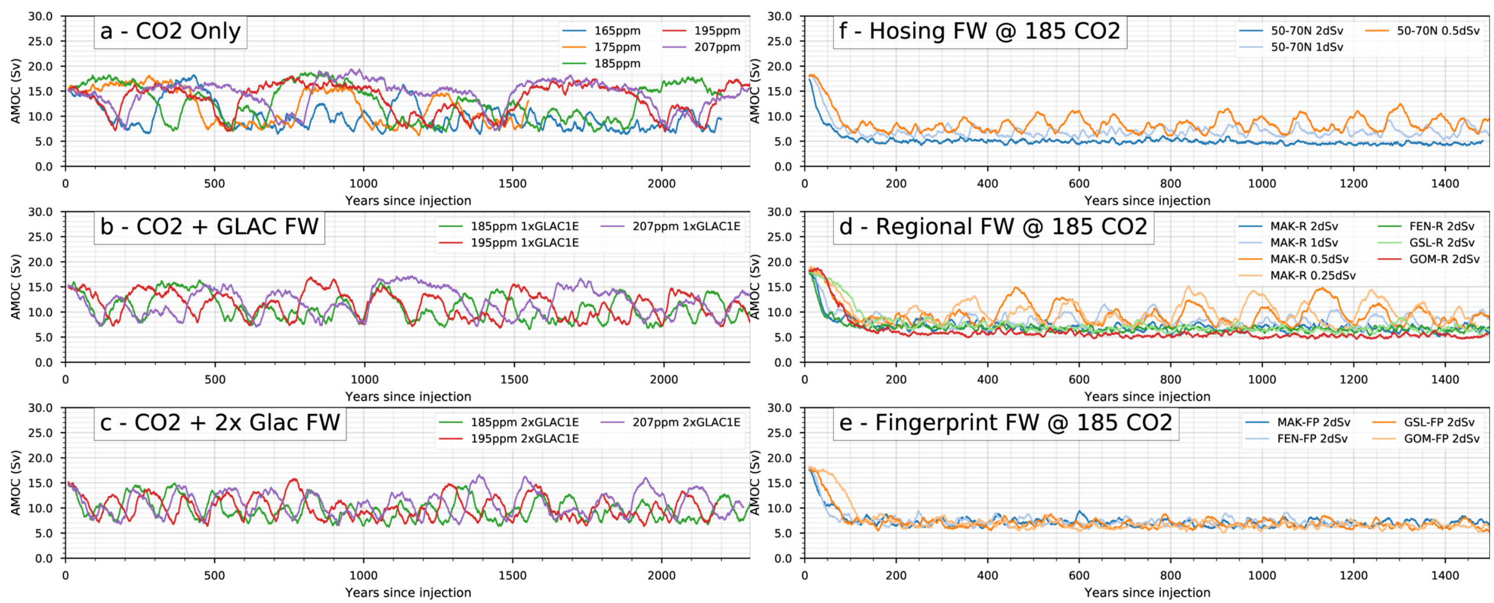

Figure 4.6: AMOC from our various freshwater forcing scenarios. Panel a shows unforced simulations where the atmospheric pCO_2 concentration was varied between 165ppmv to 207ppmv. Panels b and c show the same model configuration as those in panel a, but with the addition of glacial runoff at 1× and 2× the flux from the change in ice volume, respectively, as described in the experimental design. Panels d, e, and f show additional freshwater injection scenarios, traditional hosing, regional injection (-R), and fingerprint injection (-FP) methods respectively. Simulations shown in panels f,d,e were branched from the aso_1ELoCo2 run (185ppm pCO_2) 800 years after starting. A 30-year running mean has been applied to monthly data.

Bibliography

Florian Adolphi, Christopher Bronk Ramsey, Tobias Erhardt, R. Lawrence Edwards, Hai Cheng, Chris S. M. Turney, Alan Cooper, Anders Svensson, Sune O. Rasmussen, Hubertus Fischer, and et al. Connecting the greenland ice-core and u/th timescales via cosmogenic radionuclides: testing the synchroneity of dansgaard-oeschger events. *Climate of the Past*, 14(11):1755–1781, Nov 2018. ISSN 1814-9332. doi: 10.5194/cp-14-1755-2018. URL http://dx.doi.org/10.5194/cp-14-1755-2018.

Heather J. Andres and Lev Tarasov. Towards understanding potential atmospheric contributions to abrupt climate changes: characterizing changes to the north atlantic eddy-driven jet over the last deglaciation. *Climate of the Past*, 15(4):16211646, Aug 2019. ISSN 1814-9332. doi: 10.5194/cp-15-1621-2019. URL http://dx.doi.org/10.5194/cp-15-1621-2019.

R. C. Bales and E. W. Wolff. Interpreting natural climate signals in ice cores. *Eos, Transactions American Geophysical Union*, 76(47):477477, 1995. ISSN 0096-3941. doi: 10.1029/95eo00293. URL http://dx.doi.org/10.1029/95EO00293.

Thomas K. Bauska, Shaun A. Marcott, and Edward J. Brook. Abrupt changes in the global carbon cycle during the last glacial period. *Nature Geoscience*, 14(2):9196, Feb 2021. ISSN 1752-0908. doi: 10.1038/s41561-020-00680-2. URL http://dx.doi.org/10.1038/s41561-020-00680-2.

Bernhard Bereiter, Sarah Eggleston, Jochen Schmitt, Christoph Nehrbass-Ahles, Thomas F. Stocker, Hubertus Fischer, Sepp Kipfstuhl, and Jerome Chappellaz. Revision of the epica dome c co2 record from 800 to 600kyr before present. *Geophysical Research Letters*, 42(2):542549, Jan 2015. ISSN 0094-8276. doi: 10.1002/2014gl061957. URL http://dx.doi.org/10.1002/2014GL061957.

André L Berger. Long-term variations of caloric insolation resulting from the earth's orbital elements1. *Quaternary research*, 9(2):139–167, 1978.

G. Edward Birchfield and Wallace S. Broecker. A salt oscillator in the glacial atlantic? 2. a scale analysis model. *Paleoceanography*, 5(6):835843, Dec 1990. ISSN 0883-8305. doi: 10.1029/pa005i006p00835. URL http://dx.doi.org/10.1029/PA005i006p00835.

Niklas Boers, Michael Ghil, and Denis-Didier Rousseau. Ocean circulation, ice shelf, and sea ice interactions explain dansgaardoeschger cycles. *Proceedings of the National Academy of Sciences*, 115(47):E11005E11014, Nov 2018. ISSN 1091-6490. doi: 10.1073/pnas.1802573115. URL http://dx.doi.org/10.1073/pnas.1802573115.

Robert D Briggs, David Pollard, and Lev Tarasov. A data-constrained large ensemble analysis of antarctic evolution since the eemian. *Quaternary Science Reviews*, 103:91–115, 2014.

Wallace S. Broecker, Gerard Bond, Millie Klas, Georges Bonani, and Willy Wolfli. A salt oscillator in the glacial atlantic? 1. the concept. *Paleoceanography*, 5(4):469477, Aug 1990. ISSN 0883-8305. doi: 10.1029/pa005i004p00469. URL http://dx.doi.org/10.1029/PA005i004p00469.

Nicolas Brown and Eric D. Galbraith. Hosed vs. unhosed: interruptions of the atlantic meridional overturning circulation in a global coupled model, with and without freshwater forcing. *Climate of the Past*, 12(8):16631679, Aug 2016. ISSN 1814-9332. doi: 10.5194/cp-12-1663-2016. URL http://dx.doi.org/10.5194/cp-12-1663-2016.

Anders E. Carlson, Lev Tarasov, and Tamara Pico. Rapid laurentide ice-sheet advance towards southern last glacial maximum limit during marine isotope stage 3. *Quaternary Science Reviews*, 196:118123, Sep 2018. ISSN 0277-3791. doi: 10.1016/j.quascirev.2018.07.039. URL http://dx.doi.org/10.1016/j.quascirev.2018.07.039.

A. Condron and P. Winsor. Meltwater routing and the younger dryas. *Proceedings of the National Academy of Sciences*, 109(49):1992819933, Nov 2012. ISSN 1091-6490. doi: 10.1073/pnas.1207381109. URL http://dx.doi.org/10.1073/pnas.1207381109.

Ellen C. Corrick, Russell N. Drysdale, John C. Hellstrom, Emilie Capron, Sune Olander Rasmussen, Xu Zhang, Dominik Fleitmann, Isabelle Couchoud, and Eric Wolff. Synchronous timing of abrupt climate changes during the last glacial period. *Science*, 369(6506):963969, Aug 2020. ISSN 1095-9203. doi: 10.1126/science.aay5538. URL http://dx.doi.org/10.1126/science.aay5538.

W. Dansgaard, S.J. Johnsen, H.B. Clausen, D. Dahl-Jensen, N. Gundestrup, C.U. Hammer, and H. Oeschger. North atlantic climatic oscillations revealed by deep greenland ice cores. *Geophysical Monograph Series*, page 288298, 1984. ISSN 0065-8448. doi: 10.1029/gm029p0288. URL http://dx.doi.org/10.1029/GM029p0288.

Trond M. Dokken, Kerim H. Nisancioglu, Camille Li, David S. Battisti, and Catherine Kissel. Dansgaard-oeschger cycles: Interactions between ocean and sea ice intrinsic to the nordic seas. *Paleoceanography*, 28(3):491502, Sep 2013. ISSN 0883-8305. doi: 10.1002/palo.20042. URL http://dx.doi.org/10.1002/palo.20042.

Andrey Ganopolski and Stefan Rahmstorf. Rapid changes of glacial climate simulated in a coupled climate model. *Nature*, 409(6817):153158, Jan 2001. ISSN 0028-0836. doi: 10.1038/35051500. URL http://dx.doi.org/10.1038/35051500.

Peter R. Gent and James C. Mcwilliams. Isopycnal mixing in ocean circulation models. *Journal of Physical Oceanography*, 20(1):150155, Jan 1990. ISSN 1520-0485. doi: 10.1175/1520-0485(1990)020⟨0150:imiocm⟩2.0.co;2. URL http://dx.doi.org/10.1175/1520-0485(1990)020<0150:IMIOCM>2.0.CO;2.

D. Genty, D. Blamart, R. Ouahdi, M. Gilmour, A. Baker, J. Jouzel, and Sandra Van-Exter. Precise dating of dansgaardoeschger climate oscillations in western europe from stalagmite data. *Nature*, 421(6925):833837, Feb 2003. ISSN 0028-0836. doi: 10.1038/nature01391. URL http://dx.doi.org/10.1038/nature01391.

Hezi Gildor and Eli Tziperman. Sea-ice switches and abrupt climate change. *Philosophical Transactions of the Royal Society of London A: Mathematical, Physical and Engineering Sciences*, 361 (1810):1935–1944, 2003. ISSN 1364-503X. doi: 10.1098/rsta.2003.1244.

Oliver Gutjahr, Nils Brggemann, Helmuth Haak, Johann H. Jungclaus, Dian A. Putrasahan, Katja Lohmann, and Jin-Song von Storch. Comparison of ocean vertical mixing schemes in the max planck institute earth system model (mpi-esm1.2). *Geoscientific Model Development*, 14(5):

23172349, May 2021. ISSN 1991-9603. doi: 10.5194/gmd-14-2317-2021. URL http://dx.doi.org/10.5194/gmd-14-2317-2021.

Feng He. *Simulating transient climate evolution of the last deglaciation with CCSM 3*, volume 72. 2011.

Yi Huang, Xiaoxiao Tan, and Yan Xia. Inhomogeneous radiative forcing of homogeneous greenhouse gases. *Journal of Geophysical Research: Atmospheres*, 121(6):27802789, Mar 2016. ISSN 2169-897X. doi: 10.1002/2015jd024569. URL http://dx.doi.org/10.1002/2015JD024569.

Mari F. Jensen, Kerim H. Nisancioglu, and Michael A. Spall. Large changes in sea ice triggered by small changes in atlantic water temperature. *Journal of Climate*, 31(12):48474863, Jun 2018. ISSN 1520-0442. doi: 10.1175/jcli-d-17-0802.1. URL http://dx.doi.org/10.1175/JCLI-D-17-0802.1.

J. H. Jungclaus, N. Keenlyside, M. Botzet, H. Haak, J.-J. Luo, M. Latif, J. Marotzke, U. Mikolajewicz, and E. Roeckner. Ocean circulation and tropical variability in the coupled model echam5/mpi-om. *Journal of Climate*, 19(16):39523972, Aug 2006. ISSN 1520-0442. doi: 10.1175/jcli3827.1. URL http://dx.doi.org/10.1175/JCLI3827.1.

J. H. Jungclaus, N. Fischer, H. Haak, K. Lohmann, J. Marotzke, D. Matei, U. Mikolajewicz, D. Notz, and J. S. Storch. Characteristics of the ocean simulations in the max planck institute ocean model (mpiom) the ocean component of the mpi-earth system model. *Journal of Advances in Modeling Earth Systems*, 5(2):422–446, Jun 2013. ISSN 1942-2466. doi: 10.1002/jame.20023. URL http://dx.doi.org/10.1002/jame.20023.

M. Kageyama, U. Merkel, B. Otto-Bliesner, M. Prange, A. Abe-Ouchi, G. Lohmann, R. Ohgaito, D. M. Roche, J. Singarayer, D. Swingedouw, and et al. Climatic impacts of fresh water hosing under last glacial maximum conditions: a multi-model study. *Climate of the Past*, 9(2):935953, Apr 2013. ISSN 1814-9332. doi: 10.5194/cp-9-935-2013. URL http://dx.doi.org/10.5194/cp-9-935-2013.

P. Kindler, M. Guillevic, M. Baumgartner, J. Schwander, A. Landais, and M. Leuenberger. Temperature reconstruction from 10 to 120 kyr b2k from the ngrip ice core. *Climate of the Past*, 10(2):887902, Apr 2014. ISSN 1814-9332. doi: 10.5194/cp-10-887-2014. URL http://dx.doi.org/10.5194/cp-10-887-2014.

M. Klockmann, U. Mikolajewicz, H. Kleppin, and J. Marotzke. Coupling of the subpolar gyre and the overturning circulation during abrupt glacial climate transitions. *Geophysical Research Letters*, 47(21), Nov 2020. ISSN 1944-8007. doi: 10.1029/2020gl090361. URL http://dx.doi.org/10.1029/2020GL090361.

Marlene Klockmann, Uwe Mikolajewicz, and Jochem Marotzke. Two amoc states in response to decreasing greenhouse gas concentrations in the coupled climate model mpi-esm. *Journal of Climate*, 31(19):79697984, Oct 2018. ISSN 1520-0442. doi: 10.1175/jcli-d-17-0859.1. URL http://dx.doi.org/10.1175/JCLI-D-17-0859.1.

Takuro Kobashi, Kenji Kawamura, Jeffrey P. Severinghaus, Jean-Marc Barnola, Toshiyuki Nakaegawa, Bo M. Vinther, Sigfs J. Johnsen, and Jason E. Box. High variability of greenland surface temperature over the past 4000 years estimated from trapped air in an ice core. *Geophysical Research Letters*, 38(21):n/an/a, Nov 2011. ISSN 0094-8276. doi: 10.1029/2011gl049444. URL http://dx.doi.org/10.1029/2011GL049444.

K. Lambeck. Sea level change through the last glacial cycle. *Science*, 292(5517):679686, Apr 2001.

ISSN 1095-9203. doi: 10.1126/science.1059549. URL http://dx.doi.org/10.1126/science.1059549.

J. Laskar, P. Robutel, F. Joutel, M. Gastineau, A. C. M. Correia, and B. Levrard. A long-term numerical solution for the insolation quantities of the earth. *Astronomy & Astrophysics*, 428(1): 261–285, Nov 2004. ISSN 1432-0746. doi: 10.1051/0004-6361:20041335. URL http://dx.doi.org/10.1051/0004-6361:20041335.

J. Laskar, A. Fienga, M. Gastineau, and H. Manche. La2010: a new orbital solution for the long-term motion of the earth. *Astronomy & Astrophysics*, 532:A89, Jul 2011. ISSN 1432-0746. doi: 10.1051/0004-6361/201116836. URL http://dx.doi.org/10.1051/0004-6361/201116836.

Camille Li and David S. Battisti. Reduced atlantic storminess during last glacial maximum: Evidence from a coupled climate model. *Journal of Climate*, 21(14):35613579, Jul 2008. ISSN 0894-8755. doi: 10.1175/2007jcli2166.1. URL http://dx.doi.org/10.1175/2007JCLI2166.1.

Lorraine E. Lisiecki and Maureen E. Raymo. A pliocene-pleistocene stack of 57 globally distributed benthic ?18o records. *Paleoceanography*, 20(1):n/a–n/a, Jan 2005. ISSN 0883-8305. doi: 10.1029/2004pa001071. URL http://dx.doi.org/10.1029/2004PA001071.

Johannes Lohmann and Peter D. Ditlevsen. Random and externally controlled occurrences of dansgaardoeschger events. *Climate of the Past*, 14(5):609617, May 2018. ISSN 1814-9332. doi: 10.5194/cp-14-609-2018. URL http://dx.doi.org/10.5194/cp-14-609-2018.

Laetitia Loulergue, Adrian Schilt, Renato Spahni, Valérie Masson-Delmotte, Thomas Blunier, Bénédicte Lemieux, Jean-Marc Barnola, Dominique Raynaud, Thomas F. Stocker, and Jérôme Chappellaz. Orbital and millennial-scale features of atmospheric ch4 over the past 800,000 years. *Nature*, 453(7193):383–386, May 2008. ISSN 1476-4687. doi: 10.1038/nature06950. URL http://dx.doi.org/10.1038/nature06950.

R. Love, H. Andres, A. Condron, and L. Tarasov. Eddy permitting simulations of freshwater injection from major northern hemisphere outlets during the last deglacial. *Climate of the Past Discussions*, 2021:1–16, 2021a. doi: 10.5194/cp-2021-15. URL https://cp.copernicus.org/preprints/cp-2021-15/.

R. Love, H. Andres, X. Zhang, A. Condron, G. Lohmann, and L. Tarasov. Exploring the climate system response to a range of freshwater representations: Hosing, regional, and freshwater fingerprints. *Manuscript Draft*, 2021b.

S.J. Marsland, H. Haak, J.H. Jungclaus, M. Latif, and F. Rske. The max-planck-institute global ocean/sea ice model with orthogonal curvilinear coordinates. *Ocean Modelling*, 5(2):91127, Jan 2003. ISSN 1463-5003. doi: 10.1016/s1463-5003(02)00015-x. URL http://dx.doi.org/10.1016/S1463-5003(02)00015-X.

Glenn A. Milne and Jerry X. Mitrovica. Postglacial sea-level change on a rotating earth. *Geophysical Journal International*, 133(1):119, Apr 1998. ISSN 1365-246X. doi: 10.1046/j.1365-246x.1998.1331455.x. URL http://dx.doi.org/10.1046/j.1365-246X.1998.1331455.x.

Jerry X. Mitrovica and Glenn A. Milne. On post-glacial sea level: I. general theory. *Geophysical Journal International*, 154(2):253267, Aug 2003. ISSN 1365-246X. doi: 10.1046/j.1365-246x.2003.01942.x. URL http://dx.doi.org/10.1046/j.1365-246X.2003.01942.x.

A. J. G. Nurser and S. Bacon. The rossby radius in the arctic ocean. *Ocean Science*, 10(6):967975, Nov 2014. ISSN 1812-0792. doi: 10.5194/os-10-967-2014. URL http://dx.doi.org/10.5194/os-10-967-2014.

Steffen Malskaer Olsen, Gary Shaffer, and Christian J. Bjerrum. Ocean oxygen isotope constraints on mechanisms for millennial-scale climate variability. *Paleoceanography*, 20(1):n/an/a, Feb 2005. ISSN 0883-8305. doi: 10.1029/2004pa001063. URL http://dx.doi.org/10.1029/2004PA001063.

R. C. Pacanowski and S. G. H. Philander. Parameterization of vertical mixing in numerical models of tropical oceans. *Journal of Physical Oceanography*, 11(11):14431451, Nov 1981. ISSN 1520-0485. doi: 10.1175/1520-0485(1981)011⟨1443:povmin⟩2.0.co;2. URL http://dx.doi.org/10.1175/1520-0485(1981)011<1443:POVMIN>2.0.CO;2.

W. R. Peltier, G. Vettoretti, and M. Stastna. Atlantic meridional overturning and climate response to arctic ocean freshening. *Geophysical Research Letters*, 33(6):n/a–n/a, 2006. ISSN 1944-8007. doi: 10.1029/2005GL025251. URL http://dx.doi.org/10.1029/2005GL025251. L06713.

W. Richard Peltier and Guido Vettoretti. Dansgaard-oeschger oscillations predicted in a comprehensive model of glacial climate: A kicked salt oscillator in the atlantic. *Geophysical Research Letters*, 41(20):73067313, Oct 2014. ISSN 0094-8276. doi: 10.1002/2014gl061413. URL http://dx.doi.org/10.1002/2014GL061413.

Stefan Rahmstorf. Ocean circulation and climate during the past 120,000 years. *Nature*, 419(6903): 207214, Sep 2002. ISSN 0028-0836. doi: 10.1038/nature01090. URL http://dx.doi.org/10.1038/nature01090.

Sune O. Rasmussen, Matthias Bigler, Simon P. Blockley, Thomas Blunier, Susanne L. Buchardt, Henrik B. Clausen, Ivana Cvijanovic, Dorthe Dahl-Jensen, Sigfus J. Johnsen, Hubertus Fischer, and et al. A stratigraphic framework for abrupt climatic changes during the last glacial period based on three synchronized greenland ice-core records: refining and extending the intimate event stratigraphy. *Quaternary Science Reviews*, 106:14–28, Dec 2014. ISSN 0277-3791. doi: 10.1016/j.quascirev.2014.09.007. URL http://dx.doi.org/10.1016/j.quascirev.2014.09.007.

Didier M. Roche, Ane P. Wiersma, and Hans Renssen. A systematic study of the impact of freshwater pulses with respect to different geographical locations. *Climate Dynamics*, 34(7-8): 9971013, May 2009. ISSN 1432-0894. doi: 10.1007/s00382-009-0578-8. URL http://dx.doi.org/10.1007/s00382-009-0578-8.

Adrian Schilt, Matthias Baumgartner, Thomas Blunier, Jakob Schwander, Renato Spahni, Hubertus Fischer, and Thomas F. Stocker. Glacial-interglacial and millennial-scale variations in the atmospheric nitrous oxide concentration during the last 800,000 years. *Quaternary Science Reviews*, 29(1-2):182–192, Jan 2010. ISSN 0277-3791. doi: 10.1016/j.quascirev.2009.03.011. URL http://dx.doi.org/10.1016/j.quascirev.2009.03.011.

Inger K. Seierstad, Peter M. Abbott, Matthias Bigler, Thomas Blunier, Anna J. Bourne, Edward Brook, Susanne L. Buchardt, Christo Buizert, Henrik B. Clausen, Eliza Cook, and et al. Consistently dated records from the greenland grip, gisp2 and ngrip ice cores for the past 104 ka reveal regional millennial-scale ?18o gradients with possible heinrich event imprint. *Quaternary Science Reviews*, 106:29–46, Dec 2014. ISSN 0277-3791. doi: 10.1016/j.quascirev.2014.10.032. URL http://dx.doi.org/10.1016/j.quascirev.2014.10.032.

Gary Shaffer. Ocean subsurface warming as a mechanism for coupling dansgaard-oeschger climate cycles and ice-rafting events. *Geophysical Research Letters*, 31(24), 2004. ISSN 0094-8276. doi: 10.1029/2004gl020968. URL http://dx.doi.org/10.1029/2004GL020968.

Adriana Sima, Andr Paul, and Michael Schulz. The younger dryasan intrinsic feature of late pleistocene climate change at millennial timescales. *Earth and Planetary Science Letters*, 222 (3-4):741750, Jun 2004. ISSN 0012-821X. doi: 10.1016/j.epsl.2004.03.026. URL http://dx.doi.org/10.1016/j.epsl.2004.03.026.

O. Tange. GNU Parallel - The Command-Line Power Tool. *;login: The USENIX Magazine*, 36(1): 42–47, Feb 2011. URL http://www.gnu.org/s/parallel.

Lev Tarasov and W Richard Peltier. Greenland glacial history, borehole constraints, and eemian extent. *Journal of Geophysical Research: Solid Earth*, 108(B3), 2003.

Lev Tarasov and W.R. Peltier. A calibrated deglacial drainage chronology for the north american continent: evidence of an arctic trigger for the younger dryas. *Quaternary Science Reviews*, 25(7-8):659688, Apr 2006. ISSN 0277-3791. doi: 10.1016/j.quascirev.2005.12.006. URL http://dx.doi.org/10.1016/j.quascirev.2005.12.006.

Lev Tarasov, Arthur S. Dyke, Radford M. Neal, and W.R. Peltier. A data-calibrated distribution of deglacial chronologies for the north american ice complex from glaciological modeling. *Earth and Planetary Science Letters*, 315316:30 – 40, 2012. ISSN 0012-821X. doi: http://dx.doi.org/10.1016/j.epsl.2011.09.010. URL http://www.sciencedirect.com/science/article/pii/S0012821X11005243. Sea Level and Ice Sheet Evolution: A {PALSEA} Special Edition.

Lev Tarasov, Anna Hughes, Richard Gyllencreutz, Oystein Strand Lohne, Jan Mangerud, and John-Inge Svendsen. The global GLAC-1c deglaciation chronology, melwater pulse 1-a, and a question of missing ice. In *IGS Symposium on Contribution of Glaciers and Ice Sheets to Sea-Level Change*, IGS Symposium abstracts, 2014.

Michael Vellinga and Peili Wu. Low-latitude freshwater influence on centennial variability of the atlantic thermohaline circulation. *Journal of Climate*, 17(23):44984511, Dec 2004. ISSN 0894-8755. doi: 10.1175/3219.1. URL http://dx.doi.org/10.1175/3219.1.

Guido Vettoretti and W. Richard Peltier. Thermohaline instability and the formation of glacial north atlantic super polynyas at the onset of dansgaard-oeschger warming events. *Geophysical Research Letters*, 43(10):53365344, May 2016. ISSN 0094-8276. doi: 10.1002/2016gl068891. URL http://dx.doi.org/10.1002/2016GL068891.

Guido Vettoretti and W. Richard Peltier. Fast physics and slow physics in the nonlinear dansgaardoeschger relaxation oscillation. *Journal of Climate*, 31(9):34233449, Mar 2018. ISSN 1520-0442. doi: 10.1175/jcli-d-17-0559.1. URL http://dx.doi.org/10.1175/JCLI-D-17-0559.1.

X. Zhang. "Confidential Manuscript - Personal Communication", July 2021.

Xiao Zhang, Matthias Prange, Ute Merkel, and Michael Schulz. Instability of the atlantic overturning circulation during marine isotope stage 3. *Geophysical Research Letters*, 41(12):42854293, Jun 2014a. ISSN 0094-8276. doi: 10.1002/2014gl060321. URL http://dx.doi.org/10.1002/2014GL060321.

Xu Zhang, Gerrit Lohmann, Gregor Knorr, and Conor Purcell. Abrupt glacial climate shifts controlled by ice sheet changes. *Nature*, 512(7514):290294, Aug 2014b. ISSN 1476-4687. doi: 10.1038/nature13592. URL http://dx.doi.org/10.1038/nature13592.

Xu Zhang, Gregor Knorr, Gerrit Lohmann, and Stephen Barker. Abrupt north atlantic circulation changes in response to gradual co2 forcing in a glacial climate state. *Nature Geoscience*, 10 (7):518523, Jun 2017. ISSN 1752-0908. doi: 10.1038/ngeo2974. URL http://dx.doi.org/10.1038/ngeo2974.

Chapter 5

Conclusions

5.1 Summary

The paleoclimate archive provides important insight into past climate variability, but previous work has had limited success in reproducing inferred centennial to millennial scale climate variability (CMCV). Paleoclimate records also indicate that CMCV occurred only under certain ranges of boundary conditions (e.g. intermediate ice sheet volumes). Past CMCV therefore provides the opportunity to test the question 'Can our tools capture the full range of climate variability under different mean states?'. This is of high relevance to projecting future climate variability.

However, climate modelling of CMCV has been hampered via shortcomings such as the use of inappropriate mean states (e.g. utilizing boundary conditions inconsistent with intervals which demonstrate CMCV) or simplifications in forcings (e.g. the use of simplified 'Hosing' bands for the treatment of glacial runoff). To disentangle these challenges, a step forward is to examine the sensitivity of modelled CMCV to relevant boundary conditions and forcings (i.e. ice sheet distribution, orbital configuration, greenhouse gasses such as carbon dioxide, glacial runoff/freshwater fluxes). As justified in Chapter 1, carbon dioxide (pCO_2) and glacial runoff/freshwater have been examined herein. pCO_2 was chosen for both its relevance to anthropogenic climate change and its relative simplicity to orbital configurations. Freshwater was chosen for similar relevance as pCO_2 to anthropogenic climate change due to melting glaciers, ice caps, and ice sheets, and because it provides a contrast to pCO_2 with respect to both the domain of forcing (ocean vs. atmosphere) and the spatial scale (relatively local vs. global).

However, the investigation of the impact of glacial runoff on CMCV has previously un-addressed challenges in implementation (e.g. the 'Hosing' simplification) and resolution (e.g. multi-millennial scale simulations vs. mesoscale transport features). As such I first explore issues regarding the conventional implementation method and potential mitigation strategies for both the implementation and resolution problems. I then investigate the role of pCO_2 and freshwater in modulating CMCV using boundary conditions consistent with the intervals which are inferred to demonstrate CMCV (e.g. Marine Isotope Stage (MIS) 3) and glacial runoff in the form of freshwater forcing over a range of complexities. I accomplish these goals by addressing the following research questions (as further motivated below):

- What proportion of freshwater is transported to sites of deep water formation when it originates from one of several outlets of glacial runoff? How different is this from the 'Hosing' simplification and what are the implications for understanding events like the Younger Dryas and Meltwater Pulse 1A?
- How can I utilise model output from high resolution freshwater injection experiments to compensate for the coarse ocean model resolution required for paleo-timescale experiments? How do the modelled results affect the inferences made about centennial to millennial scale climate change due to freshwater forcing?
- What are the roles of freshwater and pCO_2 in changing stadial and interstadial durations of Dansgaard-Oeschger events during Marine Isotope Stage (MIS) 3? What part of the range of variability seen in the paleoclimate record can be attributed to changes in these forcings?

Freshwater transport, from both glacial and river runoff, is generally poorly resolved in paleoclimate simulations. A core reason for this shortcoming is the necessarily coarse resolution required to conduct multi-centennial to multi-millennial scale experiments being at odds with the fine-scale transport mechanisms for coastally released freshwater. As such, freshwater injection investigations tend to rely on a simplified freshwater injection distribution for the representation of glacial runoff, the 'Hosing' belt approach, which effectively covers sites of deep water formation with the injection region. This motivates the first question above, which can be expanded to "how much freshwater from outlets of glacial runoff is transported to the sites of deep water formation when processes such as boundary currents and mesoscale eddies are resolved rather than parametrized?".

To investigate this question, in Chapter 2 I provide the first assessment of freshwater transport to deepwater formation regions under Younger Dryas (YD) conditions using realistic freshwater injection amounts applied to a range of plausible source regions in a suite of eddy-permitting simulations. In doing so, I find that one year of 2 dSv injection at the mouth of the Mackenzie River (for a closed Bering Strait configuration) yields a freshening equivalent to direct regional hosing by amounts of ≈ 0.31 dSv in the Labrador Sea, ≈ 0.33 dSv in the northern North Atlantic, and $\approx$ 1.85 dSv in the GIN Seas. These results indicate that the transport of freshwater from the coast to sites of deepwater formation leads to a reduction in the effective freshwater forcing compared to that of direct Hosing with the same injected flux of freshwater. Thus, while the practice of hosing, such as used in the experiments listed in 1.1, may mitigate the inability of coarse resolution models to adequately resolve small-scale features that are key to freshwater transport, like (e.g. boundary currents and mesoscale eddies), applying freshwater fluxes directly onto sites of deep water formation is an inaccurate representation when considering the transport processes involved. A caveat is that this work examines only liquid freshwater fluxes, not solid (i.e. icebergs) contributions from ice sheets. However, recent investigation [Condron and Hill, 2021] indicates that the 'Hosing' distribution may not be reflective of the distribution of solid freshwater.

Using the results of Chapter 2, I examine an outstanding issue regarding the role of freshwater and CMCV: the delay between Meltwater Pulse 1A (MWP1A) and the YD return to stadial conditions. Based upon pre-existing experiments and physical reasoning, it is expected that glacial runoff at the scale of MWP1A should result in a sudden transition to stadial climate conditions. When considering the total discharge due to net ice mass loss during MWP1A, a 10 to 15m rise of sea level over one third of a millennium [Deschamps et al., 2012] translates to a discharge of 3 to 5dSv. The scale of this discharge has been shown in multiple studies, see table 1.1, to strongly suppress AMOC (when considering only the 'Hosing' simplification). Instead, the Bølling-Allerød warm interval lasted for $>$ 1000 years after MWP1A with only gradual cooling before the sudden return to stadial conditions at the onset of the YD.

I examine this disconnect from the perspective of the simulated salinity anomaly distributions and the lack of reconstructed impact on deepwater formation during the Bølling-Allerød (where deep water formation ought to be taking place in the Greenland-Iceland-Norwegian (GIN) Seas). Of the North American outlets explored, freshwater from the Mackenzie River results in the strongest freshening effect of the GIN seas deep water formation site, and would thus be most effective at reducing AMOC with the associated sudden climate cooling. By comparison, freshwater from the Mississippi River/Gulf of Mexico results in $\approx \frac{1}{8}$ the freshening impact of the GIN seas relative to the Mackenzie River routed freshwater, while the Gulf of St. Lawrence routed freshwater results in $\approx \frac{1}{4}$. The implications of these results to the overarching question of how significant freshwater fluxes, such as occurred during MWP1A, could occur without a consequent effect on DWF rates and climate is that the majority of freshwater from North American Ice Sheets needs to enter the ocean from either (of those outlets investigated herin) the Gulf of St. Lawrence or the Mississippi River in order to minimally impact sites of DWF. Note, my results do not help resolve the outstanding issue regarding MWP1A contributions from Eurasia [inferred to be ≈ 2 dSv, Brendryen et al., 2020], instead showing that runoff from Fennoscandia is very effective at freshening the GIN seas region and ought to result in a strong reduction of DWF.

Given the computational resource trade-offs between resolving mesoscale features for accurate transport of glacial runoff and performing multi-millennial scale simulations to examine CMCV, a method which assists in mitigating this shortcoming would allow for more robust examination of the role of freshwater in the paleoclimate system and CMCV. Therefore, in Chapter 3 I developed the novel 'freshwater fingerprint' injection distribution using the freshwater distributions obtained from the eddy-permitting simulations in Chapter 2. The goal of this injection method is to incorporate information from the eddy-permitting configuration into the eddy-parametrizing model configuration. I compare this technique to two other methods of freshwater injection and analyse the climatological impacts using a coarse (3° ocean/T31 atmosphere) resolution coupled Earth Systems Model to address the second research question and also contributing to question 1.

To perform these comparisons I implement and evaluate three different forms of freshwater injection, the typical 'Hosing' method, regional injection, and the 'freshwater fingerprint' method. Hosing involves uniformly distributing freshwater over a band in the North Atlantic that covers common deep-water formation regions ($50 - 70°$ N). Regional injection places freshwater at the mouth of major outlets in the Northern Hemisphere and allow the relatively coarse model to transport the freshwater. The freshwater fingerprint method distributes the freshwater according to its transport in the eddy-permitting model configuration of the MITgcm discussed in Chapter 2.

In the case of the COSMOS model, a relatively comprehensive Earth Systems Model running at coarse resolution, I find that regional freshwater injection can reproduce some, but not all, of the major features observed at the eddy permitting scale, with my investigation finding better agreement for the Mackenzie River and Fennoscandia. The distributions of freshwater from the Gulf of St. Lawrence (GSL) and the Mississippi River/Gulf of Mexico (GOM) are those most different from regional to fingerprint injection, largely due to resolution related model issues. The response of the system to freshwater from the GSL regional injection is much weaker than with the fingerprint method when comparing AMOC, and Greenland and European surface temperature changes within the first century of hosing. Those same responses are inverted for the GOM regional and fingerprint simulations. These results demonstrate that the use of the fingerprint method in COSMOS reduces errors that arise from the representation of freshwater transport at coarse resolutions in a coupled Earth Systems Model.

Comparing these methods against the typical 'Hosing' methodology I find the overall climate response of hosing is both faster and greater in magnitude, over-emphasizing the cooling aspect of glacial runoff. In particular I find that using hosing leads to greater surface cooling in Greenland, Europe, and North Asia as well as an exaggerated growth of northern hemisphere sea ice. As such, the interpretation of past studies using hosing, such as the 10 studies listed in Table 1.1, need to take into account this unphysical enhancement of cooling. These types of biases need to be addressed when designing modelling experiments for climate stability and/or sensitivity, or for future climate simulations if choosing to represent freshwater injection as a simple band over sites of deep water formation.

Dansgaard-Oeschger (DO) events are centennial to millennial scale climate excursions first identified in the Greenland ice core records [Dansgaard et al., 1984]. During the last glacial cycle these events are most common during the MIS3 interval, and do not occur during more recent intervals (with the notable exception of the YD/BA which demonstrate comparable climate changes to DO events). These excursions are associated with temperature changes over Europe [Genty et al., 2003] and the Nordic seas [Dokken et al., 2013] of the $O(5 - 10° C)$, and changes in precipitation patterns in the monsoon regions of South Asia and South America Corrick et al. [2020]. As discussed, these events occur within a window of boundary conditions, of which I explore variations of pCO_2 and glacial runoff/freshwater in Chapter 4. This is done via the same modelling configuration from Chapter 3 but using a range of MIS3 appropriate pCO_2 and freshwater injection scenarios, including the novel freshwater fingerprint. Unlike most modelling studies to date, this work is distinguished by the the generation and investigation of CMCV under boundary conditions (land ice, land-sea-mask, orbital, and GHGs) consistent with MIS3, rather than with intervals which do not exhibit DO events such as the last glacial maximum (as in Peltier and Vettoretti [2014] and Klockmann et al. [2020]).

Given the structural uncertainties of climate models, meaningful interpretation of climate modelling results needs attention on isolating relevant key processes and feedbacks and comparing these to similar modelling studies. Investigations of DO events can be loosely categorized as describing simulated CMCV as via either a 'salinity oscillator' or a 'thermohaline oscillator' hypothesis. In my investigation I find the pacing of the simulated CMCV appears to be related to the subsurface temperature gradient between the Atlantic and the GIN seas. This behaviour is in agreement with the thermohaline oscillator hypothesis (shown further in Chapter 4) of DO events as per Brown and Galbraith [2016]. I find that there is a clear relationship between pCO_2 and interstadial durations, where increasing pCO_2 leads to longer interstadial intervals. This relationship is found in the paleoclimate record (when examining CMCV during the MIS3 interval) as well as the COSMOS simulations.

The maximum stadial duration of my simulated CMCV is related to background pCO_2, where increasing background pCO_2 results in a decreasing upper limit on the duration of stadial intervals. This feature of the simulated events is also seen in the paleoclimate record, but there are limited stadial events at higher pCO_2 values during MIS3 to compare against. This limiting of stadial duration arises as a result of the greater transport of subsurface heat from the Atlantic to the Nordic seas, where the temperature gradient between these regions increases with pCO_2. The result of this increased heat transport is a shortening of the interval before deep water formation in the Nordic Seas is reinvigorated by a build-up of subsurface heat.

When exploring the role of freshwater on CMCV, I find that freshwater injections can result in one of three different behaviours depending both upon the flux amount and the location of the injection. Continual freshwater injection of 2dSv results in a complete suppression of AMOC and a continual stadial state for all injection locations and methods investigated. This result is the expected behaviour of the addition of freshwater into the climate system and is in agreement with previous work, which indicates that this behaviour is robust. Intermediate injections of $0.25-0.5$dSv using regional injection locations and the $50-70°$ N band in the North Atlantic result in regular periodic changes. For this range of freshwater injection flux I find the period depends more strongly on the location of the injection than the injection amount, with the $50-70°$ N band having a higher frequency. This feature seems to be tied to the effective freshening of the deep water formation region in the Nordic seas by a given method/outlet. When using the glacial runoff distribution from ice sheet reconstruction, I find freshwater decreases interstadial durations but does not impact stadial durations. These latter two results are unexpected given previous work examining the role of freshwater in the glacial climate system, as the intuitive behaviour would be extended stadial durations via suppressed AMOC. As such, further examination with additional lower-flux freshwater injection experiments (as detailed in Section 5.2), and potentially multi-model comparisons, are required to elucidate if these results are a property of COSMOS or are robust results.

The full range of stadial/interstadial durations present in the paleoclimate archive is not captured by COSMOS under this mean state for the inferred range of pCO_2 and freshwater forcing. My experiments are unable to reproduce the longer-duration/lower-frequency events during the MIS3 interval via changes to the mean state. However, those boundary condition changes explored here successfully capture the range of higher frequency variability. These results indicate that the longer-duration/lower-frequency events may be more dependent upon features of the unexplored boundary conditions (e.g. ice sheet reconstructions) than upon those explored here.

5.2 Future Work

Given the time limitations of a PhD there are invariably unresolved questions to address and further experiments to perform. The following discussion is focused around observations which arose in the construction of individual chapters rather than the cross-chapter research questions as above.

With regards Chapter 2 and the role of freshwater in triggering rapid (centennial to millennial scale) climate change events such as the Younger Dryas, two additional research questions and two technical questions are of interest to me. It is observed that freshwater had a tendency to accumulate in marginal seas, which motivates the question: "Could a build-up and subsequent flushing (via changing oceanic gateways or changes in perennial sea ice) of freshwater in a partially isolated region, such as Baffin Bay, lead to a delayed onset of cooling after changing routing or increase in glacial runoff?". Given all outlets have some freshening effects at sites of deep water formation there remains the issue of how to reconcile high discharge during MWP1A and with limited impact on interstadial conditions. When considering this result and that MWP1A occurred coincident with the onset of the Bølling-Allerød warming period, the question: "Can a transition from a stadial to an interstadial climate provide some means of stabilizing AMOC to the effects of freshwater and thus allow for both increased glacial runoff and increased warming such as seen at the onset of the Bølling-Allerød?" is motivated. Both of these questions arise as a direct result of observations during the investigation, the latter of which may provide further insight into the mechanisms of CMCV.

In the more technical vein, one of the shortcomings discussed in Chapter 2 is the use of last glacial maximum surface boundary conditions, and so directly addressing this shortcoming via the question: "What is the sensitivity of the proportions of freshwater transported to sites of deep water formation to atmospheric conditions (e.g. interglacial vs. glacial forcings, temporal and spatial resolution)?" is a logical next step. Finally, the role of seasonality in freshwater forcing in general is an open question at present. Despite the readily apparent seasonal cycle to glacial runoff [Arnold et al., 2014], this feature has not been explored in freshwater injection experiments. As such, it seems a natural extension of the work of both Chapters 2 and 3, to ask the question "What is the impact of seasonal variability in glacial runoff in freshwater forcing simulations?" Seasonal variation can be evaluated using tools appropriate (e.g. the infrastructure used in Chapter 2) for examining the transport of glacial runoff as well as can be incorporated into the freshwater fingerprint.

Similarly, additional questions are motivated by the work in Chapter 3 where the novel freshwater fingerprint method is described and the ability of an intermediate resolution climate model to accurately represent freshwater transports from outlets of glacial runoff is evaluated. One of the clearest avenues of extension to this work is the generation of fingerprints using a closed Bering Strait configuration for all outlets rather than only the Mackenzie River. While the impact of the Bering Strait on the other outlets of interest is considered to be low for the use of the fingerprints as an initial step (when considering the high compute cost) in Chapters 3 and 4, it is reasonable to conclude that having a set for both open and closed Bearing Strait would increase the utility of the fingerprints for the climate modelling community at large and allow for validation of this assumption. This extension, and the associated analysis, is a final step before consideration of this chapter for publication.

With respect to Chapter 4 and the relationships between freshwater, pCO_2, and attributes of centennial- to millennial scale climate variability during MIS3; while evaluating the triggering of the events, several other potential triggering mechanisms arose as discussion points. In examining the ice core records of Greenland it is readily seen that there are tephra horizons coincident with many of the sudden changes in δ^{18}O representative of DO events [Bourne et al., 2015]. Volcanism is understood to have a negative radiative forcing impact which can be global in impact Zanchettin et al. [2014]. As discussed in Chapters 1 and 4, changes in sea ice [whose extent can be enhanced by by volcanism Gagn et al., 2017] are an important feature of the transitions between interstadial and stadial states. As such, the question of "Can volcanic events trigger, or extend, stadial conditions via sudden decreases in radiative forcing associated with volcanic events?" arises. Similarly, given the connection between the termination of stadial conditions (shown in both Chapter 4, Klockmann et al. [2020], and inferred Dokken et al. [2013]) and sea ice changes in the Nordic seas, two additional questions arise: "Can a simulated event be artificially triggered through the creation of an artificial polyna or artificially extended via preventing polynia formation? If so, what preconditioning of the system is required?" and "Can a simulated event be triggered in the absence of these large openings in sea ice cover or is this another component of preconditioning the climate system?". As noted in Chapter 4, additional simulations may help elucidate the interactions between glacial runoff and CMCV under the salinity oscillator and thermohaline hypotheses.

Under the salinity oscillator hypothesis, there should be sensitivity to the location of the freshwater injection, as freshwater introduced into the subpolar gyre intensifies the salinity gradient between the subtropical and subpolar gyres and thus affects the pacing. The simulations presented in Chapter 4 are not sufficient to test this idea at present, however this can be achieved by conducting additional simulations at lower fluxes using the same injection locations. Using 0.5dSv in line with the estimates of glacial runoff in the 1xGLAC1E (the flux in line with changes to ice sheet volume) simulations and evaluating the behaviour would be a logical approach given the aforementioned suppression of AMOC at flux rates > 0.5dSv when using regional or fingerprint injection. Of the injection locations to evaluate at lower fluxes, GSL and GOM provide an opportunity to test the salinity oscillator hypotheses further as they introduce freshwater into the subpolar and subtropical gyres respectively. These simulations would also be of use for evaluating the relationship between injection location (and freshwater delivery to sites of deep water formation), and oscillation frequency. A multi-model comparison would also assist in determining the robustness of these relationships. As well, extending some simulations presented in Chapter 4, to better resolve the distribution of stadial/interstadial durations as a function of pCO_2 and freshwater, is a next-step prior to consideration for publication. Two other primary forcings were not examined in this investigation but are inferred to be significant for CMCV: the effects of varied ice sheet geometry and orbital configurations. As such, these results raise the question of how impactful differences in ice sheet geometry, particularly areal extent which remains untested at present, and orbital configurations are upon CMCV characteristics.

Bibliography

L. Ackermann, C. Danek, P. Gierz, and G. Lohmann. Amoc recovery in a multicentennial scenario using a coupled atmosphere-ocean-ice sheet model. *Geophysical Research Letters*, 47(16), Aug 2020. ISSN 1944-8007. doi: 10.1029/2019gl086810. URL http://dx.doi.org/10.1029/2019GL086810.

Florian Adolphi, Christopher Bronk Ramsey, Tobias Erhardt, R. Lawrence Edwards, Hai Cheng, Chris S. M. Turney, Alan Cooper, Anders Svensson, Sune O. Rasmussen, Hubertus Fischer, and et al. Connecting the greenland ice-core and u/th timescales via cosmogenic radionuclides: testing the synchroneity of dansgaard-oeschger events. *Climate of the Past*, 14(11):1755–1781, Nov 2018. ISSN 1814-9332. doi: 10.5194/cp-14-1755-2018. URL http://dx.doi.org/10.5194/cp-14-1755-2018.

Paul Aharon. Entrainment of meltwaters in hyperpycnal flows during deglaciation superfloods in the gulf of mexico. *Earth and Planetary Science Letters*, 241(1-2):260270, Jan 2006. ISSN 0012-821X. doi: 10.1016/j.epsl.2005.10.034. URL http://dx.doi.org/10.1016/j.epsl.2005.10.034.

Katrine K Andersen, Anders Svensson, Sigfus J Johnsen, Sune O Rasmussen, Matthias Bigler, Regine Röthlisberger, Urs Ruth, Marie-Louise Siggaard-Andersen, Jørgen Peder Steffensen, Dorthe Dahl-Jensen, et al. The greenland ice core chronology 2005, 15–42ka. part 1: Constructing the time scale. *Quaternary Science Reviews*, 25(23):3246–3257, 2006.

Heather J. Andres and Lev Tarasov. Towards understanding potential atmospheric contributions to abrupt climate changes: characterizing changes to the north atlantic eddy-driven jet over the last deglaciation. *Climate of the Past*, 15(4):16211646, Aug 2019. ISSN 1814-9332. doi: 10.5194/cp-15-1621-2019. URL http://dx.doi.org/10.5194/cp-15-1621-2019.

N. S. Arnold, A. F. Banwell, and I. C. Willis. High-resolution modelling of the seasonal evolution of surface water storage on the greenland ice sheet. *The Cryosphere*, 8(4):11491160, Jul 2014. ISSN 1994-0424. doi: 10.5194/tc-8-1149-2014. URL http://dx.doi.org/10.5194/tc-8-1149-2014.

Yosef Ashkenazy, Martin Losch, Hezi Gildor, Dror Mirzayof, and Eli Tziperman. Multiple sea-ice states and abrupt moc transitions in a general circulation ocean model. *Climate Dynamics*, 40 (7-8):1803–1817, 2013. ISSN 0930-7575. doi: 10.1007/s00382-012-1546-2. URL http://dx.doi.org/10.1007/s00382-012-1546-2.

Taimaz Bahadory, Lev Tarasov, and Heather Andres. Last glacial inception trajectories for the northern hemisphere from coupled ice and climate modelling. *Climate of the Past*, 17(1):397418, Feb 2021. ISSN 1814-9332. doi: 10.5194/cp-17-397-2021. URL http://dx.doi.org/10.5194/cp-17-397-2021.

Jostein Bakke, yvind Lie, Einar Heegaard, Trond Dokken, Gerald H. Haug, Hilary H. Birks, Peter

Dulski, and Trygve Nilsen. Rapid oceanic and atmospheric changes during the younger dryas cold period. *Nature Geoscience*, 2(3):202205, Feb 2009. ISSN 1752-0908. doi: 10.1038/ngeo439. URL http://dx.doi.org/10.1038/ngeo439.

R. C. Bales and E. W. Wolff. Interpreting natural climate signals in ice cores. *Eos, Transactions American Geophysical Union*, 76(47):477477, 1995. ISSN 0096-3941. doi: 10.1029/95eo00293. URL http://dx.doi.org/10.1029/95EO00293.

Christine L. Batchelor, Martin Margold, Mario Krapp, Della K. Murton, April S. Dalton, Philip L. Gibbard, Chris R. Stokes, Julian B. Murton, and Andrea Manica. The configuration of northern hemisphere ice sheets through the quaternary. *Nature Communications*, 10(1), Aug 2019. ISSN 2041-1723. doi: 10.1038/s41467-019-11601-2. URL http://dx.doi.org/10.1038/s41467-019-11601-2.

Thomas K. Bauska, Shaun A. Marcott, and Edward J. Brook. Abrupt changes in the global carbon cycle during the last glacial period. *Nature Geoscience*, 14(2):9196, Feb 2021. ISSN 1752-0908. doi: 10.1038/s41561-020-00680-2. URL http://dx.doi.org/10.1038/s41561-020-00680-2.

Bernhard Bereiter, Sarah Eggleston, Jochen Schmitt, Christoph Nehrbass-Ahles, Thomas F. Stocker, Hubertus Fischer, Sepp Kipfstuhl, and Jerome Chappellaz. Revision of the epica dome c co2 record from 800 to 600 kyr before present. *Geophysical Research Letters*, 42(2):542–549, Jan 2015. ISSN 0094-8276. doi: 10.1002/2014gl061957. URL http://dx.doi.org/10.1002/2014GL061957.

André L Berger. Long-term variations of caloric insolation resulting from the earth's orbital elements1. *Quaternary research*, 9(2):139–167, 1978.

Ingo Bethke, Camille Li, and Kerim H. Nisancioglu. Can we use ice sheet reconstructions to constrain meltwater for deglacial simulations? *Paleoceanography*, 27(2):n/an/a, Apr 2012. ISSN 0883-8305. doi: 10.1029/2011pa002258. URL http://dx.doi.org/10.1029/2011PA002258.

Alan K. Betts and John H. Ball. Albedo over the boreal forest. *Journal of Geophysical Research: Atmospheres*, 102(D24):2890128909, Dec 1997. ISSN 0148-0227. doi: 10.1029/96jd03876. URL http://dx.doi.org/10.1029/96JD03876.

Matthias Bigler, Anders Svensson, Ernesto Kettner, Paul Vallelonga, Maibritt E. Nielsen, and Jrgen Peder Steffensen. Optimization of high-resolution continuous flow analysis for transient climate signals in ice cores. *Environmental Science & Technology*, 45(10):44834489, Apr 2011. ISSN 1520-5851. doi: 10.1021/es200118j. URL http://dx.doi.org/10.1021/es200118j.

G. Edward Birchfield and Wallace S. Broecker. A salt oscillator in the glacial atlantic? 2. a scale analysis model. *Paleoceanography*, 5(6):835843, Dec 1990. ISSN 0883-8305. doi: 10.1029/pa005i006p00835. URL http://dx.doi.org/10.1029/PA005i006p00835.

Niklas Boers. Observation-based early-warning signals for a collapse of the atlantic meridional overturning circulation. *Nature Climate Change*, 11(8):680688, Aug 2021. ISSN 1758-6798. doi: 10.1038/s41558-021-01097-4. URL http://dx.doi.org/10.1038/s41558-021-01097-4.

Niklas Boers, Michael Ghil, and Denis-Didier Rousseau. Ocean circulation, ice shelf, and sea ice interactions explain dansgaardoeschger cycles. *Proceedings of the National Academy of Sciences*, 115(47):E11005E11014, Nov 2018. ISSN 1091-6490. doi: 10.1073/pnas.1802573115. URL http://dx.doi.org/10.1073/pnas.1802573115.

A.J. Bourne, E. Cook, P.M. Abbott, I.K. Seierstad, J.P. Steffensen, A. Svensson, H. Fischer, S. Schpbach, and S.M. Davies. A tephra lattice for greenland and a reconstruction of volcanic events spanning 2545 ka b2k. *Quaternary Science Reviews*, 118:122141, Jun 2015. ISSN 0277-3791. doi: 10.1016/j.quascirev.2014.07.017. URL http://dx.doi.org/10.1016/j.quascirev.2014.07.017.

P. Braconnot, B. Otto-Bliesner, S. Harrison, S. Joussaume, J.-Y. Peterchmitt, A. Abe-Ouchi, M. Crucifix, E. Driesschaert, Th. Fichefet, C. D. Hewitt, and et al. Results of pmip2 coupled simulations of the mid-holocene and last glacial maximum part 1: experiments and large-scale features. *Climate of the Past*, 3(2):261–277, Jun 2007. ISSN 1814-9332. doi: 10.5194/cp-3-261-2007. URL http://dx.doi.org/10.5194/cp-3-261-2007.

P. Braconnot, S.P. Harrison, B. Otto-Bliesner, Ayako Abe-Ouchi, J. Jungclaus, and J.-Y Peterschmitt. The paleoclimate modeling intercomparison project contribution to cmip5. *CLIVAR Exchanges*, 56:15–19, 01 2011.

Jo Brendryen, Haflidi Haflidason, Yusuke Yokoyama, Kristian Agasoester Haaga, and Bjarte Hannisdal. Eurasian ice sheet collapse was a major source of meltwater pulse 1a 14,600 years ago. *Nature Geoscience*, 13(5):363–368, Apr 2020. ISSN 1752-0908. doi: 10.1038/s41561-020-0567-4. URL http://dx.doi.org/10.1038/s41561-020-0567-4.

Robert D Briggs, David Pollard, and Lev Tarasov. A data-constrained large ensemble analysis of antarctic evolution since the eemian. *Quaternary Science Reviews*, 103:91–115, 2014.

W. S. Broecker. Geology: Was the younger dryas triggered by a flood? *Science*, 312(5777):11461148, May 2006. ISSN 1095-9203. doi: 10.1126/science.1123253. URL http://dx.doi.org/10.1126/science.1123253.

Wallace S. Broecker, James P. Kennett, Benjamin P. Flower, James T. Teller, Sue Trumbore, Georges Bonani, and Willy Wolfli. Routing of meltwater from the laurentide ice sheet during the younger dryas cold episode. *Nature*, 341(6240):318321, Sep 1989. ISSN 1476-4687. doi: 10.1038/341318a0. URL http://dx.doi.org/10.1038/341318a0.

Wallace S. Broecker, Gerard Bond, Millie Klas, Georges Bonani, and Willy Wolfli. A salt oscillator in the glacial atlantic? 1. the concept. *Paleoceanography*, 5(4):469477, Aug 1990. ISSN 0883-8305. doi: 10.1029/pa005i004p00469. URL http://dx.doi.org/10.1029/PA005i004p00469.

Wallace S. Broecker, George H. Denton, R. Lawrence Edwards, Hai Cheng, Richard B. Alley, and Aaron E. Putnam. Putting the younger dryas cold event into context. *Quaternary Science Reviews*, 29(9-10):10781081, May 2010. ISSN 0277-3791. doi: 10.1016/j.quascirev.2010.02.019. URL http://dx.doi.org/10.1016/j.quascirev.2010.02.019.

Nicolas Brown and Eric D. Galbraith. Hosed vs. unhosed: interruptions of the Atlantic Meridional Overturning Circulation in a global coupled model, with and without freshwater forcing. *Climate of the Past*, 12:1663–1679, 2016. doi: 10.5194/cp-12-1663-2016.

Frank Bryan. High-latitude salinity effects and interhemispheric thermohaline circulations. *Nature*, 323(6086):301304, Sep 1986. ISSN 1476-4687. doi: 10.1038/323301a0. URL http://dx.doi.org/10.1038/323301a0.

S. J. Burns. Indian ocean climate and an absolute chronology over dansgaard/oeschger events 9 to 13. *Science*, 301(5638):13651367, Sep 2003. ISSN 1095-9203. doi: 10.1126/science.1086227. URL http://dx.doi.org/10.1126/science.1086227.

L. Caesar, S. Rahmstorf, A. Robinson, G. Feulner, and V. Saba. Observed fingerprint of a weakening atlantic ocean overturning circulation. *Nature*, 556(7700):191196, Apr 2018. ISSN 1476-4687. doi: 10.1038/s41586-018-0006-5. URL http://dx.doi.org/10.1038/s41586-018-0006-5.

L. Caesar, G. D. McCarthy, D. J. R. Thornalley, N. Cahill, and S. Rahmstorf. Current atlantic meridional overturning circulation weakest in last millennium. *Nature Geoscience*, Feb 2021. ISSN 1752-0908. doi: 10.1038/s41561-021-00699-z. URL http://dx.doi.org/10.1038/s41561-021-00699-z.

Anders E. Carlson, Lev Tarasov, and Tamara Pico. Rapid laurentide ice-sheet advance towards southern last glacial maximum limit during marine isotope stage 3. *Quaternary Science Reviews*, 196:118123, Sep 2018. ISSN 0277-3791. doi: 10.1016/j.quascirev.2018.07.039. URL http://dx.doi.org/10.1016/j.quascirev.2018.07.039.

Dudley Chelton and Shang-Ping Xie. Coupled ocean-atmosphere interaction at oceanic mesoscales. *Oceanography*, 23(4):5269, Dec 2010. ISSN 1042-8275. doi: 10.5670/oceanog.2010.05. URL http://dx.doi.org/10.5670/oceanog.2010.05.

Dudley B. Chelton, Roland A. deSzoeke, Michael G. Schlax, Karim El Naggar, and Nicolas Siwertz. Geographical variability of the first baroclinic rossby radius of deformation. *Journal of Physical Oceanography*, 28(3):433460, Mar 1998. ISSN 1520-0485. doi: 10.1175/1520-0485(1998)028⟨0433:gvotfb⟩2.0.co;2. URL http://dx.doi.org/10.1175/1520-0485(1998)028<0433:GVOTFB>2.0.CO;2.

John A Church, Peter U Clark, Anny Cazenave, Jonathan M Gregory, Svetlana Jevrejeva, Anders Levermann, Mark A Merrifield, Glenn A Milne, R Steven Nerem, Patrick D Nunn, et al. Sea level change. In *Climate Change 2013-The Physical Science Basis: Contribution of Working Group I to the Fifth Assessment Report of the Intergovernmental Panel on Climate Change*, pages 1136–1216. Cambridge University Press, 2013.

Matthew Collins, Reto Knutti, Julie Arblaster, Jean-Louis Dufresne, Thierry Fichefet, Pierre Friedlingstein, Xuejie Gao, William J Gutowski, Tim Johns, Gerhard Krinner, et al. Long-term climate change: projections, commitments and irreversibility. In *Climate Change 2013-The Physical Science Basis: Contribution of Working Group I to the Fifth Assessment Report of the Intergovernmental Panel on Climate Change*, pages 1029–1136. Cambridge University Press, 2013.

A. Condron and P. Winsor. Meltwater routing and the younger dryas. *Proceedings of the National Academy of Sciences*, 109(49):1992819933, Nov 2012. ISSN 1091-6490. doi: 10.1073/pnas.1207381109. URL http://dx.doi.org/10.1073/pnas.1207381109.

Alan Condron and Jenna C. Hill. Timing of iceberg scours and massive ice-rafting events in the subtropical north atlantic. *Nature Communications*, 12(1), Jun 2021. ISSN 2041-1723. doi: 10.1038/s41467-021-23924-0. URL http://dx.doi.org/10.1038/s41467-021-23924-0.

Ellen C. Corrick, Russell N. Drysdale, John C. Hellstrom, Emilie Capron, Sune Olander Rasmussen, Xu Zhang, Dominik Fleitmann, Isabelle Couchoud, and Eric Wolff. Synchronous timing of abrupt climate changes during the last glacial period. *Science*, 369(6506):963969, Aug 2020. ISSN 1095-9203. doi: 10.1126/science.aay5538. URL http://dx.doi.org/10.1126/science.aay5538.

Kurt M. Cuffey and Eric J. Steig. Isotopic diffusion in polar firn: implications for interpretation of seasonal climate parameters in ice-core records, with emphasis on central greenland. *Journal of Glaciology*, 44(147):273284, 1998. ISSN 1727-5652. doi: 10.3189/s0022143000002616. URL http://dx.doi.org/10.3189/S0022143000002616.

W. Dansgaard, S.J. Johnsen, H.B. Clausen, D. Dahl-Jensen, N. Gundestrup, C.U. Hammer, and H. Oeschger. North atlantic climatic oscillations revealed by deep greenland ice cores. *Geophysical*

Monograph Series, page 288298, 1984. ISSN 0065-8448. doi: 10.1029/gm029p0288. URL http://dx.doi.org/10.1029/GM029p0288.

W. Dansgaard, S. J. Johnsen, H. B. Clausen, D. Dahl-Jensen, N. S. Gundestrup, C. U. Hammer, C. S. Hvidberg, J. P. Steffensen, A. E. Sveinbjrnsdottir, J. Jouzel, and et al. Evidence for general instability of past climate from a 250-kyr ice-core record. *Nature*, 364(6434):218220, Jul 1993. ISSN 1476-4687. doi: 10.1038/364218a0. URL http://dx.doi.org/10.1038/364218a0.

Will Dansgaard, Sigfus J Johnsen, Jesper Møller, and Chester C Langway. One thousand centuries of climatic record from camp century on the greenland ice sheet. *Science*, 166(3903):377–380, 1969.

Willi Dansgaard, HB Clausen, N Gundestrup, CU Hammer, SF Johnsen, PM Kristinsdottir, and Niels Reeh. A new greenland deep ice core. *Science*, 218(4579):1273–1277, 1982.

Robert M. DeConto and David Pollard. Contribution of antarctica to past and future sea-level rise. *Nature*, 531(7596):591597, Mar 2016. ISSN 1476-4687. doi: 10.1038/nature17145. URL http://dx.doi.org/10.1038/nature17145.

Gilles Delaygue. *Oxygen Isotopes*, pages 666–673. Springer Netherlands, Dordrecht, 2009. ISBN 978-1-4020-4411-3. doi: 10.1007/978-1-4020-4411-3_163. URL https://doi.org/10.1007/978-1-4020-4411-3_163.

Pierre Deschamps, Nicolas Durand, Edouard Bard, Bruno Hamelin, Gilbert Camoin, Alexander L. Thomas, Gideon M. Henderson, Jun'ichi Okuno, and Yusuke Yokoyama. Ice-sheet collapse and sea-level rise at the boelling warming 14,600 years ago. *Nature*, 483(7391):559–564, Mar 2012. ISSN 1476-4687. doi: 10.1038/nature10902. URL http://dx.doi.org/10.1038/nature10902.

Brendan T Doherty and Dana R Kester. *Freezing point of seawater*. Sears Foundation for Marine Research, 1974.

Trond M. Dokken, Kerim H. Nisancioglu, Camille Li, David S. Battisti, and Catherine Kissel. Dansgaard-oeschger cycles: Interactions between ocean and sea ice intrinsic to the nordic seas. *Paleoceanography*, 28(3):491502, Sep 2013. ISSN 0883-8305. doi: 10.1002/palo.20042. URL http://dx.doi.org/10.1002/palo.20042.

Mark B Dyurgerov, Mark F Meier, et al. *Glaciers and the changing Earth system: a 2004 snapshot*, volume 58. 2005.

John H. England and Mark F.A. Furze. New evidence from the western canadian arctic archipelago for the resubmergence of bering strait. *Quaternary Research*, 70(1):6067, Jul 2008. ISSN 1096-0287. doi: 10.1016/j.yqres.2008.03.001. URL http://dx.doi.org/10.1016/j.yqres.2008.03.001.

M. Etminan, G. Myhre, E. J. Highwood, and K. P. Shine. Radiative forcing of carbon dioxide, methane, and nitrous oxide: A significant revision of the methane radiative forcing. *Geophysical Research Letters*, 43(24), Dec 2016. ISSN 1944-8007. doi: 10.1002/2016gl071930. URL http://dx.doi.org/10.1002/2016GL071930.

Richard G. Fairbanks. A 17,000-year glacio-eustatic sea level record: influence of glacial melting rates on the younger dryas event and deep-ocean circulation. *Nature*, 342(6250):637642, Dec 1989. ISSN 1476-4687. doi: 10.1038/342637a0. URL http://dx.doi.org/10.1038/342637a0.

Cdric G. Fichot, Karl Kaiser, Stanford B. Hooker, Rainer M. W. Amon, Marcel Babin, Simon Blanger, Sally A. Walker, and Ronald Benner. Pan-arctic distributions of continental runoff in the arctic ocean. *Scientific Reports*, 3(1), Jan 2013. ISSN 2045-2322. doi: 10.1038/srep01053. URL http://dx.doi.org/10.1038/srep01053.

M.-. Gagn, M. C. Kirchmeier-Young, N. P. Gillett, and J. C. Fyfe. Arctic sea ice response to the eruptions of agung, el chichn, and pinatubo. *Journal of Geophysical Research: Atmospheres*, 122 (15):80718078, Aug 2017. ISSN 2169-897X. doi: 10.1002/2017jd027038. URL http://dx.doi.org/10.1002/2017JD027038.

Andrey Ganopolski and Stefan Rahmstorf. Rapid changes of glacial climate simulated in a coupled climate model. *Nature*, 409(6817):153158, Jan 2001. ISSN 0028-0836. doi: 10.1038/35051500. URL http://dx.doi.org/10.1038/35051500.

Peter R. Gent and James C. Mcwilliams. Isopycnal mixing in ocean circulation models. *Journal of Physical Oceanography*, 20(1):150155, Jan 1990. ISSN 1520-0485. doi: 10.1175/1520-0485(1990) 020⟨0150:imiocm⟩2.0.co;2. URL http://dx.doi.org/10.1175/1520-0485(1990)020<0150:IMIOCM>2.0.CO;2.

D. Genty, D. Blamart, R. Ouahdi, M. Gilmour, A. Baker, J. Jouzel, and Sandra Van-Exter. Precise dating of dansgaardoeschger climate oscillations in western europe from stalagmite data. *Nature*, 421(6925):833837, Feb 2003. ISSN 0028-0836. doi: 10.1038/nature01391. URL http://dx.doi.org/10.1038/nature01391.

Hezi Gildor and Eli Tziperman. Sea-ice switches and abrupt climate change. *Philosophical Transactions of the Royal Society of London A: Mathematical, Physical and Engineering Sciences*, 361 (1810):1935–1944, 2003. ISSN 1364-503X. doi: 10.1098/rsta.2003.1244.

Xun Gong, Gregor Knorr, Gerrit Lohmann, and Xu Zhang. Dependence of abrupt atlantic meridional ocean circulation changes on climate background states. *Geophysical Research Letters*, 40(14):36983704, Jul 2013. ISSN 0094-8276. doi: 10.1002/grl.50701. URL http://dx.doi.org/10.1002/grl.50701.

Xun Gong, Xiangdong Zhang, Gerrit Lohmann, Wei Wei, Xu Zhang, and Madlene Pfeiffer. Higher laurentide and greenland ice sheets strengthen the north atlantic ocean circulation. *Climate Dynamics*, 45(1-2):139150, Feb 2015. ISSN 1432-0894. doi: 10.1007/s00382-015-2502-8. URL http://dx.doi.org/10.1007/s00382-015-2502-8.

Vivien Gornitz. *Encyclopedia of paleoclimatology and ancient environments*. Springer Science & Business Media, 2008.

Lauren J. Gregoire, Bette Otto-Bliesner, Paul J. Valdes, and Ruza Ivanovic. Abrupt boelling warming and ice saddle collapse contributions to the meltwater pulse 1a rapid sea level rise. *Geophysical Research Letters*, 43(17):9130–9137, Sep 2016. ISSN 0094-8276. doi: 10.1002/2016gl070356. URL http://dx.doi.org/10.1002/2016GL070356.

PM Grootes and M Stuiver. Oxygen 18/16 variability in greenland snow and ice with 10- 3-to 105-year time resolution. *Journal of Geophysical Research: Oceans*, 102(C12):26455–26470, 1997.

PM Grootes, Minze Stuiver, JWC White, S Johnsen, and J Jouzel. Comparison of oxygen isotope records from the gisp2 and grip greenland ice cores. 1993.

Oliver Gutjahr, Nils Brggemann, Helmuth Haak, Johann H. Jungclaus, Dian A. Putrasahan, Katja Lohmann, and Jin-Song von Storch. Comparison of ocean vertical mixing schemes in the max planck institute earth system model (mpi-esm1.2). *Geoscientific Model Development*, 14(5): 23172349, May 2021. ISSN 1991-9603. doi: 10.5194/gmd-14-2317-2021. URL http://dx.doi.org/10.5194/gmd-14-2317-2021.

T. Hanebuth. Rapid flooding of the sunda shelf: A late-glacial sea-level record. *Science*, 288 (5468):10331035, May 2000. ISSN 1095-9203. doi: 10.1126/science.288.5468.1033. URL http://dx.doi.org/10.1126/science.288.5468.1033.

Feng He. *Simulating transient climate evolution of the last deglaciation with CCSM 3*, volume 72. 2011.

W. D. Hibler. A dynamic thermodynamic sea ice model. *Journal of Physical Oceanography*, 9(4): 815846, Jul 1979. ISSN 1520-0485. doi: 10.1175/1520-0485(1979)009⟨0815:adtsim⟩2.0.co;2. URL http://dx.doi.org/10.1175/1520-0485(1979)009<0815:ADTSIM>2.0.CO;2.

Jenna C. Hill and Alan Condron. Subtropical iceberg scours and meltwater routing in the deglacial western north atlantic. *Nature Geoscience*, 7(11):806810, Oct 2014. ISSN 1752-0908. doi: 10.1038/ngeo2267. URL http://dx.doi.org/10.1038/ngeo2267.

Linda A Hinnov, Michael Schulz, and Pascal Yiou. Interhemispheric spacetime attributes of the dansgaardoeschger oscillations between 100 and 0ka. *Quaternary Science Reviews*, 21 (10):12131228, May 2002. ISSN 0277-3791. doi: 10.1016/s0277-3791(01)00140-8. URL http://dx.doi.org/10.1016/S0277-3791(01)00140-8.

Jol J.M. Hirschi, Bernard Barnier, Claus Bning, Arne Biastoch, Adam T. Blaker, Andrew Coward, Sergey Danilov, Sybren Drijfhout, Klaus Getzlaff, Stephen M. Griffies, and et al. The atlantic meridional overturning circulation in high-resolution models. *Journal of Geophysical Research: Oceans*, 125(4), Apr 2020. ISSN 2169-9291. doi: 10.1029/2019jc015522. URL http://dx.doi.org/10.1029/2019JC015522.

Jeremy S. Hoffman, Anders E. Carlson, Kelsey Winsor, Gary P. Klinkhammer, Allegra N. LeGrande, John T. Andrews, and Jeffrey C. Strasser. Linking the 8.2 ka event and its freshwater forcing in the labrador sea. *Geophysical Research Letters*, 39(18), Sep 2012. ISSN 0094-8276. doi: 10.1029/2012gl053047. URL http://dx.doi.org/10.1029/2012GL053047.

A. Hu, G. A. Meehl, W. Han, A. Timmermann, B. Otto-Bliesner, Z. Liu, W. M. Washington, W. Large, A. Abe-Ouchi, M. Kimoto, and et al. Role of the bering strait on the hysteresis of the ocean conveyor belt circulation and glacial climate stability. *Proceedings of the National Academy of Sciences*, 109(17):64176422, Apr 2012. ISSN 1091-6490. doi: 10.1073/pnas.1116014109. URL http://dx.doi.org/10.1073/pnas.1116014109.

Aixue Hu, Gerald A. Meehl, and Weiqing Han. Role of the bering strait in the thermohaline circulation and abrupt climate change. *Geophysical Research Letters*, 34(5), Mar 2007. ISSN 0094-8276. doi: 10.1029/2006gl028906. URL http://dx.doi.org/10.1029/2006GL028906.

Aixue Hu, Gerald A. Meehl, Weiqing Han, Bette Otto-Bliestner, Ayako Abe-Ouchi, and Nan Rosenbloom. Effects of the bering strait closure on amoc and global climate under different background climates. *Progress in Oceanography*, 132:174196, Mar 2015. ISSN 0079-6611. doi: 10.1016/j.pocean.2014.02.004. URL http://dx.doi.org/10.1016/j.pocean.2014.02.004.

Yi Huang, Xiaoxiao Tan, and Yan Xia. Inhomogeneous radiative forcing of homogeneous greenhouse gases. *Journal of Geophysical Research: Atmospheres*, 121(6):27802789, Mar 2016. ISSN 2169-897X. doi: 10.1002/2015jd024569. URL http://dx.doi.org/10.1002/2015JD024569.

René FB Isarin, Hans Renssen, and Jef Vandenberghe. The impact of the north atlantic ocean on the younger dryas climate in northwestern and central europe. *Journal of Quaternary Science*, 13(5):447–453, 1998.

L. C. Jackson and R. A. Wood. Hysteresis and resilience of the amoc in an eddy-permitting gcm. *Geophysical Research Letters*, 45(16):85478556, Aug 2018. ISSN 1944-8007. doi: 10.1029/2018gl078104. URL http://dx.doi.org/10.1029/2018GL078104.

Martin Jakobsson, Christof Pearce, Thomas M. Cronin, Jan Backman, Leif G. Anderson, Natalia Barrientos, Göran Björk, Helen Coxall, Agatha de Boer, Larry A. Mayer, and et al. Post-glacial flooding of the bering land bridge dated to 11 cal ka bp based on new geophysical and sediment records. *Climate of the Past*, 13(8):991–1005, Aug 2017. ISSN 1814-9332. doi: 10.5194/cp-13-991-2017. URL http://dx.doi.org/10.5194/cp-13-991-2017.

Mari F. Jensen, Kerim H. Nisancioglu, and Michael A. Spall. Large changes in sea ice triggered by small changes in atlantic water temperature. *Journal of Climate*, 31(12):48474863, Jun 2018. ISSN 1520-0442. doi: 10.1175/jcli-d-17-0802.1. URL http://dx.doi.org/10.1175/JCLI-D-17-0802.1.

Knud Jessen. *Archaeological dating in the history of North Jutland's vegetation*. Munksgaard, 1935.

J Jouzel, C Genthon, C Lorius, JR Petit, and NI Barkov. Vostok ice core-a continuous isotope temperature record over the last climatic cycle (160,000 years). *Nature*, 329:403–408, 1987.

J. H. Jungclaus, N. Keenlyside, M. Botzet, H. Haak, J.-J. Luo, M. Latif, J. Marotzke, U. Mikolajewicz, and E. Roeckner. Ocean circulation and tropical variability in the coupled model echam5/mpi-om. *Journal of Climate*, 19(16):39523972, Aug 2006. ISSN 1520-0442. doi: 10.1175/jcli3827.1. URL http://dx.doi.org/10.1175/JCLI3827.1.

J. H. Jungclaus, N. Fischer, H. Haak, K. Lohmann, J. Marotzke, D. Matei, U. Mikolajewicz, D. Notz, and J. S. Storch. Characteristics of the ocean simulations in the max planck institute ocean model (mpiom) the ocean component of the mpi-earth system model. *Journal of Advances in Modeling Earth Systems*, 5(2):422–446, Jun 2013. ISSN 1942-2466. doi: 10.1002/jame.20023. URL http://dx.doi.org/10.1002/jame.20023.

M. Kageyama, U. Merkel, B. Otto-Bliesner, M. Prange, A. Abe-Ouchi, G. Lohmann, R. Ohgaito, D. M. Roche, J. Singarayer, D. Swingedouw, and et al. Climatic impacts of fresh water hosing under last glacial maximum conditions: a multi-model study. *Climate of the Past*, 9(2):935953, Apr 2013. ISSN 1814-9332. doi: 10.5194/cp-9-935-2013. URL http://dx.doi.org/10.5194/cp-9-935-2013.

Masa Kageyama, Sandy P. Harrison, Marie-L. Kapsch, Marcus Lofverstrom, Juan M. Lora, Uwe Mikolajewicz, Sam Sherriff-Tadano, Tristan Vadsaria, Ayako Abe-Ouchi, Nathaelle Bouttes, and et al. The pmip4 last glacial maximum experiments: preliminary results and comparison with the pmip3 simulations. *Climate of the Past*, 17(3):10651089, May 2021. ISSN 1814-9332. doi: 10.5194/cp-17-1065-2021. URL http://dx.doi.org/10.5194/cp-17-1065-2021.

Per Kållberg, Adrian Simmons, Sakari Uppala, and Manuel Fuentes. The era-40 archive. *ERA-40 project report series*, 17:31, 2004.

Mehdi Pasha Karami, Paul G. Myers, Anne de Vernal, L. Bruno Tremblay, and Xianmin Hu. The role of arctic gateways on sea ice and circulation in the arctic and north atlantic oceans: a sensitivity study with an ocean-sea-ice model. *Climate Dynamics*, May 2021. ISSN 1432-0894. doi: 10.1007/s00382-021-05798-6. URL http://dx.doi.org/10.1007/s00382-021-05798-6.

Ralph F Keeling and Charles D. Keeling. Atmospheric monthly in situ co2 data - mauna loa observatory, hawaii. in scripps co2 program data, 2017. URL https://library.ucsd.edu/dc/object/bb3859642r.

L. D. Keigwin, S. Klotsko, N. Zhao, B. Reilly, L. Giosan, and N. W. Driscoll. Deglacial floods in the Beaufort Sea preceded Younger Dryas cooling. *Nature Geoscience*, 11:599–604, 2018. doi: 10.1038/s41561-018-0169-6.

P. Kindler, M. Guillevic, M. Baumgartner, J. Schwander, A. Landais, and M. Leuenberger. Temperature reconstruction from 10 to 120 kyr b2k from the ngrip ice core. *Climate of the Past*, 10(2):887902, Apr 2014. ISSN 1814-9332. doi: 10.5194/cp-10-887-2014. URL http://dx.doi.org/10.5194/cp-10-887-2014.

Hannah Kleppin, Markus Jochum, Bette Otto-Bliesner, Christine A. Shields, and Stephen Yeager. Stochastic atmospheric forcing as a cause of Greenland climate transitions. *Journal of Climate*, 28:7741–7764, 2015. doi: 10.1175/JCLI-D-14-00728.1.

M. Klockmann, U. Mikolajewicz, H. Kleppin, and J. Marotzke. Coupling of the subpolar gyre and the overturning circulation during abrupt glacial climate transitions. *Geophysical Research Letters*, 47(21), Nov 2020. ISSN 1944-8007. doi: 10.1029/2020gl090361. URL http://dx.doi.org/10.1029/2020GL090361.

Marlene Klockmann, Uwe Mikolajewicz, and Jochem Marotzke. Two AMOC states in response to decreasing greenhouse gas concentrations in the coupled climate model MPI-ESM. *Journal of Climate*, 31:7969–7985, 2018. doi: 10.1175/JCLI-D-17-0859.1.

Takuro Kobashi, Kenji Kawamura, Jeffrey P. Severinghaus, Jean-Marc Barnola, Toshiyuki Nakaegawa, Bo M. Vinther, Sigfs J. Johnsen, and Jason E. Box. High variability of greenland surface temperature over the past 4000 years estimated from trapped air in an ice core. *Geophysical Research Letters*, 38(21):n/an/a, Nov 2011. ISSN 0094-8276. doi: 10.1029/2011gl049444. URL http://dx.doi.org/10.1029/2011GL049444.

Nikolay V. Koldunov, Detlef Stammer, and Jochem Marotzke. Present-day arctic sea ice variability in the coupled echam5/mpi-om model. *Journal of Climate*, 23(10):25202543, May 2010. ISSN 0894-8755. doi: 10.1175/2009jcli3065.1. URL http://dx.doi.org/10.1175/2009JCLI3065.1.

K. Lambeck. Sea level change through the last glacial cycle. *Science*, 292(5517):679686, Apr 2001. ISSN 1095-9203. doi: 10.1126/science.1059549. URL http://dx.doi.org/10.1126/science.1059549.

Lamy, Klump, Hebbeln, and Wefer. Late quaternary rapid climate change in northern chile. *Terra Nova*, 12(1):813, Feb 2000. ISSN 1365-3121. doi: 10.1046/j.1365-3121.2000.00265.x. URL http://dx.doi.org/10.1046/j.1365-3121.2000.00265.x.

Chester C. Langway. The history of early polar ice cores. *Cold Regions Science and Technology*, 52(2):101117, Apr 2008. ISSN 0165-232X. doi: 10.1016/j.coldregions.2008.01.001. URL http://dx.doi.org/10.1016/j.coldregions.2008.01.001.

J. Laskar, P. Robutel, F. Joutel, M. Gastineau, A. C. M. Correia, and B. Levrard. A long-term numerical solution for the insolation quantities of the earth. *Astronomy & Astrophysics*, 428(1): 261–285, Nov 2004. ISSN 1432-0746. doi: 10.1051/0004-6361:20041335. URL http://dx.doi.org/10.1051/0004-6361:20041335.

J. Laskar, A. Fienga, M. Gastineau, and H. Manche. La2010: a new orbital solution for the long-term motion of the earth. *Astronomy & Astrophysics*, 532:A89, Jul 2011. ISSN 1432-0746. doi: 10.1051/0004-6361/201116836. URL http://dx.doi.org/10.1051/0004-6361/201116836.

Mathieu Le Corre, Jonathan Gula, and Anne-Marie Trguier. Barotropic vorticity balance of the north atlantic subpolar gyre in an eddy-resolving model. *Ocean Science*, 16(2):451468, Apr

2020. ISSN 1812-0792. doi: 10.5194/os-16-451-2020. URL http://dx.doi.org/10.5194/os-16-451-2020.

Camille Li and David S. Battisti. Reduced atlantic storminess during last glacial maximum: Evidence from a coupled climate model. *Journal of Climate*, 21(14):35613579, Jul 2008. ISSN 0894-8755. doi: 10.1175/2007jcli2166.1. URL http://dx.doi.org/10.1175/2007JCLI2166.1.

Yucheng Lin, Fiona D. Hibbert, Pippa L. Whitehouse, Sarah A. Woodroffe, Anthony Purcell, Ian Shennan, and Sarah L. Bradley. A reconciled solution of meltwater pulse 1a sources using sea-level fingerprinting. *Nature Communications*, 12(1), Apr 2021. ISSN 2041-1723. doi: 10.1038/s41467-021-21990-y. URL http://dx.doi.org/10.1038/s41467-021-21990-y.

Lorraine E. Lisiecki and Maureen E. Raymo. A pliocene-pleistocene stack of 57 globally distributed benthic δ18o records. *Paleoceanography*, 20(1):n/an/a, Jan 2005. ISSN 0883-8305. doi: 10.1029/2004pa001071. URL http://dx.doi.org/10.1029/2004PA001071.

Jean Liu, Glenn A. Milne, Robert E. Kopp, Peter U. Clark, and Ian Shennan. Sea-level constraints on the amplitude and source distribution of meltwater pulse 1a. *Nature Geoscience*, 9 (2):130134, Dec 2015. ISSN 1752-0908. doi: 10.1038/ngeo2616. URL http://dx.doi.org/10.1038/NGEO2616.

Yonggang Liu, Robert Hallberg, Olga Sergienko, Bonnie L. Samuels, Matthew Harrison, and Michael Oppenheimer. Climate response to the meltwater runoff from greenland ice sheet: evolving sensitivity to discharging locations. *Climate Dynamics*, 51(5-6):17331751, Nov 2017. ISSN 1432-0894. doi: 10.1007/s00382-017-3980-7. URL http://dx.doi.org/10.1007/s00382-017-3980-7.

Z. Liu, B. L. Otto-Bliesner, F. He, E. C. Brady, R. Tomas, P. U. Clark, A. E. Carlson, J. Lynch-Stieglitz, W. Curry, E. Brook, and et al. Transient simulation of last deglaciation with a new mechanism for bolling-allerod warming. *Science*, 325(5938):310314, Jul 2009. ISSN 1095-9203. doi: 10.1126/science.1171041. URL http://dx.doi.org/10.1126/science.1171041.

M. Löfverström, R. Caballero, J. Nilsson, and J. Kleman. Evolution of the large-scale atmospheric circulation in response to changing ice sheets over the last glacial cycle. *Climate of the Past*, 10 (4):14531471, Jul 2014. ISSN 1814-9332. doi: 10.5194/cp-10-1453-2014. URL http://dx.doi.org/10.5194/cp-10-1453-2014.

Marcus Löfverström and Juan M. Lora. Abrupt regime shifts in the north atlantic atmospheric circulation over the last deglaciation. *Geophysical Research Letters*, 44(15):80478055, Aug 2017. ISSN 0094-8276. doi: 10.1002/2017gl074274. URL http://dx.doi.org/10.1002/2017GL074274.

Gerrit Lohmann, Xu Zhang, and Gregor Knorr. Abrupt climate change experiments: the role of freshwater, ice sheets and deglacial warming for the atlantic meridional overturning circulation. *Polarforschung*, 85(2):161–170, 2016.

Gerrit Lohmann, Martin Butzin, Nina Eissner, Xiaoxu Shi, and Christian Stepanek. Abrupt climate and weather changes across time scales. *Paleoceanography and Paleoclimatology*, 35(9), Sep 2020. ISSN 2572-4525. doi: 10.1029/2019pa003782. URL http://dx.doi.org/10.1029/2019PA003782.

Johannes Lohmann and Peter D. Ditlevsen. Random and externally controlled occurrences of dansgaardoeschger events. *Climate of the Past*, 14(5):609617, May 2018. ISSN 1814-9332. doi: 10.5194/cp-14-609-2018. URL http://dx.doi.org/10.5194/cp-14-609-2018.

Laetitia Loulergue, Adrian Schilt, Renato Spahni, Valérie Masson-Delmotte, Thomas Blunier, Bénédicte Lemieux, Jean-Marc Barnola, Dominique Raynaud, Thomas F. Stocker, and Jérôme Chappellaz. Orbital and millennial-scale features of atmospheric ch4 over the past 800,000 years. *Nature*, 453(7193):383–386, May 2008. ISSN 1476-4687. doi: 10.1038/nature06950. URL http://dx.doi.org/10.1038/nature06950.

R. Love, H. Andres, A. Condron, and L. Tarasov. Eddy permitting simulations of freshwater injection from major northern hemisphere outlets during the last deglacial. *Climate of the Past Discussions*, 2021:1–16, 2021a. doi: 10.5194/cp-2021-15. URL https://cp.copernicus.org/preprints/cp-2021-15/.

R. Love, H. Andres, X. Zhang, A. Condron, G. Lohmann, and L. Tarasov. Exploring the climate system response to a range of freshwater representations: Hosing, regional, and freshwater fingerprints. *Manuscript Draft*, 2021b.

Ryan Love, Glenn A. Milne, Lev Tarasov, Simon E. Engelhart, Marc P. Hijma, Konstantin Latychev, Benjamin P. Horton, and Torbjrn E. Trnqvist. The contribution of glacial isostatic adjustment to projections of sealevel change along the atlantic and gulf coasts of north america. *Earths Future*, 4(10):440464, Oct 2016. ISSN 2328-4277. doi: 10.1002/2016ef000363. URL http://dx.doi.org/10.1002/2016EF000363.

Syukuro Manabe and Ronald Stouffer. The rle of thermohaline circulation in climate. *Tellus B*, 51(1), 1999. ISSN 1600-0889. URL http://www.tellusb.net/index.php/tellusb/article/view/16262.

Syukuro Manabe and Ronald J. Stouffer. Simulation of abrupt climate change induced by freshwater input to the north atlantic ocean. *Nature*, 378(6553):165167, Nov 1995. ISSN 1476-4687. doi: 10.1038/378165a0. URL http://dx.doi.org/10.1038/378165a0.

Syukuro Manabe and Ronald J. Stouffer. Coupled ocean-atmosphere model response to freshwater input: Comparison to younger dryas event. *Paleoceanography*, 12(2):321336, Apr 1997. ISSN 0883-8305. doi: 10.1029/96pa03932. URL http://dx.doi.org/10.1029/96PA03932.

Syukuro Manabe and Ronald J Stouffer. Study of abrupt climate change by a coupled oceanatmosphere model. *Quaternary Science Reviews*, 19(15):285 – 299, 2000. ISSN 0277-3791. doi: http://dx.doi.org/10.1016/S0277-3791(99)00066-9. URL http://www.sciencedirect.com/science/article/pii/S0277379199000669.

JAN Mangerud, Svend T Andersen, BJÖRN E BERGLUND, and Joakim J Donner. Quaternary stratigraphy of norden, a proposal for terminology and classification. *Boreas*, 3(3):109–126, 1974.

Jan Mangerud, Steinar Gulliksen, and Eiliv Larsen. 14c-dated fluctuations of the western flank of the scandinavian ice sheet 45-25 kyr bp compared with boelling-younger dryas fluctuations and dansgaard-oeschger events in greenland. *Boreas*, 39(2):328–342, Apr 2010. ISSN 1502-3885. doi: 10.1111/j.1502-3885.2009.00127.x. URL http://dx.doi.org/10.1111/j.1502-3885.2009.00127.x.

John Marshall, Alistair Adcroft, Chris Hill, Lev Perelman, and Curt Heisey. A finite-volume, incompressible navier stokes model for studies of the ocean on parallel computers. *Journal of Geophysical Research: Oceans*, 102(C3):57535766, Mar 1997. ISSN 0148-0227. doi: 10.1029/96jc02775. URL http://dx.doi.org/10.1029/96JC02775.

S.J. Marsland, H. Haak, J.H. Jungclaus, M. Latif, and F. Rske. The max-planck-institute global ocean/sea ice model with orthogonal curvilinear coordinates. *Ocean Modelling*, 5(2):91127, Jan

2003. ISSN 1463-5003. doi: 10.1016/s1463-5003(02)00015-x. URL http://dx.doi.org/10.1016/S1463-5003(02)00015-X.

J. F. McManus, R. Francois, J.-M. Gherardi, L. D. Keigwin, and S. Brown-Leger. Collapse and rapid resumption of atlantic meridional circulation linked to deglacial climate changes. *Nature*, 428(6985):834837, Apr 2004. ISSN 1476-4687. doi: 10.1038/nature02494. URL http://dx.doi.org/10.1038/nature02494.

DA Meese, RB Alley, T Gow, PM Grootes, P Mayewski, M Ram, K Taylor, E Waddington, and G Zielinski. Preliminary depth-age scale of the gisp2 ice core. *Special CRREL Report*, 94(1), 1994.

Dimitris Menemenlis, Jean-Michel Campin, Patrick Heimbach, Chris Hill, Tong Lee, An Nguyen, Michael Schodlok, and Hong Zhang. Ecco2: High resolution global ocean and sea ice data synthesis. *Mercator Ocean Quarterly Newsletter*, 31(October):13–21, 2008.

Glenn A. Milne and Jerry X. Mitrovica. Postglacial sea-level change on a rotating earth. *Geophysical Journal International*, 133(1):119, Apr 1998. ISSN 1365-246X. doi: 10.1046/j.1365-246x.1998.1331455.x. URL http://dx.doi.org/10.1046/j.1365-246X.1998.1331455.x.

Jerry X. Mitrovica and Glenn A. Milne. On post-glacial sea level: I. general theory. *Geophysical Journal International*, 154(2):253267, Aug 2003. ISSN 1365-246X. doi: 10.1046/j.1365-246x.2003.01942.x. URL http://dx.doi.org/10.1046/j.1365-246X.2003.01942.x.

Juan Muglia and Andreas Schmittner. Glacial atlantic overturning increased by wind stress in climate models. *Geophysical Research Letters*, 42(22):98629868, Nov 2015. ISSN 0094-8276. doi: 10.1002/2015gl064583. URL http://dx.doi.org/10.1002/2015GL064583.

Dirk Notz, F. Alexander Haumann, Helmuth Haak, Johann H. Jungclaus, and Jochem Marotzke. Arctic seaice evolution as modeled by max planck institute for meteorologys earth system model. *Journal of Advances in Modeling Earth Systems*, 5(2):173194, Apr 2013. ISSN 1942-2466. doi: 10.1002/jame.20016. URL http://dx.doi.org/10.1002/jame.20016.

A. J. G. Nurser and S. Bacon. The rossby radius in the arctic ocean. *Ocean Science*, 10(6):967975, Nov 2014. ISSN 1812-0792. doi: 10.5194/os-10-967-2014. URL http://dx.doi.org/10.5194/os-10-967-2014.

Elizabeth A. Obbink, Anders E. Carlson, and Gary P. Klinkhammer. Eastern north american freshwater discharge during the bølling-allerød warm periods. *Geology*, 38(2):171174, Feb 2010. ISSN 0091-7613. doi: 10.1130/g30389.1. URL http://dx.doi.org/10.1130/G30389.1.

Steffen Malskaer Olsen, Gary Shaffer, and Christian J. Bjerrum. Ocean oxygen isotope constraints on mechanisms for millennial-scale climate variability. *Paleoceanography*, 20(1):n/an/a, Feb 2005. ISSN 0883-8305. doi: 10.1029/2004pa001063. URL http://dx.doi.org/10.1029/2004PA001063.

Bette L. Otto-Bliesner and Esther C. Brady. The sensitivity of the climate response to the magnitude and location of freshwater forcing: last glacial maximum experiments. *Quaternary Science Reviews*, 29(1-2):5673, Jan 2010. ISSN 0277-3791. doi: 10.1016/j.quascirev.2009.07.004. URL http://dx.doi.org/10.1016/j.quascirev.2009.07.004.

R. C. Pacanowski and S. G. H. Philander. Parameterization of vertical mixing in numerical models of tropical oceans. *Journal of Physical Oceanography*, 11(11):14431451, Nov 1981. ISSN 1520-0485. doi: 10.1175/1520-0485(1981)011⟨1443:povmin⟩2.0.co;2. URL http://dx.doi.org/10.1175/1520-0485(1981)011<1443:POVMIN>2.0.CO;2.

Jeffrey D. Parsons, John W. M. Bush, and James P. M. Syvitski. Hyperpycnal plume formation from riverine outflows with small sediment concentrations. *Sedimentology*, 48(2):465478, Apr 2001. ISSN 1365-3091. doi: 10.1046/j.1365-3091.2001.00384.x. URL http://dx.doi.org/10.1046/j.1365-3091.2001.00384.x.

W. R. Peltier and G. Vettoretti. Dansgaard-Oeschger oscillations predicted in a comprehensive model of glacial climate: A "kicked" salt oscillator in the Atlantic. *Geophysical Research Letters*, 41:7306–7313, 2014. doi: 10.1002/2014GL061413.

W. R. Peltier, G. Vettoretti, and M. Stastna. Atlantic meridional overturning and climate response to arctic ocean freshening. *Geophysical Research Letters*, 33(6):n/a–n/a, 2006a. ISSN 1944-8007. doi: 10.1029/2005GL025251. URL http://dx.doi.org/10.1029/2005GL025251. L06713.

W. R. Peltier, G. Vettoretti, and M. Stastna. Atlantic meridional overturning and climate response to arctic ocean freshening. *Geophysical Research Letters*, 33(6):n/a–n/a, 2006b. ISSN 1944-8007. doi: 10.1029/2005GL025251. URL http://dx.doi.org/10.1029/2005GL025251. L06713.

Simon Pendleton, Alan Condron, and Jeffrey Donnelly. The potential of hudson valley glacial floods to drive abrupt climate change. *Communications Earth & Environment*, 2(1), Aug 2021. ISSN 2662-4435. doi: 10.1038/s43247-021-00228-1. URL http://dx.doi.org/10.1038/s43247-021-00228-1.

Stefan Rahmstorf. Ocean circulation and climate during the past 120,000 years. *Nature*, 419(6903): 207214, Sep 2002. ISSN 0028-0836. doi: 10.1038/nature01090. URL http://dx.doi.org/10.1038/nature01090.

S. O. Rasmussen, K. K. Andersen, A. M. Svensson, J. P. Steffensen, B. M. Vinther, H. B. Clausen, M.-L. Siggaard-Andersen, S. J. Johnsen, L. B. Larsen, D. Dahl-Jensen, and et al. A new greenland ice core chronology for the last glacial termination. *Journal of Geophysical Research*, 111(D6), 2006. ISSN 0148-0227. doi: 10.1029/2005jd006079. URL http://dx.doi.org/10.1029/2005JD006079.

Sune O. Rasmussen, Matthias Bigler, Simon P. Blockley, Thomas Blunier, Susanne L. Buchardt, Henrik B. Clausen, Ivana Cvijanovic, Dorthe Dahl-Jensen, Sigfus J. Johnsen, Hubertus Fischer, and et al. A stratigraphic framework for abrupt climatic changes during the last glacial period based on three synchronized greenland ice-core records: refining and extending the intimate event stratigraphy. *Quaternary Science Reviews*, 106:14–28, Dec 2014. ISSN 0277-3791. doi: 10.1016/j.quascirev.2014.09.007. URL http://dx.doi.org/10.1016/j.quascirev.2014.09.007.

Sune Olander Rasmussen, Inger Kathrine Seierstad, Katrine Krogh Andersen, Matthias Bigler, Dorthe Dahl-Jensen, and Sigfus Johann Johnsen. Synchronization of the NGRIP, GRIP, and GISP2 ice cores across MIS 2 and palaeoclimatic implications. *Quaternary Science Reviews*, 27 (1):18–28, 2008.

T. P. Rippeth, B. J. Lincoln, H. A. Kennedy, M. R. Palmer, J. Sharples, and C. A. J. Williams. Impact of vertical mixing on sea surfacepco2in temperate seasonally stratified shelf seas. *Journal of Geophysical Research: Oceans*, 119(6):38683882, Jun 2014. ISSN 2169-9275. doi: 10.1002/2014jc010089. URL http://dx.doi.org/10.1002/2014JC010089.

Didier M. Roche, Ane P. Wiersma, and Hans Renssen. A systematic study of the impact of freshwater pulses with respect to different geographical locations. *Climate Dynamics*, 34(7-8): 9971013, May 2009. ISSN 1432-0894. doi: 10.1007/s00382-009-0578-8. URL http://dx.doi.org/10.1007/s00382-009-0578-8.

William F. Ruddiman. Late quaternary deposition of ice-rafted sand in the subpolar north atlantic (lat 40 to 65n). *Geological Society of America Bulletin*, 88(12):1813, 1977. ISSN 0016-7606. doi: 10.1130/0016-7606(1977)88⟨1813:lqdois⟩2.0.co;2. URL http://dx.doi.org/10.1130/0016-7606(1977)88<1813:LQDOIS>2.0.CO;2.

Adrian Schilt, Matthias Baumgartner, Jakob Schwander, Daphn Buiron, Emilie Capron, Jrme Chappellaz, Laetitia Loulergue, Simon Schpbach, Renato Spahni, Hubertus Fischer, and et al. Atmospheric nitrous oxide during the last 140,000years. *Earth and Planetary Science Letters*, 300(1-2):3343, Nov 2010. ISSN 0012-821X. doi: 10.1016/j.epsl.2010.09.027. URL http://dx.doi.org/10.1016/j.epsl.2010.09.027.

Uwe Schulzweida. Cdo user guide, October 2019. URL https://doi.org/10.5281/zenodo.3539275.

Dan Seidov, Olga K. Baranova, Mathew Biddle, Timothy P. Boyer, Daphne R. Johnson, Alexey V. Mishonov, Christopher Paver, and Melissa Zweng. Greenland-Iceland-Norwegian Seas Regional Climatology (NCEI Accession 0112824). . 2016. doi: doi:10.7289/V5GT5K30.

Inger K. Seierstad, Peter M. Abbott, Matthias Bigler, Thomas Blunier, Anna J. Bourne, Edward Brook, Susanne L. Buchardt, Christo Buizert, Henrik B. Clausen, Eliza Cook, and et al. Consistently dated records from the greenland grip, gisp2 and ngrip ice cores for the past 104 ka reveal regional millennial-scale ?18o gradients with possible heinrich event imprint. *Quaternary Science Reviews*, 106:29–46, Dec 2014. ISSN 0277-3791. doi: 10.1016/j.quascirev.2014.10.032. URL http://dx.doi.org/10.1016/j.quascirev.2014.10.032.

Albert J. Semtner. A model for the thermodynamic growth of sea ice in numerical investigations of climate. *Journal of Physical Oceanography*, 6(3):379389, May 1976. ISSN 1520-0485. doi: 10.1175/1520-0485(1976)006⟨0379:amfttg⟩2.0.co;2. URL http://dx.doi.org/10.1175/1520-0485(1976)006<0379:AMFTTG>2.0.CO;2.

Gary Shaffer. Ocean subsurface warming as a mechanism for coupling dansgaard-oeschger climate cycles and ice-rafting events. *Geophysical Research Letters*, 31(24), 2004. ISSN 0094-8276. doi: 10.1029/2004gl020968. URL http://dx.doi.org/10.1029/2004GL020968.

Adriana Sima, Andr Paul, and Michael Schulz. The younger dryasan intrinsic feature of late pleistocene climate change at millennial timescales. *Earth and Planetary Science Letters*, 222 (3-4):741750, Jun 2004. ISSN 0012-821X. doi: 10.1016/j.epsl.2004.03.026. URL http://dx.doi.org/10.1016/j.epsl.2004.03.026.

Sharon B. Sneed, Paul A. Mayewski, W.G. Sayre, Michael J. Handley, Andrei V. Kurbatov, Kendrick C. Taylor, Pascal Bohleber, Dietmar Wagenbach, Tobias Erhardt, and Nicole E. Spaulding. New la-icp-ms cryocell and calibration technique for sub-millimeter analysis of ice cores. *Journal of Glaciology*, 61(226):233242, 2015. ISSN 1727-5652. doi: 10.3189/2015jog14j139. URL http://dx.doi.org/10.3189/2015JoG14J139.

Qingtao Song, Dudley B. Chelton, Steven K. Esbensen, Nicolai Thum, and Larry W. ONeill. Coupling between sea surface temperature and low-level winds in mesoscale numerical models. *Journal of Climate*, 22(1):146164, Jan 2009. ISSN 0894-8755. doi: 10.1175/2008jcli2488.1. URL http://dx.doi.org/10.1175/2008JCLI2488.1.

Eric J Steig, Pieter M Grootes, and Minze Stuiver. Seasonal precipitation timing and ice core records. *Science (Washington, DC);(United States)*, 266(5192), 1994.

Rüdiger Stein. The expedition ps115/2 of the research vessel polarstern to the arctic ocean in 2018. Technical report, 2019.

Thomas F. Stocker, Lawrence A. Mysak, and Daniel G. Wright. A zonally averaged, coupled ocean-atmosphere model for paleoclimate studies. *Journal of Climate*, 5(8):773797, Aug 1992. ISSN 1520-0442. doi: 10.1175/1520-0442(1992)005⟨0773:azacoa⟩2.0.co;2. URL http://dx.doi.org/10.1175/1520-0442(1992)005<0773:AZACOA>2.0.CO;2.

Henry Stommel. Thermohaline convection with two stable regimes of flow. *Tellus*, 13(2):224–230, 1961.

R. J. Stouffer, J. Yin, J. M. Gregory, K. W. Dixon, M. J. Spelman, W. Hurlin, A. J. Weaver, M. Eby, G. M. Flato, H. Hasumi, and et al. Investigating the causes of the response of the thermohaline circulation to past and future climate changes. *Journal of Climate*, 19(8):13651387, Apr 2006. ISSN 1520-0442. doi: 10.1175/jcli3689.1. URL http://dx.doi.org/10.1175/JCLI3689.1.

Minze Stuiver, Pieter M Grootes, and Thomas F Braziunas. The gisp2 δ 18 o climate record of the past 16,500 years and the role of the sun, ocean, and volcanoes. *Quaternary Research*, 44(3): 341–354, 1995.

Anders Svensson, Katrine K Andersen, Matthias Bigler, Henrik B Clausen, Dorthe Dahl-Jensen, Siwan M Davies, Sigfus J Johnsen, Raimund Muscheler, Sune O Rasmussen, Regine Röthlisberger, et al. The greenland ice core chronology 2005, 15–42ka. part 2: comparison to other records. *Quaternary Science Reviews*, 25(23):3258–3267, 2006.

Didier Swingedouw, Juliette Mignot, Pascale Braconnot, Eloi Mosquet, Masa Kageyama, and Ramdane Alkama. Impact of freshwater release in the north atlantic under different climate conditions in an oagcm. *Journal of Climate*, 22(23):63776403, Dec 2009. ISSN 0894-8755. doi: 10.1175/2009jcli3028.1. URL http://dx.doi.org/10.1175/2009JCLI3028.1.

O. Tange. GNU Parallel - The Command-Line Power Tool. *;login: The USENIX Magazine*, 36(1): 42–47, Feb 2011. URL http://www.gnu.org/s/parallel.

L Tarasov, A Hughes, R Gyllencreutz, OS Lohne, J Mangerud, and JI Svendsen. The global glac-1c deglaciation chronology, melwater pulse 1-a, and a question of missing ice. In *IGS Symposium: Contribution of Glaciers and Ice Sheets to Sea-Level Change, Chamonix, France*, pages 26–30, 2014a.

Lev Tarasov and W Richard Peltier. Greenland glacial history, borehole constraints, and eemian extent. *Journal of Geophysical Research: Solid Earth*, 108(B3), 2003.

Lev Tarasov and W.R. Peltier. Arctic freshwater forcing of the younger dryas cold reversal. *Nature*, 435(7042):662665, Jun 2005. ISSN 1476-4687. doi: 10.1038/nature03617. URL http://dx.doi.org/10.1038/nature03617.

Lev Tarasov and W.R. Peltier. A calibrated deglacial drainage chronology for the north american continent: evidence of an arctic trigger for the younger dryas. *Quaternary Science Reviews*, 25(7-8):659688, Apr 2006. ISSN 0277-3791. doi: 10.1016/j.quascirev.2005.12.006. URL http://dx.doi.org/10.1016/j.quascirev.2005.12.006.

Lev Tarasov, Arthur S. Dyke, Radford M. Neal, and W.R. Peltier. A data-calibrated distribution of deglacial chronologies for the north american ice complex from glaciological modeling. *Earth and Planetary Science Letters*, 315316:30 – 40, 2012a. ISSN 0012-821X. doi: http://dx.doi.org/10.1016/j.epsl.2011.09.010. URL http://www.sciencedirect.com/science/

article/pii/S0012821X11005243. Sea Level and Ice Sheet Evolution: A {PALSEA} Special Edition.

Lev Tarasov, Arthur S. Dyke, Radford M. Neal, and W.R. Peltier. A data-calibrated distribution of deglacial chronologies for the north american ice complex from glaciological modeling. *Earth and Planetary Science Letters*, 315316:30 – 40, 2012b. ISSN 0012-821X. doi: http://dx.doi.org/10.1016/j.epsl.2011.09.010. URL http://www.sciencedirect.com/science/article/pii/S0012821X11005243. Sea Level and Ice Sheet Evolution: A {PALSEA} Special Edition.

Lev Tarasov, Anna Hughes, Richard Gyllencreutz, Oystein Strand Lohne, Jan Mangerud, and John-Inge Svendsen. The global GLAC-1c deglaciation chronology, melwater pulse 1-a, and a question of missing ice. In *IGS Symposium on Contribution of Glaciers and Ice Sheets to Sea-Level Change*, IGS Symposium abstracts, 2014b.

J. T. Teller. Importance of freshwater injections into the arctic ocean in triggering the younger dryas cooling. *Proceedings of the National Academy of Sciences*, 109(49):1988019881, Nov 2012. ISSN 1091-6490. doi: 10.1073/pnas.1218344109. URL http://dx.doi.org/10.1073/pnas.1218344109.

James T Teller, David W Leverington, and Jason D Mann. Freshwater outbursts to the oceans from glacial lake agassiz and their role in climate change during the last deglaciation. *Quaternary Science Reviews*, 21(8-9):879–887, 2002.

S. Toucanne, S. Zaragosi, J.F. Bourillet, M. Cremer, F. Eynaud, B. Van Vliet-Lano, A. Penaud, C. Fontanier, J.L. Turon, and E. Cortijo. Timing of massive fleuve manche discharges over the last 350kyr: insights into the european ice-sheet oscillations and the european drainage network from mis 10 to 2. *Quaternary Science Reviews*, 28(13-14):12381256, Jun 2009. ISSN 0277-3791. doi: 10.1016/j.quascirev.2009.01.006. URL http://dx.doi.org/10.1016/j.quascirev.2009.01.006.

A. M. Treguier, S. Theetten, E. P. Chassignet, T. Penduff, R. Smith, L. Talley, J. O. Beismann, and C. Bning. The north atlantic subpolar gyre in four high-resolution models. *Journal of Physical Oceanography*, 35(5):757774, May 2005. ISSN 0022-3670. doi: 10.1175/jpo2720.1. URL http://dx.doi.org/10.1175/JPO2720.1.

D. J. Ullman, A. N. LeGrande, A. E. Carlson, F. S. Anslow, and J. M. Licciardi. Assessing the impact of laurentide ice sheet topography on glacial climate. *Climate of the Past*, 10(2):487507, Mar 2014. ISSN 1814-9332. doi: 10.5194/cp-10-487-2014. URL http://dx.doi.org/10.5194/cp-10-487-2014.

S. M. Uppala, P. W. KÅllberg, A. J. Simmons, U. Andrae, V. Da Costa Bechtold, M. Fiorino, J. K. Gibson, J. Haseler, A. Hernandez, G. A. Kelly, and et al. The era-40 re-analysis. *Quarterly Journal of the Royal Meteorological Society*, 131(612):29613012, Oct 2005. ISSN 1477-870X. doi: 10.1256/qj.04.176. URL http://dx.doi.org/10.1256/qj.04.176.

Michael Vellinga and Peili Wu. Low-latitude freshwater influence on centennial variability of the atlantic thermohaline circulation. *Journal of Climate*, 17(23):44984511, Dec 2004. ISSN 0894-8755. doi: 10.1175/3219.1. URL http://dx.doi.org/10.1175/3219.1.

Guido Vettoretti and W. Richard Peltier. Thermohaline instability and the formation of glacial North Atlantic super polynyas at the onset of Dansgaard-Oeschger warming events. *Geophysical Research Letters*, 43:5336–5344, 2016. doi: 10.1002/2016GL068891.

Guido Vettoretti and W. Richard Peltier. Fast physics and slow physics in the nonlinear Dansgaard-Oeschger relaxation oscillation. *Journal of Climate*, 31:3423–3450, 2018. doi: 10.1175/JCLI-D-17-0559.1.

Guido Vettoretti, Marc d Orgeville, William R. Peltier, and Marek Stastna. Polar climate instability and climate teleconnections from the arctic to the midlatitudes and tropics. *Journal of Climate*, 22(13):35133539, Jul 2009. ISSN 0894-8755. doi: 10.1175/2009jcli2481.1. URL http://dx.doi.org/10.1175/2009JCLI2481.1.

Miren Vizcaino, Uwe Mikolajewicz, Florian Ziemen, Christian B. Rodehacke, Ralf Greve, and Michiel R. Broeke. Coupled simulations of greenland ice sheet and climate change up to a.d. 2300. *Geophysical Research Letters*, 42(10):39273935, May 2015. ISSN 1944-8007. doi: 10.1002/2014gl061142. URL http://dx.doi.org/10.1002/2014GL061142.

Antje H.L. Voelker. Global distribution of centennial-scale records for marine isotope stage (mis) 3: a database. *Quaternary Science Reviews*, 21(10):11851212, May 2002. ISSN 0277-3791. doi: 10.1016/s0277-3791(01)00139-1. URL http://dx.doi.org/10.1016/S0277-3791(01)00139-1.

Xianfeng Wang, Augusto S. Auler, R. Lawrence Edwards, Hai Cheng, Patricia S. Cristalli, Peter L. Smart, David A. Richards, and Chuan-Chou Shen. Wet periods in northeastern brazil over the past 210 kyr linked to distant climate anomalies. *Nature*, 432(7018):740–743, Dec 2004. ISSN 1476-4687. doi: 10.1038/nature03067. URL http://dx.doi.org/10.1038/nature03067.

Xianfeng Wang, Augusto S. Auler, R. Lawrence Edwards, Hai Cheng, Emi Ito, and Maniko Solheid. Interhemispheric anti-phasing of rainfall during the last glacial period. *Quaternary Science Reviews*, 25(23-24):33913403, Dec 2006. ISSN 0277-3791. doi: 10.1016/j.quascirev.2006.02.009. URL http://dx.doi.org/10.1016/j.quascirev.2006.02.009.

Y. J. Wang. A high-resolution absolute-dated late pleistocene monsoon record from hulu cave, china. *Science*, 294(5550):23452348, Dec 2001. ISSN 1095-9203. doi: 10.1126/science.1064618. URL http://dx.doi.org/10.1126/science.1064618.

W. Weijer, M. E. Maltrud, M. W. Hecht, H. A. Dijkstra, and M. A. Kliphuis. Response of the atlantic ocean circulation to greenland ice sheet melting in a strongly-eddying ocean model. *Geophysical Research Letters*, 39(9):n/an/a, May 2012. ISSN 0094-8276. doi: 10.1029/2012gl051611. URL http://dx.doi.org/10.1029/2012GL051611.

G. Wendler, B. Moore, B. Hartmann, M. Stuefer, and R. Flint. Effects of multiple reflection and albedo on the net radiation in the pack ice zones of antarctica. *Journal of Geophysical Research: Atmospheres*, 109(D6):n/an/a, Mar 2004. ISSN 0148-0227. doi: 10.1029/2003jd003927. URL http://dx.doi.org/10.1029/2003JD003927.

Matteo Willeit and Andrey Ganopolski. The importance of snow albedo for ice sheet evolution over the last glacial cycle. *Climate of the Past*, 14(5):697707, May 2018. ISSN 1814-9332. doi: 10.5194/cp-14-697-2018. URL http://dx.doi.org/10.5194/cp-14-697-2018.

Jiayan Yang. On the importance of resolving the western boundary layer in wind-driven ocean general circulation models. *Ocean Modelling*, 5(4):357379, Jan 2003. ISSN 1463-5003. doi: 10.1016/s1463-5003(02)00058-6. URL http://dx.doi.org/10.1016/S1463-5003(02)00058-6.

D. Zanchettin, O. Bothe, C. Timmreck, J. Bader, A. Beitsch, H.-F. Graf, D. Notz, and J. H. Jungclaus. Inter-hemispheric asymmetry in the sea-ice response to volcanic forcing simulated by mpi-esm (cosmos-mill). *Earth System Dynamics*, 5(1):223242, Jun 2014. ISSN 2190-4987. doi: 10.5194/esd-5-223-2014. URL http://dx.doi.org/10.5194/esd-5-223-2014.

X. Zhang. "Confidential Manuscript - Personal Communication", July 2021.

X. Zhang, G. Lohmann, G. Knorr, and X. Xu. Different ocean states and transient characteristics in last glacial maximum simulations and implications for deglaciation. *Climate of the Past*, 9(5): 23192333, Oct 2013. ISSN 1814-9332. doi: 10.5194/cp-9-2319-2013. URL http://dx.doi.org/10.5194/cp-9-2319-2013.

Xiao Zhang, Matthias Prange, Ute Merkel, and Michael Schulz. Instability of the atlantic overturning circulation during marine isotope stage 3. *Geophysical Research Letters*, 41(12):42854293, Jun 2014a. ISSN 0094-8276. doi: 10.1002/2014gl060321. URL http://dx.doi.org/10.1002/2014GL060321.

Xu Zhang, Gerrit Lohmann, Gregor Knorr, and Conor Purcell. Abrupt glacial climate shifts controlled by ice sheet changes. *Nature*, 512(7514):290294, Aug 2014b. ISSN 1476-4687. doi: 10.1038/nature13592. URL http://dx.doi.org/10.1038/nature13592.

Xu Zhang, Gregor Knorr, Gerrit Lohmann, and Stephen Barker. Abrupt North Atlantic circulation changes in response to gradual CO_2 forcing in a glacial climate state. *Nature Geoscience*, 10: 518–524, 2017. doi: 10.1038/NGEO2974.

Appendix A

Supplementary Materials : Model Descriptions

A.1 Model Descriptions

Over the course of the thesis, two main numerical models have been used: the MITgcm in an eddy-permitting configuration, and the COSMOS Earth System model. Here I describe some of the relevant basic model characteristics. For each investigation, the specifics of the model configurations are detailed in the experimental design sections of the relevant chapters.

A.1.1 COSMOS

An examination of CMCV via numerical modelling necessitates the ability to perform multi-millennial timescale simulations within a reasonable time-frame and computational expense. Simultaneously, the model needs to be comprehensive enough to capture features and processes known to be important to CMCV (such as realistic ocean transports and atmosphere-ocean-sea-ice processes and feedbacks). This limits the choice to coupled climate models operating at coarse [1] horizontal resolutions. In this thesis, I use the COSMOS model for this purpose.

COSMOS is a fully coupled Earth System model composed of the ECHAM atmosphere model, the JSBACH land surface model, the MPIOM ocean model, and the OASIS coupler. The Max Plank Institute Ocean Model (MPIOM) is a primitive-equation ocean model using the hydrostatic and Boussinesq approximations Jungclaus et al. [2006]. We use a configuration which has a horizontal resolution of approximately 3° at the equator with 40 unevenly spaced levels with support for partial vertical grid cells and a free surface (grid geometry of 120x101x40, bathymetry is shown in Fig. A.1). The grid (GR30) features a displaced pole over Greenland, which results in enhanced horizontal resolution in adjacent regions like the Labrador and Nordic Seas. This enhanced resolution averages $\approx$ 160 km with minimums of $\approx$ 20 km for regions poleward of 60° N, while the global average is $\approx$ 270 km. Sea ice is modelled in COSMOS via an integrated sea ice model in MPIOM. This sea ice model is a dynamic-thermodynamic model utilising a viscous-plastic rheology based on Hibler [1979] and Semtner [1976]. The model's capability to displace the ice pack is of utility when

[1] relative to climate models used for short-future/short-timespan projects like the Climate Model Intercomparison Project Phase 5 (CMIP5), which forms part of the recent International Panel on Climate Change (IPCC) report.

evaluating the behaviours of the sea ice hysteresis and polynyas, which are understood to play roles in Dansgaard-Oeschger variability. The atmosphere model, ECHAM5, was derived from the European Center (EC) for Medium Range Weather Forecasts (ECMWF) by developers at Hamburg (HAM). The model has a horizontal resolution of T31 with 19 unevenly spaced sigma-hybrid levels in the configuration used here. COSMOS has had relative success in reproducing present day climate [Notz et al., 2013, Koldunov et al., 2010] though it does have outstanding issues, like MPIOM's high sensitivity to the state of the atmosphere driving it during summer months.

COSMOS is well suited to the workload of examining CMCV, as it is relatively efficient considering the complexity of the model. On contemporary hardware (e.g. one dual-socket compute-node using 2xIntel Xeon Gold 6248 processors clocked at 2.5 GHz) $>$ 100yrs of simulation time can be completed in one wall-day. COSMOS is also well suited to paleoclimate modelling as the model inputs (e.g. bathymetry, orbital configuration, greenhouse gasses) are comparatively easy to modify. As such it has been used in many paleoclimate investigations like Gong et al. [2013], Zhang et al. [2013, 2014a,b]. However, one shortcoming of COSMOS is the river and surface runoff scheme cannot be readily modified for different topographic configurations, thus it is not suitable for ensemble studies exploring ice sheet effects.

A.1.2 MITgcm

In my investigations the MITgcm plays the role of an eddy permitting ocean model configuration, largely structured around the configuration used in Condron and Winsor [2012] and the Estimating the Circulation and Climate of the Ocean, Phase II (ECCO2) project [Menemenlis et al., 2008]. The MITgcm is atypical relative to most ocean (or atmosphere) models in that it has a very flexible framework for either atmospheric or oceanic simulations (using the same code-base), around which specific configurations can be developed. The configuration which I use is a primitive-equation ocean model setup using the hydrostatic and Boussinesq approximations and a non-linear free surface, with bathymetry appropriate for the YD interval. Due to the high resolutions employed (bathymetry for the Arctic and North Atlantic are shown in Fig. A.2), 18km globally which is

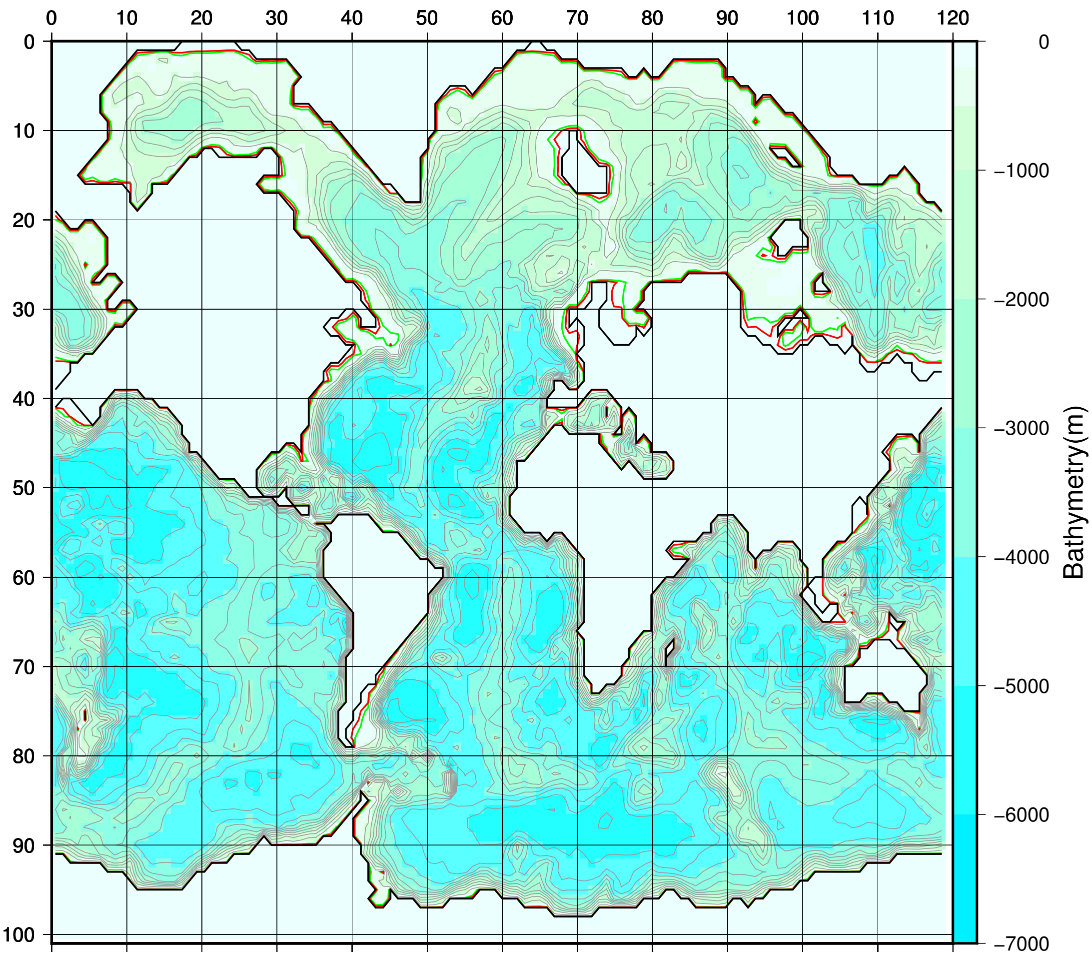

Figure A.1: Un-projected MPIOM bathymetry for the experiments in Chapters 3 and 4. Black contours denote the coastline, while the red and green contours denote 50 m and 100 m depth contours, grey contours denote 500 m depth intervals. Due to the coarse grid resolution, contours are smoothed and do not follow grid-cell edges cleanly, resulting in small visual artefacts (e.g. land discontinuity around Central America).

below the internal Rossby radius for regions equatorward of 60° N [Nurser and Bacon, 2014], the Gent-McWilliams parametrization is not enabled. The model configuration uses an unusual grid geometry, where the surface of the Earth is decomposed into 6-faces, each of which is further broken down into individual 510×510 grids with 50 vertical levels. This approach avoids issues at the North pole and results in a much more uniform distribution of grid-cell sizes relative to using a displaced pole grid. The dynamic-thermodynamic sea ice model, using a viscous-plastic rheology based on Hibler [1979] and Semtner [1976], is computed on the same model grid and time-step as the ocean model. Unfortunately, due to the high resolution, this model is both too slow and expensive to integrate on timescales longer than several decades. On contemporary hardware (with the MITgcm most simulations were done on the Niagara national cluster using nodes with 2xIntel Xeon Gold 6148 processors clocked at 2.40 GHz) one simulation year has a wall time of ≈ 9.5 h using 9-nodes (360 compute cores). However, it is readily modified to operate using different bathymetry configurations, a feature not common in most general circulation models.

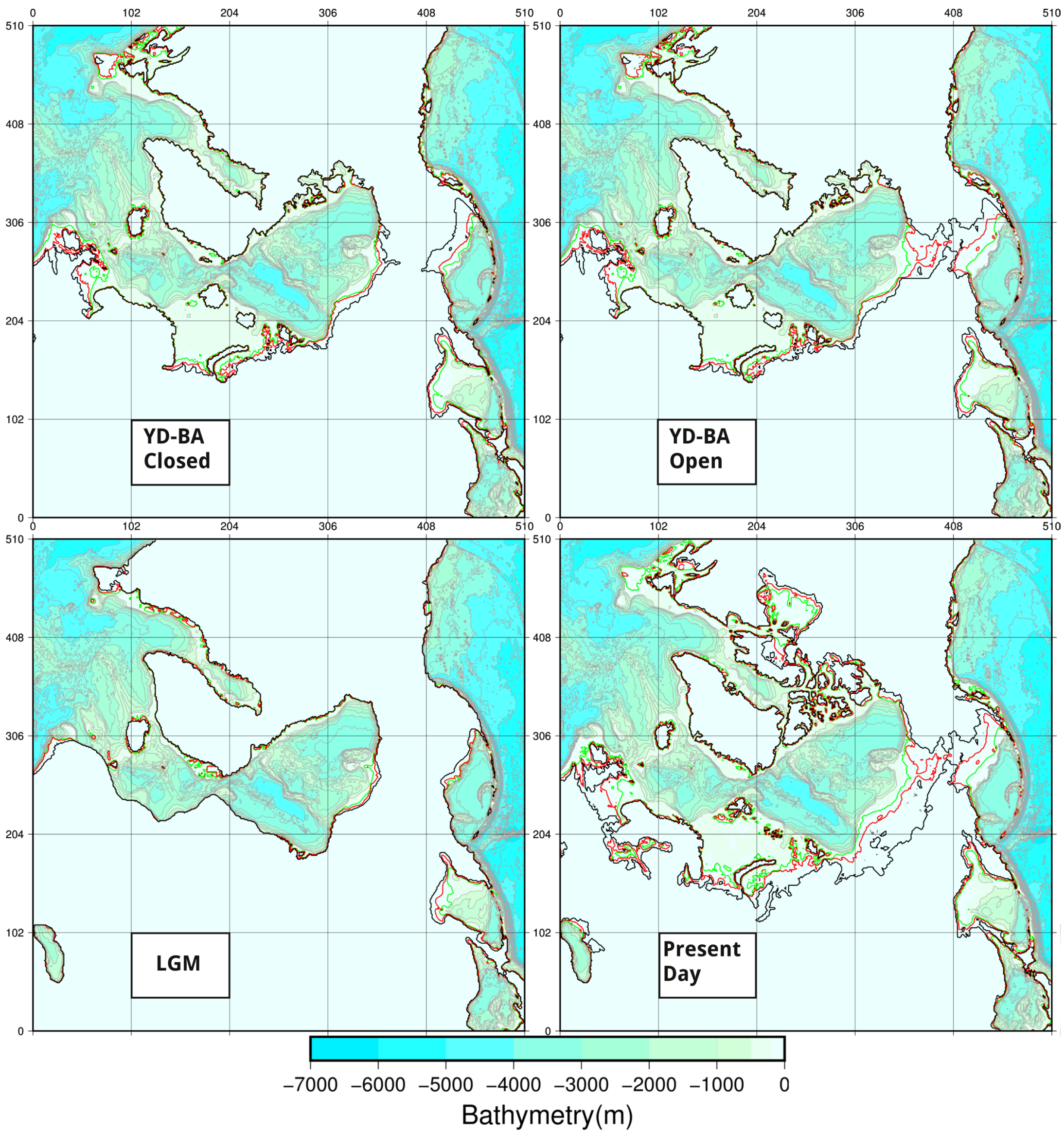

Figure A.2: MITgcm bathymetry for Arctic and North Atlantic for the investigations in Chapters 2 and 3. The bathymetry is shown on the native $\approx \frac{1}{6}$ resolution grid for the top face of the cubed-sphere grid topology, each face is 510×510 grid cells wide. Black contours denote the coastline, while the red and green contours denote 50 m and 100 m depth contours, grey contours denote 500 m depth intervals. Top panels show configurations utilized in this thesis, while the bottom panels are provided for context (bathymetry used in Condron and Winsor [2012] and present day bathymetry on the left and right respectively).

Appendix B

Supplementary Materials : Freshwater Routing In Eddy-permitting Simulations Of The Last Deglacial:Impact Of Realistic Freshwater Discharge

Supplement: Freshwater Routing In Eddy-permitting Simulations Of The Last Deglacial:Impact Of Realistic Freshwater Discharge

Ryan Love[1], Heather J. Andres[1], Alan Condron[2], and Lev Tarasov[1]

[1]Department of Physics and Physical Oceanography, Memorial University of Newfoundland, St. John's, Newfoundland, Canada

[2]Geology & Geophysics, Woods Hole Oceanographic Institution, Woods Hole, Massachusetts, USA

B.1 Supplemental Figures

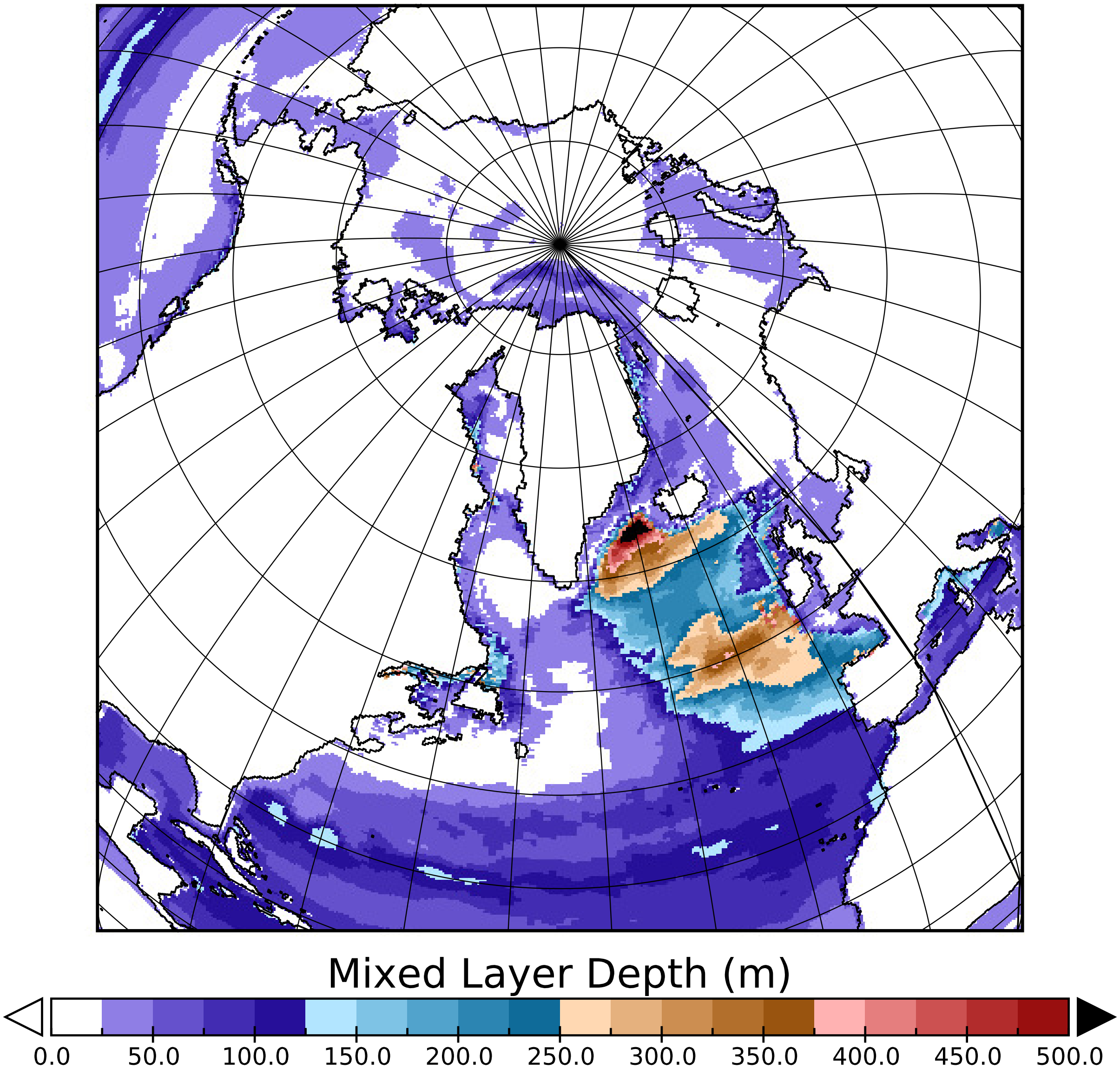

Figure B.1: Mixed layer depth in the North Atlantic from the last 5 years of our open Bering Strait control simulation. The most significant region of mixing is between -40E to 0E, 50N to 65N. This is the region which we examine the salinity anomaly to evaluate the impact of each of our injection scenarios. Latitude and longitude lines represent 10 degree increments.

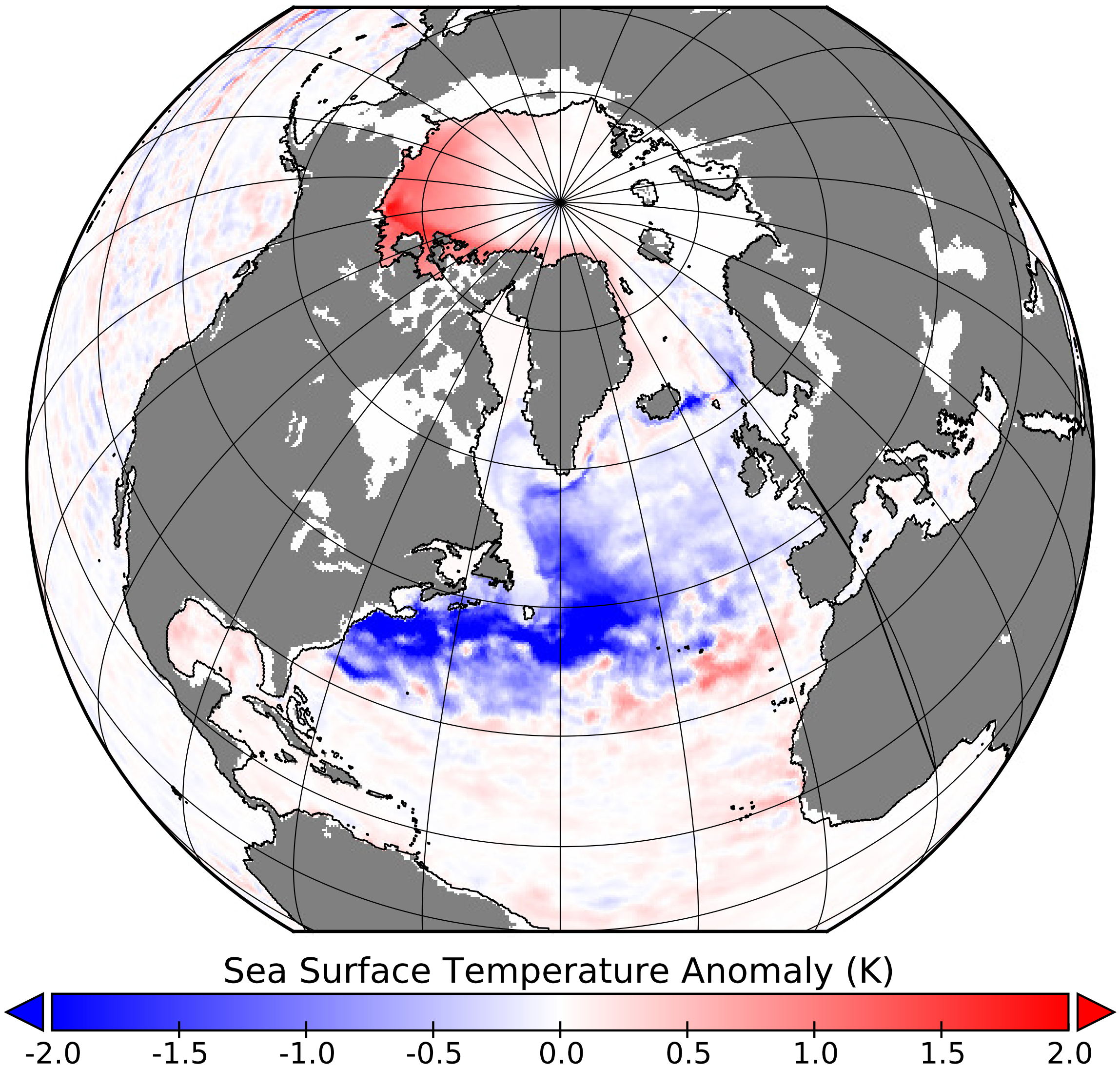

Figure B.2: Sea surface temperature differences for the closed Bering Strait 2dSv Mackenzie River forcing. Given our model configuration is uncoupled the differences observed here should be used only for context.

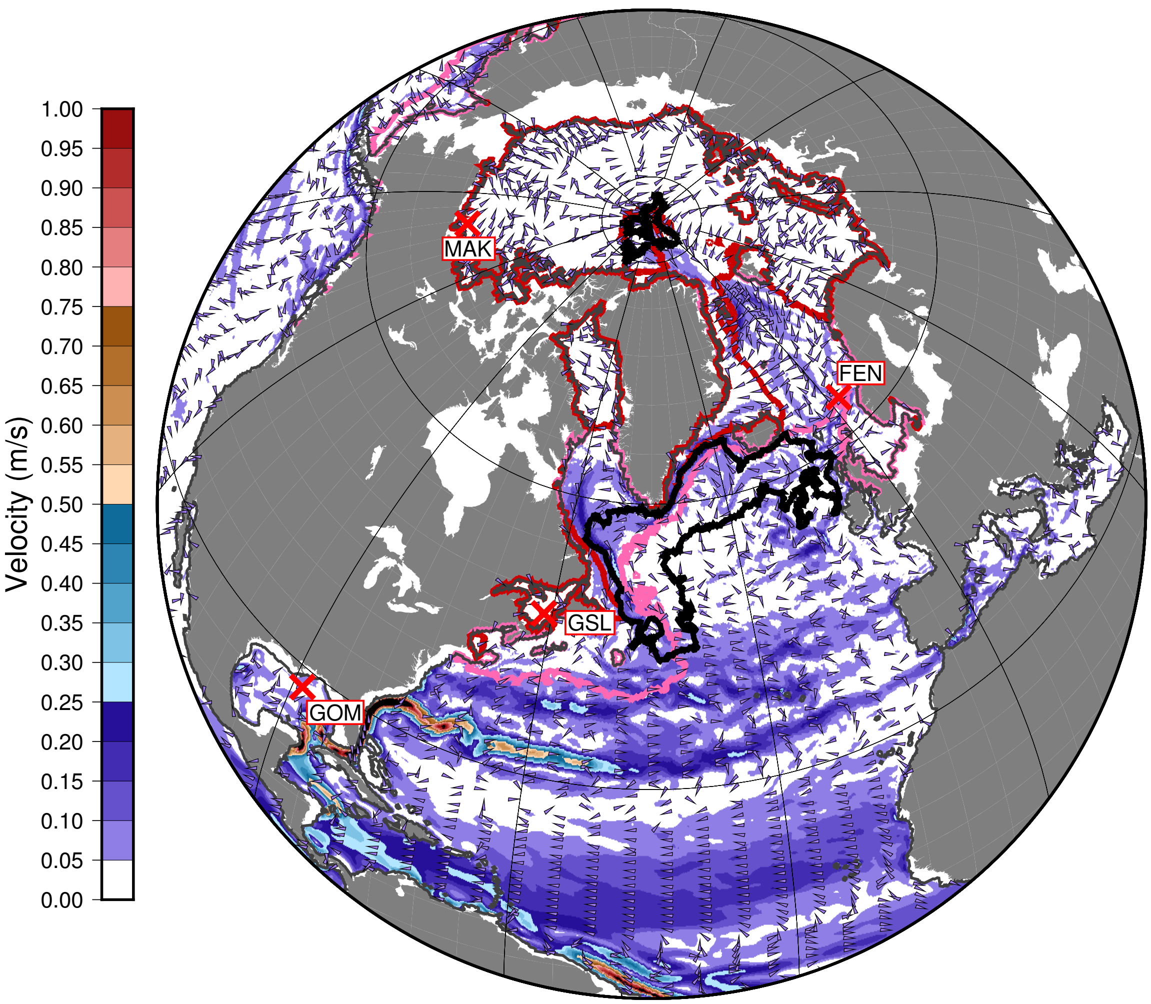

Figure B.3: Average sea surface velocity for the last 5 years of our CBS Control run with arrows denoting the direction. Present day land-sea mask is shown in light grey while simulation land-sea mask is contoured in a darker shade of grey. The dark red and pink contours denotes the time minimum and maximum sea ice extent respectively, of at least 15% sea ice coverage calculated over the last 5 years of the simulation. When comparing the sea ice maximal extent to the mixed layer depth shown in B.1 (for the OBS case) and black contour, denoting 1000m mixed layer depth, in the current plot we see the mixing is just off the outer limit of the sea ice maximum. The arrows denoting direction are shown at a lesser density than the native grid to aid in visualization.

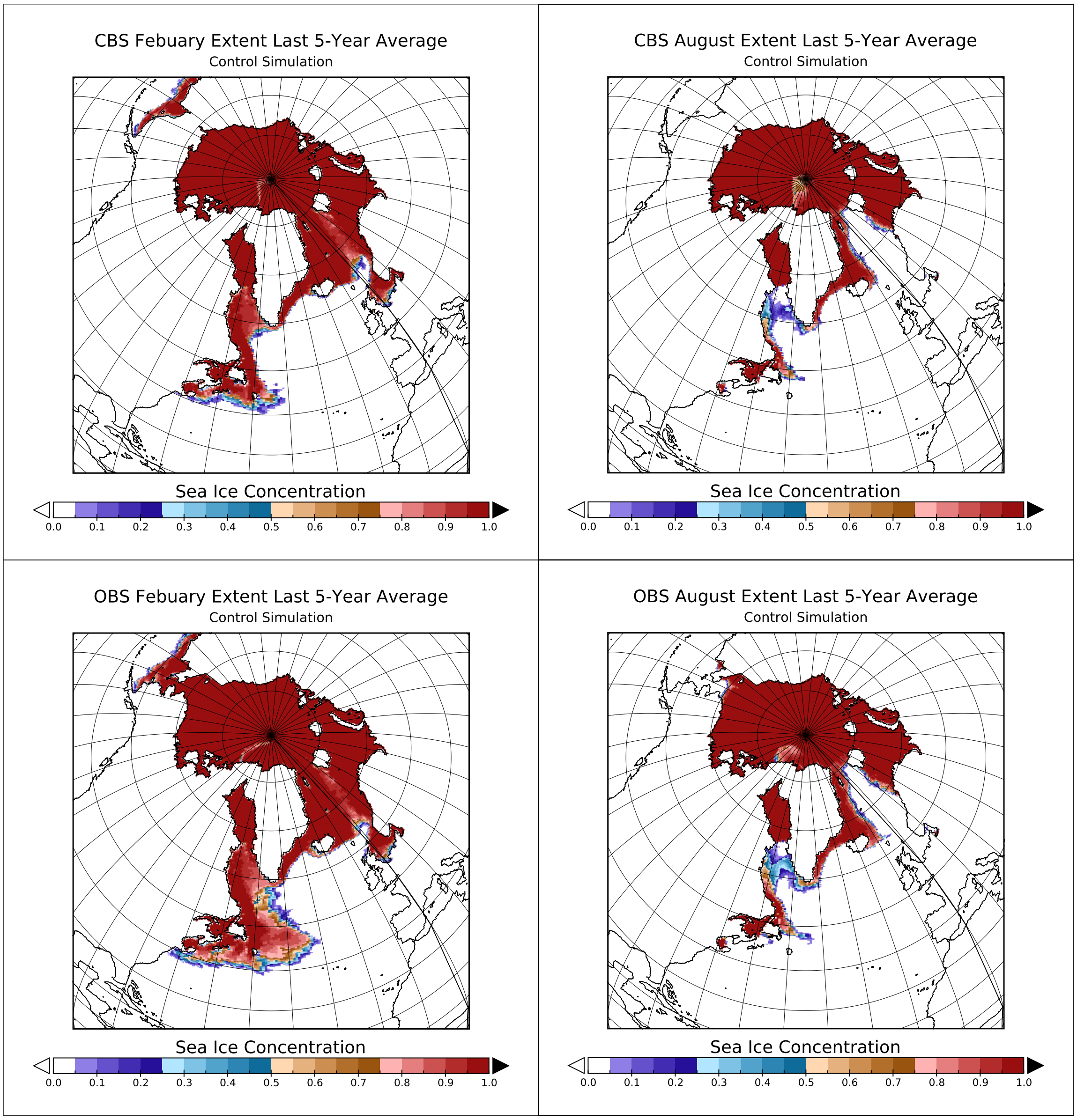

Figure B.4: Sea ice minimal and maximal extent for both the open and closed Bering Strait control simulations. Sea ice concentration values range from 0 (no sea ice) to 1 (full grid cell coverage). Minimum/maximum extents correspond to August and February respectively, the averages are generated as monthly means from the last 5 years of simulation data for each run (whose duration is approximately 30 simulation years each).

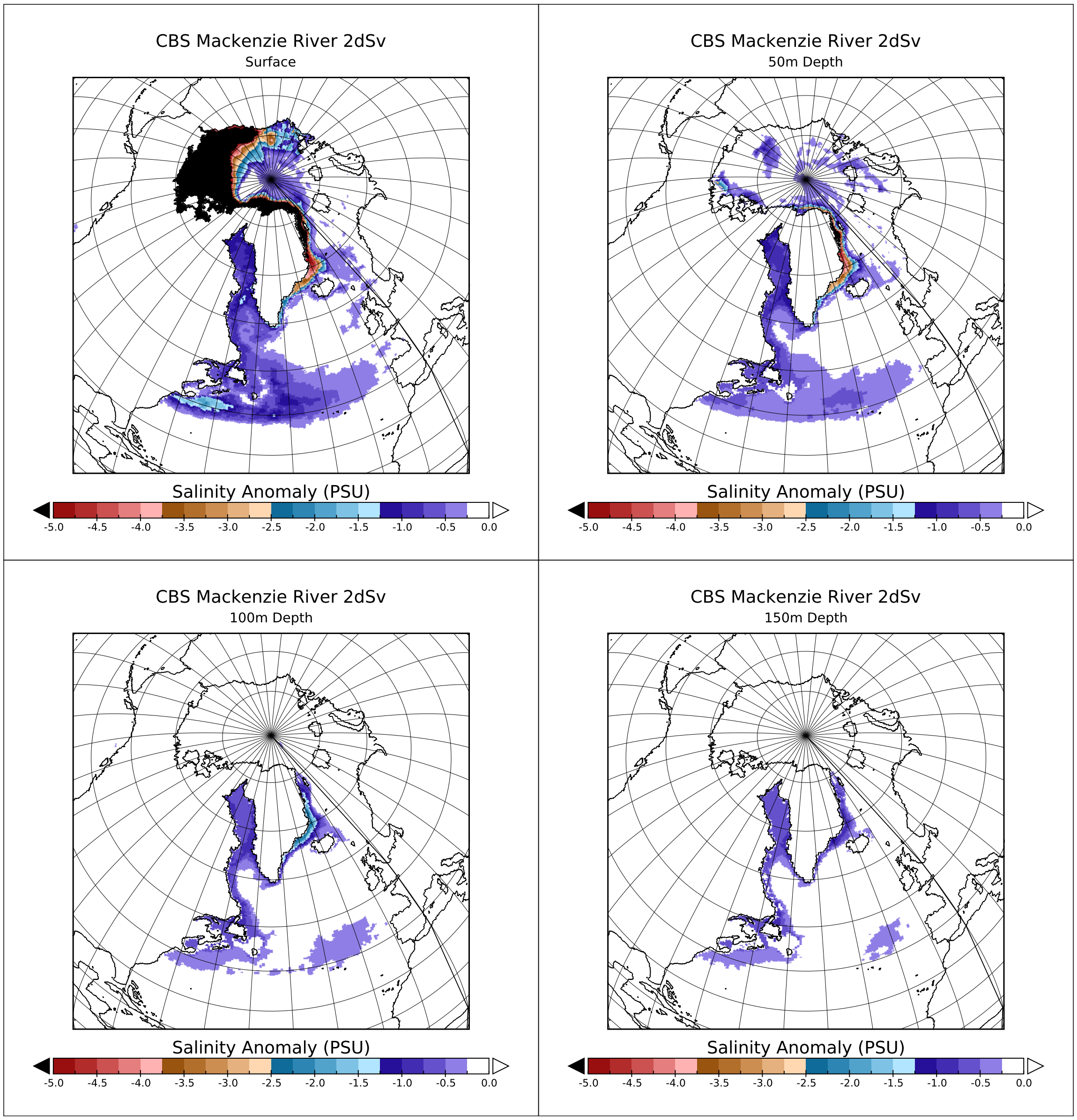

Figure B.5: Salinity anomaly distribution at a selection of depths for the Closed Bering Strait Mackenzie River 2dSv continual injection scenario. This distribution is the average of the anomaly field over the last 5 years of model integration.

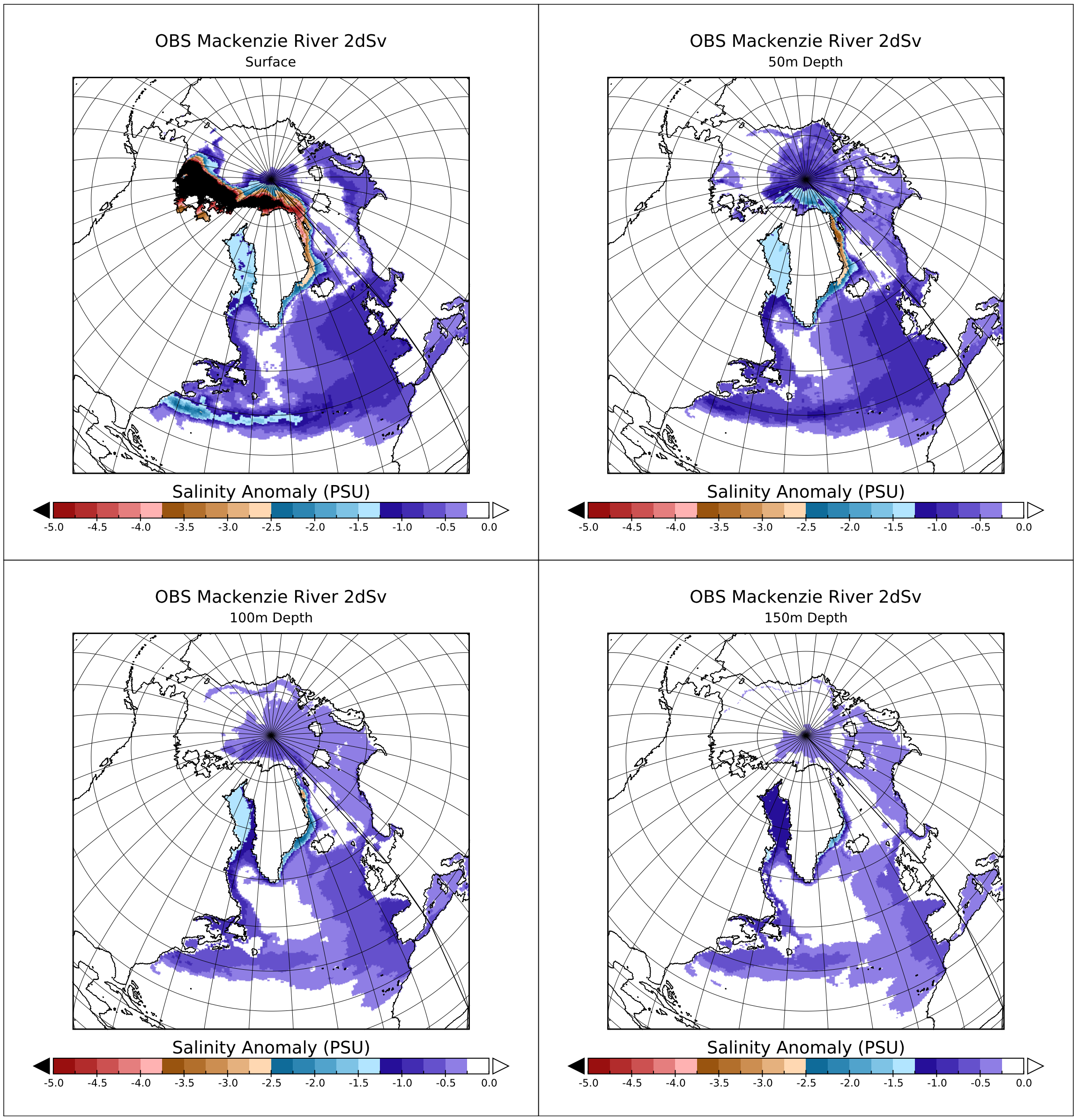

Figure B.6: Salinity anomaly distribution at a selection of depths for the Open Bering Strait Mackenzie River 2dSv continual injection scenario. This distribution is the average of the anomaly field over the last 5 years of model integration.

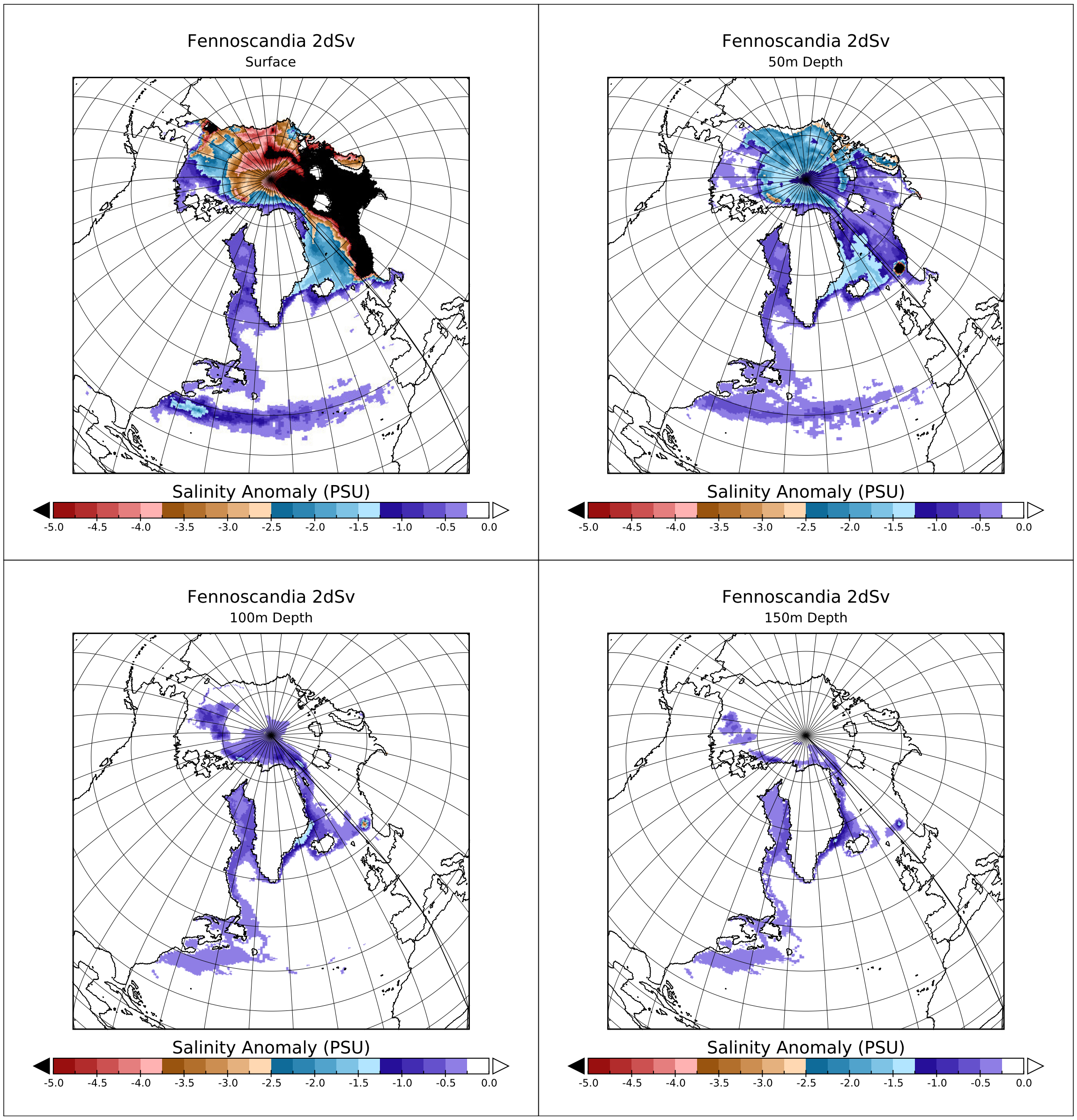

Figure B.7: Salinity anomaly distribution at a selection of depths for the Open Bering Strait Fennoscandia 2dSv continual injection scenario. This distribution is the average of the anomaly field over the last 5 years of model integration.

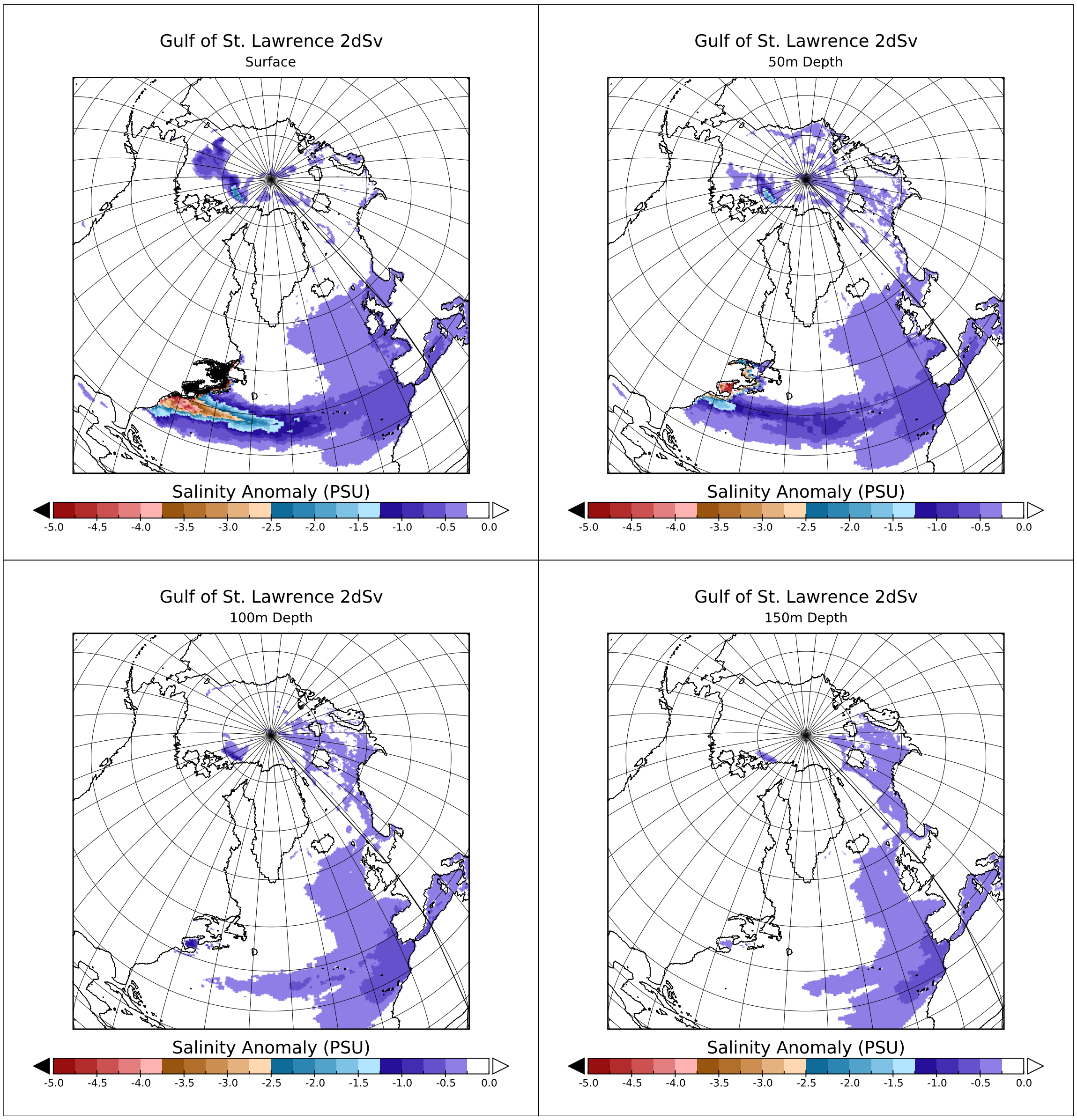

Figure B.8: Salinity anomaly distribution at a selection of depths for the Open Bering Strait Gulf of St. Lawrence 2dSv continual injection scenario. This distribution is the average of the anomaly field over the last 5 years of model integration.

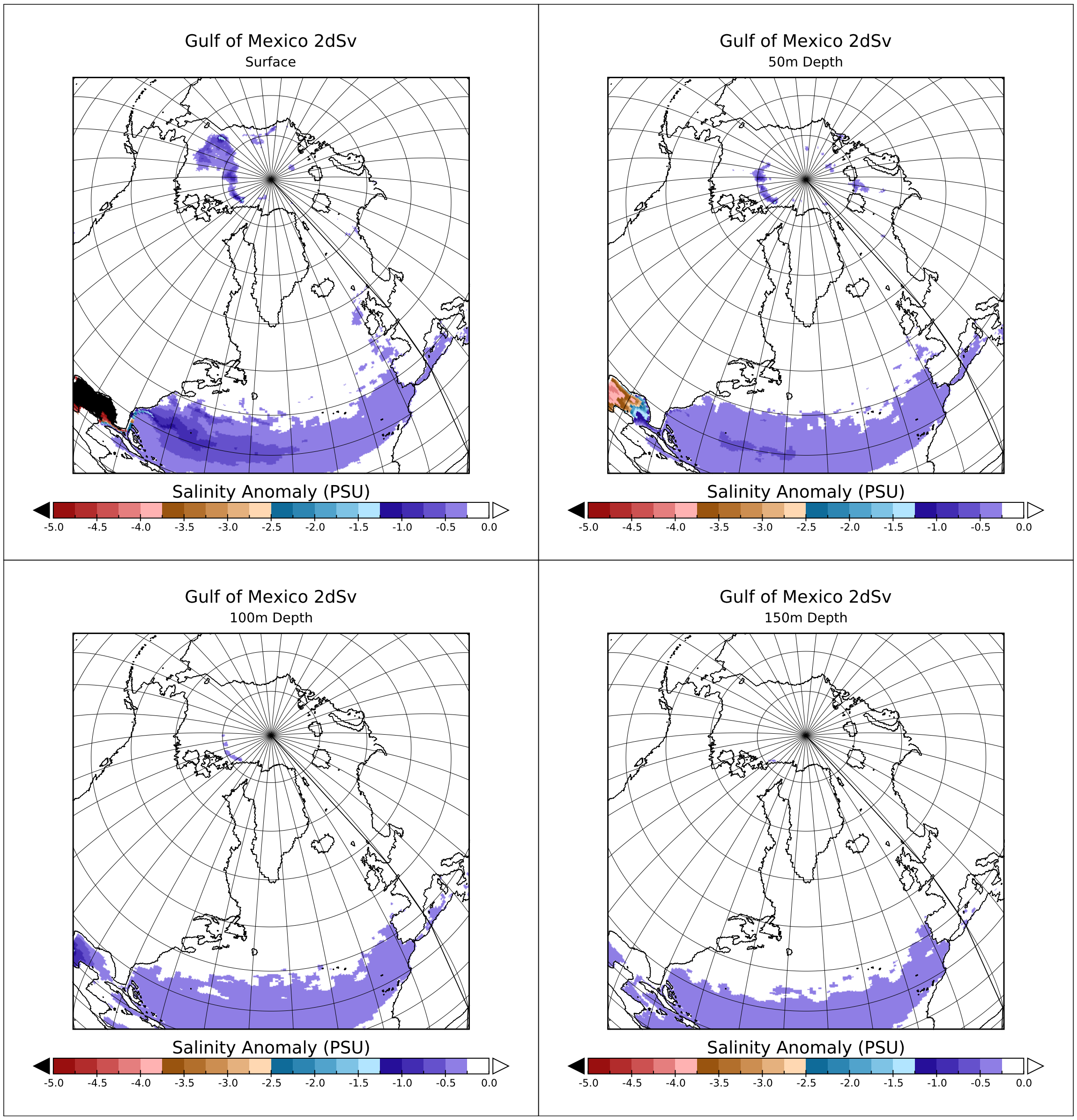

Figure B.9: Salinity anomaly distribution at a selection of depths for the Open Bering Strait Gulf of Mexico 2dSv continual injection scenario. This distribution is the average of the anomaly field over the last 5 years of model integration.

B.2 Model Drift

For the Barents-Kara sea region we observe a maximum drift of ≈ 0.75psu/a for the open Bering Strait YD case and a maximum of ≈ 0.3psu/a for the closed Bering Strait YD case. The drift is calculated over the duration of the respective control run. This trend is observed in the region directly where the surface runoff is introduced into the model and only in the uppermost ≈ 50m of the water column, with the greatest drift present in the surface layer. For the drift of ≈ 0.75psu/a for the open Bering Strait YD case the magnitude reduces by an order of magnitude at the 30m depth. Elsewhere in the simulation the calculated trend is generally below 0.05psu/a, a trend which may be an artefact of the short run time and reflect ongoing longer timescale internal variability.

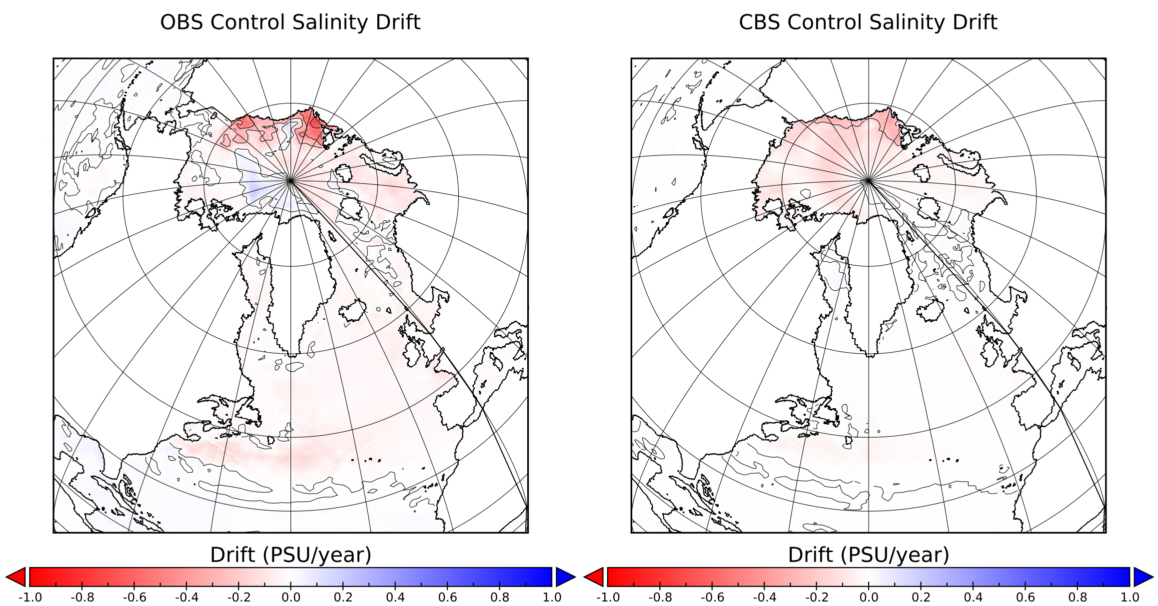

Figure B.10: Drift for each of the control runs at the ocean surface calculated over the duration of the control run. Major scale intervals are contoured, most contours denote the 0-line. Continental outlines reflect the land-sea mask as used in each of the control simulations and are identical with the exception of the regions surrounding the Bering Strait. The drift is accounted for as part of the fingerprint processing routine. There is correspondence between the observed drift and the sources of runoff in the model boundary conditions, but is more noticeable in the open Bering Strait configuration.

B.3 AMOC Discussion

Since the focus of the study is the surface transport of freshwater, here we discuss the immediate impact of freshwater on rates of DWF and AMOC purely for context. This is done given the significant limitations in using this metric for such short durations, which renders these simulations unsuitable for examination of AMOC and deeper ocean trends. The simulated state of the AMOC is shown in fig. B.11. The AMOC in the control simulations shows an overall similar structure (not shown) but weaker values compared to comparable high-resolution members of the multi-model, present-day ensemble in Hirschi et al. [2020]. The strength of the AMOC at 26N in the control simulations is around 4Sv with a one-sigma annual variation of 1Sv, and a strong seasonality. Using 26N to coinicide with previous studies and the RAPID array results in an offset of -6Sv relative to the peak as is common in studies where this feature can be adequately resolved. Consistently with Hu et al. [2015], the CBS control run shows a stronger AMOC than OBS when examined using a 1 year running mean. However, unlike previous studies (e.g. Condron and Winsor [2012]), freshwater forcing in the injection simulations does not influence the AMOC variability or the southward flow from the Labrador Sea above the threshold of internal variability on the time scales examined. The weak AMOC values obtained here indicate that the model is operating in a 'Glacial' mode relative to the previous study by Condron and Winsor [2012], which showed AMOC values around 18Sv under present-day boundary conditions. The ocean operating in a glacial mode is reasonable given the glacial surface forcing and initialization conditions implemented here, although it is unlikely that in reality the ocean was in such a state just prior to the Younger Dryas [McManus et al., 2004]. We expect that otherwise identical simulations performed using surface forcing and initialization conditions more consistent with the start of the Younger Dryas would generate more realistic AMOC values under both control and forcing conditions. Relative to a stronger AMOC we would expect that Gulf Stream, which is highlighted in the main manuscript as being a key feature to reducing meridional transport of freshwater, would be both shifted northwards and closer to shore [Caesar et al., 2018]. However, this does not change the impact of the Gulf Stream on our simulations or conclusions.

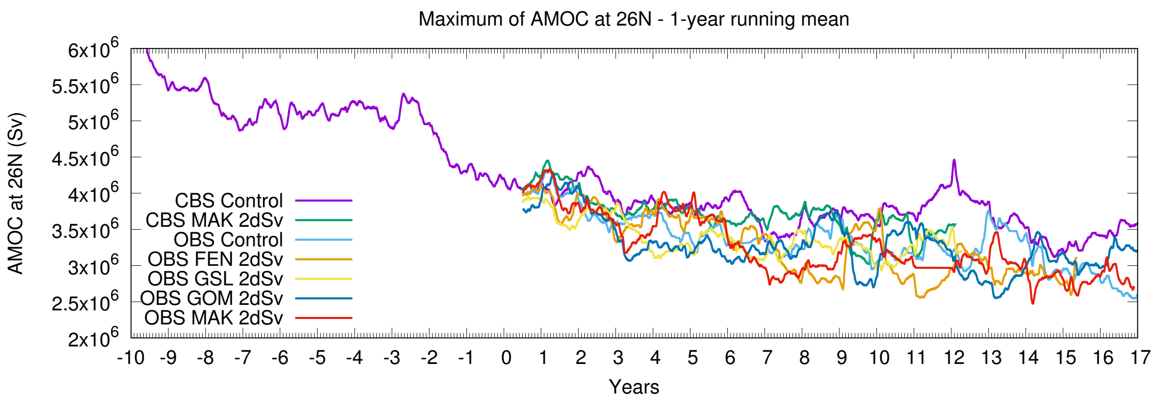

Figure B.11: AMOC calculated as the maximum of the meridional overturning stream function at 26N, to coincide with the RAPID array, at depths below 700m. Comparing to the more common metric of maximum of the meridional overturning stream function in the North Atlantic basin below 700m, we find a roughly -6Sv offset, that is the AMOC is roughly 9.5Sv rather than 3.5Sv. Timeseries shown are 1 year running means where year 0 is when glacial runoff is introduced into the model. The standard deviation of this time series, calculated annually, ranges between 1-1.5Sv.

B.4 Experimental Design Additional Information

Run name	Bathymetry	Freshwater Forcing	Purpose	Duration (years)	Parent Run
LGMCS510	As in Condron & Hill 2014	None	Spin-up and Preliminary investigations	20	Hill and Condron [2014] Control (not end of simulations)
LGMCS510 YD13kaControl	13kaBP GLAC (CBS)	None	LGM $\rightarrow$ YD spin up	10	LGMCS510 (T&S field restart due to modified bathymetry)
YDCS510 Control	13kaBP GLAC (CBS)	None	YD CBS Spin-up and control	33	LGMCS510 YD13kaControl
YDCS510 ERA40	13kaBP GLAC (CBS)	None	LGM vs. PD wind comparison	20	LGMCS510 YD13kaControl
YDCS510 ERA40 OBS GOM 0p2C	13kaBP GLAC (CBS)	None	ERA40 Mississippi River Outlet Forcing	10	YDCS510 ERA40 (at year 10)
YDCS510 openBeringControl	13kaBP GLAC (OBS)	None	YD OBS Spin-up and control	33	LGMCS510 YD13kaControl
YDCS510 0p2SvMack	13kaBP GLAC (CBS)	2dSv Mackenzie River (221.25E, 71.15N)	Mackenzie River Outlet Forcing	24	YDCS510 Control (at year 10)
YDCS510 openBering 0p2MackRiver	13kaBP GLAC (OBS)	2dSv Mackenzie River (221.25E, 71.15N)	Mackenzie River Outlet Forcing	23	YDCS510 openBeringControl (at year 10)
YDCS510 OBS FEN 0p2C	13kaBP GLAC (OBS)	2dSv Fennoscandia (2.5E, 63.6N)	Fennoscandian Forcing	22	YDCS510 openBeringControl (at year 10)
YDCS510 OBS GSL 0p2C	13kaBP GLAC (OBS)	2dSv Gulf of St. Lawrence (298.75E, 47.6N)	Gulf of St. Lawrence Outlet Forcing	23	YDCS510 openBeringControl (at year 10)
YDCS510 OBS GOM 0p2C	13kaBP GLAC (OBS)	2dSv Mississippi River (271.25E, 27.8N)	Mississippi River Outlet Forcing	23	YDCS510 openBeringControl (at year 10)

Table B.1: A summary of all the runs conducted in this investigation. All runs (excepting YDCS510 ERA40 and YDCS510 ERA40 OBS GOM 0p2C which used ERA40 wind fields) use the same surface forcing as in Hill and Condron [2014] which corresponds with Last Glacial Maximum conditions. Data from 'LGMCS510' and 'LGMCS510 YD13kaControl' are not shown in any figures.

B.5 Effects of modern wind forcing on the Gulf Stream

To explore the impact that our overly zonal Gulf Stream has on one of the injection locations most sensitive to this feature we performed a pair of brief sensitivity runs. These sensitivity use an identical configuration to our other YDCS510 runs except the wind forcing has been replaced by fields from the ERA40 atmospheric re-analysis [Kållberg et al., 2004]. We observe that the salinity anomaly field is zonal as in our other simulations but with additional freshwater being transported north-east in the direction of the more modern path of the Gulf Stream. Examining the sea surface velocity fields between the ERA40 Control and the YD Open Bering Strait Control we find that the YD OBS Control has faster surface currents relative to the ERA40 simulation, as well as a Gulf Stream located $\approx 5^{\circ}$ closer to the equator. Despite these differences, the blocking behaviour observed in the YDCS510 OBS GOM run and discussed in the main text remains.

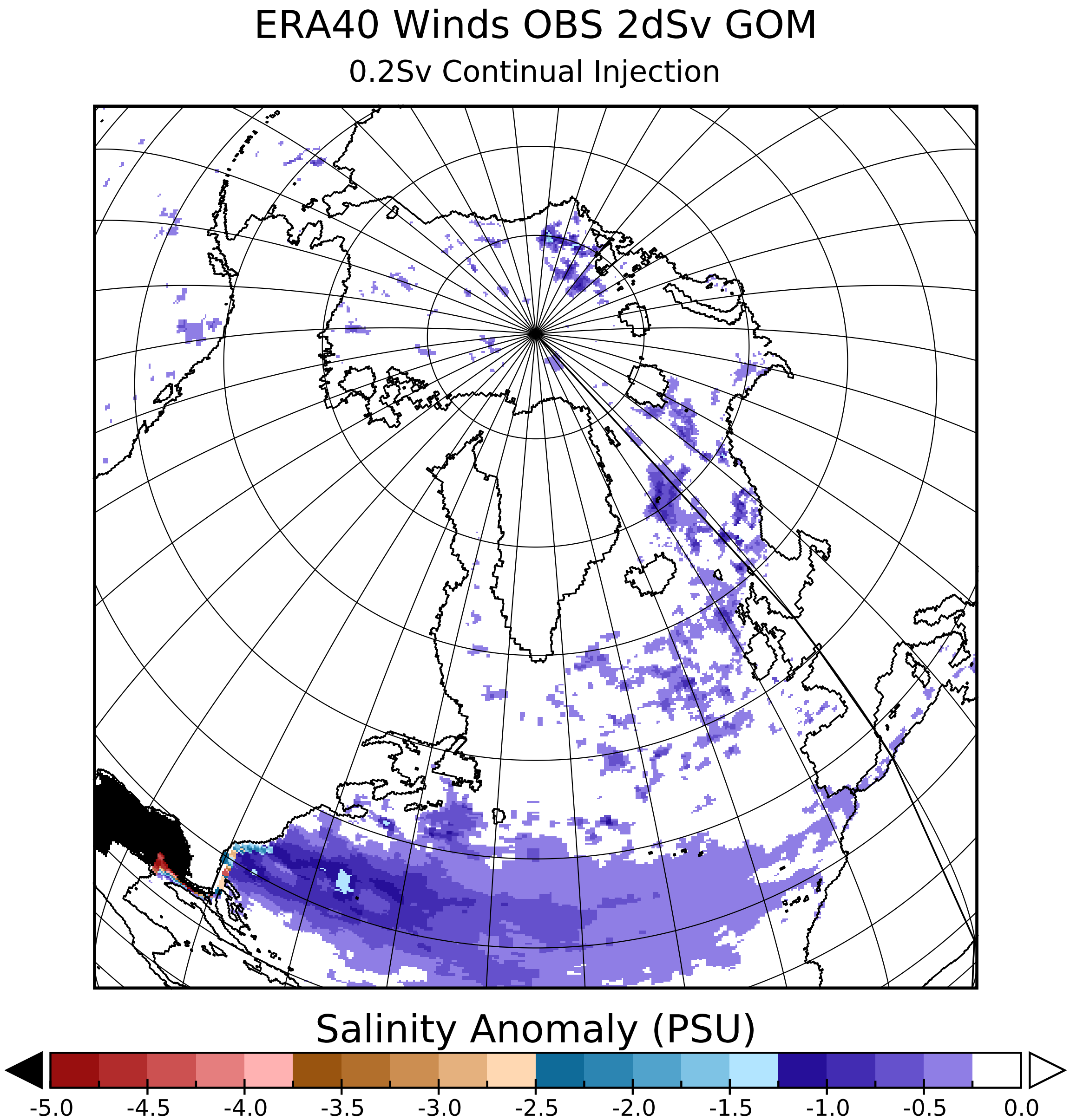

Figure B.12: Sea surface salinity anomaly distribution for our OBS 2dSv GOM injection run with ERA40 surface wind forcing. This distribution is the average of the anomaly field over the last year of model integration.

B.6 Hosing difference approximation

When comparing the freshening effect of direct injection into the regions of interest, we use the following: we assume that the freshwater displaces existing seawater from the regions, that the injection region is evenly inundated with freshwater, and the freshwater is evenly mixed over the top 50m of the water column. Also, given this is a very simplified approximation, we assume the density of sea water and freshwater are the same, neglecting the $O(3\%)$ error.

$$S_{displaced} = q_{fw}\Delta t S_{avg}\rho_w \tag{B.1}$$

$$S_{total} = A\Delta z\rho_w \tag{B.2}$$

$$S_{diff} = (S_{total} - S_{displaced})/(A\Delta z\rho_w) \tag{B.3}$$

Where $S_{displaced}$ is the salt we are displacing with freshwater(g) , S_{total} is the total salt in the volume (g), S_{diff} is the resulting salinity difference (psu), S_{avg} is the average salinity of the region (taken directly from the model and over the top 50m, psu), q_{fw} is the freshwater flux (2dSv in our calculations), Δt is the time over which the flux is considered (1 year), ρ_w is the density of water we use 1000kg/m^3, A is the area of the region, and Δz is the depth which we are considering the freshwater is mixing (50m).

Bibliography

L. Caesar, S. Rahmstorf, A. Robinson, G. Feulner, and V. Saba. Observed fingerprint of a weakening atlantic ocean overturning circulation. *Nature*, 556(7700):191196, Apr 2018. ISSN 1476-4687. doi: 10.1038/s41586-018-0006-5. URL http://dx.doi.org/10.1038/s41586-018-0006-5.

A. Condron and P. Winsor. Meltwater routing and the younger dryas. *Proceedings of the National Academy of Sciences*, 109(49):1992819933, Nov 2012. ISSN 1091-6490. doi: 10.1073/pnas.1207381109. URL http://dx.doi.org/10.1073/pnas.1207381109.

Jenna C. Hill and Alan Condron. Subtropical iceberg scours and meltwater routing in the deglacial western north atlantic. *Nature Geoscience*, 7(11):806810, Oct 2014. ISSN 1752-0908. doi: 10.1038/ngeo2267. URL http://dx.doi.org/10.1038/ngeo2267.

Jol J.M. Hirschi, Bernard Barnier, Claus Bning, Arne Biastoch, Adam T. Blaker, Andrew Coward, Sergey Danilov, Sybren Drijfhout, Klaus Getzlaff, Stephen M. Griffies, and et al. The atlantic meridional overturning circulation in high-resolution models. *Journal of Geophysical Research: Oceans*, 125(4), Apr 2020. ISSN 2169-9291. doi: 10.1029/2019jc015522. URL http://dx.doi.org/10.1029/2019JC015522.

Aixue Hu, Gerald A. Meehl, Weiqing Han, Bette Otto-Bliestner, Ayako Abe-Ouchi, and Nan Rosenbloom. Effects of the bering strait closure on amoc and global climate under different background climates. *Progress in Oceanography*, 132:174196, Mar 2015. ISSN 0079-6611. doi: 10.1016/j.pocean.2014.02.004. URL http://dx.doi.org/10.1016/j.pocean.2014.02.004.

Per Kållberg, Adrian Simmons, Sakari Uppala, and Manuel Fuentes. The era-40 archive. *ERA-40 project report series*, 17:31, 2004.

J. F. McManus, R. Francois, J.-M. Gherardi, L. D. Keigwin, and S. Brown-Leger. Collapse and rapid resumption of atlantic meridional circulation linked to deglacial climate changes. *Nature*, 428(6985):834837, Apr 2004. ISSN 1476-4687. doi: 10.1038/nature02494. URL http://dx.doi.org/10.1038/nature02494.

Appendix C

Supplementary Materials : Exploring the Glacial Climate System Response to a Range of Freshwater Representations: Hosing, Regional, and Freshwater Fingerprints

Supplement : Exploring the Glacial Climate System Response to a Range of Freshwater Representations: Hosing, Regional, and Freshwater Fingerprints

Ryan Love[1], Heather J. Andres[1], Xu Zhang[5,6], Alan Condron[2], Gerrit Lohmann[3,4], and Lev Tarasov[1]

[1]Department of Physics and Physical Oceanography, Memorial University of Newfoundland, St. John's, Newfoundland, Canada
[2]Geology & Geophysics, Woods Hole Oceanographic Institution, Woods Hole, Massachusetts, USA
[3]Group of Alpine Paleoecology and Human Adaptation (ALPHA), State Key Laboratory of Tibetan Plateau Earth System, Resources and Environment (TPESRE), Institute of Tibetan Plateau Research, Chinese Academy of Sciences, Beijing 100101, China
[4]Department of Environmental Physics & MARUM, University of Bremen, Bremen, Germany
[5]Group of Alpine Paleoecology and Human Adaptation (ALPHA), State Key Laboratory of Tibetan Plateau Earth System, Resources and Environment (TPESRE), Institute of Tibetan Plateau Research, Chinese Academy of Sciences, Beijing 100101, China
[6]Key Laboratory of Western Chinas Environmental Systems (Ministry of Education), College of Earth and Environmental Sciences, Lanzhou University, Lanzhou, 730000, China

C.1 Supplemental Figures

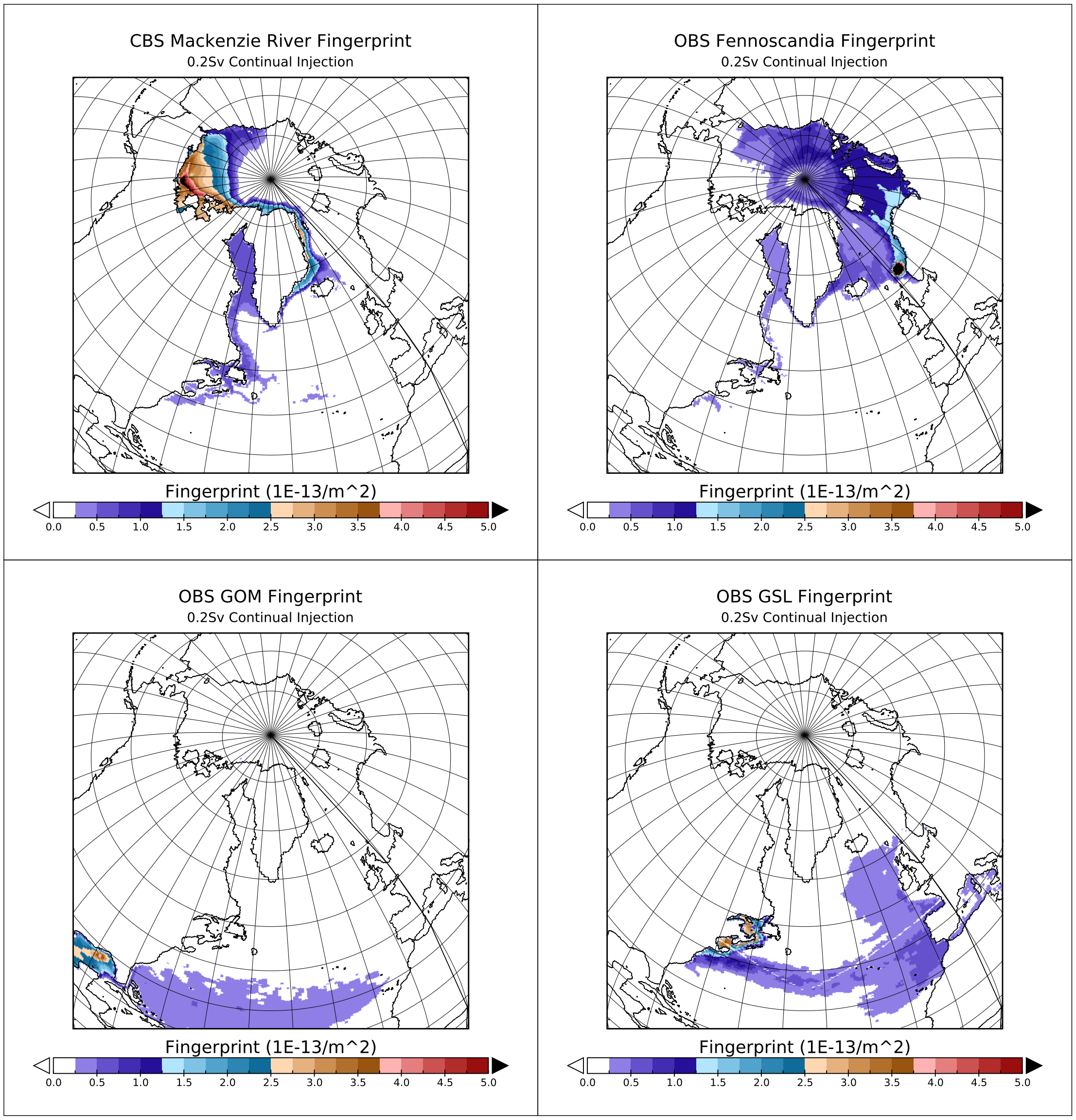

Figure C.1: Each of the freshwater fingerprints used in this study. Values shown are the normalized values as on a regular $\frac{1}{6}^{\circ}$ global grid. To obtain an injection rate in $\frac{m}{s}$ for a given fingerprint simply multiply the shown distribution by the desired volume flux.

Figure C.2: Freshwater injection locations for the generation of the fingerprints and regional injection locations. MAK is Mackenzie River, FEN is Fennoscandia, GSL is Gulf of St. Lawrence, GOM is Gulf of Mexico. Present day land-sea mask is shown in grey, Younger Dryas land-sea mask as used in Love et al. [2021] and the generation of the fingerprints is contoured in black, and the 38ka land-sea mask used in COSMOS is contoured in red. The 50-70N injection region is shown in yellow. The Barents-Kara sea region over which our freshwater flux calculation is done is shown in Green.

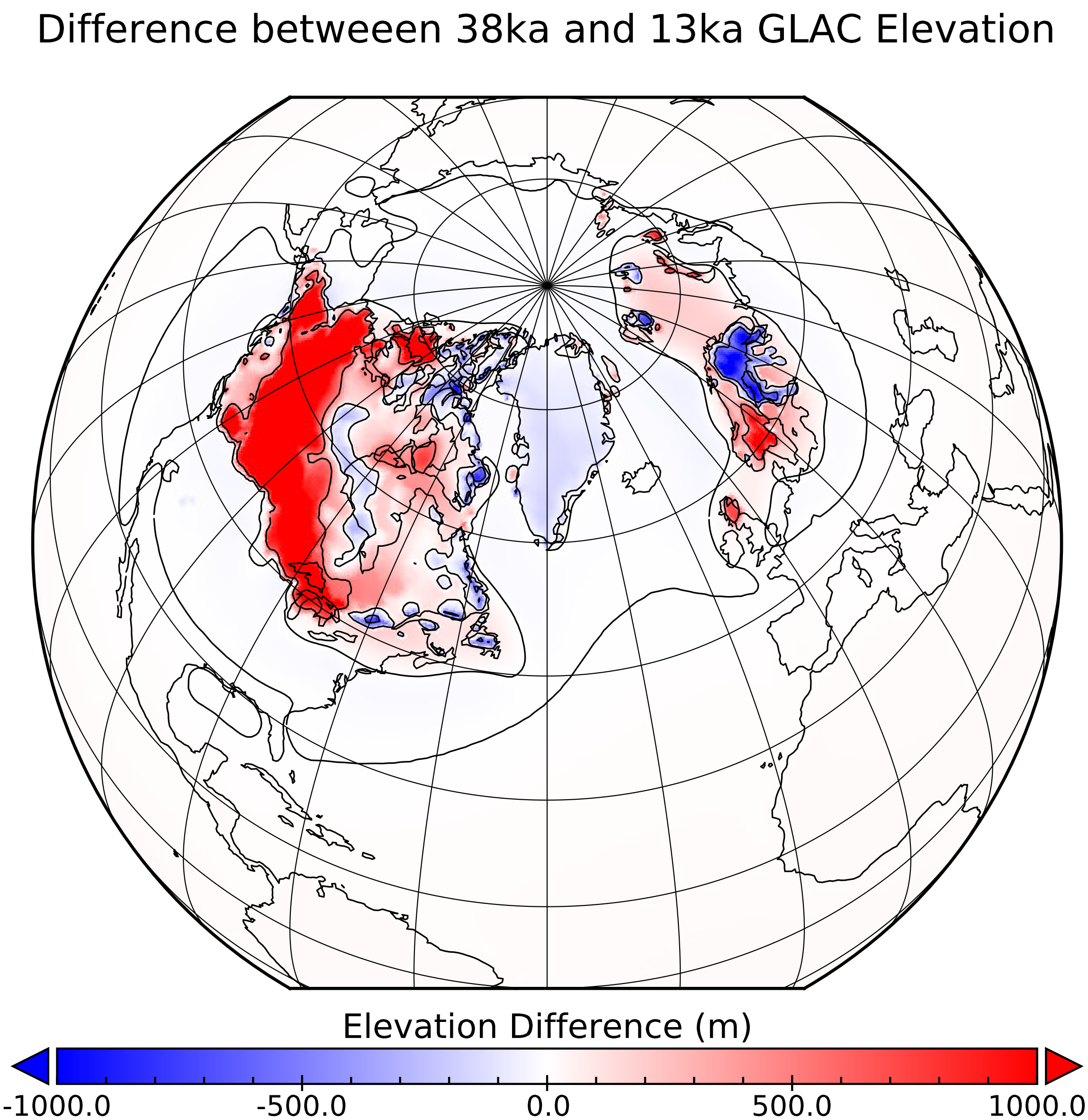

Figure C.3: Difference in elevation at 38ka and 13ka from our reconstruction. Ice extent is largely the same except over western Canada where the North American Ice Complex is more extensive at 38ka. Sea level over the North Atlantic and Arctic is generally less than 10m difference while far field locations are ≈ 15m.

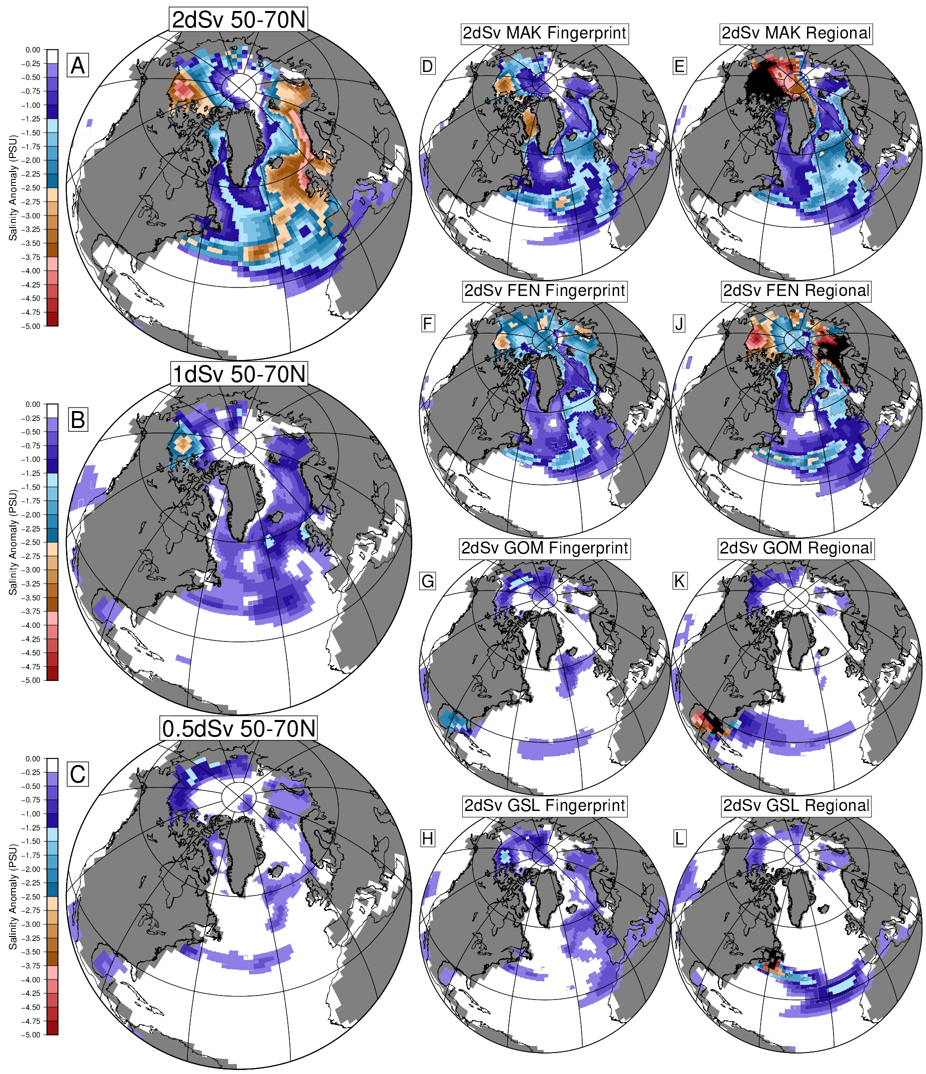

Figure C.4: Salinity anomaly averaged over years $20-30$ of injection averaged over the top 30m of the water column. Subfigures a,b,c show the impact of a 50-70N injection with varying fluxes uniformly distributed over the band. Subfigures d,f,g,h, show the salinity anomalies resulting from using the fingerprint distributions with a 2dSv flux. Similarly, subfigures e,j,k,l show the salinity anomalies resulting from the regional injection locations.

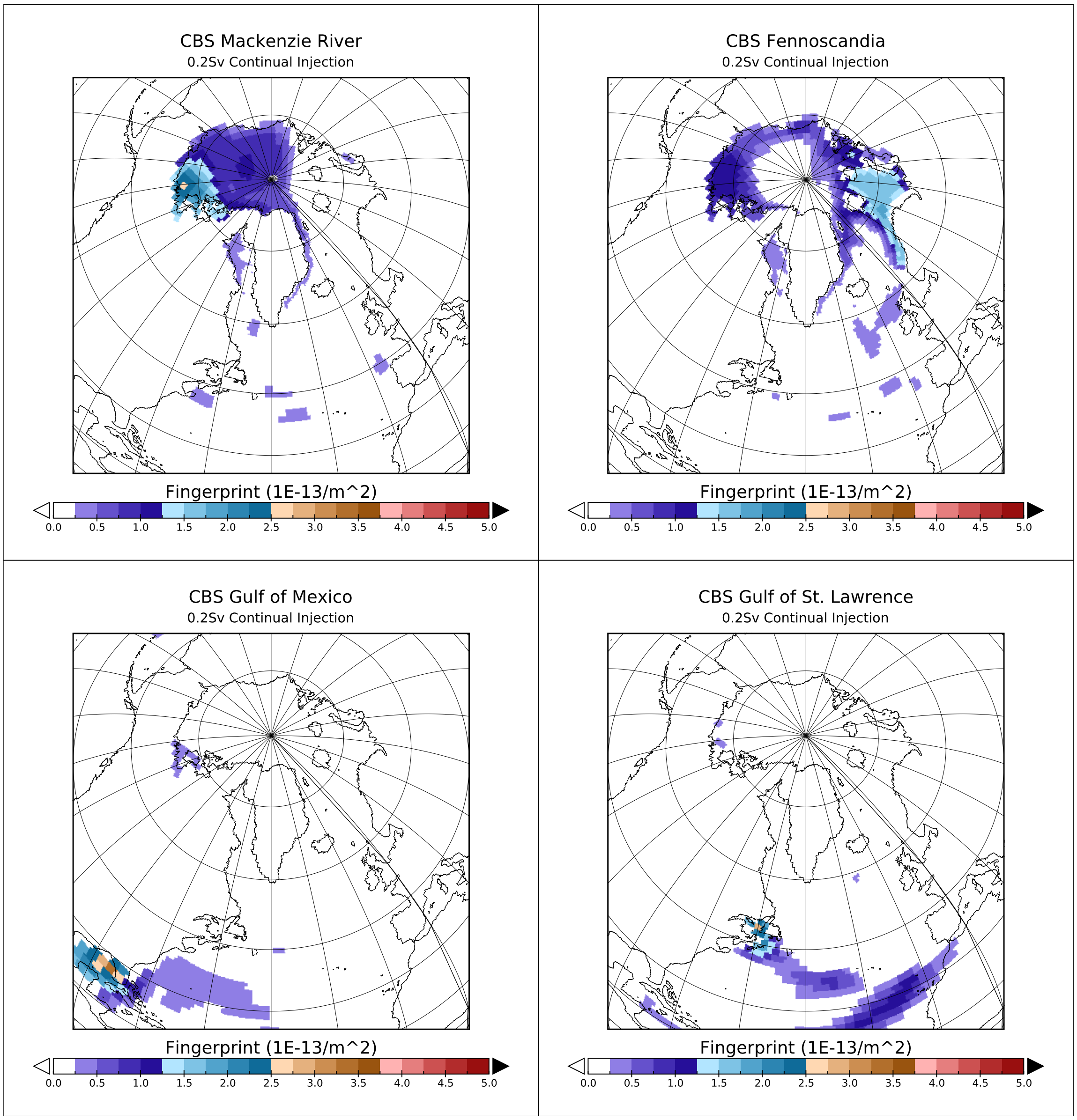

Figure C.5: Freshwater distribution in the COSMOS simulation using a comparible time range as their corresponding MITGCM fingerprint simulation (for Mackenzie River the CBS fingerprint time range was used rather than the OBS). The distribution was calculated using the same methods as to generate the corresponding MITGCM fingerprint. We note that the distribution of the freshwater anomaly in the coarser resolution COSMOS simulation was much more diffuse than in the MITGCM simulations.

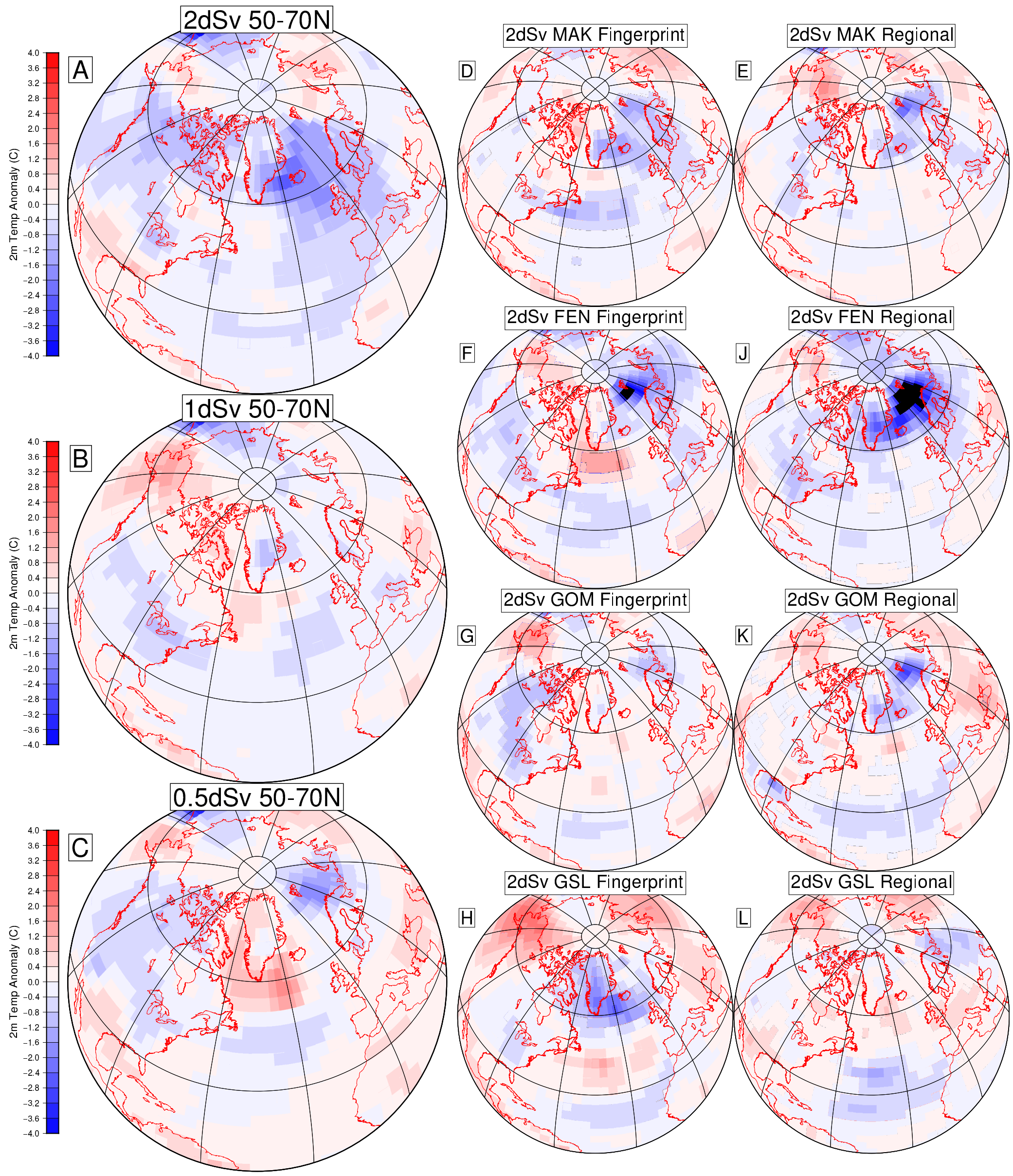

Figure C.6: 2m temperature anomaly averaged over the first 10yr of injection. Subfigures a,b,c show the impact of a 50-70N injection with varying fluxes uniformly distributed over the band. Subfigures d,f,g,h, show the salinity anomalies resulting from using the fingerprint distributions with a 2dSv flux. Similarly, subfigures e,j,k,l show the salinity anomalies resulting from the regional injection locations.

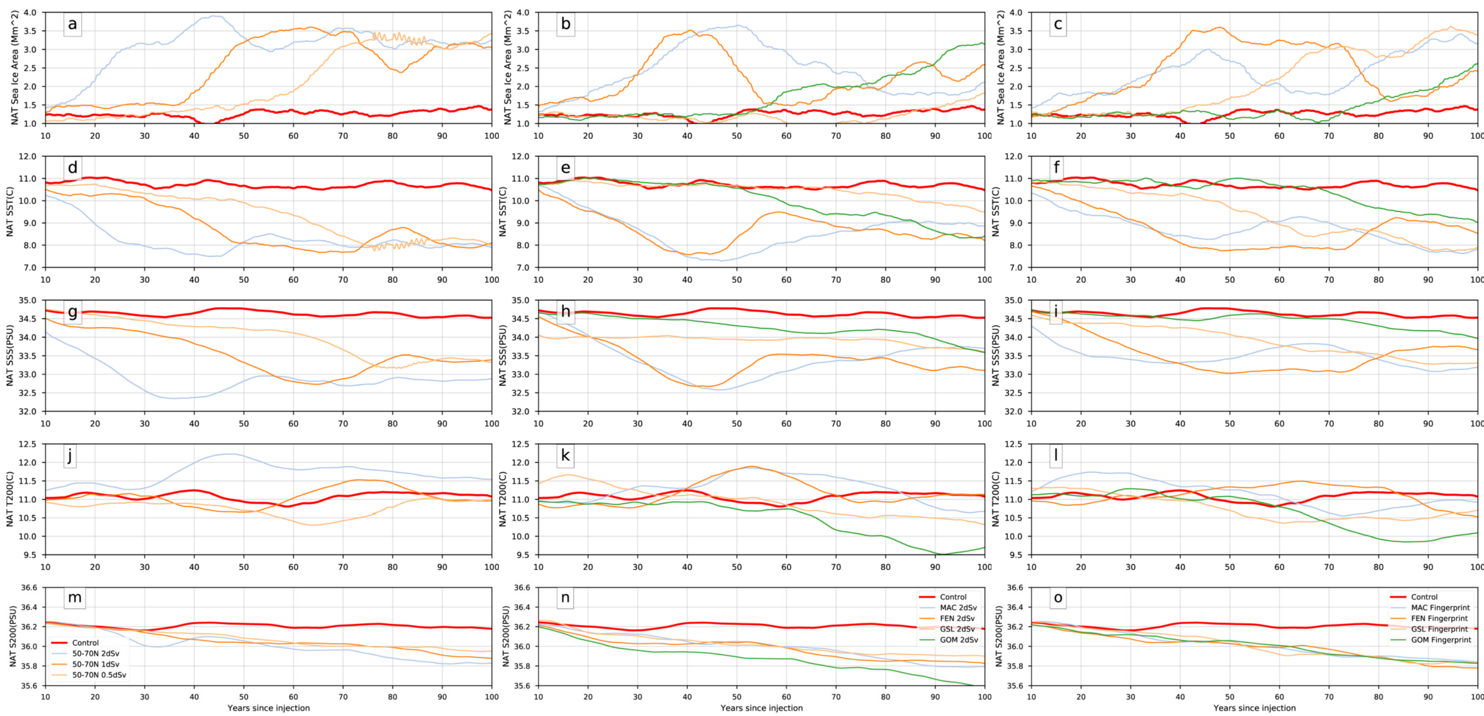

Figure C.7: Ocean domain metrics for the upper layers of the North Atlantic Ocean. Each of the timeseries shown are boxcar running mean with a 10 year window.

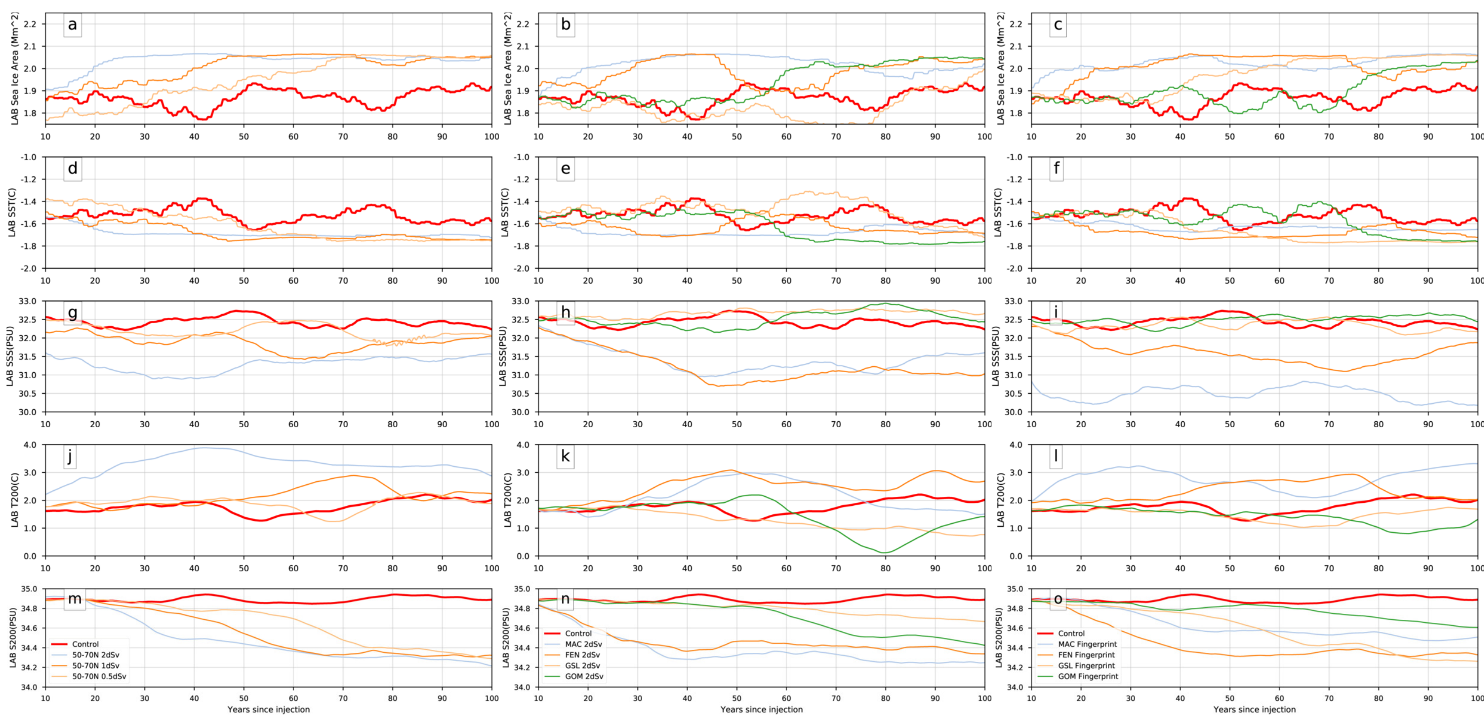

Figure C.8: Ocean domain metrics for the upper layers of the Labrador Sea. Each of the timeseries shown are boxcar running mean with a 10 year window.

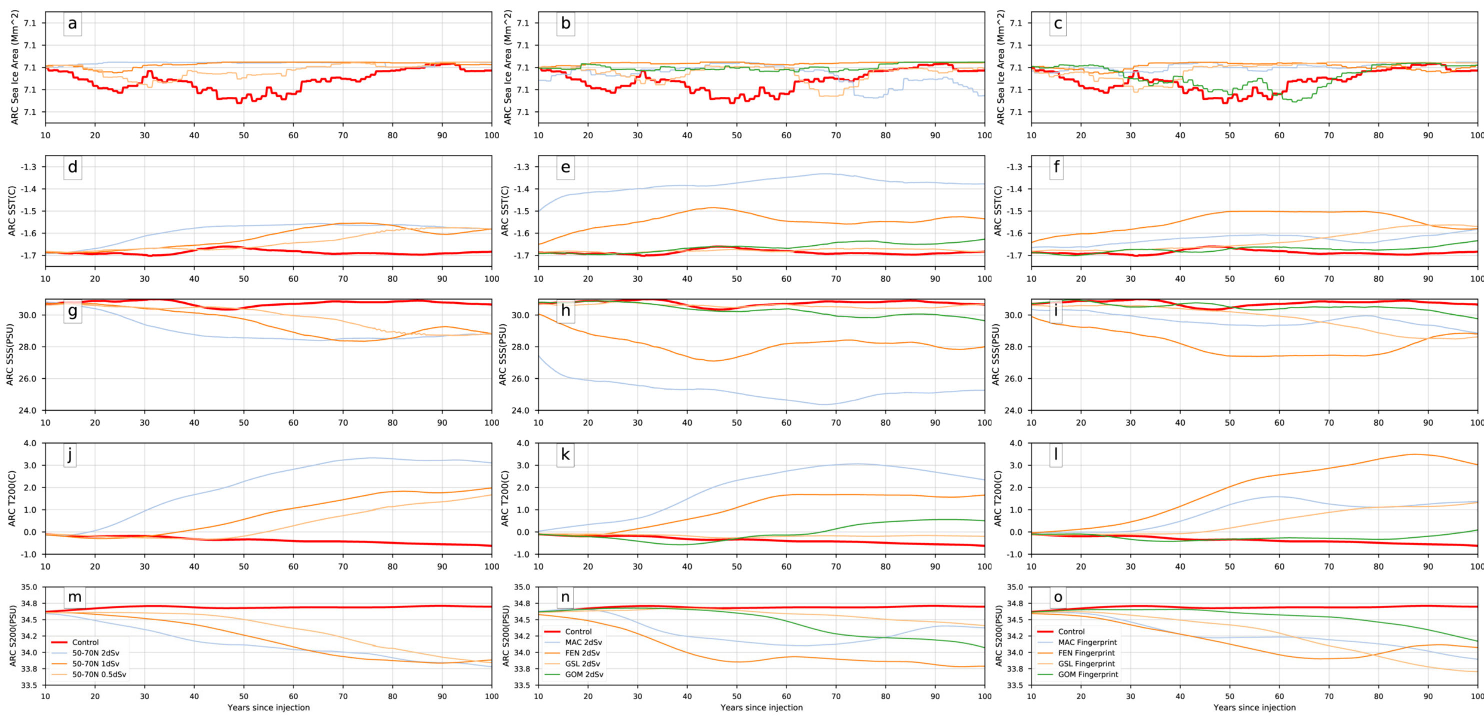

Figure C.9: Ocean domain metrics for the upper layers of the Arctic Ocean. Each of the timeseries shown are boxcar running mean with a 10 year window.

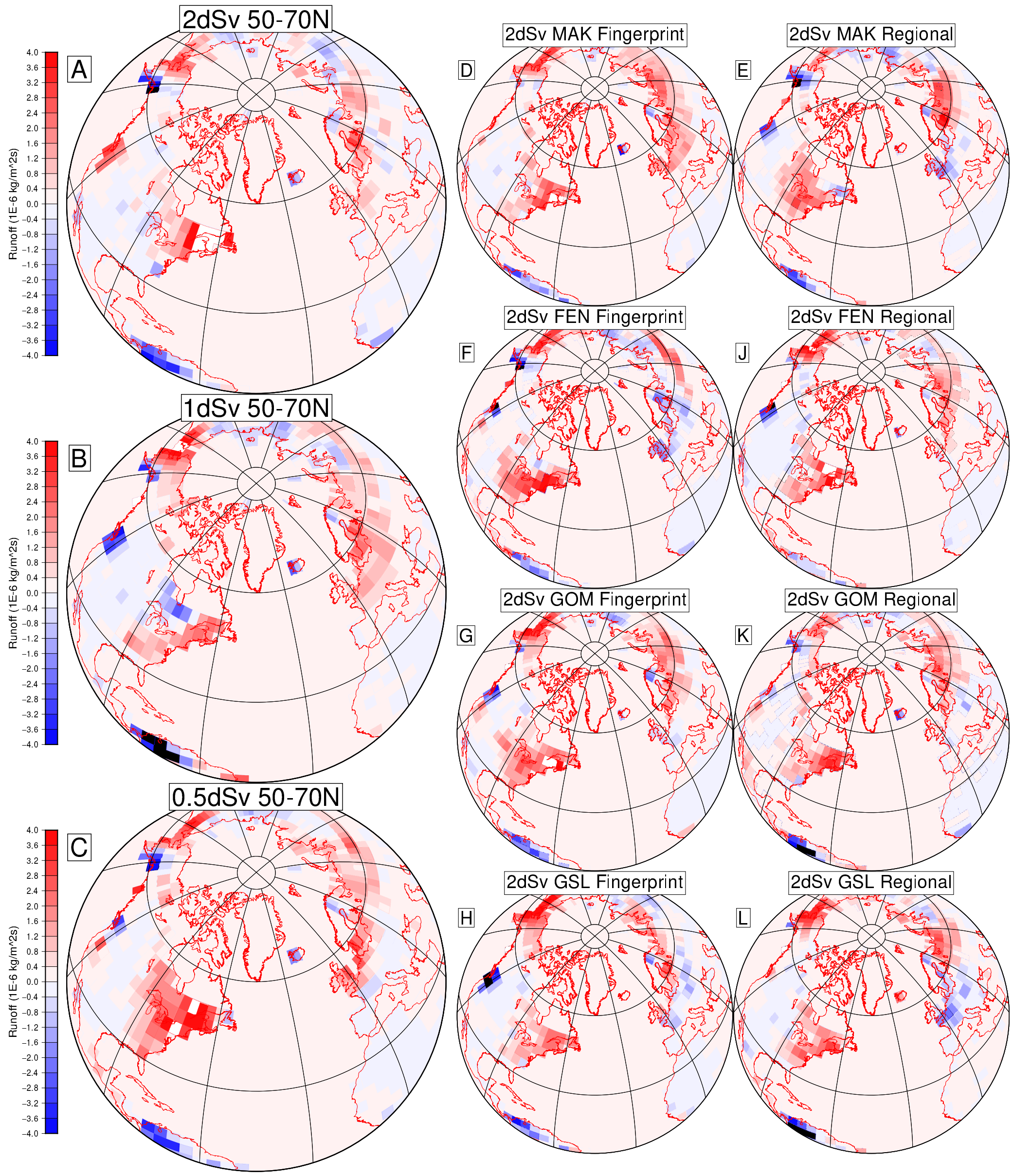

Figure C.10: Surface runoff anomaly averaged over the first 10yr of injection. Subfigures a,b,c show the impact of a 50-70N injection with varying fluxes uniformly distributed over the band. Subfigures d,f,g,h, show the salinity anomalies resulting from using the fingerprint distributions with a 2dSv flux. Similarly, subfigures e,j,k,l show the salinity anomalies resulting from the regional injection locations.

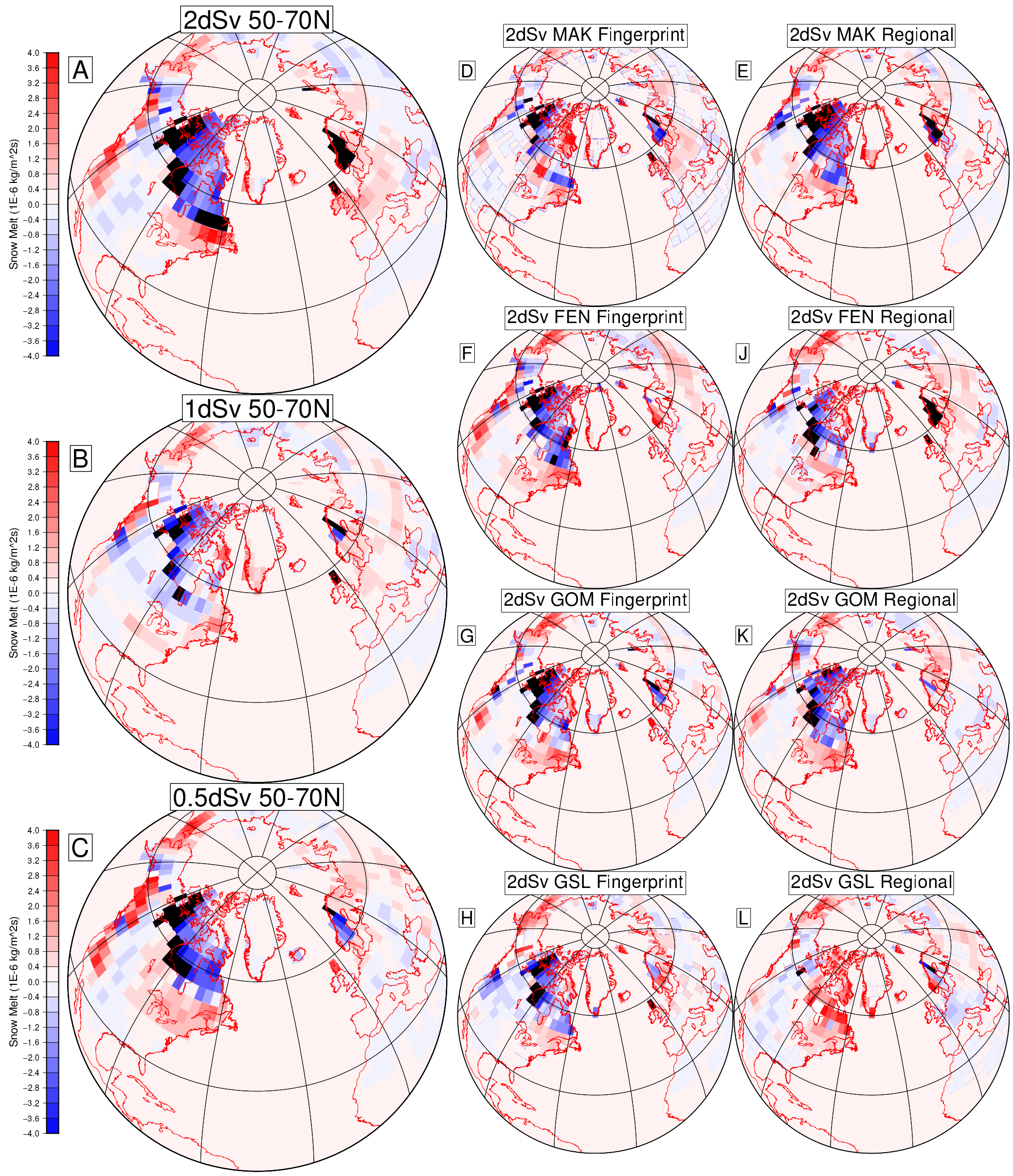

Figure C.11: Snow melt anomaly averaged over the first 10yr of injection. Subfigures a,b,c show the impact of a 50-70N injection with varying fluxes uniformly distributed over the band. Subfigures d,f,g,h, show the salinity anomalies resulting from using the fingerprint distributions with a 2dSv flux. Similarly, subfigures e,j,k,l show the salinity anomalies resulting from the regional injection locations.

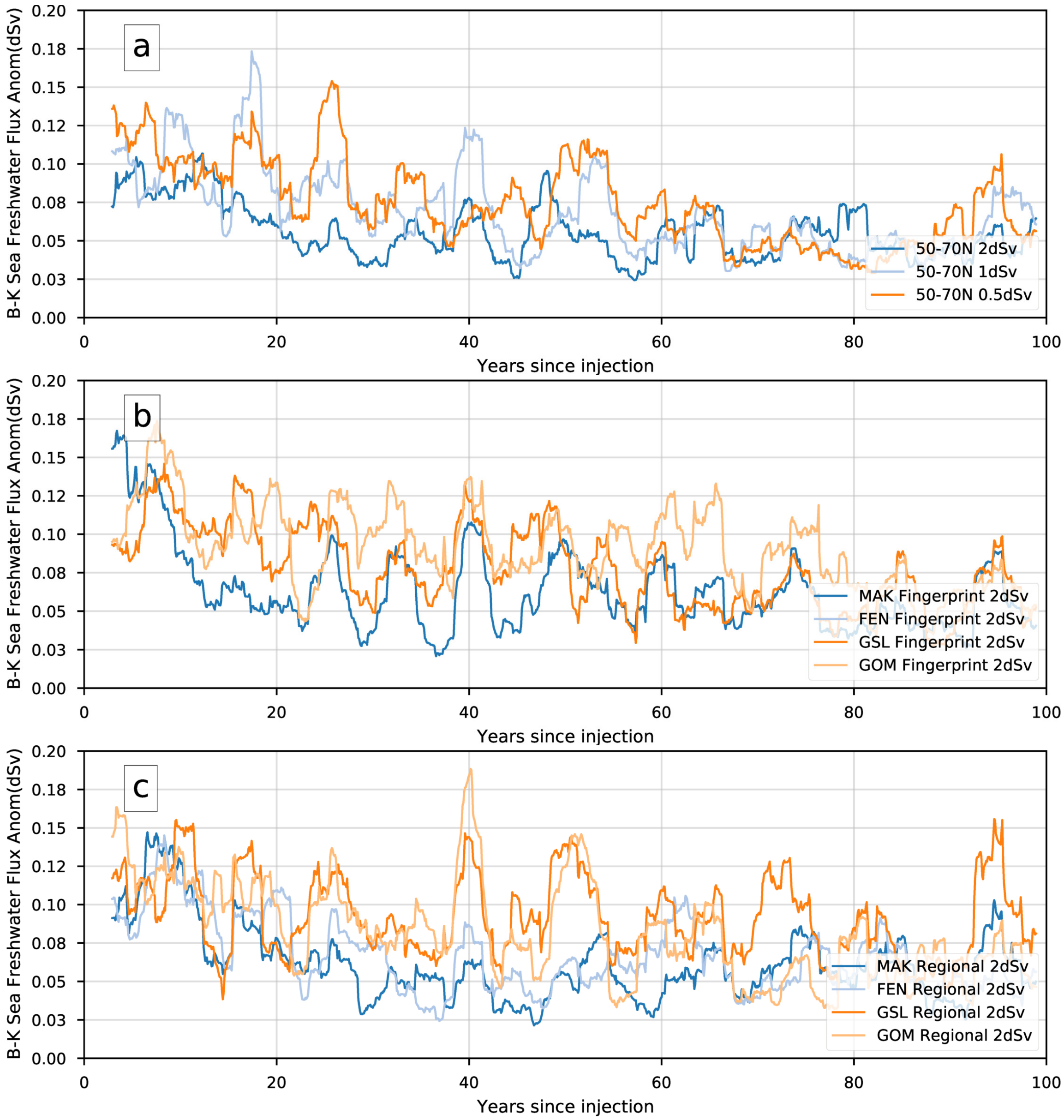

Figure C.12: Freshwater flux into the Barents-Kara Sea, the green region in fig. C.2. In subfigure b the Fennoscandia fingerprint run is off the scale due to the fingerprint injection itself overlapping with the region. We note that it does not show the rise in variability as in the other timeseries shown.

C.2 Why do we have such a strong salinity anomaly in Barents-Kara?

A feature common to all our injection scenarios is a strong salinity anomaly in the Barents Kara sea. Examination of the runoff field shows that all simulations show enhanced surface runoff into this region, see fig C.10. This runoff is explained by enhanced surface warming and snow-melt over North Asia and Eastern Europe, see figs C.6 and C.11 respectively. This enhanced runoff into the Barents-Kara sea, and to a lesser extent the GIN seas, serves to amplify the climate response of a given flux of freshwater by $\approx 4 - 10\%$ of the total freshwater signal. Figure C.12 shows that the peak of the enhanced runoff is short-lived but an enhanced runoff signal is present in all injection scenarios. This feature is similarly replicated around the Mackenzie River for our FEN-R simulation.

Bibliography

R. Love, H. Andres, A. Condron, and L. Tarasov. Eddy permitting simulations of freshwater injection from major northern hemisphere outlets during the last deglacial. *Climate of the Past Discussions*, 2021:1–16, 2021. doi: 10.5194/cp-2021-15. URL https://cp.copernicus.org/preprints/cp-2021-15/.

Appendix D

Supplementary Materials : The Role of CO2 and Glacial Runoff in Modulating Dansgaard-Oeschger Oscillations in an Earth Systems Model

Supplement: The Role of Glacial Runoff in Modulating Dansgaard-Oeschger Oscillations in an Earth Systems Model

Ryan Love[1], Heather J. Andres[1], and Lev Tarasov[1]

[1]Department of Physics and Physical Oceanography, Memorial University of Newfoundland, St. John's, Newfoundland, Canada

D.1 Supplement Figures

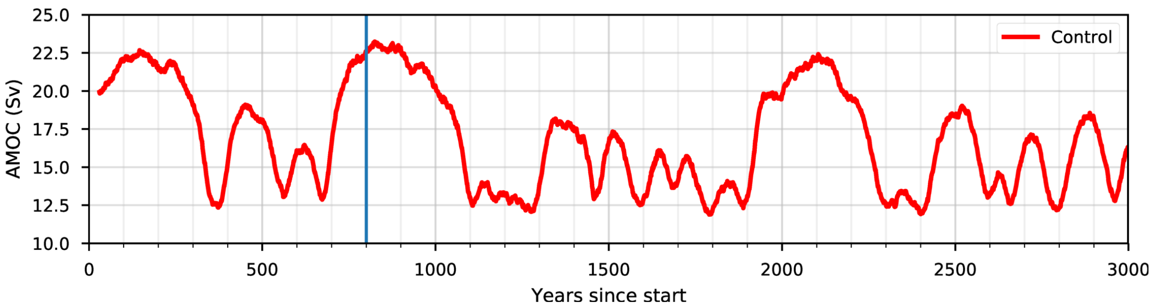

Figure D.1: AMOC from our 185ppm pCO2 simulation demonstrating the internal variability in the system. The pacing is similar to what is expected from the paleoclimate record [Rasmussen et al., 2014] but has a shorter period. The vertical blue line indicates the point at which we branch our injection simulations.

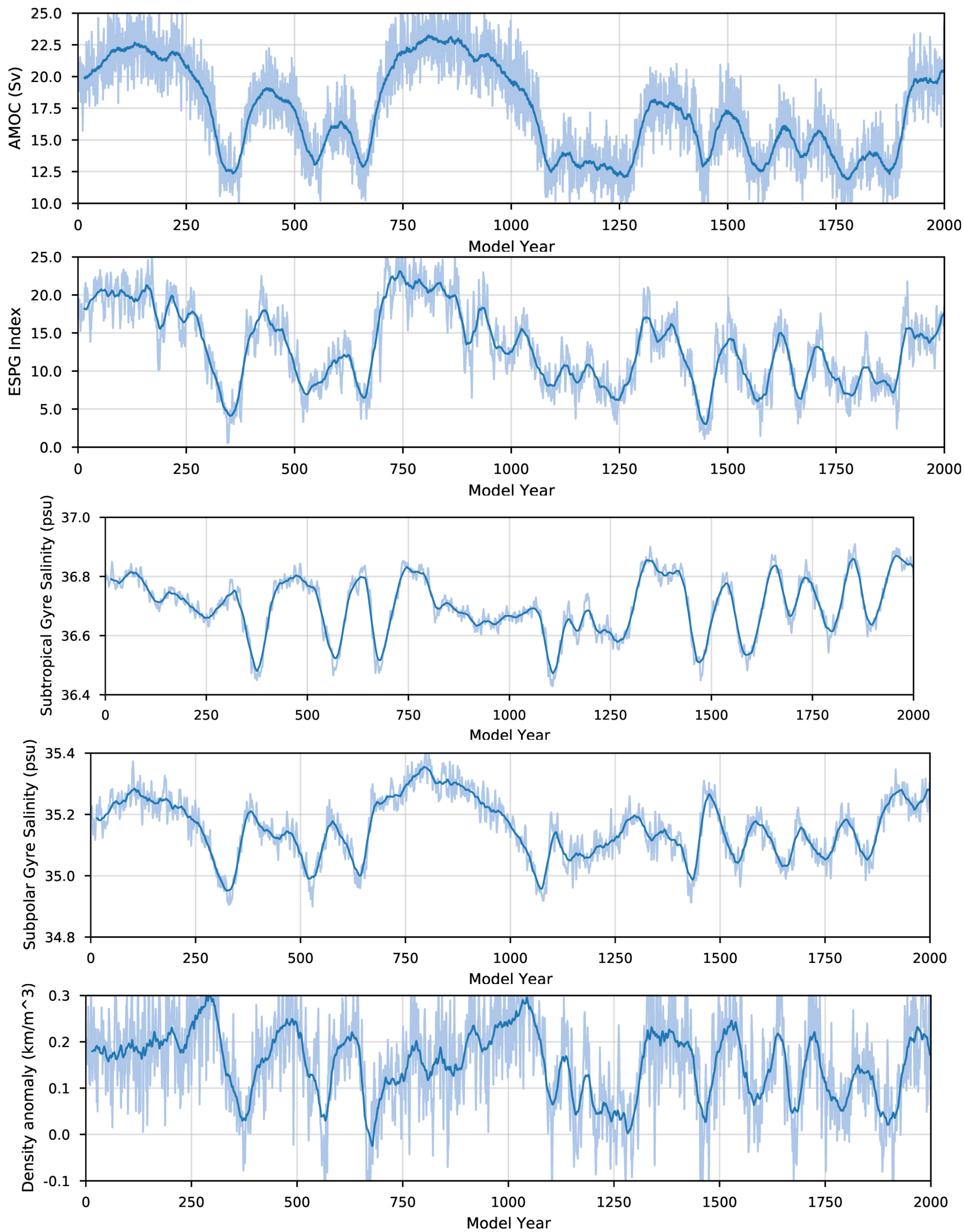

Figure D.2: Comparisons of the fields for the Salinity Oscillator hypothesis. Eastern Subpolar Gyre (ESPG) index and Density anomaly are as in Klockmann et al. [2020].

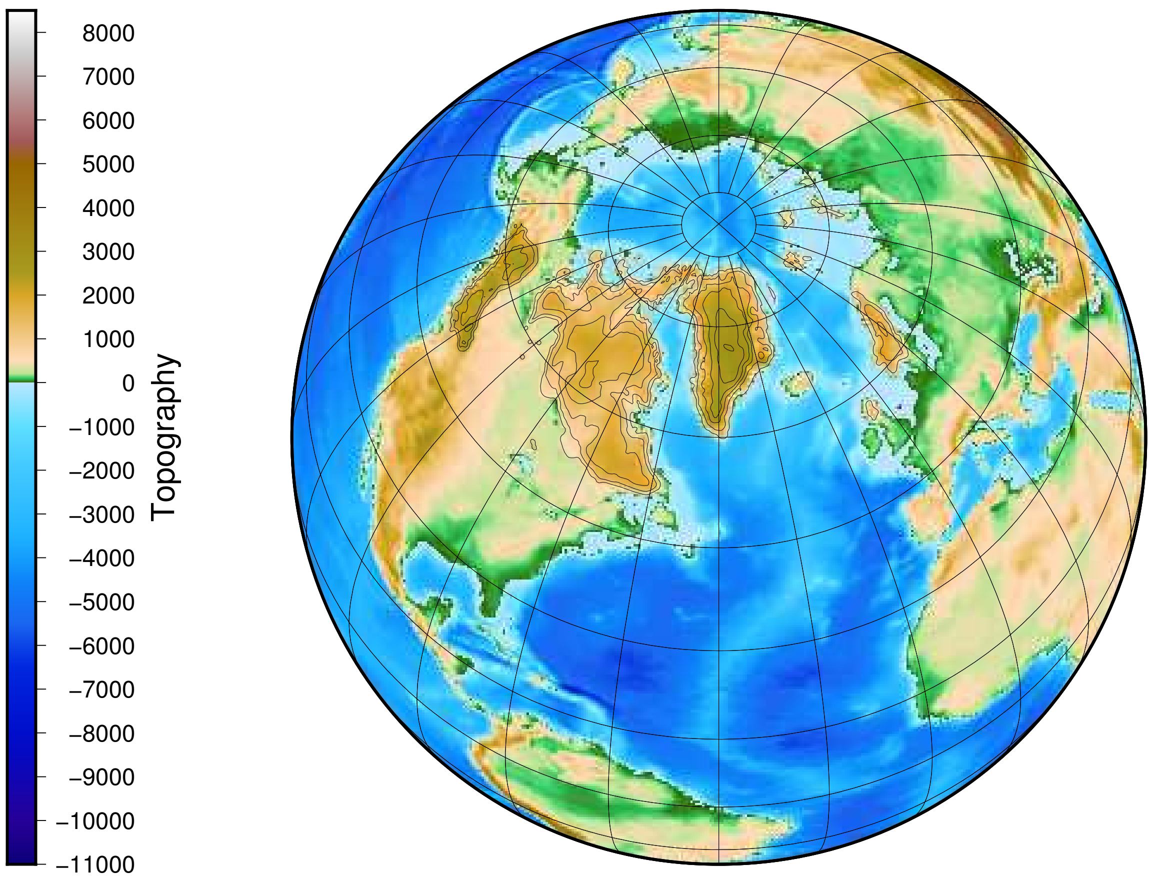

Figure D.3: Topography at 38 ka as per the GLAC1E reconstruction. Ice sheet thickness are contoured at 500m intervals.

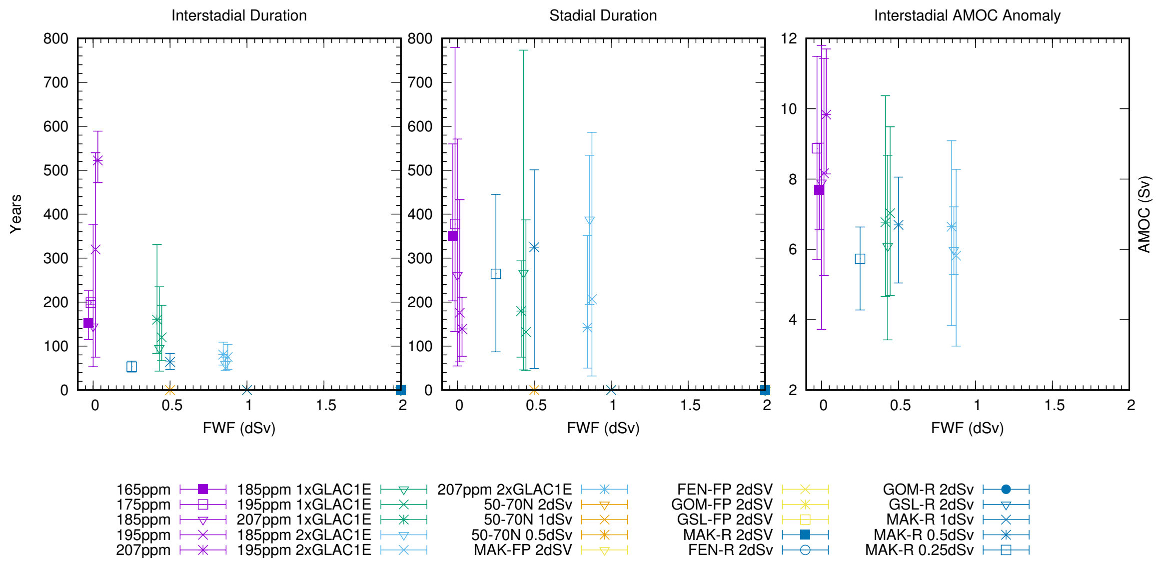

Figure D.4: The relationship between freshwater flux, stadial and interstadial durations, and difference of the peak amplitude of the interstadial vs. the preceding AMOC value. Vertical error bars are indicative of the maximum/minimum values for the interstadial/stadial durations or AMOC peak. Stadial/interstadial durations for configurations in which no CMCOs were detected are set to zero, however in all such cases the model operated in a stadial mode with suppressed AMOC. Where values overlap due to using the same flux value (0, 0.43dSv, 0.86dSv) they have been shifted on the x-axis by a small amount to assist clarity.

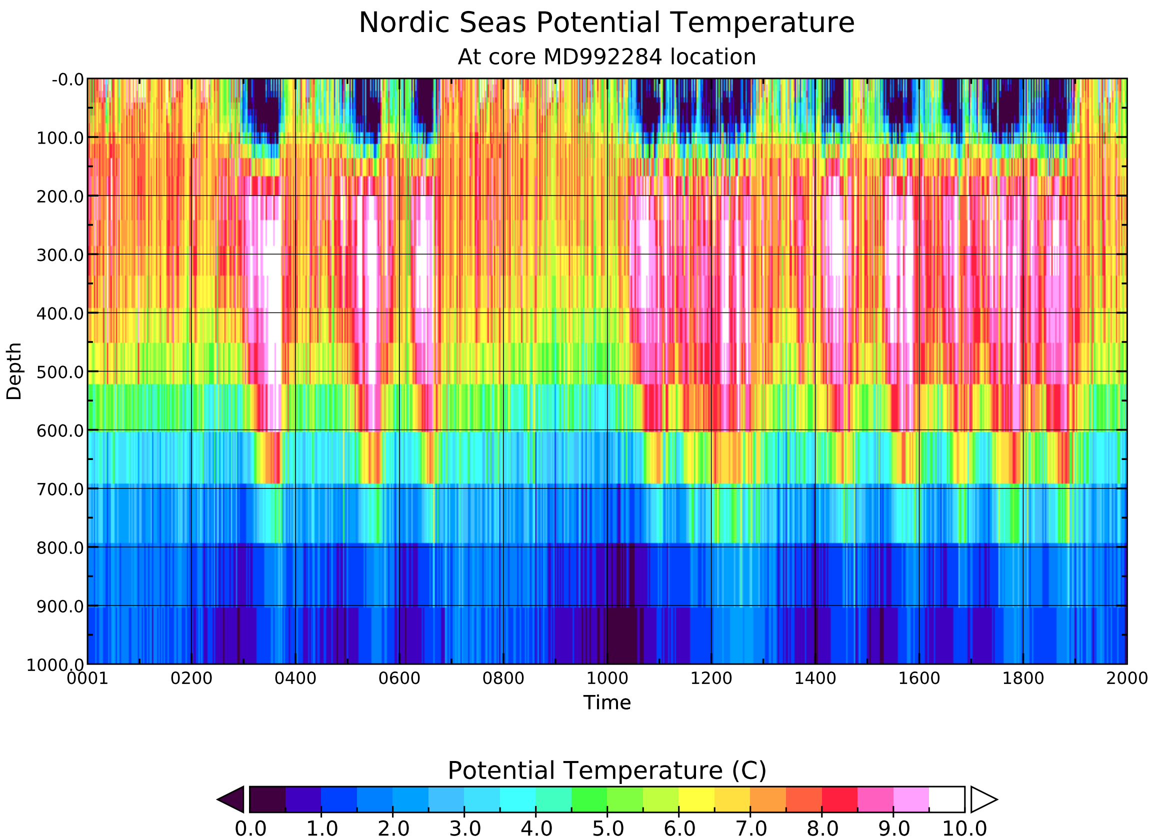

Figure D.5: Potential temperature in the Nordic Seas for the 185ppm pCO2 simulation at the core MD992284 which is examined in Dokken et al. [2013].

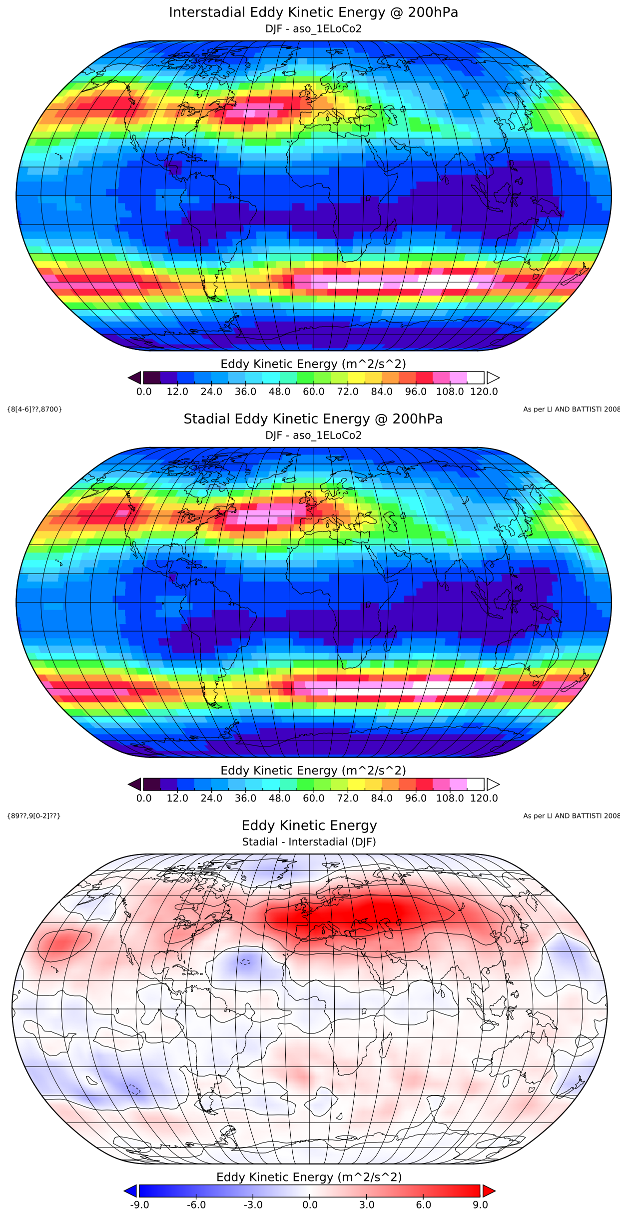

Figure D.6: Spatial map of EKE during stadial and interstadial periods. 200hPa eddy kinetic energy for our typical stadial and interstadial periods and the difference between the periods. We calculate eddy kinetic energy as in Li and Battisti [2008] and we find agreement between the predictions of Dokken et al. [2013] and our results. However, the agreement is not strong, as the main feature of the difference in eddy kinetic energy at elevation is the intensification of EKE during the stadial period relative to the interstadial. In our simulation the storm track is similarly strongly zonal over the North Atlantic and south of the Fennoscandian ice sheet. A brief summary of the eddy kinetic energy calculation is in Section D.3.

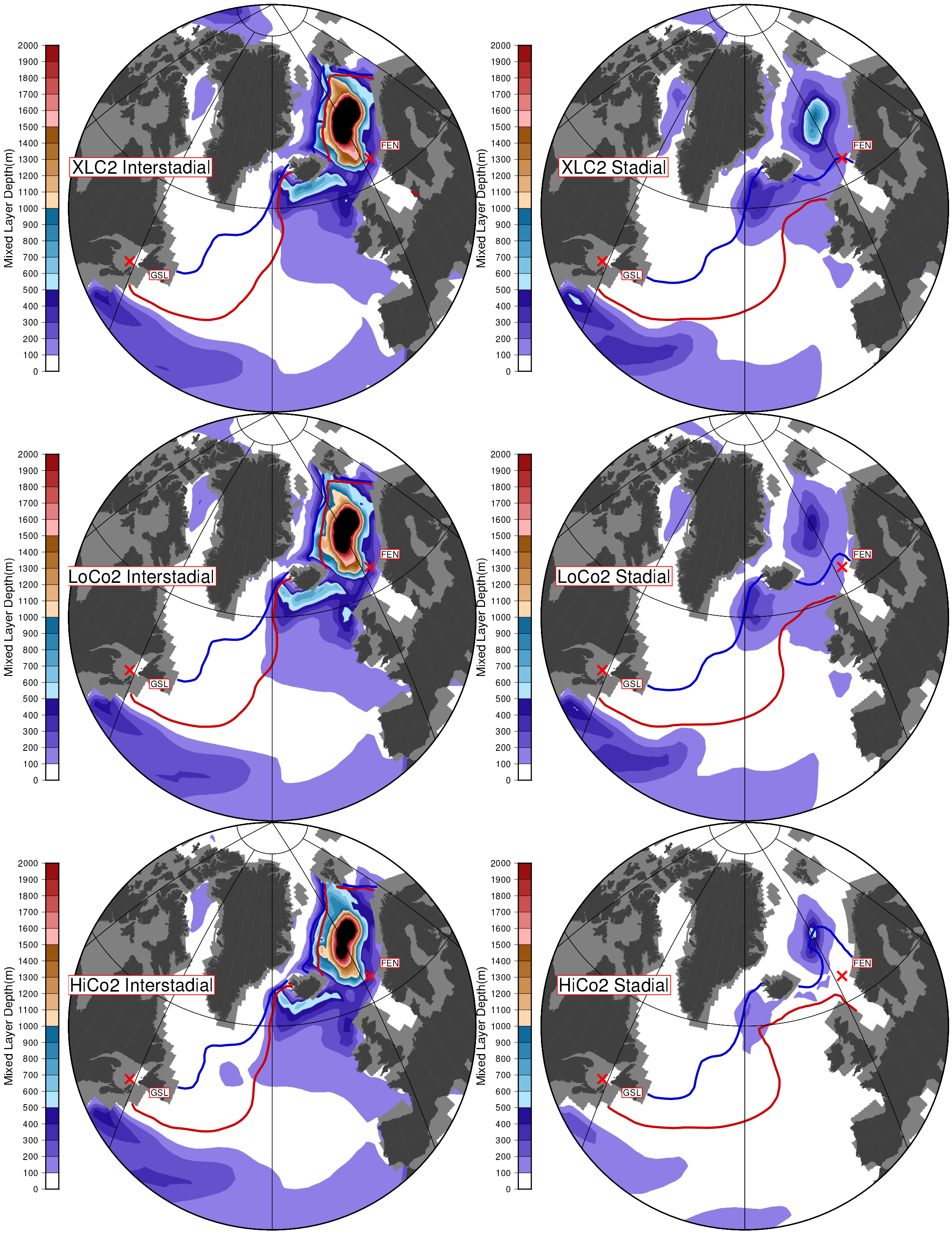

Figure D.7: Mixed layer depth for stadial and interstadial states across a range of background pCO2 values. Blue contour denotes December/January/February 15% sea ice area coverage, while the red contour denotes the June/July/August 15% sea ice area coverage.

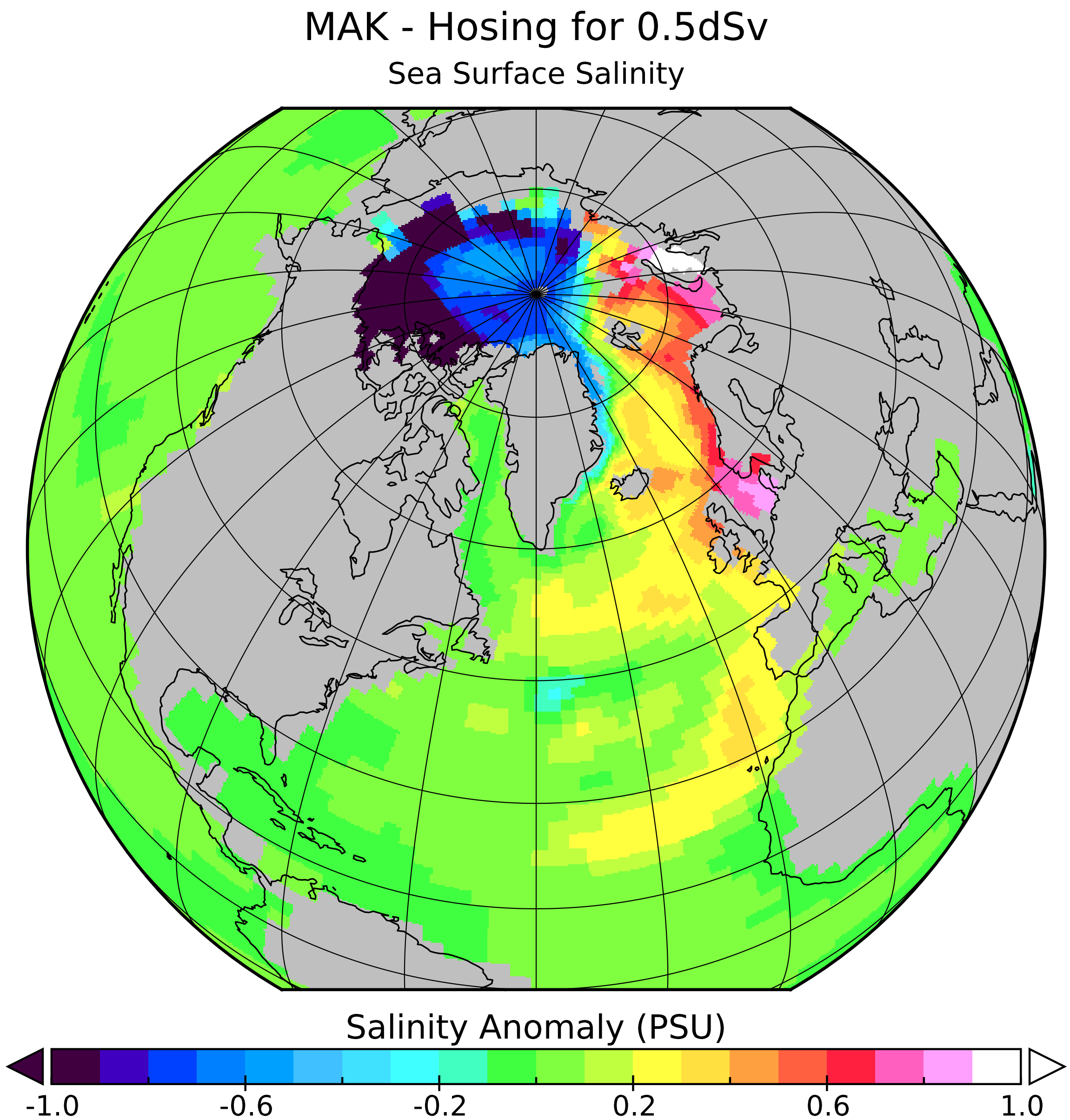

Figure D.8: Sea surface difference between the 0.5dSv MAK and Hosing simulations for the AMOC strong intervals. AMOC strong intervals were determined from the annual mean AMOC, with values $> 10Sv$ for the MAK injection and $> 8Sv$ for the Hosing simulation. Fields were averaged over all years with AMOC greater than their respective limits, except for the first 200 years of each run which exhibited a very clear transition period.

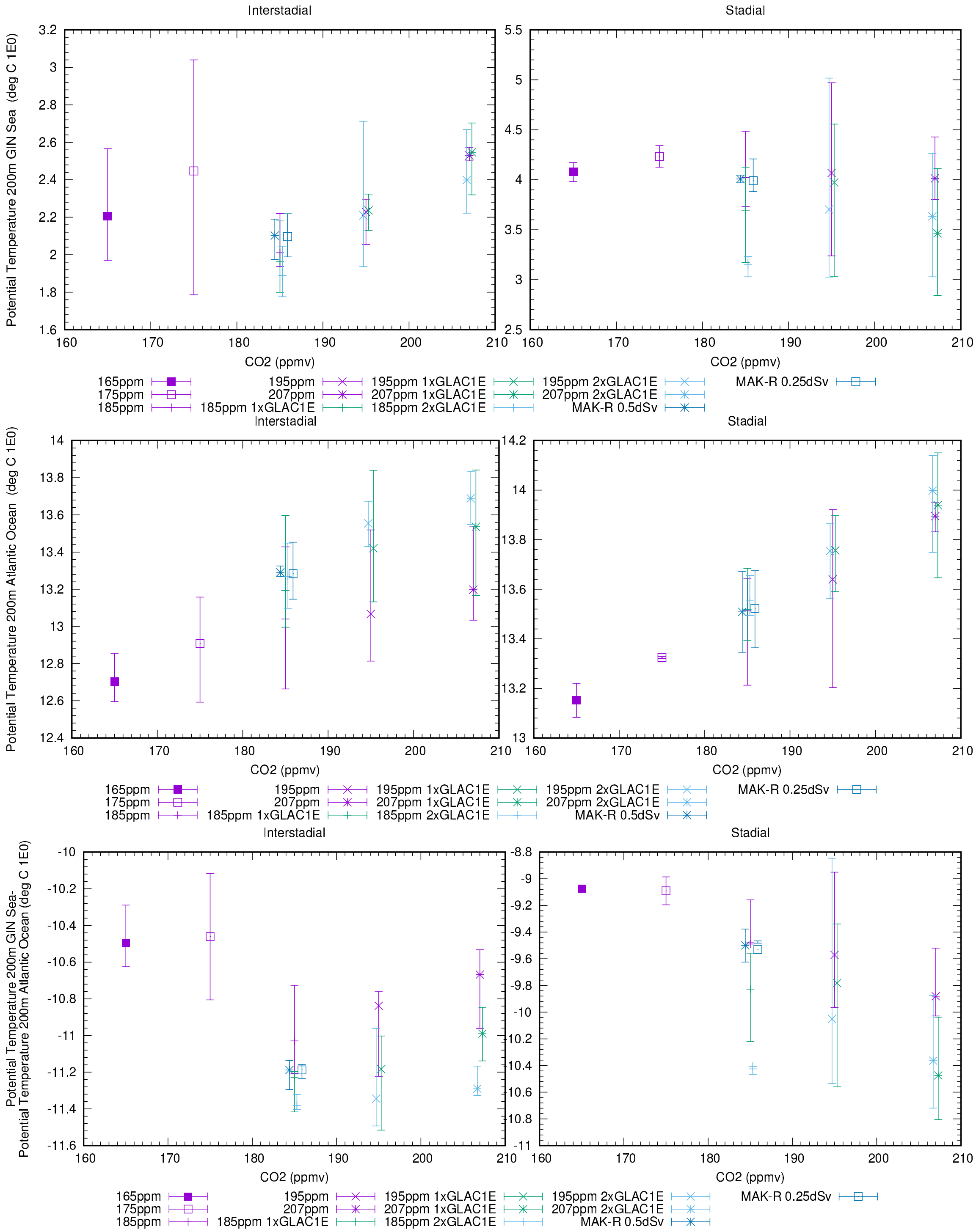

Figure D.9: 200m Potential Temperature in the GIN Seas, the Atlantic, and the difference between the two as a function of CO2 for interstadial periods and stadial periods.

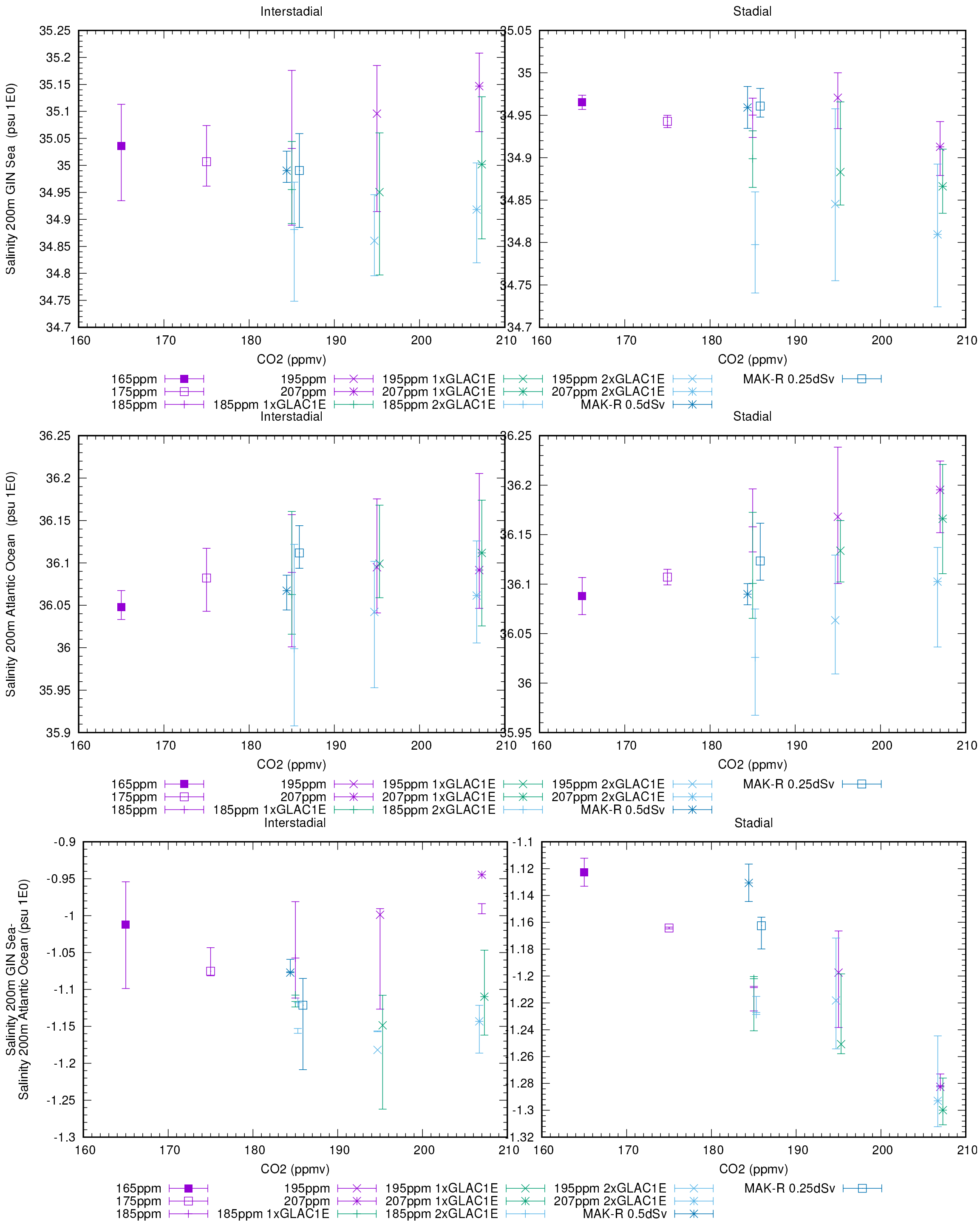

Figure D.10: 200m Salinity in the GIN Seas, the Atlantic, and the difference between the two as a function of CO2 for interstadial periods and stadial periods.

D.2 Bathymetry/Topography Adjustment Methodology

For both bathymetry and topography we have elected to use data from the Tarasov et al. [2012] Glacial Systems Model (GSM) reconstructions. The topography for 38ka is taken directly from the GLAC1E reconstructions. The bathymetry was modified by using the anomaly between the respective time slices and present day in the GSM reconstruction. This anomaly is then applied to the preindustrial ocean bathymetry data while accounting for features in the reconstruction such as closed gateways and ice shelves. The bathymetry is also modified to remove features which may cause instabilities in the model, these adjustments are minor and mainly reflect refinements (e.g. isolated ocean cells). This methodology allows us to account not only for the eustatic sea level change but the spatial variability in sea level change between present day and the chosen time-slice. We are able to do this as the GSM features a gravitationally self consistent sea level solver and can output relative sea level taking into account deflection of the geoid and other such features as in [Mitrovica and Milne, 2003] with the exception of the rotational component [Milne and Mitrovica, 1998].

D.3 Eddy Kinetic Energy

A brief summary of the eddy kinetic energy calculation follows;

1. Starting from 6 hourly atmospheric velocity fields on hybrid elevation levels we take daily averages of the data
2. Remap from the hybrid elevation scheme to 200hPa
3. Highpass filter the fields to retain variability with periods less than 8 days using CDO; cdo highpass,$(echo "365.0/8.0|bc -l") -del29feb

4. Our measure of eddy kinetic energy is then the sum of

$$u^2 + v^2$$

5. We then take seasonal (DJF,MAM,JJA,SON) averages of the resulting field for analysis

Bibliography

Trond M. Dokken, Kerim H. Nisancioglu, Camille Li, David S. Battisti, and Catherine Kissel. Dansgaard-oeschger cycles: Interactions between ocean and sea ice intrinsic to the nordic seas. *Paleoceanography*, 28(3):491502, Sep 2013. ISSN 0883-8305. doi: 10.1002/palo.20042. URL http://dx.doi.org/10.1002/palo.20042.

M. Klockmann, U. Mikolajewicz, H. Kleppin, and J. Marotzke. Coupling of the subpolar gyre and the overturning circulation during abrupt glacial climate transitions. *Geophysical Research Letters*, 47(21), Nov 2020. ISSN 1944-8007. doi: 10.1029/2020gl090361. URL http://dx.doi.org/10.1029/2020GL090361.

Camille Li and David S. Battisti. Reduced atlantic storminess during last glacial maximum: Evidence from a coupled climate model. *Journal of Climate*, 21(14):35613579, Jul 2008. ISSN 0894-8755. doi: 10.1175/2007jcli2166.1. URL http://dx.doi.org/10.1175/2007JCLI2166.1.

Glenn A. Milne and Jerry X. Mitrovica. Postglacial sea-level change on a rotating earth. *Geophysical Journal International*, 133(1):119, Apr 1998. ISSN 1365-246X. doi: 10.1046/j.1365-246x.1998.1331455.x. URL http://dx.doi.org/10.1046/j.1365-246X.1998.1331455.x.

Jerry X. Mitrovica and Glenn A. Milne. On post-glacial sea level: I. general theory. *Geophysical Journal International*, 154(2):253267, Aug 2003. ISSN 1365-246X. doi: 10.1046/j.1365-246x.2003.01942.x. URL http://dx.doi.org/10.1046/j.1365-246X.2003.01942.x.

Sune O. Rasmussen, Matthias Bigler, Simon P. Blockley, Thomas Blunier, Susanne L. Buchardt, Henrik B. Clausen, Ivana Cvijanovic, Dorthe Dahl-Jensen, Sigfus J. Johnsen, Hubertus Fischer, and et al. A stratigraphic framework for abrupt climatic changes during the last glacial period based on three synchronized greenland ice-core records: refining and extending the intimate event stratigraphy. *Quaternary Science Reviews*, 106:14–28, Dec 2014. ISSN 0277-3791. doi: 10.1016/j.quascirev.2014.09.007. URL http://dx.doi.org/10.1016/j.quascirev.2014.09.007.

Lev Tarasov, Arthur S. Dyke, Radford M. Neal, and W.R. Peltier. A data-calibrated distribution of deglacial chronologies for the north american ice complex from glaciological modeling. *Earth and Planetary Science Letters*, 315316:30 – 40, 2012. ISSN 0012-821X. doi: http://dx.doi.org/10.1016/j.epsl.2011.09.010. URL http://www.sciencedirect.com/science/article/pii/S0012821X11005243. Sea Level and Ice Sheet Evolution: A {PALSEA} Special Edition.